Dissecting the mechanisms of pacemaking in the heart using photo-affinity probes and pharmacological intervention



Islom Nazarov

Corpus Christi

University of Oxford

A thesis submitted for the degree of

Doctor of Philosophy

Trinity 2016

Dissecting the mechanisms of pacemaking in the heart using photo-affinity probes and pharmacological intervention

Islom Nazarov, Corpus Christi College, University of Oxford. A thesis submitted for the degree of Doctor of Philosophy, Trinity 2016

The aim of the work described in this thesis was to dissect the mechanisms underlying pacemaking in the heart using both pharmacological and chemical tools. The mechanisms underlying pacemaker activity in the sino-atrial node are controversial, with some researchers giving prominence to the role of the 'funny' current, I_f, others emphasising a 'calcium clock', and with still others highlighting the elusive sustained inward current, I_{st}.

Autonomic modulators, particularly adrenaline and noradrenaline regulate all the proposed mechanisms. To investigate which adrenoceptors are responsible for driving positive chronotropic action in the heart, adrenoceptors α_1, β_1 and β_2 were studied using selective blockers (prazosin, CGP20712A and ICI118551, respectively). The results imply that activation of the β_1-adrenoceptor pathway is responsible for most positive chronotropic actions in the mouse heart.

Selective blockers of I_f (ZD7288, ivabradine) and sarcoplasmic reticulum (SR) [ryanodine and cylopiazonic acid (CPA)] were used to explore the contributions of I_f and Ca^{2+} release from SR to cardiac pacemaking in the absence and presence of β adrenoceptor stimulation. The results showed that both I_f and Ca^{2+} release from SR significantly contribute to pacemaking both in the presence or absence of β adrenoceptor stimulation. They also show that the effects of ivabradine and ZD7288 on heart rate are substantially reduced following CPA or ryanodine administration; this may reflect a possible effect of reduced activity of Ca^{2+}-stimulated adenylyl cyclases (AC) present in SAN cells. To investigate this phenomenon genetically modified mice lacking Ca^{2+}-stimulated (AC) were used. Contrary to predictions, the resting heart rates and responses to I_f blockers, CPA blockers and isoprenaline from genetically modified mice showed only small differences relative to control mice.

With aim of identifying the sequence of the I_{st} protein a series of photo-affinity probes were developed to enable covalent photocapture of the I_{st} ion channel following exposure to UV light. Proof of concept studies involved for photo-crosslinking and pull-down experiments in pursuit of identifying the $Ca_v1.2$ channel. Subsequent to cross-linking the photo-affinity probe to its target, Western blot analysis identified a ~190 kD band, consistent with the L-type Ca^{2+} channel.

Acknowledgements

I would like to express my sincere gratitude to my supervisors Professor Derek Terrar, Professor Chris Schofield, Dr. Akane Kawamura, Dr. Jacob Bush and Dr. Duncan Hay, for their patience, trust, guidance and continuous support throughout my D.Phil. Professor Schofield's support and belief enabled me to follow my interest in the cardiovascular field.

I thank both Professor Terrar and Schofield for giving me access to their laboratory and research facilities. In particular, I am grateful to Cynthia Sam for her never-ending support through the highs and lows. I would also like to thank Colin Robey for his support and advice throughout this journey; who always managed to make the dark days bright.

Besides my advisors, I would like to thank the Pharmacology administrative team, in particular Paula Savin without whose constant support my journey would have not been a successful one.

Last but not the least, my heartfelt gratitude goes out to my family: my parents without their sacrifices this goal would have been unattainable and my sister, the biggest pillar of my life, for her constant never ending support and belief in me.

Full paper

Nazarov, IB, Schofield, CJ & Terrar, DA (2015). Contributions of cardiac "funny" (f) channels and sarcoplasmic reticulum Ca^{2+} in regulating beating rate of mouse and guinea pig sinoatrial node. *Physiol Rep* **3**, pp 1-13.

Abstracts presented at:

- BHF Centre of Research Excellence Annual Symposium, Oxford (2012)
- Cardiac & Respiratory Physiology Conference, Manchester (2012)
- Biophysical Society's 57th Annual Meeting, Philadelphia (2013)
- BHF Centre of Research Excellence Annual symposium, Oxford (2014)
- Biophysical Society's 58th Annual Meeting, San Francisco, California (2014)

Author contributions

I performed all the experiments described in this thesis unless otherwise stated in the text. A description of the contributions from collaborators is given bellow.

Chapter 4. Results in **Figure 4.8** were the only results collected in collaboration with Kamal Ibrahim (my supervisee for an MSc in Pharmacology 2014).

Abbreviations

AC	Adenylyl Cyclase
AC1	Adenylyl Cyclase 1
$AC1^{(-/-)}$	Knockout mice lacking AC1 enzyme
$AC1\&8^{(-/-)}$	Double knockout mice lacking both AC1 and AC8 enzyme
AC3	Adenylyl Cyclase 3
AC5	Adenylyl Cyclase 5
AC6	Adenylyl Cyclase 6
AC8	Adenylyl Cyclase 8
$AC8^{(-/-)}$	Knockout mice lacking AC8 enzyme
ACh	Acetylcholine
AP	Action Potential
BL6	C57BL/6J
bpm	Beats per minute
CaM	Calmodulin
CaMKII	Ca^{2+} calmodulin-dependent protein kinase II
cAMP	Cyclic adenosine monophosphate
CCh	Carbachol
CGP	CGP20712A
CICR	Calcium-induced calcium release
CPA	Cyclopiazonic acid
CV	Column volumes
DD	Diastolic depolarization
DMSO	Dimethyl sulfoxide
GIRK	G protein-coupled inwardly-rectifying potassium channel
HCN	Hyperpolarization-activated cyclic nucleotide-gated
HPLC	High Performance Liquid Chromatography
Hz	Hertz
I_f	Funny current
I_{NCX}	Sodium-calcium exchange current
Iso	Isoprenaline
I_{st}	Sustained inward current
KN-93	N-[2-[[[3-(4-chlorophenyl)-2-propen-1-yl]methylamino]methyl]phenyl]-N-(2-hydroxyethyl)-4-methoxy-benzenesulfonamide
K_r	Rapid-activated voltage-gated delayed rectifier K^+ channel
K_s	Slow-activated voltage-gated delayed rectifier K^+ channel
K_v	Voltage-gated K^+ channel
LCR	Localized calcium release
MDL-12,330A	cis-*N*-(2-Phenylcyclopentyl)-azacyclotridec-1-en-2-amine hydrochloride
Me	Methyl
NCX	Sodium-calcium exchanger
NMR	Nuclear magnetic resonance
Nor	Noradrenaline

PCR	Polymerase chain reaction
PDE	Phosphodiesterases
Phen	Phenylephrine
PIP_2	Phosphatidylinositol 4,5-bisphosphate
PKA	Protein Kinase A
PLB	Phospholamban
Praz	Prazosin
PSS	Physiological Salt Solution
Reb	Reboxetine
RT-PCR	Reverse transcription polymerase chain reaction
RY	Ryanodine
RYR	Ryanodine receptor
SAN	Sino atrial node
SAR	Structure-activity relationship
SERCA	Sarcoendoplasmic reticulum Ca^{2+} ATPase
SR	Sarcoplasmic reticulum
TEA	Tetraethylammonium
TTX	Tetrodotoxin
UV	Ultraviolet
W-7	N-(6-Aminohexyl)-5-chloro-1-naphthalenesulfonamide hydrochloride
ZD7288	4-(*N*-Ethyl-N-phenylamino)-1,2-dimethyl-6(methylamino) pyridinium chloride

Table of Contents

CHAPTER 1: INTRODUCTION 1

1.1. Introduction 2

1.2. Surface Membrane Currents (M-clocks) 4

1.2.1. K^+ channels 6
1.2.1.1. Lack of inwardly rectifying K^+ channel (K_1) 6
1.2.1.2. Delayed rectifier potassium current (K_v) 7
1.2.1.3. ACh-activated K^+ channels (K_{Ach}) 7
1.2.2. Na^+ channel 8
1.2.3. Background current, I_{bNa} 9
1.2.4. Ca^{2+} channels 11
1.2.5. Ca^{2+}-activated nonselective cation channel, TRPM4 11
1.2.6. Sustained inward current (I_{st}) 13
1.2.7. Hyperpolarization-activated current, I_f 15
1.2.7.1 The K^+ - decay hypothesis 15
1.2.7.2. Indirect modulation of I_f by intracellular calcium 18

1.3. Intracellular Mechanisms of Pacemaking 20

1.3.1. The role of intracellular Ca^{2+} at the foot of the AP 21
1.3.2. The involvement of the Na^+-Ca^{2+} exchanger (NCX) current in pacemaking 22
1.3.3. The role of elevated cAMP levels in the generation of LCRs 26
1.3.4. Is LCR essential for pacemaking? 27

1.4. A coupled mechanism of intracellular Ca^{2+}-clocks and M-clocks 27

1.4.1. The control of the Ca^{2+} clock by PKA 30
1.4.2. Minor contribution of Ca^{2+} transients to the pacemaker rhythm 32

1.5. Autonomic modulation of the pacemaker 33

1.5.1. Sympathetic modulation of the pacemaker 34
1.5.2. Parasympathetic modulation of the pacemaker 36

1.6. Clinical implications 37

1.7. Aims 40

CHAPTER 2: METHODS 41

2.1. Atrial node preparation 42
2.2. Organ bath sinoatrial node preparations 42
2.3. Optical fluorescent Ca^{2+} transient measurement sinoatrial node preparation 44
2.4. Imaging system for Ca^{2+} transient measurements from intact SAN preparation 46
2.5. Imaging system for Ca^{2+} transient measurements from guinea pig SAN cells 46
2.6. Cell isolation (guinea pig) 47
2.6.1. Ventricular isolation (guinea pig) 47
2.6.2. SAN cell isolation (guinea pig) 48
2.7. Knockout mice models: $AC1^{(-/-)}$, $AC8^{(-/-)}$ and $AC1\&8^{(-/-)}$ 49

2.8. Drug Exposure Times 50
2.9. Statistical analysis 51
2.10. Solutions used for pharmacological studies: 51
2.11. Chemicals used for Pharmacology studies: 52
2.12. Pharmacodynamics profile of used compounds 53
2.13. Representative traces from atrial preparations 54
2.14. Lysis buffers 55
2.15. Sample preparation from mouse whole heart 55
2.16. Cell lysis (guinea pig) 56
2.17. UV irradiation of samples 56
2.18. Click Chemistry reaction 57
2.19. Magnetic beads pull-down 57
2.20. Electrophoresis protocol 58
2.21. Western blotting protocol 58
2.22. Antibodies 59

CHAPTER 3: IDENTIFICATION OF ADRENOCEPTOR ACTIVATION RESPONSIBLE FOR DRIVING THE POSITIVE CHRONOTROPIC ACTION 60

3.1. Introduction 61

3.2. Results 63

3.3. The effects of adrenergic receptor stimulation on positive chronotropy 63

3.3.1. β_1-adrenergic receptor (isoprenaline) 63
3.3.2. β_1-adrenergic receptor (noradrenaline) 65
3.3.3. Chronotropic contribution of α_1-adrenergic receptor (noradrenaline) 66
3.3.4. Chronotropic contribution of β_2-adrenergic receptor (isoprenaline) 66

3.4. Discussion 68

CHAPTER 4: THE EFFECTS OF I_F AND SR Ca^{2+} RELEASE INHIBITORS ON BASAL SPONTANEOUSLY BEATING RATE IN THE ABSENCE AND PRESENCE OF β_1-ADRENOCEPTOR STIMULATION WITH ISOPRENALINE. 73

4.1. Introduction 74

4.2. Results 78

4.3. Modulation of spontaneous beating rate at rest 78

4.3.1. The role of I_f at rest 78
4.3.2. The role of Ca^{2+} release from SR at rest 78
4.3.3. Effect of Ca^{2+} release from SR on I_f's modulation of basal beating rate 80
4.3.4. Contribution of MDL-12,330A (AC inhibitor) to I_f's effect modulation of basal beating rate 80
4.3.5. Assessing effective concentration of I_f and SR inhibitors 82

4.4. Fluorescent Ca^{2+} transient measurements 86

4.4.1. Control ... 86
4.4.2. The role of I_f at rest assessed via Ca^{2+} transient measurements ... 88
4.4.3. The role of Ca^{2+} release from SR at rest assessed via Ca^{2+} transient measurements ... 89
4.4.4. Contribution of Ca^{2+} release from SR to I_f's modulation of basal beating rate assessed via Ca^{2+} transient measurements ... 90
4.4.5. Effective time course and concentration of I_f and SR inhibitors assessed via Ca^{2+} transient measurements ... 92

4.5. Modulation of β-adrenergic receptor-stimulated beating rate ... 94

4.5.1. The role of I_f in β-adrenergic pathway in mouse ... 94
4.5.2. The role of Ca^{2+} release from SR in β-adrenergic pathway in mouse ... 95
4.5.3. Contribution of Ca^{2+} release from SR and I_f combined on the β-adrenergic pathway in mouse ... 96
4.5.4. The role of I_f in the β-adrenergic pathway in guinea pig ... 96
4.5.5. Contribution of Ca^{2+} release from SR alone and in combination with I_f to β-adrenergic pathway in guinea pig ... 97
4.5.6. Contribution of PKA and I_f to pacemaking in the β-adrenergic pathway in mouse ... 99
4.5.7. Contribution of PKA and I_f to pacemaking in mouse ... 100

4.6. Contribution of K_{ACh} to pacemaking ... 103

4.7. Discussion ... 106

4.7.1. The role of I_f at rest ... 106
4.7.2. The role of Ca^{2+} release from SR at rest ... 108
4.7.3. Contribution of Ca^{2+} release from SR to I_f's modulation of basal beating rate ... 111
4.7.4. The role of PKA at rest ... 117
4.7.5. Contribution of AC to modulation of basal beating rate by I_f ... 119

4.8. Fluorescent Ca^{2+} transient measurements ... 120

4.8.1. The role of I_f in modulation of Ca^{2+} transient amplitude ... 120
4.8.2. The role of Ca^{2+} release from SR in modulation of Ca^{2+} transient amplitude ... 122

4.9. Modulation of β-adrenergic receptor-stimulated beating rate ... 124

4.9.1. Role of I_f under β-adrenergic receptor stimulation ... 124
4.9.2. Role of Ca^{2+} release from the SR under β-adrenergic receptor stimulation ... 127
4.9.3. Contribution of I_f and the SR Ca^{2+} store to the chronotropic effect of isoprenaline ... 128
4.9.4. Role of K_{ACh} at rest and under β-adrenergic and muscarinic receptor pre-stimulation ... 130
4.9.5. Role of PKA under β-adrenergic receptor stimulation ... 132

4.10. Limitations ... 133

4.11. Underlying mechanism of Cs^+ action ... 137

CHAPTER 5: EFFECTS OF I_F AND SR CA^{2+} RELEASE INHIBITORS ON BASAL SPONTANEOUS BEATING RATE IN MICE WITH DIFFERENT EXPRESSION OF CA^{2+}-STIMULATED ACS IN THE ABSENCE AND PRESENCE OF β_1 -ADRENOCEPTOR STIMULATION WITH ISOPRENALINE. ... 140

5.1. Introduction 141

5.2. Results 150

5.3. The role of Ca^{2+}-stimulated ACs at rest 150

5.4. Effects of changes in extracellular Ca^{2+} concentration in modulating basal beating rate in mice with differential expression of Ca^{2+}-stimulated ACs. 151

5.5. Influence of ZD7288/ivabradine on basal beating rate at different extracellular Ca^{2+} concentrations in double knockout mouse model lacking both AC1&8 isoforms. 153

5.6. Modulation of spontaneous beating rate at rest in mice with differential expression of Ca^{2+}-stimulated ACs 154

5.6.1. Influence of ZD7288/ivabradine (I_f inhibition) at rest in mice with differential expression of Ca^{2+} stimulated ACs 154
5.6.2. Influence of CPA (inhibition of Ca^{2+} release from SR) at rest in mice with differential expression of Ca^{2+}-stimulated ACs 157
5.6.3. The influence of CPA (inhibition of Ca^{2+} release from SR) on I_f's modulation of basal beating rate in mice with differential expression of Ca^{2+} stimulated ACs 158

5.7. Assessing effective I_f blockade 159

5.8. Fluorescent Ca^{2+} transient measurements 161

5.8.1. Influence of ZD7288/ivabradine (I_f inhibition) at rest in mice with differential expression of Ca^{2+}-stimulated ACs, assessed via Ca^{2+} transient measurements. 161
5.8.2. Influence of CPA (inhibition of Ca^{2+} release from SR) at rest in mice with differential expression of Ca^{2+}-stimulated ACs, assessed via Ca^{2+} transient measurements. 162
5.8.3. The influence of CPA (inhibition of Ca^{2+} release from SR) on I_f's modulation of basal beating rate in mice with differential expression of Ca^{2+}-stimulated ACs, assessed via Ca^{2+} transient measurements 163

5.9. The effect of differential expression of Ca^{2+}-stimulated ACs on β-adrenergic receptor-stimulated beating rate 167

5.9.1. The contribution of Ca^{2+}-stimulated AC to I_f's influence on mouse beating rate in the presence of β-adrenergic pathway stimulation, assessed using I_f blockers. 167
5.9.2. The contribution of Ca^{2+}-stimulated AC to Ca^{2+} release from SR's influence on mouse beating rate in the presence of β-adrenergic pathway stimulation, assessed using SR blocker. 170
5.9.3. The influence of Ca^{2+}-stimulated AC on the contribution of Ca^{2+} release from SR and I_f combined on beating rate via the β-adrenergic pathway, assessed from the effects of combined application of CPA and I_f blockers 171
5.9.4. Contribution of Ca^{2+}-stimulated AC on the influence of L-type Ca^{2+} channels in the β-adrenergic pathway in mouse, assessed by partial blockade with nifedipine 174

5.10. Discussion 176

5.10.1. The role of Ca^{2+}-stimulated AC at rest in mice with differential expression of Ca^{2+}-stimulated ACs 176
5.10.2. Influence of ZD7288/ivabradine (I_f inhibition) and CPA (inhibition of Ca^{2+} release from SR) at rest in mice with differential expression of Ca^{2+}-stimulated ACs 177
5.10.3. The influence of the CPA (inhibition of Ca^{2+} release from SR) on I_f's modulation of basal beating rate in mice with differential expression of Ca^{2+}-stimulated ACs 179
5.10.4. The influence of ZD7288/ivabradine (I_f inhibition) and CPA (inhibition of Ca^{2+} release from SR) on β-adrenergic pathway activation in mice with differential expression of Ca^{2+}-stimulated ACs 180
5.10.6. Assessing effective I_f channel blockade in the modulation of beating rate. 182
5.10.7. Effects of changes in extracellular Ca^{2+} concentration on its ability to modulate basal beating rate in mice with differential expression of Ca^{2+} stimulated ACs 183
5.10.8. The influence of nifedipine (L-type Ca^{2+} channel inhibition) on β-adrenergic pathway activation in mice with differential expression of Ca^{2+}-stimulated ACs 184

5.11. Future experiments: 185

CHAPTER 6: PHOTO-CROSSLINKING 186

6.1. Introduction 187

6.1.2. Ligand-protein interaction methods 187
6.1.3. Photo-affinity probes 188
6.1.4. Development of Photo-affinity Probes 190

6.2. Photo-affinity probes synthesis' results and discussion 192

Figure 6.2 A general synthesis of probes using modified Hantzsch synthesis 192

6.2.1 Probe Synthesis 192
6.2.1.1 Probes 1 & 2 192

Figure 6.7 Reaction scheme for synthesis of azidobenzaldehyde using iodobenzaldehyde. 195

6.2.1.2 Probes 4 & 5 197
6.2.1.3 Probes 3a & 3b 199

Figure 6.13 Reaction scheme for addition of the 3-oxobutanoate group. 201

6.3. Biological assay's results and discussion 203

6.3.1. Photo-affinity enrichment of the I_{st} channel 205
6.3.2. Immunoblotting for $Ca_v1.2$ using ACC-003 207
6.3.3. Blotting for $Ca_v1.2$ using streptavidin-horseradish peroxidase conjugate 209

6.4. Experimental section 213

6.4.1 Chemical syntheses 213
6.4.1.1 3-Azidobenzaldehyde (Li et al., 2010) [1.1] 214
6.4.1.2 2-((3-azidobenzyl)(methyl)amino)ethan-1-ol [1.2] 215
6.4.1.3 2-((3-azidobenzyl)(methyl)amino)ethyl 3-oxobutanoate [1.3] 215
6.4.1.4 But-3-yn-1-yl 3-oxobutanoate (Yadav et al., 2007) [1.4] 216

6.4.1.5 But-3-yn-1-yl-(E)-3-aminobut-2-enoate [1.5] *217*
6.4.1.6 3-(2-((3-azidobenzyl)(methyl)amino)ethyl) 5-(but-3-yn-1-yl) 2,6-dimethyl-4-(3-nitrophenyl)pyridine-3,5-dicarboxylate [Probe 1] *218*
6.4.1.7 Prop-2-yn-1-yl 3-oxobutanoate [2.1] *219*
6.4.1.8 Prop-2-yn-1-yl-(E)-3-aminobut-2-enoate [2.2] *220*
6.4.1.9 3-(2-((3-azidobenzyl)(methyl)amino)ethyl) 5-(prop-2-yn-1-yl) 2,6-dimethyl-4-(3-nitrophenyl)pyridine-3,5-dicarboxylate [Probe 2] *221*
6.4.1.10. 2-(benzyl(methyl)amino)ethyl3-oxobutanoate (Noyola et al., 2003) [3.1] *222*
6.4.1.11 3-(2-(benzyl(methyl)amino)ethyl) 5-methyl 4-(3-azidophenyl)-2,6 dimethylpyridine-3,5-dicarboxylate [Probe 3a] *223*
6.4.1.12 3-(2-(benzyl(methyl)amino)ethyl) 5-(but-3-yn-1-yl) 4-(3-azidophenyl)-2,6-dimethylpyridine-3,5-dicarboxylate [Probe 3b] *224*
6.4.1.13 (4-((methyl(2-((3-oxobutanoyl)oxy)ethyl)amino)methyl)phenyl)boronic acid [3.4] 225
6.4.1.14 2-((4-azidobenzyl)(methyl)amino)ethan-1-ol [3.5] *226*
6.4.1.15 2-((4-azidobenzyl)(methyl)amino)ethyl 3-oxobutanoate [3.6] *227*
6.4.1.16 3-(2-(4-azido-N-methylbenzamido)ethyl) 5-(but-3-yn-1-yl) 2,6-dimethyl-4-(3-nitrophenyl)pyridine-3,5-dicarboxylate [Probe 4] *228*
6.4.1.17 3-(2-((4-azidobenzyl)(methyl)amino)ethyl) 5-(prop-2-yn-1-yl) 2,6-dimethyl-4-(3-nitrophenyl)pyridine-3,5-dicarboxylate [Probe 5] *229*
6.4.1.18 2-(prop-2-yn-1-ylamino)ethan-1-ol (Vergnaud et al., 2011) [4.1] *230*
6.4.1.19 2-((3-azidobenzyl)(prop-2-yn-1-yl)amino)ethan-1-ol[4.2] *231*
6.4.1.20 4-azidobenzaldehyde (Grimes et al., 2010) [5.1] *232*

CHAPTER 7: GENERAL DISCUSSION **234**

7.1. General Dissuasion **235**

References **243**

Appendix **263**

CHAPTER 1: INTRODUCTION

1.1. Introduction

The heart is an autonomous organ that acts as a pump that transports blood, oxygen, nutrients, waste products, and heat around the body. The rhythm of the heart plays a vital role in maintaining a state of homeostasis in the cardiovascular system. The initiation and modulation of heart rate occurs at the pacemaker site of the heart, the sino-atrial node (SAN), which was discovered in 1907 (Keith and Flack, 1907). Davies and Francis (1946) showed that the SAN consists of modified myocyte cells located on the posterior wall of the right atrium, adjacent to the superior vena cava. Anatomically, the sinoatrial node region differs from atrial tissue in that it is translucent and in being positioned close to the crista terminalis and away from the interatrial septum. The SAN is only a few cells in depth but spans all the way across the wall of the right atrium.

SAN cells differ anatomically relative to other non-pacemaker cardiomyocytes, and can therefore be easily distinguished. One of the apparent differences is that unlike ventricular or atrial cells, SAN cells either lack striation or have very faint visible striations (Rigg *et al.,* 2000). This is because SAN cells have a less extensive contractile apparatus that consists of actin and myosin fibers, arranged in a specific orientation. SAN cells are much smaller than other cardiomyocytes; their approximate dimensions are 30-100 μM length, 2-25 μM width and 2-5 μM depth (Honjo *et al.,* 1996). Ventricular and atrial cells have larger dimensions of 100μM length, 20μM width and 6μM depth (Severs *et al.,* 1985). Also unlike ventricular and atrial cells, SAN cells lack a transverse tubule network (Boyett *et al.,* 2000). There exists a morphological spectrum of

pacemaker cells named after their shapes: these include spindle, elongated spindle and spider cells (Wu *et al.,* 2001). However, some studies have indicated that the centrally located SAN cells are the true pacemaking cells and that the peripheral cells are somewhat transitionary in that they have both SAN-like and atrial characteristics (Honjo *et al.,* 1996, Wu *et al.,* 2001).

SAN cells exhibit intrinsic electrical activity that is responsible for the initiation and modulation of heart rate. This in turn gives SAN cells a unique action potential (AP) profile relative to atrial and ventricular cells; these properties give rise to automaticity (Boyett *et al.,* 2000). The unique electrical profile of SAN cells arises from an unstable membrane potential, which results in spontaneous depolarization towards the action potential threshold during diastole. This is also referred to as the pacemaker potential or diastolic depolarization (DD). Although this activity does not depend on extrinsic nerves, the slope of the pacemaker potential, and consequently, the frequency of action potentials, can be modified by the autonomic nervous system (**Figure 1.1.**).

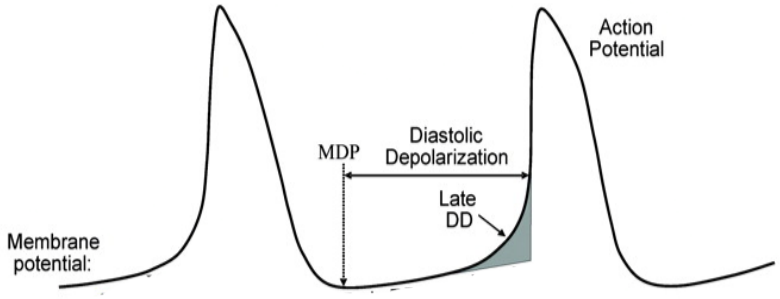


Figure 1.1 The SAN has an unstable membrane potential, resulting in spontaneous depolarization towards the action potential threshold during diastole. This is also referred to as the pacemaker potential or diastolic depolarization [permission was granted by Copyright Clearance Center to reproduce **Figure 1.1**, Maltsev & Lakatta (2007), license number: 3830340658189].

There is interest in pacemaking from a biomedical perspective: both as to how it works, and because of diseases that stem from misregulation of pacemaking. Thus, understanding the underlying mechanism of the SAN is valuable for creating better interventions. Sick Sinus Syndrome is an example in which the loss of SAN pacemaker function causes symptomatic bradycardia, which can lead to syncope and even sudden death (Schulze-Bahr *et al.,* 2003; Ueda *et al.,* 2004; Milanesi *et al.,* 2006). While electronic pacemakers remain a satisfactory therapy for Sick Sinus Syndrome, they have limitations: size, the need for replacement, the possibility of infection, and the absence of autonomic rate modulation (Rosen *et al.,* 2004).

The mechanisms underlying the pacemaker activity of SAN cells are still debated, with some researchers giving greatest prominence to I_f (DiFrancesco *et al.,* 2010), others emphasising a 'calcium clock' (Lakatta *et al.,* 2010), and still others favouring membrane currents other than I_f, such as the sustained inward current, I_{st} (Himeno *et al.,* 2011).

1.2. Surface Membrane Currents (M-clocks)

Different ionic currents are involved in the generation of pacemaker activity, but the functional importance of each individual ionic current in the generation of diastolic depolarization remains controversial. In general, it is thought that diastolic depolarization is generated through interaction of the decaying outward ionic current of the voltage-activated K^+ channel (K_v) with the activation of the inward ionic current [hyperpolarization-activated current I_f,

sustained inward current I_{st}, low-voltage-activated T-type Ca^{2+} channel, high-voltage-activated L-type Ca^{2+} current, and Na^{+}-Ca^{2+} exchanger (NCX)] (Irisawa et al., 1993; Boyett et al., 2000; Dobrzynski et al., 2007). Thus, no one ionic current system is likely responsible for pacemaking in the SAN. It is now known that a number of ionic currents underlie pacemaking, although the relative contribution/importance of each is still being elucidated. Table 1.1 provides a summary of the different ionic currents involved in the generation of pacemaker activity along with their functional contribution to pacemaking, which is explained in greater detail in the following sections.

Table 1.1 Ionic currents thought to be involved in the generation of pacemaker activity.

Current	**Contribution to pacemaker depolarization**
I_{Kr}, I_{Ks}	De-activation of voltage-gated delayed rectifier K^{+} channels
I_f	Activation of hyperpolarization-activated 'funny' current
I_{NCX}	Activation of sodium-calcium exchanger (NCX)
$I_{Ca,T}$	Activation of transient T-type Ca^{2+} channel towards the end of pacemaker depolarization
$I_{Ca,L}$	Activation of L-type Ca^{2+} channel determined the upstroke of the AP
I_{st}	Activation of sustained inward current
TRPM4	Activation of Ca^{2+}-activated nonselective cation channel
$I_{B,Na}$	Presence of background current
I_{K1}	Absence of this stabilizing current in SAN pacemaker cells
Current	**Contribution to pacemaker repolarization**
I_{Kr}, I_{Ks}	Activation of voltage-gated delayed rectifier K^{+} channels
K_{Ach}	Activation of ACh-activated K^{+} channels via M_2 receptors
$I_{Ca,T}$, $I_{Ca,L}$	De-activation of voltage-gated Ca^{2+} channels

1.2.1. K^+ channels

1.2.1.1. Lack of inwardly rectifying K^+ channel (K_1)

The lack of the inward-rectifier potassium current (I_{K1}) in SAN cells significantly alters the SAN's current-voltage profile compared to other myocardial cells (Giles *et al.,* 1986). In ventricular myocytes, the K_1 channels are mainly in their open state during the diastolic phase of an action potential (AP), which maintains the resting membrane potential at a strongly negative potential (-75mV). However, a lack of these channels in the SAN means that its resting potential will be unstable and less negative (in the range of -50 to -60mV). As there is a small resting membrane current, a very small fluctuation in the membrane current can cause a large deflection of the membrane potential to reach AP threshold unlike other myocardium cells. Thus, one can infer that SAN cells have evolved to have high membrane resistance such that they are stimulated at sub-threshold currents relative to other myocardium cells.

Evidence for this theory was put forward by Hirano *et al.,* (1988), who showed that the suppression of I_{K1} using Ba^{2+} ions induces automaticity in ventricular cardiomyocytes. However, as Ba^{2+} also permeates L-type calcium channels in mixed solutions of Ca^{2+} and Ba^{2+}, it is difficult to interpret Ba^{2+}'s effect strictly in terms of I_{K1}. Miake *et al.'s* (2002) findings, on the other hand, were more convincing. The authors showed that knockdown of the gene responsible for encoding K_1 channels (Kir2.1) converts ventricular cells into pacemaker cells that spontaneously depolarize.

1.2.1.2. Delayed rectifier potassium current (K_v)

K_v channels are crucial in controlling the current-voltage profile of SAN cells through depolarization and repolarization (see **Table 1.1**) (Denyer and Brown 1990). K_v channels repolarize the membrane potential, inactivating L-type Ca^{2+} channels and activating HCN channels, which can induce diastolic depolarization. Lei and Brown (1996) in rabbit SAN cells reported that there are two types of delayed rectifier potassium channels, K_r and K_s. Dofetilide, a specific K_r channel blocker, was shown to slow spontaneous activity, suggesting that K_r is dominant over K_s and contributes to the pacemaker activity of SAN cells (Lei and Brown 1996). Subsequent studies in rabbit SAN cells revealed that K_r channels are dominant during the basal condition, however K_s contributes significantly to spontaneous pacemaker rate during β-adrenoceptor stimulation, with isoprenaline, 10 nM, (Lei *et al.,* 2002). However, this results contrasts with the findings of Anumonwo *et al.,* (1992), who reported that K_s predominates in the guinea pig SAN, as blocking the K_s channel slowed spontaneous activity. These apparent differences between rabbit and guinea pig SAN are likely to be due to species differences (Ono *et al.,* 1995; *Lei et al.,* 1996)

1.2.1.3. ACh-activated K^+ channels (K_{Ach})

Activation of M_2 receptors via ACh activates K_{ACh} channels (Krapivinsky *et al.,* 1995), which then reduces heart rate by hyperpolarizing the cell membrane and inactivating L-type Ca^{2+} channels. The inactivation of L-type

Ca^{2+} channels, in turn, reduces excitability and the generation of APs. The underlying mechanism for this phenomenon was discovered by Huang *et al.* (1998) when studying the effect of PIP_2 in the modulation of K^+ channels. PIP_2 activates K_{ir} channels by directly binding to their C-terminals. For K_{ACh} channels in particular, the initial experimental evidence indicated that in excised patches perfused with exogenous PIP_2, conductance was significantly lower compared to 'on cell' (Huang *et al.,* 1998). However, further experiments revealed that the conductance level of K_{ACh} channels equalled 'on cell' conductance only when PIP_2 was applied in the presence of the $\beta\gamma_{i/o}$ subunit, which was not present in excision patch recordings (Huang *et al.,* 1998). Expression of the $\beta\gamma_{i/o}$ subunit in the absence of PIP_2 did not activate the K_{ACh} channels. It became clear that the $\beta\gamma_{i/o}$ subunit is critical for stabilising the PIP_2-GIRK channel complex, whereas PIP_2 activates the channels (Huang *et al.,* 1998). Hence, the rapid parasympathetic action of reducing heart rate is due to $\beta\gamma_{i/o}$ subunit stabilization of the PIP_2-K_{ACh} channel. A secondary, slower action occurs via inhibition of adenylyl cyclase (AC), which reduces the concentration of cytosolic cAMP (the role of cAMP in modulation of heart rate is discussed below [DiFrancesco and Tromba, 1987]).

1.2.2. Na^+ channel

Work by Nathan (1986) indicated that SAN cells lack a fast inward Na^+ current (I_{Na}); as such, the rate of rise of the action potential is very slow, as shown in **Figure 1**. Nathen further argued that even if Na^+ channels were present within SAN cells, the negative membrane potential of SAN cell (-55mV)

would tend to keep the channel in its inactive state. Tetrodotoxin (TTX), a Na^+ channel blocker, has no effect on the cells of the primary pacemaker (Lipsius and Vassalle 1978; Kreitner 1985). However, the contribution of I_{Na} cannot be dismissed. This is because a study by Lei *et al.* (2004) revealed that Na^+ channels ($Na_v1.1$, $Na_v1.3$ and $Na_v1.6$) are present and play functionally important roles within mice SAN cells. $Na_v1.5$ is predominantly expressed in peripheral SAN cells and is absent in central SAN cells (Lei *et al.,* 2004). The role of I_{Na} in contributing to pacemaking has been somewhat unclear, however direct mechanistic links between Na^+ channel (SCN5A) mutations and pacemaking associated miss-regulation in Sick Sinus Syndrome (SSS) were shown to exist (Benson *et al.,* 2003). Butters *et al.* (2010) used computational models to further explore SCN5A mutation's contribution for pacemaking and it was shown that the mutation slowed beating in the peripheral SAN cells but not the central SAN cells. However, in tissue simulations, it was found that not only the rate of pacemaking was reduced but AP conduction was also compromised across the SAN-atrium junction, causing SAN exit block or sinus arrest. Further experimental works are required to uncover the exact underlying mechanistic contribution of Na^+ cannels for pacemaking.

1.2.3. Background current, I_{bNa}

Inhibition of all voltage gated, exchange and pump currents in a given SAN cell results to "pseudo resting" reverse potential in the region of −30 to −40 mV (Hagiwara *et al.,* 1992). Inhibition of all the known currents; Ca^{2+} current, K^+ current, N^+-K^+ pump current, Na^+-Ca^{2+} exchange current, and I_f current results in a presence of residual Na^+-dependent inward current. This inward current

was referred to as a background current, I_{bNa}, (Hagiwara *et al.,* 1992). Using the whole-cell patch clamp method authors observed the following electrophysiological profile for the I_{bNa}:

- The current amplitude was directly proportional to extracellular concentration of Na^+ concentration (0 - 200 mM)
- The reversal potential of the current was - 21 mV, at a physiological condition
- The current density was 0.73± 0.21 pA/pF at -50 mV

Furthermore, recent studies by Cheng *et al.* (2016) on rabbit and mouse AV node cells also discovered the presence of the background current, with a similar profile to I_{bNa} observed in SAN (Hagiwara *et al.,* 1992). At - 50 mV the slope conductance of I_{bNa} increased from 0.54 ± 0.03 to 0.91 ± 0.05 nS and its magnitude varied in proportion to extracellular Na^+ concentration. It was also estimated that the single-channel conductance was 3.2 ± 1.2 pS.

As well as being present at the pacemaker potential range, the background current is present throughout generation of the AP (Hagiwara *et al.,* 1992). Therefore, it seems likely that the I_{bNa} may contribute towards generation of diastolic depolarization.

1.2.4. Ca^{2+} channels

Experiments by Hagiwara *et al.* (1988) revealed that blocking T-type Ca^{2+} channels with Ni^{2+} reduces pacemaker potential. The authors recorded single calcium channel activity in rabbit SAN cells, and, on the basis of the activation thresholds of the channels, suggested that the physiological role of the T-type Ca^{2+} channel was to contribute to the late phase of diastolic depolarization to the activation threshold of $I_{Ca,L}$, which is responsible for the AP's upstroke.

Studies by Mangoni *et al.* (2003, 2006) showed that the $Ca_v1.3$ L-type calcium channel (the α_{1D} subtype of the pore forming subunit) is found in cells of the SAN in mice and is activated at more negative voltages than in ventricular cells. It is possible that this lower potential for activation is able to kick-start the pacemaker potential upstroke. Mangoni studied this by knocking out the gene that encodes for the α_{1D} ($Ca_v1.3$) calcium channel in the mouse ($Ca_v1.3^{(-/-)}$); this knockout model induced a strong reduction in the $I_{Ca,L}$ of SAN pacemaker cells (specifically, in the voltage range that corresponds to diastolic depolarization). However, lack of $Ca_v1.3$ did not stop pacemaker activity, demonstrating that different ionic channels control SAN pacemaking.

1.2.5. Ca^{2+}-activated nonselective cation channel, TRPM4

The presence of voltage & Ca^{2+}-activated nonselective cation channel, specifically TRPM4, has been implicated in contribution of pacemaking (Demion *et al.,* 2006; Hof *et al.,* 2013). TRPM4 channels are shown to be present and

their function has been investigated in different mammalian cardiomyocytes (Guinamard *et al.,* 2002; Guinamard *et al.,* 2006). TRPM4 is activated by: Ca^{2+} (with Kd of 10 μM), PKC and PIP_2, yet it is inhibited by cytosolic ATP (with IC_{50} of 10 μM) [Nilius *et al.,* 2003; Nilius *et al.,* 2004; Guinamard *et al.,* 2004].

The first evidence of TRPM4 being expressed in SAN cells came from studies by Demion et al. (2006). Authors validated the presence of TRPM4 in mouse SAN cells using RT-PCR and Western blotting techniques. Also using the inside-out patch-clamp technique on mouse SAN cells, the characteristics of the channel were found to be similar to those observed in previous studies in different non-pacemaker cardiomyocytes (Demion *et al.* 2006):

- Voltage dependent with a conductance of 20.9 ± 0.5 pS
- Permeable to both Na^+ and K^+ but not to divalent ions
- Activated by rise in intracellular Ca^{2+} concentrations
- Blocked by intracellular ATP
- Activated by phosphatidylinositol 4,5-bisphosphate, PIP_2

There were no specific inhibitors available at the time for TRPM4 to assess the channel's physiological implication for pacemaking. However, due to its contribution towards cell depolarization at negative potentials it was hypothesized that TRPM4 contributes towards peacemaking (Demion *et al.* 2006). Moreover, with identification of TRPM4 inhibitor, 9-phenanthrol (Grand *et al.,* 2008), Hof *et al.* (2013) assess the contribution of 9-phenanthrol towards pacemaking on mice. 9-phenanthrol reduced the AP rate in a concertation-dependent manner, with an EC_{50} of 8 μM. The overall AP rate reduced by 62%.

Assessing the AP profile revealed that 9-phenanthrol reduced the DD slope without effecting other parameters of the AP. Also the effect of 9-phenanthrol was absent in TRPM4 knockout (KO) mice model. Application of 9-phenanthrol did not alter AP profile of mice lacking TRPM4. These results suggest that in mouse TRPM4 directly contributes in pacemaking. Therefore, future models need to take the contribution of TRPM4 to pacemaking into account.

1.2.6. Sustained inward current (I_{st})

In the mid-90s, a novel inward current, I_{st}, was identified in the spontaneously active SA node cells of rabbits, guinea pigs, and rats (Guo *et al.,* 1995; Guo *et al.,* 1997; Mitsuiye *et al.,* 2000). I_{st} is mainly carried by Na^+ and is activated by depolarization within the range of slow diastolic depolarization (from -80 mV to between -70 and -50 mV). Thus, it has been suggested that the I_{st} ion channel contributes to pacemaker depolarization.

The pharmacological profile of the I_{st} channel has been characterized (Guo *et al.,* 1997). I_{st} increases two-fold upon adrenergic stimulation by isoprenaline (100 nM) (Guo *et al.,* 1997). This increase can be reversed by application of acetylcholine (5 μM). The I_{st} channel is insensitive to tetrodotoxin (TTX; 30 μM). Furthermore, the I_{st} channel shows similar pharmacological properties to L-type Ca^{2+} channels, as it is blocked by Ca^{2+} channel antagonists [verapamil (1 μM); nicardipine (0.2 to 0.5 μM)] and its current is augmented by Ca^{2+} channel agonists [Bay K 8644 (1 μM)] in guinea pig SAN cells (Guo *et al.,* 1997).

Due to its L-type Ca^{2+} channel-like characteristics (blocked and activated by Ca^{2+} channel antagonists and antagonist respectively), the existence of I_{st} has been challenged (Lakatta *et al.,* 2010). The channel mainly carries Na^{+} ions however, its current conductance is increased by lowering extracellular Ca^{2+} and is reduced by decreasing extracellular Na^{+} ions. These features imply that the I_{st} channel behaves like both the NCX and L-type Ca^{2+} channels. As such, Lakatta *et al.* (2010) proposed that the current might be due to both the direct and indirect effects of the NCX and L-type channels.

Despite this challenge by Lakatta, there exists evidence supporting the existence of I_{st} channels. In particular, the reversal potential of +37 mV recorded in the presence of 0.1 mM extracellular Ca^{2+} is unlikely to result from the combination of separate currents (Guo *et al.,* 1995). Also, its activation threshold of ~ -70 mV, is very distinct from that of L-type Ca^{2+} channels (-40 mV) (Guo *et al.,* 1995). Even though the research group of Noma has described the channel (Guo *et al.,* 1995, 1997, Mitsuiye *et al.,* 2000; Shinagawa *et al.,* 2000), a review of the literature reveals that similar currents to I_{st} have been identified in the past, but have been incorrectly assigned to the L-type Ca^{2+} current (Mitsuiye *et al.,* 2000). For example, the ramp pulse experiment (0.1 mV/ms from -70 to +30mV) carried out by Denyer and Brown (1990) revealed an inward current activation past -60 mV and a current density of 2pA/pF analogous to the I_{st} current recorded in rabbit SAN cells (Guo *et al.,* 1997). However, during the experiment, addition of nifedipine (2 μM) inhibited the current, causing the authors to conclude that the current belonged to L-type Ca^{2+} channels. A similar current was observed by DiFrancesco *et al.* (1991);

however, once again, the current was assigned to L-type channels, as it was inhibited by application of nitrendipine.

The I_{st} channel could be a new medical target for the treatment of angina and hypertension, and inhibitors of the channel may provide a promising alternative to current drugs for heart disease. For example, some patients are intolerant to beta-blockers (European Medicine Agency, 2010), and whilst ivabradine is a particularly useful alternative; its use is associated with a number of adverse effects (European Medicine Agency, 2010). Ivabradine is contra-indicated during pregnancy, as it has been shown to cause embryotoxic and teratogenic effects (European Medicine Agency, 2010). It also has been shown to reversibly alter retinal function due to modulation of hyperpolarisation-activated I_h currents in the retina, which are homologous to the cardiac pacemaker I_f current (European Medicine Agency, 2010). Thus, targeting the I_{st} channel would provide a unique pharmacological pathway for the treatment of angina and hypertension.

1.2.7. Hyperpolarization-activated current, I_f

1.2.7.1 The K^+ - decay hypothesis

Through experimental evidence obtained using Purkinje fibers, Noble and Tsien (1969) concluded that the decay of the delayed K^+ current was responsible for controlling pacemaker automaticity. The term "I_{K2} - decay hypothesis" was coined to describe the findings (Noble and Tsien 1969). The

concept was based on evidence that the current reversal occurred near the K^+ equilibrium potential and that it was directly involved in increasing the frequency of APs stimulated by sympathetic stimulation. However, the following observations could not be explained: the disappearance of the I_{K2} current at low extracellular Na^+ concentration, and the reversal potential for I_{K2} being too negative for it to be due to a pure K^+ current (Noble and Tsien 1969).

Brown *et al.* (1979) identified the "funny current" (I_f) in SAN cells, work which not merely challenged but also invalidated the "I_{K2} - decay hypothesis." It turned out that the original discovery of I_{K2} and the suggestion of the "I_{K2} - decay hypothesis" for the control of pacemaker automaticity had been incorrectly interpreted (Noble and Tsien, 1969). The pacemaker current was not an outward, but rather an inward, current, activated not during depolarization, but during hyperpolarisation—identical to I_f in SAN cells. Crucially, during voltage clamp experiments, altering the extracellular concentration of K^+ did not affect either the kinetics or maximum conductance of the current (Brown *et al.,* 1979). It was revealed that the activation of I_f and the decay of K_v channels during the hyperpolarisation phase of the AP superimposed one another and produced an equilibrium potential that was close to the K^+ equilibrium potential. Furthermore, Ba^{2+} ions were used to block the decaying K_v component, showing that the inward nature of Purkinje fibers' pacemaker current is due to activation of I_f. Thus, the authors reinterpreted the I_{K2} current as an inward hyperpolarisation activated current, I_f.

The threshold for activation of I_f is between -40 to -50 mV, and the current is fully activated at -100 mV (DiFrancesco *et al.,* 1986). The I_f channel

lacks a specific selectivity filter; therefore, it permits K^+ and Na^+ ions through the channel and is also known to allow other cations through. This was further confirmed by a reversal potential of -25 mV, indicating that the channel is not selective for a specific ion (Yanagihara and Irasawa, 1980). In 1991, DiFrancesco and Tortora provided the first evidence that I_f channels are activated by cAMP as well as hyperpolarization (DiFrancesco and Tortora 1991). Upon binding of cAMP, the threshold voltage activation range of the channel is shifted to a more depolarized potential in excess of 10mV. It was also noted that cAMP increased the open-state probability of the channel. This activation by cAMP was direct, rather than occurring via phosphorylation of the channel by PKA, as the catalytic subunit of PKA did not produce an activating current. The dual regulation of I_f channels gave rise to their name: Hyperpolarization-activated cyclic nucleotide-gated (HCN) channels. Four isoforms of HCN (HCN_{1-4} families) have been cloned and identified, with the HCN_4 isoform specifically expressed in SAN cells (She *et al.,* 1999; Altomare *et al.,* 2003).

Considerable controversy surrounds the exact role of I_f in pacemaking. At low doses of CsCl (Cs^+), I_f is selectively blocked, and a substantial slowing of beating rate is observed, indicating that I_f contributes to the pacing of SAN cells (DiFrancesco, 1981; Denyer and Brown, 1990). However, Cs^+ does not completely stop beating, indicating that I_f is not essential for pacemaking (Irisawa *et al.,* 1993). Presently, ivabradine is the only clinically used selective I_f channel blocker, with a high degree of use dependency (Bois *et al.,* 1996; Bucchi *et al.,* 2002; DiFrancesco and Camm, 2004). Inhibition of I_f slows down heart rate (by 6 beats/min) by selectively reducing the steepness of diastolic

depolarization (DiFrancesco and Camm, 2004). Interestingly, over-expression of HCN channels not only accelerates the rate of pacing cells, but can also induce spontaneous activity in resting cardiomyocytes (Rosen *et al.,* 2004). Over-expression of HCN channels could be another approach to developing "biological pacemakers" (Rosen *et al.,* 2004).

1.2.7.2. Indirect modulation of I_f by intracellular calcium

Using a whole cell patch configuration, Hagiwara *et al.* (1989) detected that the I_f current is modulated by a change in intercellular Ca^{2+} concentration. When the Ca^{2+} concentration was increased, the activation voltage for I_f was shifted to a more positive potential: thus, Ca^{2+} was thought to directly modulate I_f. However, using an inside out macropatch, Zaza *et al.* (1991) did not see a direct effect of Ca^{2+} on the I_f current. In 2003, Rigg *et al.* further investigated the possible regulation of I_f by cytosolic calcium in guinea pig SAN cells using a perforated patch clamp technique to record I_f activated by hyperpolarizing voltage steps. Loading the cells with 10μM BAPTA-AM (a calcium chelator) significantly reduced the amplitude of I_f. Calmodulin (CaM) antagonists (10 μM W-7 and 25 μM calmidazolium) caused a similar reduction in the amplitude of I_f. However, 1 μM KN-93 (CaMKII inhibitor) did not affect I_f, indicating that both calcium and calmodulin are involved in the modulation of I_f, via a mechanism that is independent of CaMKII. Furthermore, when SAN cells were exposed to BAPTA in the presence of W-7, there was no significant change in I_f amplitude, indicating that calcium acts through calmodulin and not through direct activation

of the HCN channel. Thus, it was speculated that a Ca^{2+}-sensitive AC might be involved in the underlying mechanism (Rigg *et al.,* 2003).

Terrar's group (Mattick *et al.,* 2007) further characterized the regulation of I_f by cytosolic Ca^{2+} in 2006, when they used RT-PCR and immunoblotting with a specific antibody to show that the mRNA and protein forms of Ca^{2+}-stimulated Type 1 ACs (AC1) were present in the SAN, but not in the ventricular muscle, of the guinea pig heart. Another Ca^{2+}-stimulated adenylyl cyclase, AC8, was detected by immunocytochemistry in SAN cells. An inhibitor of AC (MDL-12,330A) reduced I_f, and an inhibitor of phosphodiesterase (IBMX) increased I_f, indicating that AC1 and AC8 in the SAN provide background production of cAMP, even in the absence of β-adrenoceptor stimulation. A functional interaction between AC1 and HCN_2 has also been shown in myocytes in which HCN_2 was co-expressed with AC1, AC6, or GFP (Kryukova *et al.,* 2012). When Ca^{2+}-stimulated AC1 was co-expressed with HCN_2, the I_f current was activated at potentials approximately 10 mV more depolarized than when HCN_2 expression was coupled with AC6 or GFP (Kryukova *et al.,* 2012). It remains to be seen whether Ca^{2+}-stimulated ACs regulated other channels.

Moreover, Terrar group's findings shed some light on the previous controversy regarding I_f currents' role in the absence of β-adrenoceptor stimulation. Previously in voltage clamp experiments, it was shown that the I_f current is only fully active at -100mV (DiFrancesco *et al.,* 1986). However, the SA node membrane potential only reaches approximately -60mV, meaning that at basal beating levels, the channels are not fully active. This low basal membrane potential questioned the importance of I_f channels in the absence of

β-adrenoceptor stimulation. However, it was noted that inhibition of I_f channels does indeed slow beating rate in the absence of β-adrenoceptor stimulation (Denyer & Brown 1990). Thus, it is possible that under a conventional voltage clamp technique, the resting level of cytosolic Ca^{2+} in beating cells is reduced (see Sanders *et al.,* 2006) and hence I_f may be underestimated if Ca^{2+}-stimulated AC activity is reduced under these conditions due to Ca^{2+} reduction.

1.3. Intracellular Mechanisms of Pacemaking

For almost half a century, it was thought that voltage-gated ion channels in the surface membrane (membrane clocks; M-clocks) underlie the origin of pacemaker rhythm in the heart (Irisawa *et al.,* 1993). Recently, however, pacemaker cell research has largely focused on the contribution of spontaneous intracellular Ca^{2+} release from SR to pacemaking and their interplay with surface membrane currents (Rigg *et al.,* 1996, 2000; Bogdanov *et al.,* 2001; Vinogradova *et al.,* 2006). It is now thought that the rhythm is initiated, sustained, and regulated by oscillatory calcium release (Ca^{2+} clock) from the sarcoplasmic reticulum (SR), whereas the M-clocks merely represent the immediate cause for depolarization and the generation of APs (Maltsev and Lakatta 2012).

1.3.1. The role of intracellular Ca^{2+} at the foot of the AP

Rigg and Terrar (1996) conducted a simple and elegant experiment to demonstrate the effect of blocking SR calcium cycling on heart rate using pharmacological intervention. When 2 μM ryanodine was added to spontaneously beating guinea pig SAN preparations, the rate of beating reduced from 225 bpm to 125 bpm, and other characteristics of the action potentials were modified. Similar observations were recorded when 100 μM cyclopiazonic acid (CPA; an inhibitor of the SR Ca^{2+} ATPase) was added to the preparation. Although not explicitly investigated in that experiment, it was suggested that changes in action potential characteristics were due to cytosolic calcium regulating a variety of sarcolemmal ionic currents.

Rigg *et al.* (2000) showed that ryanodine also significantly reduces the positive chronotropic effect of isoprenaline in single guinea pig SAN cells. Furthermore, ryanodine receptor (RyR) labelling through immunocytochemistry revealed that within SA node cells, there exist regular organized patterns of RyRs within the cytosol (Rigg *et al.,* 2000). Populations of RyR that were localised close to sarcolemma were identified. Furthermore, increases in Ca^{2+} just before the Ca^{2+} transient and before the upstroke of the action potential were observed.

One may question how this subsarcolemmal co-localization of RyR occurs. Recent work by Bennett *et al.* (2013), revealed that junctophilin-2 is responsible for the co-localization of RyR to subsarcolemmal L-type Ca^{2+} channels. Junctophilin-2 facilitates the co-localization by binding to the SR

membrane via its N terminus and to the phosphatidylinositols (PI and PIP_3) present in the plasma membrane through its C terminus. The same analogy can be seen in mGluR's ability to co-localize with IP_3Rs through homer protein dimerization (Tu *et al.,* 1998). Also, Lupu *et al.* (1998) revealed that IP3Rs are co-localised with bradykinin receptors (B_2Rs). Furthermore, IP_3R forms an inhibitory complex with PIP_2, which is imbedded within the plasma membrane (**Figure 1.2.**).

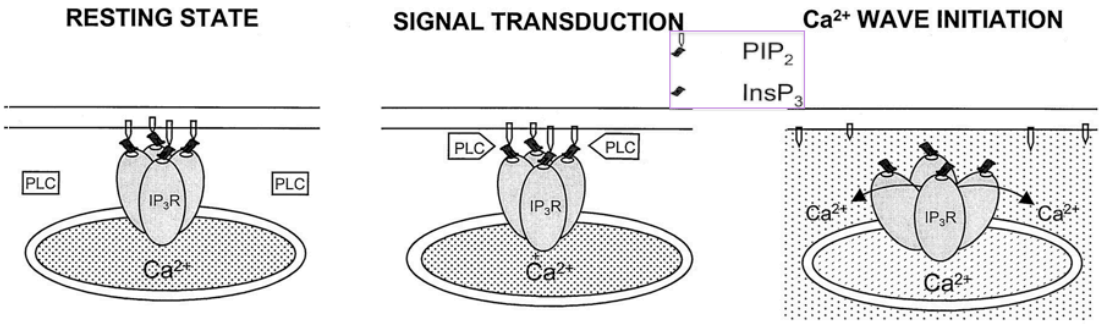


Figure 1.2 Representation of IP_3R-PIP_2 functional coupling. In unstimulated cells, $InsP_3R$ is constitutively inhibited due to interaction with PIP_2 in the juxtaposed membrane (resting state). Hormonal stimulation leads to activation of PLC, which cleaves $InsP_3R$-tethered PIP_2, simultaneously removing inhibitor (PIP_2) and generating activator ($InsP_3$) of the $InsP_3R$ (signal transduction step). PIP_2 cleavage and $InsP_3$ liberation results in immediate $InsP_3R$ opening and Ca^{2+} release (Ca^{2+} wave initiation) [letter of permission was granted by American Society for Biochemistry and Molecular Biology to reproduce **Figure 1.2**, Lupu *et al.,* (1998)].

1.3.2. The involvement of the Na^+-Ca^{2+} exchanger (NCX) current in pacemaking

Work by Zhou *et al.* (1993) on a cat latent pacemaker cells proposed that diastolic Ca^{2+} release might contribute to subsidiary pacemaker potential by

stimulating the NCX. Also work by Hancox *et al.,* 1994 on a rabbit AV node suggested that diastolic Ca^{2+} release stimulates the NCX and generates inward current. However, clear evidence of diastolic Ca^{2+} release in the pacemaker had not yet been provided, and it was not known what induced this spontaneous Ca^{2+} release.

Hüser *et al.* (2000) characterized the intracellular mechanism of pacemaking. They showed that highly localized subsarcolemmal calcium release from the SR (i.e. calcium sparks) occurs concurrently with the late phase (last third) of diastolic depolarization, which is triggered by low voltage-activated $I_{Ca,T}$. Diastolic calcium release is thought to depolarize the pacemaker potential to threshold by stimulating I_{NCX}, which has a net influx of $3Na^+$ for every $1Ca^{2+}$ released into the extracellular environment. This ratio of exchange has, however, been challenged by Kang and Hilgemann (2004), who reported that the average stoichiometry of NCX was $3.2Na^+$ to $1Ca^{2+}$. The authors also reported that under some conditions, the NCX protein might provide an inward background Na^+ current (continuous Na^+ leak pathway) that contributes to pacemaking in the SAN.

Hüser and colleagues deduced the intracellular mechanism of pacemaking through the use of drugs, a perforated patch clamp technique, and confocal fluorescence microscopy on pacemaker cells isolated from the cat right atrium (Hüser *et al.,* 2000). The addition of 20-50 μM Ni^{2+} blocked low voltage-activated $I_{Ca,T}$, decreased diastolic depolarization, prolonged the pacemaker cycle length and suppressed diastolic Ca^{2+} release. Voltage clamp analysis

showed that T-type low voltage-activated calcium channels are associated with a slow inward current, possibly due to I_{NCX}.

Further evidence for the importance of NCX was obtained by Bogdanov *et al.* (2001). They demonstrated that when fluorescence was recorded in small regions under the sarcolemma, localized rapid rises in calcium were detected. These releases resembled calcium sparks and were referred to as local Ca^{2+} release (LCR) events. Ryanodine reduced LCR in a dose-dependent manner, and abolished beating. It also decreased an inward current thought to be I_{NCX} in voltage clamped cells with slow ramps of depolarization from -70 to -45 mV. Acute blockade of the NCX channel (by slow substitution of the Na^+ bath with Li^+) abolished the beating of SAN cells, and reduced the inward current to a similar extent. Thus, the ryanodine receptor (RyR) partnering with NCX activation in SAN cells is crucial for the generation of spontaneous APs and therefore, for pacemaker function. Local subsarcolemmal calcium transients spread in a wavelike manner (via calcium-induced calcium-release; CICR) to amplify the SR activation of NCX. This provides sufficient inward current to activate any dormant L-type Ca^{2+} channels and trigger an AP.

In contrast, Sanders *et al.* (2006) showed that in the absence of SR Ca^{2+} release (achieved by blocking SR Ca^{2+} uptake with CPA), the frequency of beating is reduced (lowering the frequency of Ca^{2+} transients) but does not stop. However, in support of Bogdanov *et al.'s* (2001) results, inhibition of NCX immediately stops the beating, indicating that the NCX plays a crucial role throughout pacemaker depolarization and is not restricted to the foot of the action potential. Inhibition of NCX by *rapidly* switching to a Li^+ solution (within

the time course of a single cardiac cycle) immediately stops spontaneous beating. Experimental studies by Cho *et al.* (2000), Koushik *et al.* (2001) and Reuter *et al.* (2002) showed that the embryos of mice with the NCX gene knocked out do not survive due to the lack of a heartbeat. This again suggests the crucial importance of NCX in pacemaker potential generation. Also, in a conditional knockout experiment where NCX was selectively suppressed (partially, due to lack of NCX1) in atrial and SAN cells, the animal did not show any increase in SAN activity during the "fight or flight" response, even though the basal beating rate was unaltered (Gao *et al.,* 2013). In a separate study by Herrmann *et al.* (2013), where NCX1 was specifically suppressed through a specific Cre transgene, the animals showed progressively reduced heart rate with severe arrhythmia. Also, SAN cells lacking NCX when isolated failed to show basal rhythmic activity (Groenke *et al.,* 2013). Overall, it is clear that within SAN cells, NCX plays a crucial role in pacemaker mechanisms.

Work by Sanders *et al.* (2006) revealed that in spontaneously beating cells, cytosolic Ca^{2+} concentration between beats is maintained at a higher level (225 nM) than in resting cells, and that this elevated level of Ca^{2+} drives NCX current throughout the pacemaker potential, which is critical to spontaneous beating in these cells. In further tests of this suggestion, application of BAPTA-AM/EGTA-AM abolished spontaneous action potentials (Sanders *et al.,* 2006). This finding provides the basis for an explanation of how the pacemaker operates, which links these several lines of 'conflicting' evidence outlined above. The elevated basal cytosolic Ca^{2+} levels found specifically in pacemaker cells drive an inward Na^{+} current, either via NCX or by a continuous Na^{+} leak pathway (proposed by Kang and Hilgemann, 2004), and this makes NCX a

crucial contributor to pacemaking throughout the diastolic depolarization. Furthermore, the elevated basal cytosolic Ca^{2+} concentration helps to explain the cause of increased cytosolic cAMP concentration (Vinogradova *et al.,* 2006) and the upregulation of PKA via activation of Ca^{2+}-stimulated AC1 and AC8 (Mattick *et al.,* 2007). The elevated concentration also supports for the basal activity of CaMKII and its downstream regulation of L-type Ca^{2+} channels (Vinogradova *et al.,* 2000) and phosphorylation of phospholamban (Mundina *et al.,* 1996), and provides a mechanism by which I_f might contribute to SAN pacemaking. Nevertheless, the mechanism underlying the increased cytosolic Ca^{2+} within SAN cells remains unknown. Thus, it is not the LCR that is crucial in driving the pacemaker, but rather the elevated basal Ca^{2+} concentration within the SAN.

1.3.3. The role of elevated cAMP levels in the generation of LCRs

Attempts were made to find the reason behind the occurrence of LCR, which in turn partners with NCX to generate the inward current at the foot of the action potential, as explained by Hüser *et al.* (2000) and Bogdanov *et al.* (2001). Through experimental evidence, Vinogradova *et al.* (2006) revealed that a high level of cAMP is present in the SA node but not in rabbit ventricles or atria, and this level is key in generating the LCR. Previously in 1977, Ohsumi's group, reported that during tissue preparation, the concentration of cAMP was relatively higher in rabbit SAN relative to atrial cells in the absence of β-adrenoceptor stimulation (Taniguchi *et al.,* 1977). Work by Vinogradova *et al.* (2006) managed to link the generation of LCR with elevated cAMP

concentration in SAN cells. It was shown that inhibition of basal PKA activity (15 μM, PKI) abolishes LCR and stops spontaneous beating, overriding the notion that cAMP imposes its effect via I_f channels. Also, the basal activity of PKA is driven by high basal activity of AC, as inhibition of AC by 400 μM MDL-12,330A had the same effect of abolishing LCR. However, 400 μM is a very high concentration and it is likely that there were non-specific effects and modulation of other ion channels. Furthermore, a β-adrenoceptor antagonist and inverse agonist had no effect, so the effect was not due to a constitutively active β-adrenoceptor.

1.3.4. Is LCR essential for pacemaking?

Experiments from Terrar's group showed that in guinea pig SAN cells displayed rhythmic beating in the absence of an observed LCR (Rakovic *et al.,* 2001; Jackson *et al.,* 2002). It was also observed that the application of ryanodine or CPA, as expected, suppresses LCR (Vinogradova *et al.,* 2002) and slows the rate of pacemaking without abolishing it (Rigg and Terrar, 1996; Rigg *et al.,* 2000). Although I agree that the LCR in partnership with NCX contributes towards the late phase of diastolic depolarization, it seems that it is not essential for pacemaking.

1.4. A coupled mechanism of intracellular Ca^{2+}-clocks and M-clocks

The term 'Ca^{2+} clock' was coined to describe intracellular calcium cycling, i.e. release from, and uptake into, the SR (reviewed by Maltsev and

Lakatta, 2007). It has been proposed that the Ca^{2+} clock causes spontaneous rhythmic APs in pacemaker cells. The LCRs are tightly controlled by a high level of basal and reserve protein kinase A (PKA)-dependent protein phosphorylation. Releases of Ca^{2+} rhythmically stimulate the NCX, depolarize the membrane, and prompt the M-clocks to generate rhythmic APs. With this theory, Maltsev and Lakatta suggested the combined role of Ca^{2+}-clocks and M-clocks in the generation of pacemaker activity.

A further review by Maltsev and Lakatta (2012) proposed that the 'ticking speed' of the pacemaker is defined by the LCR period, or the delay between the AP-triggered global cytosolic Ca^{2+} transient and the LCR that emerges during diastolic depolarization. The LCR period is not solely regulated by the Ca^{2+} clock. It is regulated by both the kinetics of SR Ca^{2+} pumping and also by the sarcolemmal Ca^{2+} flux, which is regulated by membrane channels and transporters. It is well known that L-type Ca^{2+} channels are largely responsible for Ca^{2+} influx, which stimulates Ca^{2+} release from the SR, while NCX is vital in the acceleration of diastolic depolarization to reach the AP activation threshold (again via L-type Ca^{2+} channels).

However, other channels, such as K^+ channels and even HCN channels, are implicated in the Ca^{2+} balance. K^+ channels repolarize the membrane potential to inactivate L-type Ca^{2+} channels, and HCN channels (slower activation kinetics) limit hyperpolarization to activate L-type Ca^{2+} channels (almost instantaneous activation). These complex interactions between the membrane components and intracellular Ca^{2+} cycling set the LCR period, which defines the ticking speed of the coupled-clock system. The SR can indeed

oscillate Ca^{2+} independently, as has been described in earlier experiments; however, this does not underlie pacemaking. The Ca^{2+} clock simply generates a timely LCR/I_{NCX} signal during diastolic depolarization, and is then reset by the AP. Phosphorylation of the SR and membrane components allow the system to function as a clock and generate rhythmic LCRs of a stable period, generating spontaneous APs at a stable rate (**Figure 1.3**).

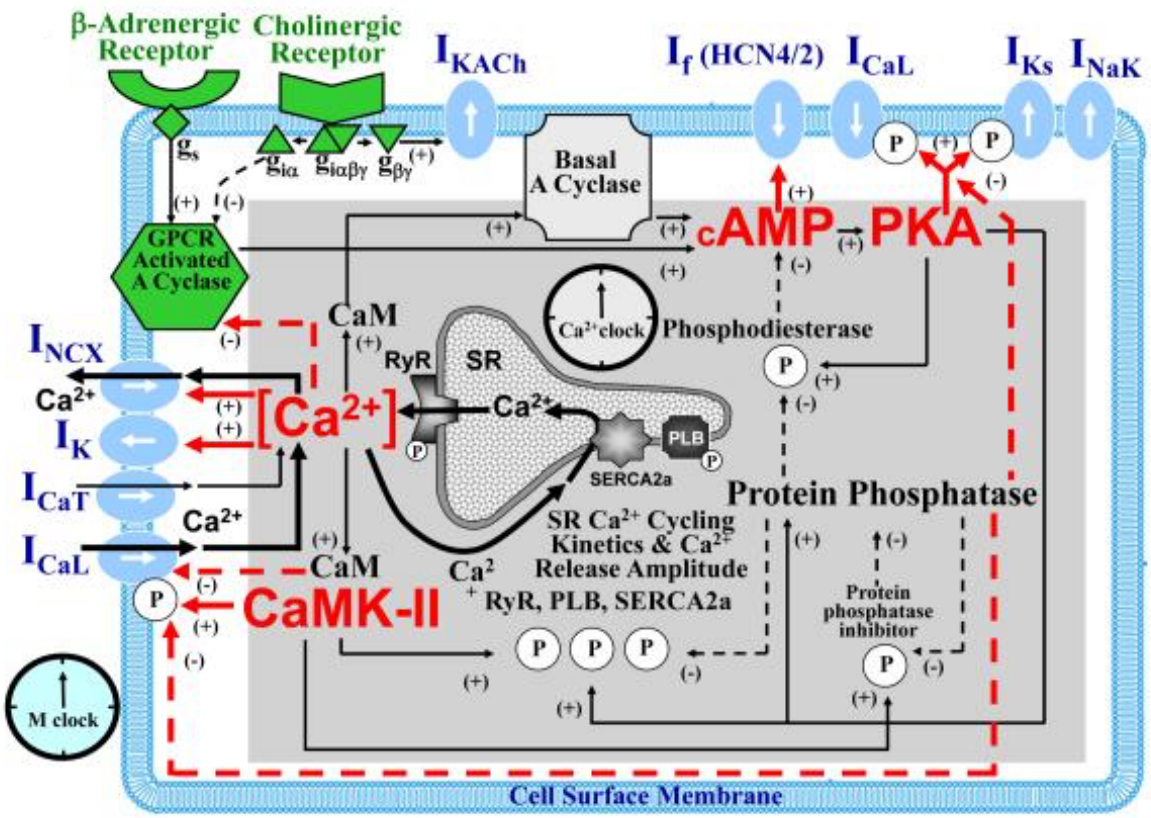


Figure 1.3 Schematic illustration of the interactions of molecules comprising the full coupled-pacemaker clock. Note that the same regulatory factors (red lettering) of the sarcoplasmic reticulum (SR) Ca^{2+} clock (grey intracellular area, black lettering) couple the Ca^{2+} clock to the M clock (blue membrane area, blue lettering). G protein–coupled receptors (green lettering) regulate both the Ca^{2+} clock and the membrane clock via those same coupling factors that are crucial nodes within the system [permission was granted by Copyright Clearance Center to reproduce **Figure 1.3**, Maltsev & Lakatta (2012), license number: 3830310968868].

1.4.1. The control of the Ca^{2+} clock by PKA

The high level of PKA-dependent phosphorylation keeps the Ca^{2+} clock operating at a rapid basal speed (Vinogradova *et al.,* 2006). This occurs even in the absence of β-adrenergic receptor stimulation (Vinogradova *et al.,* 2006). High basal levels of cAMP are due to constitutively active ACs, two isoforms of which are present in SAN cells: Type 2 AC (AC2), and Ca^{2+}-sensitive AC8. As mentioned earlier, AC1 is also present in SAN cells and provides a background production of cAMP (Mattick *et al.,* 2007).

PKA phosphorylates the following proteins in the basal state: L-type Ca^{2+} channels, phospholamban and RyRs. Phosphorylation of L-type Ca^{2+} channels increases the influx of Ca^{2+} (De *et al.,* 1996; Sculptoreanu *et al.,* 1993). Phosphorylation of phospholamban [phosphorylation of Ser^{16}, Li *et al.,* (1990)] increases the filling rate of the SR and allows extra calcium to be pumped in (due to disinhibition of the sarcoplasmic reticulum Ca^{2+}-ATPase). Phosphorylation of RyRs causes dissociation of FKBP12.6 from RyR, and this in turn causes an increased sensitivity to the release of Ca^{2+} from the SR (Marx *et al.,* 2000). Finally, phosphorylation of SR-associated phosphatase, PP1, enables the phosphorylation of phospholamban at the Thr^{17} by CaMKII, which also contributes towards a lusitropic effect (Mundina *et al.,* 1996) (**Figure 1.3**).

Vinogradova *et al.* (2000) identified basal CaMKII activity that is essential in the generation of APs, as KN93 reduced the rate and amplitude of the APs in a dose-dependent manner. Through confocal microscopy studies, it was shown that active CaMKII is localised under the cell surface membrane in the vicinity of

L-type Ca^{2+} channels. Further studies showed that CaMKII modulates L-type Ca^{2+} channels. As selective L-type channel blockers could largely mimic the inhibition of CaMKII's effect on the pacemaker.

Thus, in SAN cells the high basal levels of cAMP induce PKA phosphorylation of the above proteins; this is responsible for the spontaneous generation of LCRs which, through NCX, generates the inward current that triggers an AP. Using antibodies, Vinogradova *et al.* (2006) showed that phosphorylation of both RyR and phospholamban was high at the SA node relative to the ventricles. Although phosphorylation of L-type channels was not explicitly studied, it was postulated that it would also be high. Overall, the high level of PKA-dependent phosphorylation keeps the "Ca^{2+} clock" operating at a rapid basal speed.

The autonomic nervous system adds another layer of regulation of the Ca^{2+}- and M-clocks (Maltsev & Lakatta, 2007). Vagal stimulation predominates in the basal state, keeping the Ca^{2+} clock in check. Sympathetic stimulation (via β-adrenergic receptors) results in high levels of PKA-dependent phosphorylation, causing the Ca^{2+} clock to operate at full speed and resulting in the activation of membrane clocks at a maximum rate. This is the mechanism underlying positive chronotropism. There is also a high constitutive level of phosphodiesterase (PDE) activity in SAN cells, which keeps the Ca^{2+} cycling kinetics in check.

1.4.2. Minor contribution of Ca^{2+} transients to the pacemaker rhythm

In 2010, Noma's group challenged the importance of cytosolic Ca^{2+} transients (LCR) in pacemaker rhythm. Following rupture of the perforated patch membrane, where BAPTA was introduced into isolated guinea pig SAN cells (indicated by the arrow in **Figure 1.4**), generation of AP did not cease (Himeno *et al.,* 2011). However, Lakatta's group then challenged this result. Careful observation of the result in **Figure 1.4**, implies contraction following rupture of the membrane, where the length of the cells becomes transiently shorter before eventually reaching basal levels. This was proposal by Lakatta to be due to seal leakage, as extracellular Ca^{2+} would provide the background for APs to be generated. In my opinion, Lakatta's challenge is likely correct, as Sanders *et al.* (2006) and Vinogradova *et al.* (2000) observed that generation of AP and spontaneous beating stopped following the application of BAPTA. Sanders also used the cell-permeable BAPTA (AM-BAPTA), which can be introduced into the intracellular environment without rupturing the membrane. Further convincing evidence has recently come from a study in which Himeno *et al.'s* (2011) experimental conditions were repeated by Capel *et al.* (2015). The addition of 10 mM BAPTA to the patch pipette led to prompt cessation of rhythmic generation of AP within 5.5 s following patch rupture. An additional experiment could also be carried out to see whether UV-induced activation of the Ca^{2+}-chelating agent Diazo-2 can be utilized to determine whether rapid buffering of cytosolic Ca^{2+} slows the pacemaker to below its baseline.

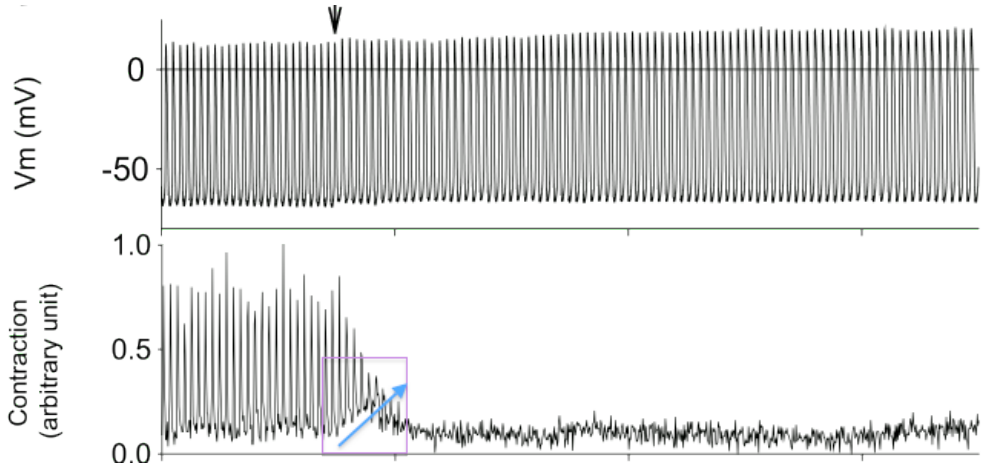


Figure 1.4 Effects of BAPTA on AP and contraction in SAN cells [permission was granted by the American Physiological Society to reproduce **Figure 1.4**, Himeno *et al.,* (*2011*)].

1.5. Autonomic modulation of the pacemaker

The spontaneous depolarization of SAN cells, which drives pacemaking, does not depend on an extrinsic nerve. However, the frequency of pacemaker potential is modulated by the autonomic nervous system. Sympathetic innervation through release of catecholamines increases the frequency of the heartbeat, while parasympathetic innervation via acetylcholine release reduces heart rate. Under normal physiological conditions, the heart is under tonic parasympathetic regulation, which reduces the heart rate by approximately 30 beats per minute reaching 70 beats per minute (Hutter and Trautwein 1956; Burnstock, 1969).

1.5.1. Sympathetic modulation of the pacemaker

Sympathetic innervation increases heart rate by predominantly activating β_1-adrenoceptors present on SAN cells. It does this by releasing the β and α-adrenoceptor agonist, noradrenaline (Hutter and Trautwein 1956; Burnstock *et al.,* 1969). Activation of the β_1-adrenoceptor (G_s-protein coupled) occurs via binding of noradrenaline to the receptor (Brodde *et al.,* 1984). Activated β_1-adrenoceptors trigger a biochemical cascade that amplifies the signal. The activated receptor undergoes a conformational change that causes the third intracellular loop of the receptor to recruit the trimeric G_s-protein ($\alpha\beta\gamma$ subunit complex). This enables activation of the heterotrimeric G_s-protein via the exchange of GDP for GTP at the α_s subunit (Brodd *et al.,* 1984). Next, the activated α_s dissociates from the $\beta\gamma$ subunit and activates the target protein, adenylyl cyclase (AC). Activated AC converts ATP to cAMP. cAMP binds directly to the I_f channels and activates them, contributing to the positive chronotropic action by accelerating the diastolic depolarization phase of the action potential (DiFrancesco *et al.,* 1991). cAMP also binds to the regulatory domain of protein kinase A (PKA) and dissociates from the catalytic subunits of PKA. The catalytic subunits of PKA catalyse and phosphorylate the following target proteins: voltage sensitive L-type Ca^{2+} channels, phospholamban, K_v channels, and ryanodine receptors (De *et al.,* 1996; Sculptoreanu *et al.,* 1993; Li *et al.,* 1990; Mundina *et al.,* 1996; Lei *et al.,* 2002) (**Figure 1.3**).

The phosphorylation of voltage sensitive L-type Ca^{2+} channels increases their open-state probability and duration, increasing the influx of Ca^{2+} ions (Kameyama *et al.,* 1985). This increase in cytosolic Ca^{2+} concentration partners

with NCX, contributing towards net inward depolarizing current and speeding up the last phase of diastolic depolarization. The action is augmented by the contribution of $Ca_v1.3$ L-type calcium channels (which have a lower activation potential), contributing to the late phase of diastolic depolarization and kick-starting the pacemaker potential upstroke (Ca^{2+}-based upstroke of the SAN action potential) [Mangoni *et al.,* 2003; Mangoni *et al.,* 2006].

Phosphorylation of phospholamban [phosphorylation of Ser^{16}, Li *et al.,* (1990)] reduces its inhibitory action on the SERCA. Removal of the inhibition of phospholamban on SERCA activity increases the Ca^{2+} affinity of SERCA and this initially boosts the rate of Ca^{2+} transfer from the cytosol into the SR; this accounts for most of the lusitropic effect (Luo *et al.,* 1994). Moreover, an increase in Ca^{2+} concentration in the SR increases the Ca^{2+} transient amplitude with each AP generated and this in turn contributes towards the positive chronotropic effect. Ju and Allen (1999) showed that β_1-adrenoceptor stimulation in toad SAN cells with caffeine-induced increases in intracellular Ca^{2+} was 14% higher. Also, following emptying of SR stores with 1 μM ryanodine, β_1-adrenoceptor stimulation was not able to restore beating rate. This suggests that the β_1-adrenoceptor-stimulated increase in Ca^{2+} concentration in the lumen of the SR contributes towards increased beating rate by increasing the amplitude of the Ca^{2+} transient. This observation was confirmed by Rigg and Terrar (1998, 2000), who found that 2 μM ryanodine significantly reduces the isoprenaline log(concentration)-response curve.

Phosphorylation of K_s channels results in an increased rate of the repolarization phase of the action potential, which leads to more excitation per minute (Marx *et al.,* 2002; Lie *et al.,* 2002).

It has also been noted that RyR phosphorylation increases the affinity of RyR for Ca^{2+}, and makes the channels more leaky. This increases Ca^{2+} efflux from the SR following each CICR mechanism. These changes to RyR induce a positive inotropic effect (Marx *et al.,* 2000).

1.5.2. Parasympathetic modulation of the pacemaker

Parasympathetic nerve terminals release acetylcholine (ACh), a muscarinic receptor agonist, which reduces heart rate through activation of the M_2 receptors present on SAN cells. M_2 receptors are $G_{i/o}$-protein coupled receptors (Breitwieser *et al.,* 1988). Following the binding of ACh to the M_2 receptor, a conformational change of the receptor occurs. Next, the third intracellular loop of the receptor recruits the trimeric $G_{i/o}$-protein ($\alpha\beta\gamma$ subunit complex), enabling activation of the heterotrimeric $G_{i/o}$-protein via attachment of GTP to the $\alpha_{i/o}$ subunit. The activated $\alpha_{i/o}$ then dissociates from the $\beta\gamma$ subunit and inhibits the function of adenylyl cyclase (AC). This in turn reduces the intracellular concentration of cAMP. The reduction in the intracellular cAMP reduces the pacemaker slope by reducing the open probability of I_f channels and the inward current (DiFrancesco and Tromba, 1987). Furthermore, the $\beta\gamma$ subunit indirectly inhibits the L-type Ca^{2+} channel as a consequence of the hyperpolarization caused by activation of the K_{ACh} channels (**Figure 1.3**). K_{ACh}

activation also directly reduces the rate of pacemaker slope decay (Breitwieser *et al.,* 1988). The underlying mechanism of K_{ACh} channel activation via the $\beta\gamma$ subunit is the stabilisation of the PIP_2-K_{ACh} complex [as explained above in Section 1.2.1.3. ACh activated K^+ channels (K_{Ach})].

1.6. Clinical implications

DiFrancesco and colleagues (2009) argue that I_f is the most important current in the regulation of pacemaker cells, while Lakatta's group favours the Ca^{2+} clock theory of pacemaking. Maltsev and Lakatta (2012) argue that I_f is a 'defensive' mechanism rather than a key player in controlling heart rate, since its most important role is to prevent bradycardia. Maltsev and Lakatta (2012) also describe I_f in the context of the coupled-clock pacemaker cell system. It is clear that I_f has a definite (secondary layer) modulatory effect on pacemaker rhythm (via vagal influences), and forms a part of the membrane clock system, which through interaction with the Ca^{2+} clock, forms the overall pacemaker clock. However, there is little evidence to suggest that I_f on its own is the sole initiator of the pacemaker. In fact, evidence shows that activation of I_f is not the primary pacemaker mechanism, since its inhibition with ivabradine does not completely stop the heart from beating but only slows heart rate. Conversely, inhibition of NCX via substitution of a Na^+ bath with Li^+ completely stops the heart from beating (Bogdanov *et al.,* 2001; Sanders *et al.,* 2006), indicating that Ca^{2+} plays a key role in the mechanisms underlying pacemaking.

I believe that the observation by Sanders *et al.* (2006) of elevated basal cytosolic Ca^{2+} concentration (225 nM) in pacemaker cells helps to explain how the pacemaker operates. The elevated basal cytosolic Ca^{2+} levels found specifically in pacemaker cells drive an inward Na^{+} current, either via NCX or via a continuous Na^{+} leak pathway (as proposed by Kang and Hilgemann, 2004); making NCX a critical contributor to pacemaking throughout diastolic depolarization. At the same time, elevated basal cytosolic Ca^{2+} concentration helps to explain the increased cytosolic cAMP concentration (Vinogradova *et al.,* 2006) and upregulation of PKA via activation of Ca^{2+}-stimulated AC1 and AC8 (Mattick *et al.,* 2007). It also helps to explain the basal activity of CaMKII and its downstream regulation of L-type Ca^{2+} channels (Vinogradova *et al.,* 2000), and phosphorylation of phospholamban (Mundina *et al.,* 1996). However, the mechanism underlying the increased cytosolic Ca^{2+} concentration within SAN cells remains unknown.

In evolutionary terms, it makes sense that there is more than one mechanism of pacemaking. Indeed, it seems that the pacemaker is imbued with multiple redundancy mechanisms in order to overcome the failure of a single layer, which would bring the heart to a standstill. For example, I_f is a 'redundancy' mechanism rather than a key player in controlling heart rate because its most important role is to prevent bradycardia. Inhibition of the I_f channel with ivabradine does not completely stop the heart from beating, only slows the heart rate.

The focus of my research was to improve our understanding of the underlying physiological signalling pathways of the biological pacemaker. I want

to increase the knowledge in this area, so that ways can be found to effectively intervene when the underlying function of pacemaking is misregulated.

1.7. Aims

The aim of the work described in this thesis were as follows:

- To investigate which adrenoceptors (α_1, β_1 or β_2) are responsible for driving positive chronotropic action in the heart (Chapter 3).

- To investigate the contributions of I_f and Ca^{2+} release from SR on the modulating basal spontaneously beating heart rate in the absence and presence of β_1-adrenocpetor stimulation. To investigate the effect of Ca^{2+} release from SR on I_f's modulation of basal beating rate via Ca^{2+} stimulated AC using pharmacological compounds (Chapter 4).

- To investigate the role of Ca^{2+}-stimulated ACs on Ca^{2+} release from SR on I_f's modulation of basal beating rate using knockout mice models differentially lacking specific Ca^{2+}-stimulated ACs isoforms; $AC1^{(-/-)}$, $AC8^{(-/-)}$ and $AC1\&8^{(-/-)}$ (Chapter 5).

- To develop photo-affinity probes from known I_{st} inhibitor (nicardipine) in pursuit of identifying of the I_{st} channel though crosslinking and pull-down protocols (Chapter 6).

CHAPTER 2: METHODS

2.1. Atrial node preparation (Rigg *et al.,* 1996)

The Oxford University ethics board, in accordance with the Home Office (UK) Code of Practice and Animals (Scientific Procedures) Act 1986 guidelines, approved all procedures involving animals. Schedule 1 was performed by initial stunning followed by cervical dislocation on male CD1, C57BL/6J, $AC1^{(-/-)}$, $AC8^{(-/-)}$, $AC1\&8^{(-/-)}$ mice, and on guinea pig. The heart was immediately excised and placed in a chamber with a "Sylgard" (Dow Corning) base filled with Physiological Salt Solution (PSS), kept at room temperature and constantly oxygenated. Next, in order to achieve an intact isolated atrial preparation, the ventricles and tissues overlying the SAN region were excised.

2.2. Organ bath sinoatrial node preparations (Rigg *et al.,* 1996)

Using a non-absorbable braded silk-waxed suture (purchased from Pearsalls Ltd), the isolated intact atrial preparation's lateral wings were carefully tied using a basic surgical knot, taking care to avoid contact with the SAN region. The preparation was then placed in a 20 mL organ bath containing 10 mL oxygenated PSS, warmed by a water jacket to 37°C. The preparation was mounted in such a way that the right atrium was attached to an isometric force transducer (AD Instruments, Oxford, UK), which ran through a "suture jacket." The left atrium was attached to a hook positioned at the bottom of the organ bath. The "suture jacket" was a 1-milliliter syringe with its tip removed (see **Figure 2.1**). Since the addition of certain drugs appeared to change the surface tension due to the formation of bubbles, which interfered with the tension

measurements, the use of the jacket protected the thread leading to the transducer, minimizing the influence of the bubbles. The beating rate was calculated from the interval between contractions using LabChart 5 software (http://www.adinstruments.com/products/labchart). Intervals between individual compounded action potentials were also used to calculate the beating rate using LabChart 5 software. The compound action potential signals were recorded using an extracellular electrode positioned close to the SAN region. Once the preparation was set up, it was left to stand for 45 min in order that a steady spontaneously beating rate would be reached before starting any experiments. For I_f inhibitors (ZD7288 and ivabradine), SR inhibitors (ryanodine and CPA) and AC inhibitor (MDL-12,330A), a 30 min incubation period required a reduced plateau steady beating rate to be reached. The beating rate was measured from beats sampled over a period of 30 sec. No irregularities in rhythm or interference with the spontaneous rhythm were observed following completion of the above procedure.

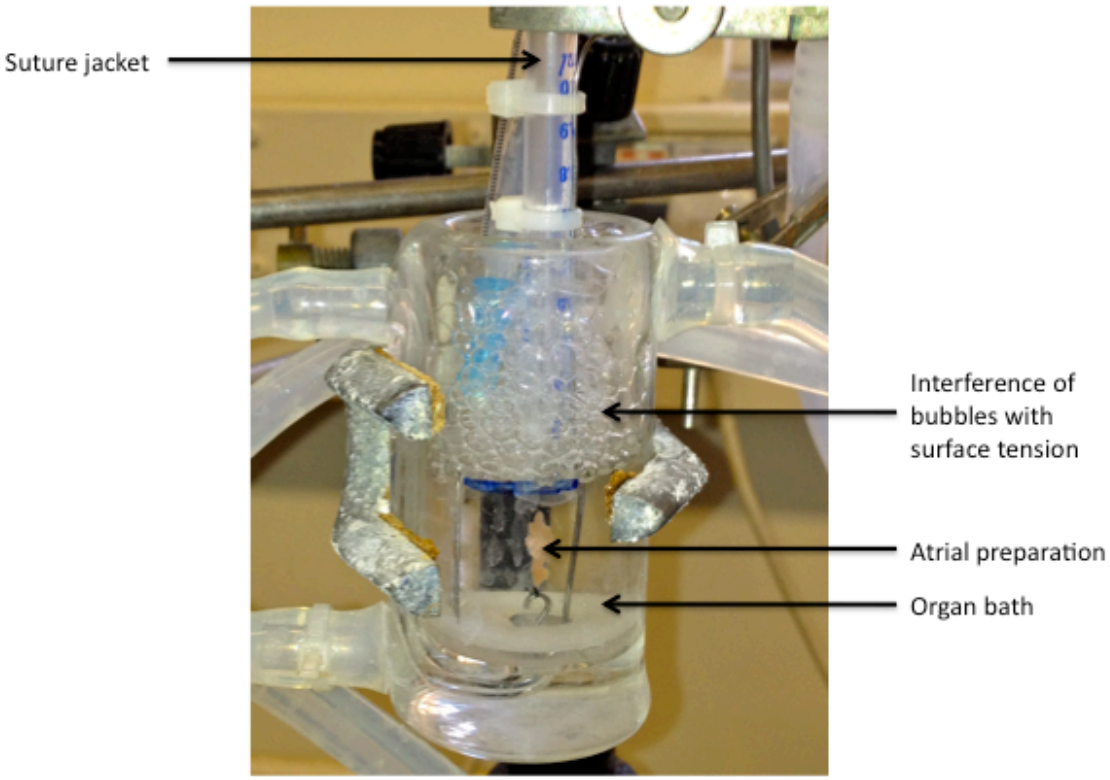


Figure 2.1 The organ bath set-up, including the suture jacket.

2.3. Optical fluorescent Ca^{2+} transient measurement sinoatrial node preparation (Lee *et al.,* 2011)

The ventricles, connective tissue, and vessels surrounding the posterior area of SA node, specifically those surrounding the superior vena cava, were carefully removed without interfering with the posterior wall of the SA node. The preparation was then transferred and pinned in a 20 mL chamber (with Sylgard base) in such a way that the left atrium was on the right with the superior vena cava was at the top. The chamber contained 10 mL of oxygenated PSS. Next, in order to reveal the SAN region, an incision was made from the bottom of the right atrium toward the superior vena cava. This exposed a clear anatomical

structure from the left-hand side of the right atrium known as the crista terminalis. To the immediate right of the crista terminalis and away from the interatrial septum, there is a unique translucent feature this is the SAN. The chamber's solution temperature was then increased to and kept at 34°C (to reduce the extrusion of the Ca^{2+} probe). Next, the tissue was pre-incubated with 10 μM blebbistatin for 30min, followed by 4 μM Rhod-2 AM for 45min. The chamber solution was then replaced and maintained with 10 μM blebbistatin, with 10 min given for the preparation to stabilize before commencing with the experiments. A stable fluorescence signal resulting from excitation of Rhod-2 AM was indicative of the location of the leading pacemaker site; it was seen to originate from the translucent site at the right atrium region near the superior vena cava, where SAN region is anatomically defined. Following detection of the leading pacemaker site, the region of interest corresponding to an area of 375 by 375 μm from its central core was selected to record Ca^{2+} transients. Throughout my experiments the leading pacemaker site remained stable during the application of drugs. For the I_f inhibitors (ZD7288 and ivabradine) and the SR inhibitor (CPA), a 30 min incubation was required in order for the preparation to reach a reduced plateau steady beating rate. The beating rate was measured using beats sampled over a period of 10 sec at a frame rate of 3000 frame/sec. No irregularities in rhythm or interference with the spontaneous rhythm were observed following completion of the above procedure. Blebbistatin and Rhod-2 AM had no effect on basal beating rate, as examined by recording of extracellular compound action potentials by surface electrode.

2.4. Imaging system for Ca^{2+} transient measurements from intact SAN preparation (Lee *et al.,* 2011)

To excite the Ca^{2+} sensitive dye, Rhod-2 AM, 4 LEDs were used to illuminate the preparation, with band pass filters of 560/50 nm. For the collection of emitted fluorescence, an ET585/40 nm emission filter was used. The LEDs and filters were purchased from Cairn Research Ltd. (Kent, UK). An EMCCD camera with 128 x 128 pixels (Evolve 128 Photometrics, Tucson) was used for optical recordings. The preparation was only exposed to light during recordings over periods of 10 seconds for each recording at a frame rate of 3000 frame/sec. The recording, quantification and visualization of the data were performed using custom software provided by Gil Bub (Department of Physiology, Anatomy and Genetics, University of Oxford). pCLAMP software was utilized for Ca^{2+} transient analysis.

2.5. Imaging system for Ca^{2+} transient measurements from guinea pig SAN cells (Collins *et al.,* 2011)

Spinning Disk Confocal Microscopy was used to record Ca^{2+} transients from guinea pig SAN cells. For visualization purposes, a Nikon Axiovert 200 inverted microscope with attached Nipkow spinning disk confocal component (CSU-10, Andor Technology, UK) was used. To excite the Ca^{2+} sensitive dye, Flour-5F AM, a 488 nm diode laser (Cairn Research Ltd, Kent, UK) was utilized to illuminate the preparation and the excitation light was delivered through the Nipkow component and exposed to sample through the objective. The emitted

light was captured by the CSU-10 component and was detected using an Andor iXON897 EM-CCD camera (Andor Technology, UK) at a frame rate of 50 Hz. The quantification and visualization of the data were performed using Andor iQ software (Andor Technology, UK). pCLAMP software was utilized for Ca^{2+} transient analysis

2.6. Cell isolation (guinea pig) (Powell *et al.,* 1980)

Powell *et al.'s* (1980) modified procedure was utilized so that both ventricular and SAN cells could be isolated from a single guinea pig's heart. After schedule 1 was performed by initial stunning followed by cervical dislocation of a male guinea pig (weighing approximately 500g), the heart was immediately excised and submerged in PSS containing heparin solution to prevent clotting. Next, via the aorta, the heart was mounted on a constant pressure Langendorff system for retrograde perfusion. The heart was first perfused with Ca^{2+} zero solution for 2 min, followed by a collagenase solution (50ml) re-circulation for 25 min. The perfusion solutions were kept at 36°C and the heart was encased in an empty organ bath with a warm water jacket to maintain the heart close to body temperature.

2.6.1. Ventricular isolation (guinea pig) (Powell *et al.,* 1980)

Following a 25 min enzymatic digestion with collagenase solution, the ventricles were cut from atrium. The ventricles was then roughly cut into ten pieces, transferred to 10 mL of collagenase solution and agitated with a

mechanical stirrer for 5 min (while the temperature was maintained at 36°C). A 250 μM mesh filter was then used to filter the cells that had been isolated, leaving the larger ventricular pieces for further isolation. The isolated cells were then transferred into a 15 mL falcon tube containing Dulbeco's Modified Eagle Medium (DMEM, Invitrogen) to prevent further digestion. In order to remove the collagenase, the cells were gently centrifuged using a manual centrifuge and the supernatant was replaced with DMEM. This was repeated two additional times, after which the cells were re-suspended in DMEM at room temperature until use.

2.6.2. SAN cell isolation (guinea pig) (Powell *et al.,* 1980)

After a 25 min enzymatic digestion with collagenase solution, the atrium was cut from the ventricles and transferred into a chamber with a "Sylgard" (Dow Corning) base that had been filled with Physiological Salt Solution (PSS), kept at room temperature and constantly oxygenated. The connective tissue and vessels surrounding the posterior area of SA node, specifically those surrounding the superior vena cava, were then carefully removed without interfering with the posterior wall of the SA node. The preparation was then pinned in such a way that the left atrium was on the right and the superior vena cava was at the top. Next, in order to expose the SAN region, an incision was made from the bottom of the right atrium toward the superior vena cava. This exposed a clear anatomical structure at the left-hand side of the right atrium known as the crista terminalis. Immediately to the right of the crista terminalis and away from the interatrial septum, the uniquely translucent SAN is located.

The SAN was excised and cut into thin strips (approximately 2 x 5 mm) and kept in warmed and oxygenated high potassium (KB) solution (5 mL). A fire-polished glass pipette was then used to gently isolate the SAN cells via trituration. Once isolated, the cells were kept at 4°C in KB solution until use.

2.7. Knockout mice models: AC1$^{(-/-)}$, AC8$^{(-/-)}$ and AC1&8$^{(-/-)}$

The mice models [AC1$^{(-/-)}$, AC8$^{(-/-)}$ and AC1&8$^{(-/-)}$] were all homozygous mutants that were kindly provided by Dr. Alana Conti's Lab (Susik *et al.,* 2014; Conti *et al.,* 2009; Wayne State University, School of Medicine, Department of Neurosurgery). To generate AC1$^{(-/-)}$, AC8$^{(-/-)}$ and AC1&8$^{(-/-)}$ mice, progeny of homozygous mutants (AC1KO, AC8KO or DKO) and C57BL/6 mice from The Jackson Laboratory (Bar Harbor, ME) were bred at the Wayne State University. Minimum of ten generation of backcrossing was carried. Western blotting analysis using anti-AC1 or anti AC8 antibodies against membrane-enriched protein extracts from the striatum of C57BL/6 or AC1&8$^{(-/-)}$ mice were carried out. Expectedly expression of both AC1 (~band at 123 kDa) and AC8 (~band at 135 kDa) proteins were detected in C57BL/6, but were absent in AC1&8$^{(-/-)}$ extracts (**Figure 2.2**).

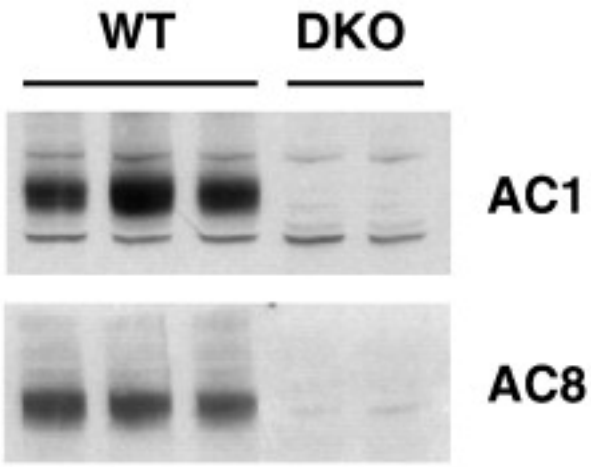


Figure 2.2 Detection of AC1 and AC8 enzymes by Western blot analysis represented by band at ~123 kDa and band at ~135 kDa respectively; in the striatum of C57BL/6 mice (WT). On the other hand in the transgenic mice the ~123 kDa and ~135 kDa bands were not present [permission was granted by Copyright Clearance Center to reproduce **Figure 2.2**, Conti *et al.,* (2009), license number: 3830320167197].

2.8. Drug Exposure Times

For I_f inhibitors (ZD7288 and ivabradine), SR inhibitors (ryanodine and CPA), AC inhibitor (MDL-12330A), L-type Ca^{2+} channel inhibitors (nifedipine and nicardipine) and synthesized probes (modified from nicardapine), all required a 30 min incubation period in order for the preparations to reach a reduced plateau steady beating rate. The reduced steady beating rate with Cs^{+} was reached within 5 min. For isoprenaline, 2 min of exposure was required to reach the increased steady state.

2.9. Statistical analysis

Results are expressed as means ± S.E.M., n = number of experiments. GraphPad Prism (version 5.0) software was used to perform statistical analysis, including Student's *t*-test, one-way ANOVA with Dunnett post-test and two-way ANOVA with Bonferroni post-test (significance level $P<0.05$).

2.10. Solutions used for pharmacological studies:

Substance (mM)	PSS	Zero Ca^{2+} solution	KB solution	Collagenase solution
$CaCl_2$	1.8			0.1
Collagenase type II				25
EGTA		0.04	0.04	
Glucose	5.5	5	10	5
HEPES			5	
K Glutamate			5	
KH_2PO4			20	
KCl	5.4	5.4	70	5.4
$MgCl_2$ $6H_2O$	1	1	5	1
Na Pyruvate		1		1
NaCl	125	137		137
NaH_2PO_4	1.2	1		1
$NaHCO_3$	25	12		12
NaOH				
pH adjusted with			KOH	
pH of	7.4	7.4	7.2	7.4
Succinic acid			5	
Taurine			20	
Aerated with 95 % O_2/5 % CO_2	YES	YES	NO	YES

2.11. Chemicals used for Pharmacology studies:

Compound	Supplier	Solvent	Stock	Storage
Blebbistatin	Tocris Inc	DMSO	10 mM	-20 °C
CGP20712A	Sigma	Water	1 mM	-20 °C
Carbachol	Tocris Inc	Water	10 mM	Fresh each day and stored in 4°C
Collagenase type II	Worthington Biochemical Corp., NJ, USA			
CsCl	Sigma	Water	100 mM	Fresh each day and stored in 4°C
Cyclopiazonic acid	Sigma	DMSO	40 mM	-20 °C
Flour-5F, AM	Invitrogen	DMSO	10 mM	-20 °C
H89	Tocris Inc	DMSO	10 mM	-20 °C
ICI118551	Sigma	Water	1 mM	-20 °C
Isoprenaline	Sigma	Water	10 mM	Fresh each day and stored in 4°C
Ivabradine	Tocris Inc	DMSO	10 mM	-20 °C
MDL-12,330A	Calbiochem	DMSO	10 mM	-20 °C
Nifedipine	Sigma	DMSO	5 mM	-20 °C
Noradrenaline	Sigma	Water	10 mM	Fresh each day and stored in 4°C
Phenylephrine	Sigma	DMSO	10 mM	Fresh each day and stored in 4°C
Prazosin	Tocris Inc	DMSO	1 mM	-20 °C
Reboxetine	Tocris Inc	Water	1 mM	-20 °C
Rhod-2 AM	Invitrogen	DMSO	10 mM	-20 °C
Ryanodine	Tocris Inc	Water	1 mM	-4 °C
Tertiapin-Q	Tocris Inc	Water	1 mM	-20 °C
ZD7288	Tocris Inc	DMSO	10 mM	-20 °C

2.12. Pharmacodynamics profile of used compounds

Target	Ki/IC50	Concentration	Compound	Reference
β_1-adrenoceptor	Ki	300 nM	ICI118551	Baker (2005)
β_2-adrenoceptor	Ki	0.55 nM	ICI118551	Baker (2005)
β_1-adrenoceptor	Ki	3.16 nM	CGP 20712A	Baker (2005)
β_2-adrenoceptor	Ki	776 nM	CGP 20712A	Baker (2005)
PKA	Ki	50 nM	H-89	Chijiwa *et al.* (1990)
Homomeric hHCN4 current in CHO cells	IC50	0.5 µM	Ivabradine	Thollon *et al.* (2007)
I_f current in isolated SAN form rabbit	IC50	2.8 µM	Ivabradine	Bois *et al.* (1996)
I_f current in isolated SAN form rabbit	IC50	1.5 µM	Ivabradine	Bucchi *et al.* (2002)
I_f current in isolated SAN from g pig	IC65	0.3 µM	ZD7288	BoSmith *et al.* (1993)
Homomeric hHCN4 current in CHO cells	IC90	2 mM	Cs^+	Thollon *et al.* (2007)
L-type Ca^{2+} channel in isolated rog atrial cardiomyocyte	IC50	1 µM	Nicardipine	Charnet *et al.* (1987)

2.13. Representative traces from atrial preparations (Figure 2.3)

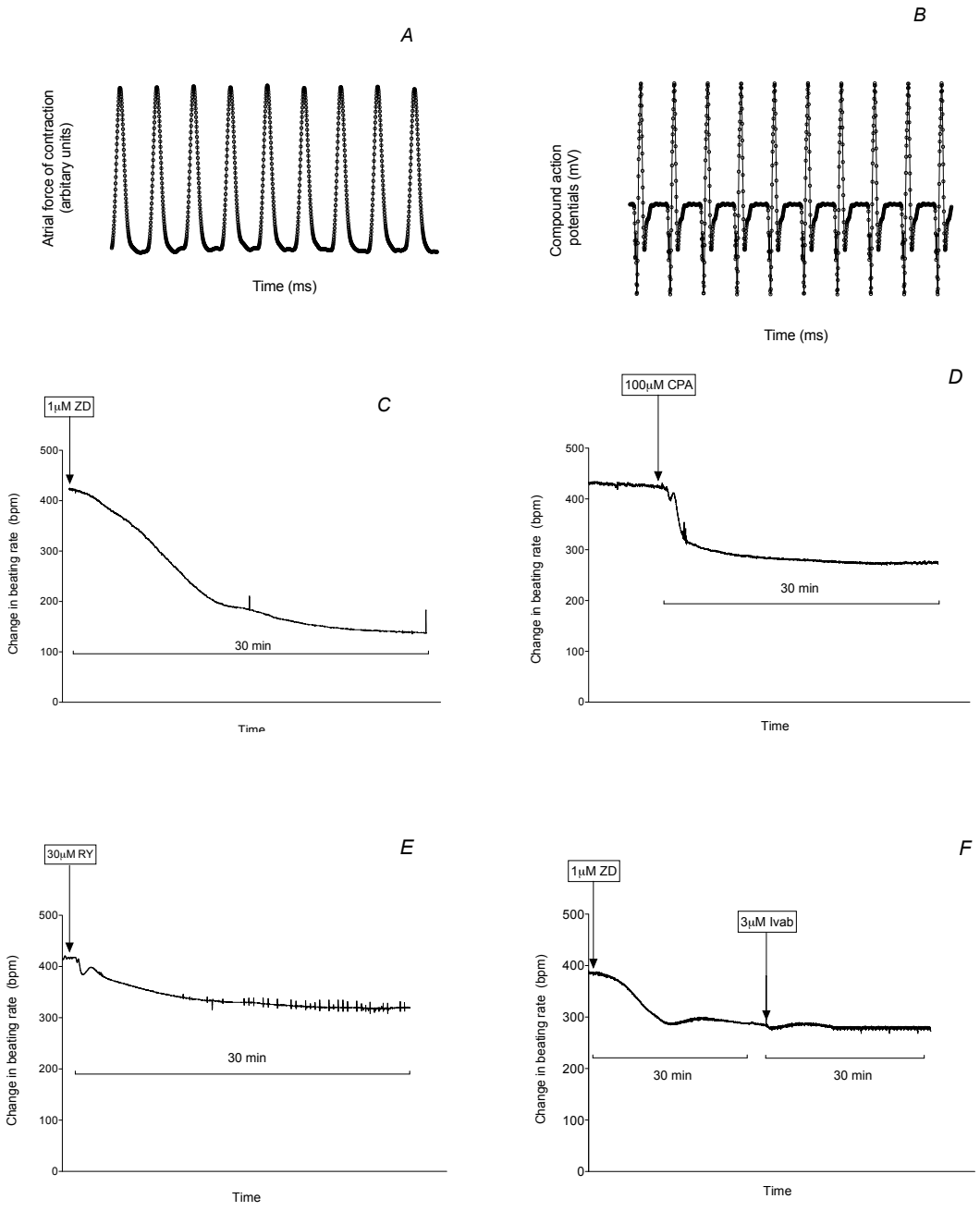


Figure 2.3 Representative traces taken from typical experiments using isolated mouse (CD1) atrial preparations in an organ bath perfused with 36°C PSS solution and with addition of drugs. ***(A)*** Representative trace of contractile force of atrial preparation. **(*B*)** Representative trace of electrical activity (compounded action potential) recorded from the surface area of SAN region. ***(C to F)*** Traces representing change in beating rate (bpm) following addition of 1μM ZD7288, 100μM CPA, 30μM ryanodine or combination of 1μM ZD7288 & 3μM ivabradine. Arrow indicates addition of a drug.

2.14. Lysis buffers, in mM (unless stated otherwise) (Rougier *et al.,* 2010; Ko *et al.,* 2012)

Substance (mM)	Lysis buffer (A)	Lysis buffer (B)	TBS-T
Deoxycholate		0.5%	
EGTA	1	1	
Glycerol	10%		
HEPES	50		
N-ethyl maleimide	10		
NaCl	150	150	150
Nonidet P-40		1%	
pH of	7.4	8	7.6
Phenylmethylsulfonyl fluoride		1	
Protease inhibitors cocktail (Roche)	Yes	Yes	
SDS		0.1%	
Tris		50	20
Triton	1%		
Tween 20			0.05%

2.15. Sample preparation from mouse whole heart (Rougier *et al.,* 2010; Ko *et al.,* 2012)

Using a Dounce homogenizer, a fresh whole heart from a C57BL/6 mouse was mechanically homogenized in the presence of 100 µL lysis buffer A/B. A further 900 µL of lysis buffer A/B was added to the final homogenized preparation. The preparation was then left for further lysis for 45 min at 4°C. Next, the membrane proteins were recovered in supernatant after 15 min of centrifugation at 13,500 rpm at 4°C.

2.16. Cell lysis (guinea pig) (Rougier *et al.,* 2010; Ko *et al.,* 2012)

Initially, the cells were suspended in PSS. Ventricular cells were manually spun down and the cells were resuspended in lysis buffer A/B (100 µl). The preparation was then digested for 45 min at 4°C. Subsequently, the sample was sonicated using 3 x 5 sec pulses separated by 30 sec intervals. After 15 min of centrifugation at 13,500 rpm at 4°C, the membrane proteins were recovered in the supernatant.

2.17. UV irradiation of samples

Firstly, the lysed sample was incubated with a photo-affinity probe for 40 min at 4°C. Secondly for crosslinking reaction 100 µL sample placed in an open top PCR Eppendorf viol followed by UV irradiation with 310 nm light at 4°C for 45 min (5 min pulses separated by 2 min intervals) in the CaproBox™ (http://www.caprotec.com). Crosslinking reactions were monitored/analysed by ESI mass spectrometry. In control experiments, the procedure was the same, with exception being that either the photo-affinity probe was not added or the probe was incubated at the same time as its competitive inhibitor, nicardipine.

2.18. Click Chemistry reaction (van Kasteren *et al.,* 2007)

Firstly, the endogenous biotinylated proteins from the sample were extracted with the use of streptavidin-coated magnetic beads. The sample was initially incubated for 1 h at 4°C with 50 µL of streptavidin magnetic beads (Dynabeads® MyOne™ Streptavidin C1, Thermo Fisher). The sample was then gently mixed every 10 min over a period of 1 h. The supernatant was collected and the magnetic beads were discarded. Next, 10µL of a freshly made copper complex solution containing 10 mg/mL of Cu(I)Br solution in acetonitrile together with 120 mg/mL tris-triazolyl amine ligand was added to a sample containing either 100 µM biotin azide or 100 µM rhodamine azide. The reaction was agitated (using a roller mixer) for 1 h at room temperature. The reaction mixture was then centrifuged to remove any precipitated Cu(II) salts.

2.19. Magnetic beads pull-down

Following the 'click reaction' in lysis buffer, the sample was incubated with 50 µL of streptavidin-coated magnetic beads (Dynabeads® MyOne™ Streptavidin C1, Thermo Fisher) for 30 min at 4°C. The beads were then collected and resuspended in 0.1% SDS buffer and the supernatant was discarded. The sample was then boiled at 100°C for 5 min in order to elute the captured protein from the beads and the magnetic beads were discarded. Captured protein was analysed by Western blotting.

2.20. Electrophoresis protocol (Rougier *et al.,* 2010; Ko *et al.,* 2012)

The samples were loaded into the gel lane (NuPAGE™ Novex™ 12% Bis-Tris Protein Gels, 1.0 mm, 10-well), with one of the lanes loaded with PageRuler^{TM} prestained protein molecular weight ladder. A Bio-Rad Mini-PROTEAN II system was used to run the gels at 200 V for 1 h.

2.21. Western blotting protocol (Rougier *et al.,* 2010; Ko *et al.,* 2012)

Using a Mini Trans-Blot Electrophore, which was filled with transfer buffer, Hybond ECL membrane (0.2 μm pore size, GE Healthcare) was used to blot the gel onto. The current was held constant at 200 mA for 2 h at 4°C. Next, the membrane was blocked overnight in blocking buffer (5% semi-skim milk or 1% Casein dissolved in TBS-T) at 4°C. The membrane was then incubated with primary antibody for 1 h at room temperature, followed by washing with TBS-T for 3 × 10 min with shaking. Next, the membrane was incubated with secondary antibody for 1 h at room temperature, followed by washing with TBS-T for 3 × 10 min with shaking. The membrane then was incubated with ECLTM detection reagents (GE Healthcare) for 1 min and exposed to AmershamTM Hyperfilm ECL film (GE Healthcare). Finally, the film was developed using a Compack X4 (Xograph) film developer.

2.22. Antibodies

ACC-003 was the primary antibody (polyclonal antibody raised in rabbit against $Ca_v1.2$, Alomone, Israel), diluted in TBS-T buffer at 1:1000 dilution.

The secondary antibody was goat anti-rabbit IgG HRP (Santa Cruz Biotech) diluted in TBS-T buffer at 1:1000 dilution.

Streptavidin-horseradish peroxidase conjugate RPN1231VS, GE Healthcare, diluted in TBS-T buffer at 1:15,000 dilution.

CHAPTER 3: IDENTIFICATION OF ADRENOCEPTOR ACTIVATION RESPONSIBLE FOR DRIVING THE POSITIVE CHRONOTROPIC ACTION

3.1. Introduction

Before investigating the mechanism underlying the pacemaker signalling pathway, I evaluated which adrenoceptor plays a major contributory role in evoking positive chronotropic effects. Three β-adrenoceptor isoforms (β_1, β_2 and β_3) have been cloned and identified as present in SAN cells (Frielle *et al.,* 1987; Dixon *et al.,* 1986; Emorine *et al.*, 1989) and are all G_s protein coupled receptors (Strader *et al.,* 1995). The β_3 adrenoceptor is the least well studied isoform. β_2 relative to β_1 adrenoceptor is thought to couple more efficiently to AC (Levy *et al.,* 1993). Through immunolabelling experiments, Barbuti *et al.* (2007) found co-localisation of I_f channels with the β_2-adrenergic receptor in the membrane caveolae of rabbit SAN. It was suggested that this co-localisation would facilitate a rapid increase in heart rate through I_f upon sympathetic stimulation. In more recent experiments by Greene *et al.* (2012) using HEK293 cells, formation of an ion channel-receptor complex via the N-terminal cytosolic tail of I_f channels with β_2-adrenoceptors was observed. Disrupting this channel-receptor complex resulted in abolition of adrenergic regulation of both the chronotropic function of SAN cells and the modulation of I_f current in isolated rat SAN cells. In contrast, using selective inhibitors in anesthetized dog heart, Takei *et al.* (1992) implicated both the β_1 & β_2 adrenoceptors in contributing to positive chronotropic action, with the predominant effect mediated through β_1-adrenoceptor. Piercy (1988) also showed that in pithed rat and in a rat right atrial preparation, the β_1-adrenoceptor is main receptor responsible for the chronotropic function of SAN cells and not the β_2-adrenoceptor. Rohrer *et al.* (1996) generated β_1-adrenoceptor knockout mice models, of which most of the offspring died prenatally, indicating the lethality of lacking the β_1-adrenoceptor.

However, the mice that did survive had a normal phenotypic character, with exception that they lacked positive chronotropic action induced by isoprenaline. Using amidephrine (α_1-adrenoceprtor agonist, while α_2, β_1 & β_2 and muscarinic receptors were inhibited with yohimbine, propranolol and atropine, respectively) in the anaesthetized open-chest dog model, Borgdorff *et al.* (1987) showed that α_1-adrenoceprtor activation did not contribute to chronotropic action. In contrast, in the pithed rat, amidephrine induced positive chronotropic action and this response was antagonized by prazosin (Flavahan *et al.,* 1981).

In order to investigate which adrenoceptor subtype (α_1, β_1 and/or β_2) is responsible for driving chronotropic action in SAN region of the heart, a series of competitive antagonists were used in mouse atrial preparation experiments.

3.2. Results

3.3. The effects of adrenergic receptor stimulation on positive chronotropy

3.3.1. β_1-adrenergic receptor (isoprenaline)

To evaluate the contribution of the β_1-adrenergic receptor on the positive chronotropic effects of pacemaking, an organ bath atrial preparation was used to assess the effect of a specific β_1 antagonist on the isoprenaline log(concentration)-response curve. It was shown that the isoprenaline log(concentration)-response curve significantly shifted in a parallel manner in the presence of a specific β_1 antagonist [CGP20712A, log(Kd) of -8.5 to -9.3 (Backer 2005)] at 10 nM CGP20712A ($P < 0.05$, two-way ANOVA with Bonferroni post-test, n = 6,), 100 nM CGP20712A ($P < 0.0001$, two-way ANOVA with Bonferroni post-test, n = 6) or 300 nM CGP20712A ($P < 0.0001$, two-way ANOVA with Bonferroni post-test, n = 6,). The 10 nM CGP20712A shifted the isoprenaline log(concentration)-response curve 7-fold (dose ratio of 7), 100 nM CGP20712A shifted the curve 107-fold (dose ratio of 107) and 300 nM CGP20712A shifted the curve 343-fold (dose ratio of 343) (**Figure 3.1*A***).

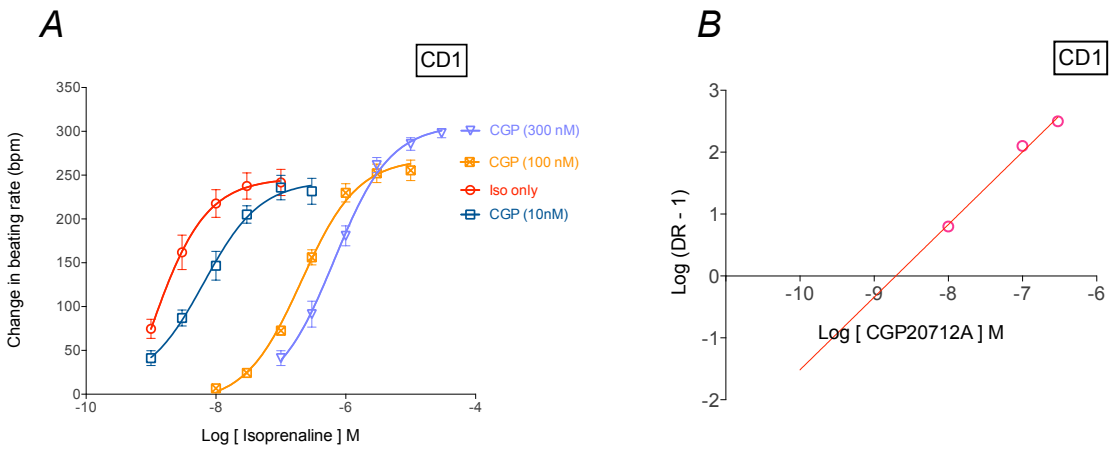


Figure 3.1 Graph changes showing in the positive chronotropic action of the β-adrenoceptor agonist isoprenaline by **(*A*)** the β_1-adrenoceptor antagonist, CGP20712A at concentrations of 10 nM (n = 6), 100 nM (n = 6) to 300 nM (n = 6) on the spontaneous beating rate of mouse atrial preparation. **(*B*)** Data from **Figure 3.1*A*** was used to calculate the dose ratios (DR). Schild analysis was performed to analyse the antagonism of isoprenaline by CGP20712A using GraphPad Prism (version 5.0) software, the resultant slope was not statistically different from 1 (demonstrating the competitive nature of CGP20712A). Data are expressed as mean ± S.E.M., n = number of experiments. GraphPad Prism (version 5.0) software was used to perform statistical analysis, including two-way ANOVA with Bonferroni post-test (significance level, $P < 0.05$).

The Schild plot revealed that log (dose ratio -1) against 10 nM, 100 nM and 300 nM concentrations of CGP20712A gave a log(Kd) of -8.7. The slope was close to unity (1.1± 0.1119) and was not statistically different from 1 ($P > 0.05$), demonstrating the competitive nature of CGP20712A (**Figure 3.1*B***).

3.3.2. β_1-adrenergic receptor (noradrenaline)

Since the natural transmitter is noradrenaline, I wanted to assess the effect of noradrenaline instead of isoprenaline. Unlike isoprenaline, noradrenaline's action is rapidly terminated by noradrenaline uptake (uptake 1). Therefore, in order to assess noradrenaline's true chronotropic action, the noradrenaline uptake needed to be taken into account. In the presence of 1 μM reboxetine (noradrenaline uptake inhibitor), the noradrenaline log(concentration)-response curve differed by 11-fold (n = 6) relative to the isoprenaline log(concentration)-response curve (n = 6). However, the noradrenaline log(concentration)-response curve in the absence of reboxetine (n = 6) differed by 99-fold relative to the isoprenaline log(concentration)-response curve (**Figure 3.2**).

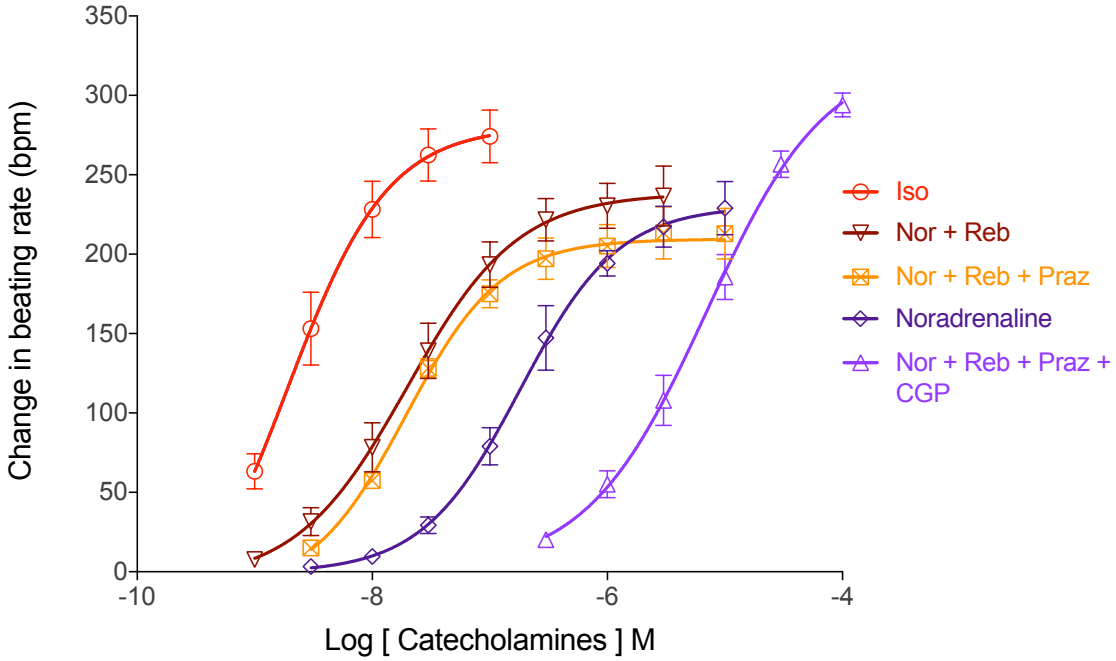


Figure 3.2 Graph representing mean change in the positive chronotropic action of isoprenaline (n = 6), noradrenaline (n = 6), noradrenaline [Nor] in the presence of: 1 μM reboxetine (n = 6), 1 μM prazosin in combination with 1 μM reboxetine (n = 6) and 1 μM prazosin combined with 1

μM reboxetine & 300 nM CGP20712A (n = 6) on the spontaneously beating mouse atrial preparation. Data are expressed as mean ± S.E.M., n = number of experiments. GraphPad Prism (version 5.0) software was used to perform statistical analysis, including two-way ANOVA with Bonferroni post-test, (significance level $P < 0.05$).

3.3.3. Chronotropic contribution of α_1-adrenergic receptor (noradrenaline)

In order to assess the chronotropic contribution of α_1-adrenoceptor stimulation, the α_1-adrenoceptor antagonist prazosin was used. Incubation with 1 μM reboxetine and 1 μM prazosin (n = 6) resulted in a slight, statistically not significant shift by a factor of 1.1 to the right, relative to incubation with 1 μM reboxetine alone (n = 6). In line with the isoprenaline's log(concentration)-response curve shift in the presence of 300 nM CGP20712A (343-fold shift), noradrenaline's log(concentration)-response curve shifted by 336-fold in the presence of 300 nM CGP20712A, 1 μM reboxetine and 1 μM prazosin (n = 6, **Figure 3.2**).

3.3.4. Chronotropic contribution of β_2-adrenergic receptor (isoprenaline)

Using a specific β_2-adrenergic receptor antagonist, I wanted to assess the contribution of the β_2-adrenergic receptor to the positive chronotropic action of isoprenaline. Initially, the preparation was incubated with either 100 nM (n = 6) or 300 nM ICI118551 (n = 6) and its impact on the isoprenaline log(concentration)-response curve was then assessed. The observed shifts of

the isoprenaline log(concentration)-response curve in the presence of either 100 nM or 300 nM ICI118551 (specific β_2 antagonist with log(Kd) of -8.3 to -9.2) were very small and statistically not significant (*P > 0.05,* two-way ANOVA with Bonferroni post-test, n = 6). Use of ICI118551at 100 nM resulted in a dose ratio of 1.8; in the presence of 300 nM ICI118551, the dose ratio was 3.9 (**Figure 3.3**).

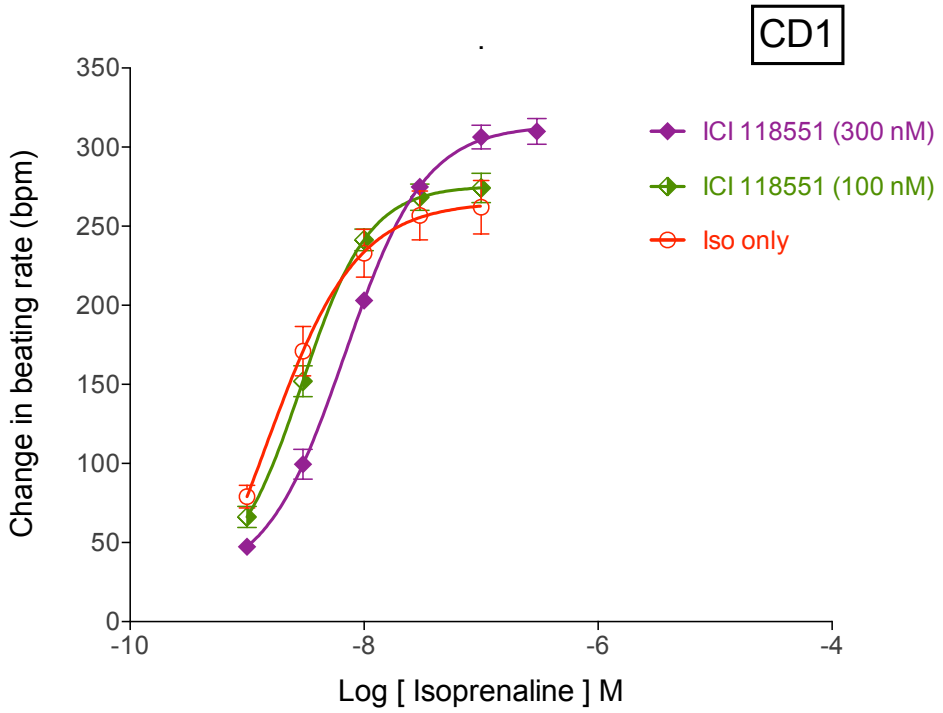


Figure 3.3 Graph representing the mean change in the positive chronotropic action of isoprenaline (n = 6) by 100 nM (n = 6) or 300 nM ICI118551 (n = 6) on the spontaneously beating mouse atrial preparation. Data are expressed as mean ± S.E.M., n = number of experiments. GraphPad Prism (version 5.0) software was used to perform statistical analysis, including two-way ANOVA with Bonferroni post-test (significance level *P < 0.05*).

3.4. Discussion

The results revealed that the major contributor in evoking the chronotropic effects of isoprenaline was occurring through the activation of β_1 pathway and not β_2 pathway. A high concentration (300 nM) of ICI118551 (a β_2 antagonist) shifted the isoprenaline log(concentration)-response curve to the right by a factor of only 3.9 (**Figure 3.3**). In contrast, 300 nM CGP20712A significantly shifted the isoprenaline log(concentration)-response curve 343-fold to the right (**Figure 3.1*A***). These observations suggest that the β_1 pathway is the dominant pathway in the positive chronotropic action of isoprenaline. This finding is in support of Piercy's (1988) observations that in pithed rat and in rat right atrial preparation, the β_1-adrenoceptor is main receptor responsible for the chronotropic function of SAN cells and not the β_2-adrenoceptor. Also, Rohrer *et al.* (1996) generated β_1-adrenoceptor knockout mice, of which most of the offspring died prenatally but where those that did survive lacked positive chronotropic action induced by isoprenaline.

The results contrast with the findings of Greene *et al.* (2012), where HEK293 cells were used to observe the formation of an I_f channel-β_2-adrenreceptor complex via the N-terminal cytosolic tail of the I_f channel with β_2-adrenoceptors. Using the epitope of the binding site, a synthetic peptide, HBAR, was synthesized to disrupt the channel-receptor complex. Pretreatment of rat SAN cells with HBAR to disrupt the channel-receptor complex resulted in the ablation of the adrenergic regulation of both the chronotropic function of SAN cells and the modulation of the I_f current. Whether the differences in our findings and those of Greene *et al.* (2012) are due to a species difference or

experimental conditions remains to be investigated.

The Schild plot for antagonism of isoprenaline by CGP20712A had a slope close to unity (1.1 ± 0.1119) and was not statistically different from 1, indicating that CGP20712A is a competitive antagonist. Furthermore, the computed affinity constant [log(Kd) = -8.7] was what would be predicted [log(Kd) from -8.3 to -9.2, (**Figure 3.1*B*)**].

From the above experiments it can be established that the β_1 receptor is the dominant pathway evoking the chronotropic effects of isoprenaline. However, I still needed to explore the role of the endogenous transmitter, noradrenaline. Initially, the potency of noradrenaline was compared to that of isoprenaline. However, the local concentration of noradrenaline around the receptors is not the same as that in the organ bath. Therefore, a direct comparison of the potencies cannot be made with accuracy, as, unlike isoprenaline, the potency of noradrenaline is underestimated due to it being subject to uptake 1. Therefore, an uptake 1 inhibitor (reboxetine) was used to assess its influence on the noradrenaline log(concentration)-response curve.

The observation that 1 μM reboxetine shifted the noradrenaline log(concentration)-response curve 11-fold to the left is strongly indicative of uptake 1 activity (**Figure 3.2**). Moreover, in the absence of reboxetine, there was a 99-fold difference between the positions of the noradrenaline log(concentration)-response curve and the isoprenaline log(concentration)-response curve (**Figure 3.2**). Thus, the potency of noradrenaline is underestimated by 1 $\log_{10}$ factor if uptake 1 activity is not taken into account.

Inhibition of uptake 1 revealed that a more accurate potency difference was 11-fold.

Before exploring the dominant effect of β_1 seen with isoprenaline, the contribution of the α_1 receptor was investigated, because noradrenaline is known to be more selective towards α adrenoceptors. Pre-treatment with 1 μM prazosin (α_1 antagonist) not significantly shifted the noradrenaline log(concentration)-response curve (in the presence of reboxetine, **Figure 3.2**). Thus, at face value, this result suggests that there is a minor contribution of the α_1 receptor towards chronotropic effects. In order to confirm the above results, I decided to increase the concentration of the β_1 & β_2 antagonists to 1 μM; instead of noradrenaline, phenylephrine (α_1 agonist) was used. The effect of phenylephrine (in the presence of the uptake 1 μM inhibitor reboxetine), combined with a high concentration of β_1 antagonist (1 μM CGP20712A), and β_2 antagonist (1 μM ICI118551), was investigated (30 min was allowed as an incubation period, n = 6, **Figure 3.4**). In doing so, I wanted to see the effect of α_1 receptor activation, which I thought might be masked by the powerful β_1-adrenoceptor pathway. However, there were no significant changes ($P > 0.05$, two-way ANOVA with Bonferroni post-test) in atrial beating rate relative to the control curve (time course recording of spontaneous basal beating rate in the absence of any drugs, n = 6), suggesting that the β_1-adrenoceptor pathway is the dominant pathway in generating positive chronotropic action (**Figure 3.4**). My results support observation of Borgdorff *et al.* (1987) using an anaesthetized open-chest dog, where amidephrine (α_1-adrenoceprtor agonist) did not cause a positive chronotropic action.

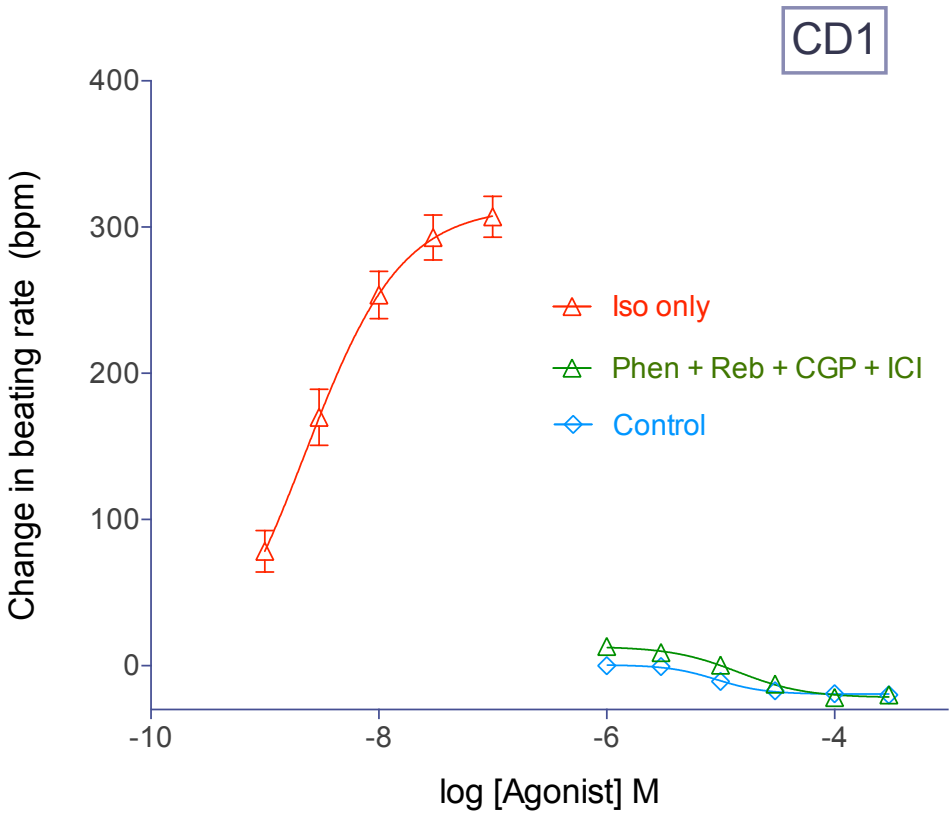


Figure 3.4 Graph representing the mean change in the time course recording of the spontaneous basal beating rate in the absence of any drugs (n = 6, control curve) and the positive chronotropic action of isoprenaline (n = 6) and phenylephrine (n = 6) on mouse spontaneously beating atrial preparation. Data are expressed as mean ± S.E.M., n = number of experiments. GraphPad Prism (version 5.0) software was used to perform statistical analysis, including two-way ANOVA with Bonferroni post-test (significance level $P < 0.05$).

From the observations described above, it seems that β_1 is the main receptor responsible for isoprenaline's chronotropic effects. The shift in the noradrenaline log(concentration)-response curve in the presence of 300 nM CGP20712A (336-fold rightward shift, **Figure 3.2**) was similar to the isoprenaline log(concentration)-response curve shift in the presence of 300 nM

CGP20712A (343-fold rightward shift, **Figure 3.1*A***). Such comparable shifts are expected based on standard receptor theory, which states that for a given competitive antagonist acting at a fixed concentration, the concentration ratio should be the same for all agonists acting through the receptors on which the antagonist acts. In line with this, the Schild plot for noradrenaline (represented by the blue asterisk) overlaps with that of isoprenaline in the presence of 300 nM CGP20712A (**Figure 3.5**).

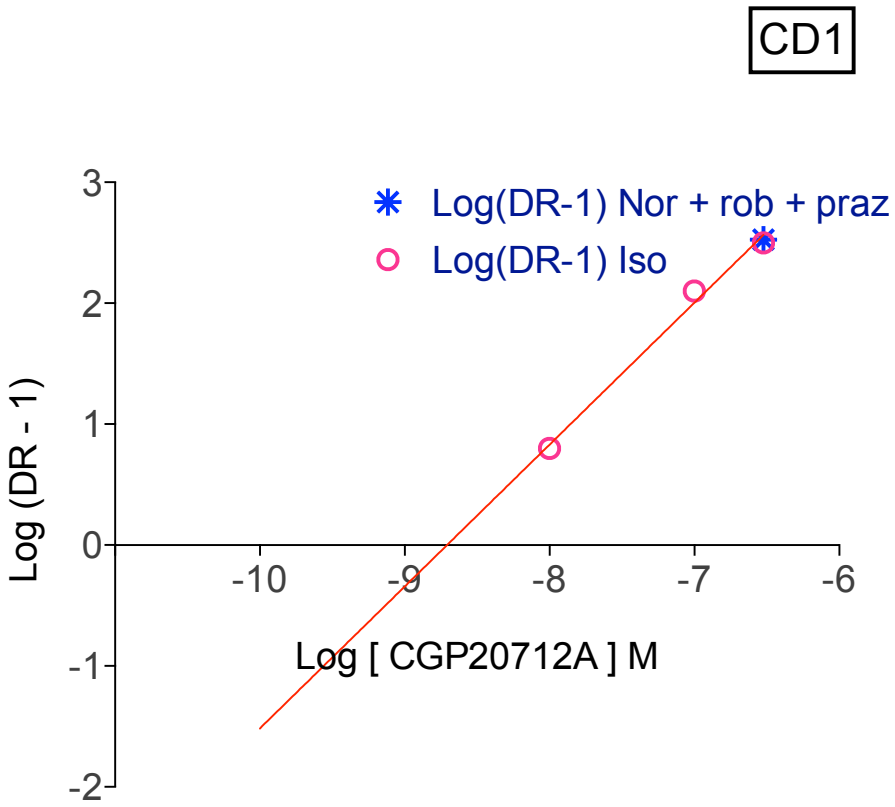


Figure 3.5 Data from **Figure 3.1*A*** were used to calculate dose ratios (DR), and Schild analysis was performed for antagonism of isoprenaline and noradrenaline by CGP20712A. The blue asterisk shows the log(DR-1) obtained with noradrenaline as the agonist in the presence of 1 μM reboxitine + 1 μM prazosin (data from **Figure 3.2)**. GraphPad Prism (version 5.0) software was used to perform statistical analysis.

CHAPTER 4: THE EFFECTS OF I_F AND SR CA^{2+} RELEASE INHIBITORS ON BASAL SPONTANEOUSLY BEATING RATE IN THE ABSENCE AND PRESENCE OF β_1-ADRENOCEPTOR STIMULATION WITH ISOPRENALINE.

4.1. Introduction

ZD7288, CsCl (Cs^+) and ivabradine were the treatments used to assess the contribution of I_f to the modulation of pacemaking. Cs^+ at 2 mM was shown by Denyer and Brown (1990) to reduce the basal spontaneous beating rate in isolated rabbit SAN cells by 30%. Earlier work by DiFrancesco (1981) in calf Purkinje fibers showed that Cs^+ inhibits I_f channels. Subsequent to that finding, the experimental drug ZD7288 was developed; at 1 μM ZD7288 selectively inhibited the I_f current by 75% without affecting other channels (BoSmith *et al.,* 1993). Presently, ivabradine is the only clinically used selective I_f channel blocker, with a high degree of use dependency (Bois *et al.,* 1996; Bucchi *et al.,* 2002). Like other I_f inhibitors, ivabradine slows down the heart rate by acting selectively on the steepness of diastolic depolarization (DiFrancesco and Camm, 2004).

There is an ongoing debate concerning the contribution of I_f in the generation of spontaneous depolarization in SAN cells, including discussion of voltage-dependence and threshold activation of the I_f current (Nakayama *et al.,* 1984; DiFrancesco *et al.,* 1991; Van Ginneken and Giles, 1991). Some authors, including DiFrancesco *et al.* (2010), believe that I_f is the driving force initiating pacemaking (see Chapter 1 for discussion). Therefore, one aim of my experiments was to assess the importance of the I_f channel in pacemaking.

Ryanodine and cyclopiazonic acid (CPA) were used to assess the contribution of mechanisms dependent on Ca^{2+} release from the SR in pacemaking. Ryanodine and CPA have been very useful experimental tools, as

they suppress Ca^{2+} release from the SR in a highly selective manner (Rousseau *et al.,* 1987; Meissner*,* 1994). Ryanodine is known to inhibit Ca^{2+} release by blocking the ryanodine receptor (Meissner, 1994), while CPA inhibits Ca^{2+} uptake by inhibiting SERCA activity (Seidler *et al.,* 1989; Yard *et al.,* 1994). Unlike CPA, ryanodine has a dual action; at lower concentrations (0.01 to 10 μM range) it increases Ca^{2+} release through the ryanodine channels, while at higher concentrations (10 to 300 μM) it blocks the ryanodine channels, preventing Ca^{2+} release from the SR (Lattanzio *et al.,* 1987).

The contribution of Ca^{2+} release from SR in SAN pacemaking was first assessed by Rigg and Terrar (1996). In their experiments, 2 μM ryanodine was used to reduce spontaneous beating in guinea pig SAN preparations by 45%. Similar observations were recorded when 100 μM CPA was added to the preparation. In contrast, Himeno *et al.* (2011) challenged the importance of cytosolic Ca^{2+} in pacemaking. Therefore, I set out to further assess the effect of Ca^{2+} release from the SR on pacemaking, using both mouse and guinea pig preparations.

The effect of Ca^{2+} release from the SR in the modulation of I_f channels was also assessed. Hagiwara *et al.* (1989) were the first to discover that the I_f current is influenced by changes in the intracellular Ca^{2+} concentration. They showed in patch-clamp recordings of the I_f channel at intracellular Ca^{2+} concentrations as low as 0.1 to 100 nM (which was assumed to be the physiological range), that there was an appreciable amount of I_f current present. It was further shown that the threshold potential of I_f channel activation was dependent on the intracellular concentration of Ca^{2+}. At concentrations of 0.1

nM and 100 nM, the channel conductance was activated at -60 mV and -40 mV, respectively. The activation of the I_f current was very steep within the physiological Ca^{2+} concentration range (0.1 to 100 nM), with I_f current being increased by approximately a factor of 2 when intracellular Ca^{2+} concentration was increased from 10 nM to 100 nM. The authors also ruled out the possibility of Ca^{2+} modulation of the I_f channel via the calmodulin (CaM) pathway, since the addition of 1 μM calmidazolium, a CaM inhibitor, did not affect the ability of Ca^{2+} to enhance the I_f current. On the contrary, using an inside-out macropatch, Zaza *et al.* (1991) did not see a direct effect of Ca^{2+} on the I_f current. In 2003, Rigg *et al.* further investigated the possible regulation of I_f by cytosolic calcium in guinea pig SAN cells using a perforated patch clamp technique to record I_f activated by hyperpolarizing voltage steps. It was shown that the effects of calcium seemed to depend on calmodulin and were not the result of direct activation of the HCN channel. Thus, it was speculated that a Ca^{2+}-sensitive AC might be involved in the underlying mechanism. Indeed, Terrar's group further characterized the regulation of I_f by cytosolic Ca^{2+} in 2007 using RT-PCR and immunoblotting with a specific antibody to show that both Ca^{2+}-stimulated AC isoforms (AC1 & AC8) were present in the SAN, but not in the ventricular muscle of guinea pig (Mattick *et al.,* 2007).

In 1977, Ohsumi's group reported that during tissue preparation, the concentration of cAMP in rabbit SAN cells was relatively higher than in atrial cells in the absence of β-adrenoceptor stimulation (Taniguchi *et al.,* 1977). Vinogradova *et al.* (2006) showed in rabbit SAN cells that elevated cytosolic cAMP caused upregulation of PKA activity, with modulation of pacemaking resulting from phosphorylation of the PKA target proteins. The inhibition of basal

PKA activity (15 μM, PKI) stopped the spontaneous beating in SAN cells (Vinogradova *et al.,* 2006). I also investigated the slowing effect of acetylcholine by assessing the contributions of PKA inhibition and activation of K_{ACh} on the basal spontaneous beating rate.

I also used various antagonists (H89, a PKA inhibitor; Tertiapin-Q, a K_{ACh} inhibitor) and agonists (isoprenaline, a β-adrenoceptor agonist; carbachol, a muscarinic agonist) to dissect the contributions of different components of the activation pathways linked to the β-adrenergic and cholinergic receptors in the contexts of I_f channel, Ca^{2+} release from the SR and K_{ACh} channels.

4.2. Results

4.3. Modulation of spontaneous beating rate at rest

4.3.1. The role of I_f at rest

Initially, the contribution of I_f, channels to spontaneous beating was assessed in the mouse and guinea pig atrial preparations. The atrial preparation was incubated for 30 min with 1 μM ZD7288. In the mouse, the basal spontaneous beating rate was reduced by 52 ± 5%, from a resting beating rate of 431 ± 14 bpm to 209 ± 14 bpm ($P < 0.05$, n = 9, **Figure 4.1*A***). In line with these observations, the guinea pig's basal spontaneous beating rate was reduced by 49 ± 4%, from a resting beating rate of 221 ± 13 bpm to 109 ± 14 bpm in the presence of 1 μM ZD7288 ($P < 0.05$, n = 6, **Figure 4.1*B***). In support of BoSmith *et al.'s* (1993) observation, an approximately 30 min incubation time was sufficient to attain the full action of ZD7288 (representative trace is presented in **Figure 2.3*C***), suggesting that with a time delay, ZD7288 is able to access SAN cells in a multicellular preparation.

4.3.2. The role of Ca^{2+} release from SR at rest

To evaluate the contribution of Ca^{2+} release from the SR on spontaneous beating, the atrial preparation was incubated with CPA or ryanodine. CPA and ryanodine suppress the SR function by blocking Ca^{2+} uptake and Ca^{2+} release from SR, respectively (Meissner, 1994; Yard *et al.,* 1994). Again, 30 min was

required for the full action of ryanodine and CPA to be reached, also suggesting that with a time delay, these drugs are able to access SAN cells in a multicellular preparation (typical representative traces are presented in **Figure 2.3*D*** & ***E***). In the presence of 100 μM CPA, the basal spontaneous beating in the mouse atrial preparation was reduced by 36 ± 4%, from 413 ± 19 bpm to 265 ± 14 bpm (*P* < *0.05*, n = 7, **Figure 4.1*A***). In the case of 30 μM ryanodine, spontaneous beating in the mouse atrial preparation was reduced by 25 ± 6%, from a resting beating rate of 425 ± 18 bpm to 320 ± 17 bpm (*P* < *0.05*, n = 6, **Figure 4.1*A***). In line with the observations in the mouse, spontaneous beating rate in the guinea pig preparation was reduced by 23 ± 4%, from a resting beating rate of 217 ± 13 bpm to 167 ± 14 bpm in the presence of 30 μM CPA (*P* < *0.05*, n = 6, **Figure 4.1*B***).

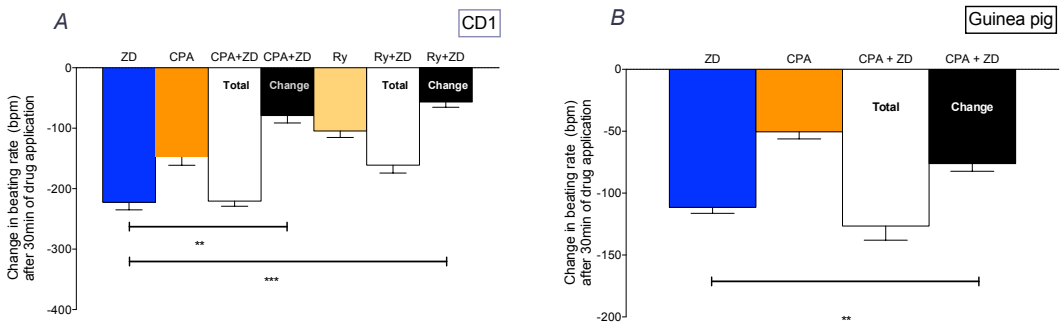


Figure 4.1 *(A)* Bar chart representing the mean effect of 1 μM ZD7288 (n = 9), 30 μM ryanodine (n = 6), 30 μM ryanodine in combination with 1 μM ZD7288 (n = 6), 100 μM CPA (n = 7) and 100 μM CPA in combination with 1 μM ZD7288 (n = 6) on basal spontaneous beating rate of mouse atrial preparations. *(B)* Bar chart representing the mean effect of 1 μM ZD7288 (n = 6), 30 μM CPA (n = 6) and 30 μM CPA in combination with 1 μM ZD7288 (n = 6) on basal spontaneous beating rate in guinea pig atrial preparations. 'Total' represents cumulative change from baseline, while 'Change' represents the relative change after ryanodine or CPA. Data are expressed as mean ± S.E.M., n = number of experiments. GraphPad Prism (version 5.0) software was used to perform statistical analysis, including Student's *t*-test, one-way ANOVA with Dunnett post-test (significance level *P* < *0.05*).

4.3.3. Effect of Ca^{2+} release from SR on I_f's modulation of basal beating rate

The effect of ZD7288 in reducing the spontaneous beating rate was investigated following inhibition of Ca^{2+} release with CPA or ryanodine. It became evident that suppression of Ca^{2+} release from SR reduced the effects of ZD7288 on the spontaneous beating rate. In the presence of 100 μM CPA or 30 μM ryanodine (incubating over 30 min), 1 μM ZD7288 applied over an additional 30 min time period reduced mouse spontaneous beating rate by 79 ± 13 bpm ($P < 0.05$, for comparison of effects of ZD7288 in the presence and absence of ryanodine, n = 6 for both datasets) and 57 ± 9 bpm ($P < 0.05$, for comparison of effects of ZD7288 in the presence and absence of CPA, n = 6 for both datasets), respectively. This was a significantly smaller reduction than seen with 1 μM ZD7288, which reduced mouse spontaneous beating rate on its own by 222 ± 13 bpm (**Figure 4.1*A***). In guinea pig atrial preparations, 1 μM ZD7288 applied over a 30 min time period in presence of 30 μM CPA (incubating over 30 min) reduced spontaneous beating rate by 76 ± 15 bpm (n = 6), again significantly lower than the 112 ± 12 bpm reduction in the absence of CPA (**Figure 4.1*B***).

4.3.4. Contribution of MDL-12,330A (AC inhibitor) to I_f's effect modulation of basal beating rate

In light of the above results I wanted to assess the influence of AC inhibition on the ability of ZD7288 to reduce spontaneous beating rate.

Pretreatment with 10 μM MDL-12,330A to inhibit all AC isoforms, including the Ca^{2+}-stimulated AC isoforms (AC1 and AC8), reduced the mouse basal beating rate from 443 ± 24 bpm to 131 ± 20 bpm (a reduction of 70 ± 4% expressed as % resting rate, $P < 0.05$, n = 6, **Figure 4.2**). Again, approximately 30 min was required to attain the full action of MDL-12,330A. In the presence of MDL-12,330A, addition of ZD7288 over a 30 min period did not produce a statistically significant further reduction (from 131 ± 20 to 107 ± 20 bpm, a reduction of 18 ± 4%, $P > 0.05$, n = 6). Any reduction was possibly due to residually active I_f channels (**Figure 4.2**).

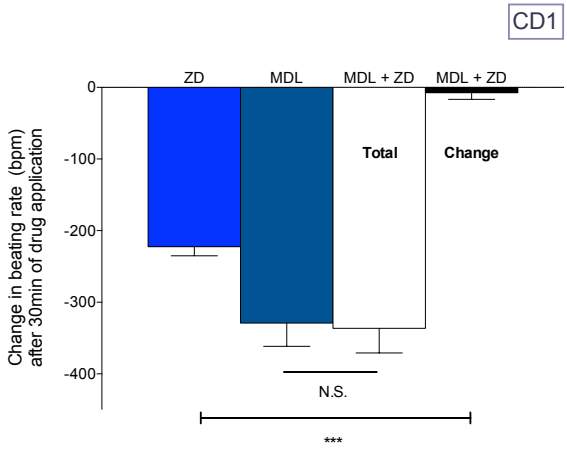


Figure 4.2. Bar chart representing the mean effect of 10 μM MDL-12,330A (n = 6), 1 μM ZD7288 (n = 9) and 1 μM ZD7288 in the presence of 10 μM MDL-12,330A (n = 6) on basal spontaneous beating rate of mouse atrial preparations. 'Total' represents cumulative change from baseline, while 'Change' represents the relative change after MDL-12,330A. Data are expressed as mean ± S.E.M., n = number of experiments. GraphPad Prism (version 5.0) software was used to perform statistical analysis, including Student's *t*-test (significance level $P < 0.05$).

4.3.5. Assessing effective concentration of I_f and SR inhibitors

In order to evaluate the selectivity of ZD7288 for I_f channels and to assess the extent of channel blockade, the concentration of ZD7288 was incrementally increased from 1 μM to 3 μM and then to 10 μM, with each concentration applied for 30 min. The initial reduction in mouse spontaneous beating rate caused by 1 μM ZD7288 was 253 ± 23 bpm ($P < 0.05$, compared to resting beating rate, n = 6), and the rate was further reduced by 46 ± 9 bpm ($P > 0.05$, one-way ANOVA, Dunnett post-test, for comparison effect of increasing the concentration of ZD7288 from 1 to 3 μM, n = 6) following the increase in concentration to 3 μM. Subsequently increasing the concentration to 10 μM marginally reduced the rate by 2 ± 6 bpm ($P > 0.05$, one-way ANOVA, Dunnett post-test, for comparison effect of increasing the concentration of ZD7288 from 3 to 10 μM, n = 6, **Figure 4.3*A***).

Like 1 μM ZD7288, Cs^+ has widely been used to inhibit I_f channels (DiFrancesco, 1981; Denyer and Brown, 1990; Bucchi *et al.,* 2002). Therefore, to assess whether ZD7288 induces near complete inhibition, I applied Cs^+ subsequent to pretreatment of the tissue with 1 μM ZD7288. Initially, the ability of Cs^+ to modulate basal spontaneous beating rate on its own was assessed by applying 2 mM Cs^+ to block I_f. This caused a reduction of mouse spontaneous beating rate from 424 ± 12 bpm to 264 ± 13 bpm (a reduction of 38 ± 3% expressed as % resting rate, $P < 0.05$, n = 9). The steady state for the effect of Cs^+ on beating rate was reached within five minutes. Pre-treatment of the preparation with 1 μM ZD7288 alone (over a 30 min time period) reduced the

initial basal beating rate from 368 ± 10 bpm to 154 ± 16 bpm (a reduction of 59 ± 4%, n = 6). Subsequent exposure to 2 mM Cs^+ caused a surprising *increase* in the spontaneous beating rate from 154 ± 16 bpm (ZD7288 alone) to 262 ± 9 bpm (ZD7288 and Cs^+), an increase of 108 ± 17 bpm (70 ± 3% increase, $P < 0.05$, n = 6, **Figure 4.3*C***). Next, in order to assess whether the increased beating rate induced by Cs^+ in the presence of ZD7288 might be linked to AC activity, the spontaneously beating mouse atrial preparation was pre-incubated with 10 μM MDL-12,330A together with 1 μM ZD7288 (over a 30 min time period). Exposure to MDL-12,330A/ZD7288 reduced the mouse basal beating rate from 443 ± 24 bpm to 107 ± 20 bpm ($P < 0.05$ n = 6). Interestingly, subsequent addition of 2 mM Cs^+ was not able to increase the beating rate (a change in the beating rate from 107 ± 20 to 110 ± 20 bpm, increase of 1 ± 1%, $P > 0.05$, n = 6; **Figure 4.3*D***).

Given the surprising result obtained with Cs^+, ivabradine was chosen as a different I_f inhibitor. Ivabradine is selective I_f blocker with little or no effect on other currents at 3 μM (Bois *et al.,* 1996; Bucchi *et al.,* 2002). The ability of ivabradine to further reduce beating rate in the presence of ZD7288 was therefore investigated (representative trace is presented in **Figure 2.3*F***). Ivabradine (3 μM) alone caused a reduction in beating rate of similar magnitude as that observed with 1 μM ZD7288 (mouse basal beating rate was reduced from 378 ± 17 bpm to 159 ± 21 bpm, a reduction of 219 ± 20 bpm or 58 ± 5%, $P < 0.05$, n = 10). Again, 30 min was sufficient to attain full action of the drug. However, in the presence of 1 μM ZD7288 (pre-incubated over 30 min), 3 μM ivabradine caused marginal change in beating rate (21 ± 5 bpm, $P > 0.05$, n = 8,

Figure 4.4*A*). Similarly, in guinea pig atrial preparations, 3 μM ivabradine had a statistically not significant effect in presence of 1 μM ZD7288. For preparations in which 1 μM ZD7288 reduced the rate by 112 ± 12 bpm from a resting beating rate of 221 ± 13 bpm to 109 ± 14 bpm ($P < 0.05$, n = 6, over a 30 min time period), subsequent addition of 3 μM ivabradine over 30 min only reduced the rate by 5 ± 30 bpm ($P > 0.05$, n = 6, **Figure 4.4*B***).

The concentration dependence of beating rate change in mouse intact SAN preparations was also assessed for CPA and ryanodine, which suppress Ca^{2+} release from SR. 30 μM CPA caused a reduction of spontaneous beating rate by 89 ± 11 bpm from 378 ± 18 bpm (a reduction of 23 ± 4% expressed as % resting rate, $P < 0.05$, n = 10, over a 30 min time period). 100 μM CPA caused a reduction of spontaneous beating rate by 177 ± 21 bpm from 380 ± 18 bpm ($P < 0.05$, n = 11, over a 30 min time period). Thus, 100 μM CPA caused a statistically significant additional reduction in the spontaneous beating rate relative to 30 μM CPA. In a similar manner, increasing ryanodine from 3 to 30 μM caused a statistically significant further reduction. At 3 μM, ryanodine reduced spontaneous beating rate by 38 ± 6 bpm, from 411 ± 15 bpm to 373 ± 13 bpm ($P < 0.05$, n = 6). In the presence of 30 μM ryanodine, spontaneous beating rate was reduced by 104 ± 10 bpm, from 409 ± 13 bpm to 305 ± 14 bpm ($P < 0.05$, n = 6). 30 min was required to attain the full action of CPA and ryanodine. With this time delay, the drugs were able to access SAN cells in a multicellular preparation (**Figure 4.3*B***).

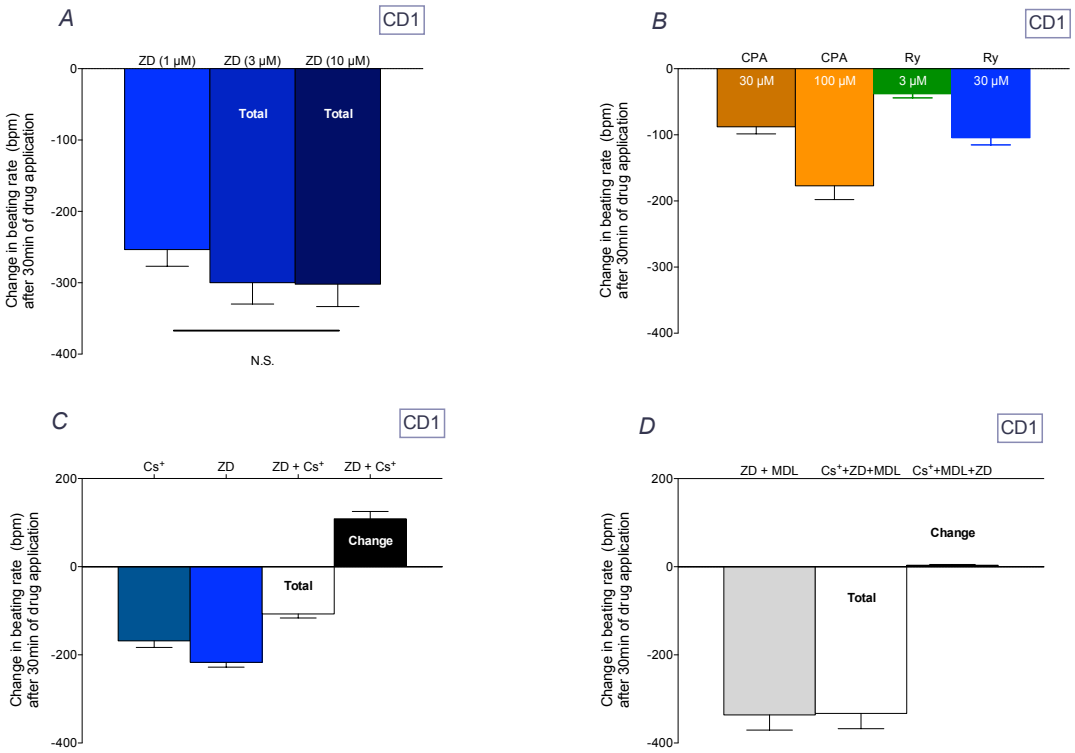


Figure 4.3 Bar chart representing the mean effects of ***(A)*** 1 µM ZD7288 (n = 6), 3 µM ZD7288 (n = 6) and 10 µM ZD7288 (n = 6); ***(B)*** 30 µM CPA (n = 10), 100 µM CPA (n = 11), 3 µM ryanodine (n = 6) and 30 µM ryanodine (n = 6); ***(C)*** 2 mM Cs^+ (n = 9), 1 µM ZD7288 (n = 6) and 1 µM ZD7288 in combination with 2 mM Cs^+ (n = 6); and ***(D)*** 10 µM MDL-12,330A together with 1 µM ZD7288 (n = 6) and 2 mM Cs^+ in the presence of 10 µM MDL-12,330A combined with 1 µM ZD7288 (n = 6) on basal spontaneous beating rate of mouse atrial preparations. 'Total' represents cumulative change from baseline, while 'Change' represents relative changes after 1 µM ZD7288 application. Data are expressed as mean ± S.E.M., n = number of experiments. GraphPad Prism (version 5.0) software was used to perform statistical analysis, including Student's *t*-test, one-way ANOVA with Dunnett post-test (significance level $P < 0.05$).

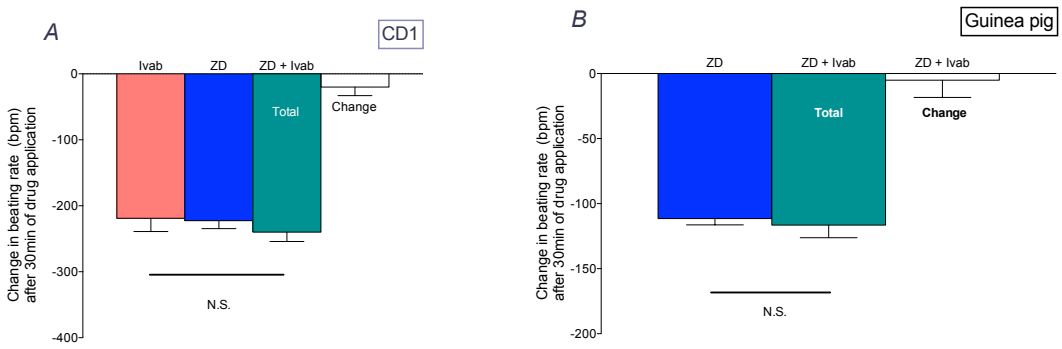


Figure 4.4 Bar chart representing the mean effect of ***(A)*** 1 μM ZD7288 (n = 9), 3 μM ivabradine (n = 10), and 1 μM ZD7288 in combination with 3 μM ivabradine (n = 8) on basal spontaneous beating rate of mouse atrial preparations; ***(B)*** 1 μM ZD7288 (n = 6) and 1 μM ZD7288 in combination with 3 μM ivabradine (n = 6) on basal spontaneous beating rate of guinea pig atrial preparations. 'Total' represents cumulative change from baseline, while 'Change' represents the relative changes after application of 1 μM ZD7288. Data are expressed as mean ± S.E.M., n = number of experiments. GraphPad Prism (version 5.0) software was used to perform statistical analysis, including Student's *t*-test (significance level $P < 0.05$).

4.4. Fluorescent Ca^{2+} transient measurements

4.4.1. Control

Possible modulation of the Ca^{2+} transient by the above drugs during their effects on pacemaking was investigated using fluorescent probes for Ca^{2+}. The effects of blockade of I_f and reduction of SR function using drugs alone and in combination were assessed under conditions in which the cytosolic Ca^{2+} transient was measured using a Ca^{2+} fluorescent probe (Rhod-2 AM, Lang *et al.,* 2011). In order to avoid movement artifacts, 10 μM blebbistatin was used to keep the atrial preparation static throughout the experiment (Lee *et al.,* 2011), as any movement would cause optical signal disturbance during Ca^{2+} transient

measurement. Blebbistatin selectively blocks contractile apparatus of cardiomyocytes, through binding to the ATPase intermediate of myosin head with ADP and phosphate bound at the active site. This prevents myosin from binding to actin (Kovacs *et al.,* 2004). Before proceeding with Ca^{2+} transient measurements, it was necessary to determine whether blebbistatin or Rhod-2 AM had any effects on the spontaneous basal beating rate of atrial preparations. An external electrode was placed near the pacemaker region of the atrial preparations in order to record the extracellular compound action potential signal. Incubation of spontaneously beating mouse atrial preparation with 10 μM blebbistatin, together with 4 μM Rhod-2 AM over 45 min, marginally reduced the rate of extracellular compound action potential by 17 ± 7 bpm (n = 11). This reduction in spontaneous beating in the mouse atrial preparation was compared with the reduction occurring after a 45 min period in the absence of drug pretreatment, which is statistically not significant ($P > 0.05$, **Figure 4.5*C***). In the absence of drugs, the reduction was 16 ± 7 bpm, (n = 8). These observations indicate that blebbistatin and Rhod-2 AM have little or no influence on pacemaker activity at the concentrations used. Therefore, for the optical recording of Ca^{2+} transients, Rhod-2 AM was incubated for 45 min prior to recording and 10 μM blebbistatin was present throughout the experiments to prevent movement artifacts.

In control experiments Ca^{2+} transient measurements were also carried out in order to assess the effect of Rhod-2 AM on Ca^{2+} handling. In the presence of Rhod-2 AM, the beating rate measured from the frequency of Ca^{2+} transients was reduced by 29 ± 5 bpm or 10 ± 1% ($P < 0.05$, n = 6, **Figure 4.5*C)*** after a 40 min time period. During this period, the Ca^{2+} transient amplitude

showed a decline of 36 ± 5% (*P* < *0.05*, n = 6), likely due to the extrusion of the Ca^{2+} probe, and/or possible dye photobleaching (**Figure 4.5*D***).

4.4.2. The role of I_f at rest assessed via Ca^{2+} transient measurements

In the presence of a combination of 1 μM ZD7288 and 3 μM ivabradine, the beating rate was reduced by 199 ± 15 bpm or 62 ± 3% (*P* < *0.05*, n = 7) after a 40 min time period (**Figure 4.5*C***). This is in line with the results obtained above in the absence of Rhod-2 AM. Over the same 40 min period, the Ca^{2+} transient amplitude was reduced by 45 ± 3%. This reduction was not statistically significantly different from observations in the absence of I_f inhibition (5 - 40 min, *P* > *0.05*, n = 6, two-way ANOVA with Bonferroni post-test, **Figure 4.5*D)***.

The isolated single SAN cells from guinea pig showed comparable results. In these experiments, Fluo-5F AM (5 μM) was used instead of Rhod-2 AM to record the Ca^{2+} transients. The single cell experiments were carried out in absence of blebbistatin, and the cells were incubated for 15 min at 36°C with Fluo-5F AM before observations began. In the presence of 1 μM ZD7288, the beating rate was reduced after 5 min of drug exposure by 173 ± 15 bpm or 78 ± 4% (*P* < *0.05*, n = 4, **Figure 4.5*E***). Over the same period of time, Ca^{2+} transient amplitude was reduced by 23 ± 5% (*P* < *0.05*, n = 4, **Figure 4.5*F***).

Taken together, the above observations are consistent with the idea that application of ZD7288/ivabradine does not have a major impact on the Ca^{2+} handling of the SAN system, as the drugs had no significant effects under the

experimental. However, upon closer inspection, a small enhancement of the rate of decline of the Ca^{2+} transient amplitude curve in presence of ZD7288/ivabradine relative to control cannot be ruled out (**Figure 4.5*D***). It is possible that such an effect could occur as a secondary consequence of the reduction in rate, leading to changes in Ca^{2+} handling (**Figure 4.5*D***).

4.4.3. The role of Ca^{2+} release from SR at rest assessed via Ca^{2+} transient measurements

Unlike the steady slow decline in Ca^{2+} transient amplitude over time observed in the presence and absence of I_f inhibitors (**Figure 4.5*D***), the application of CPA induced a rapid and pronounced reduction of the amplitude over the first 5 min (100 μM causing a reduction in amplitude of 57 ± 2%, $P < 0.05$, n = 6, whereas 30 μM reduced the amplitude by 48 ± 1%, $P < 0.05$, n = 4, **Figure 4.5*D***). Similarly, in isolated single cell guinea pig experiments, an initial rapid reduction was seen within the first 1 min, where application of 30 μM CPA reduced the amplitude by 44 ± 2% ($P < 0.05$, n = 4, **Figure 4.5*F***). This rapid reduction was most likely to be due to suppression of SR function via inhibition of Ca^{2+} uptake by SERCA (Seidler *et al.,* 1989). After the first 5 min in spontaneously beating mouse atrial preparations, the Ca^{2+} transient amplitude showed a further reduction, although the rate of change appeared to be more gradual, and this reduction was possibly due to dye extrusion and/or photobleaching (**Figure 4.5*D***). Over 40 min, the spontaneously beating atrial preparations showed a significant reduction in spontaneous rate in the presence of CPA (100 μM CPA reduced the rate by 129 ± 14 bpm, from a resting beating

rate of 299 ± 9 bpm to 170 ±14 bpm, or 43 ± 5%, P < 0.05, n = 6; and at 30 μM the rate was reduced by 99 ± 4 bpm, from 302 ± 12 bpm to 203 ± 12 bpm, or 33 ± 4%, n = 4, **Figure 4.5*C***). In isolated single cells guinea pig experiments, 30 μM CPA reduced the rate by 134 ± 7 bpm over a 5 min period (*P < 0.05*, n = 4, **Figure 4.5*E***).

4.4.4. Contribution of Ca^{2+} release from SR to I_f's modulation of basal beating rate assessed via Ca^{2+} transient measurements

In line with the organ bath studies (in the absence of Rhod-2 AM), the effect of the combination of 1 μM ZD7288 and 3 μM ivabradine was attenuated in the presence of 100 μM CPA (**Figure 4.5*C***). Addition of ZD7288/ivabradine in the presence of CPA reduced the spontaneous beating rate in the atrial preparation by 48 ± 10 bpm or 19 ± 3% (*P < 0.05*, for comparison of effects of ZD7288/ ivabradine in the presence and absence of CPA, n = 6 for both datasets) at 40 min post CPA incubation period. This was significantly lower than the reduction of 199 ± 15 bpm induced by ZD7288/ivabradine in absence of CPA (**Figure 4.5*C***). Also, over the same period, the Ca^{2+} transient amplitude was marginally reduced by 4 ± 2% (n = 6) following addition of ZD7288/ivabradine in the presence of 100 μM CPA (**Figure 4.5*D***).

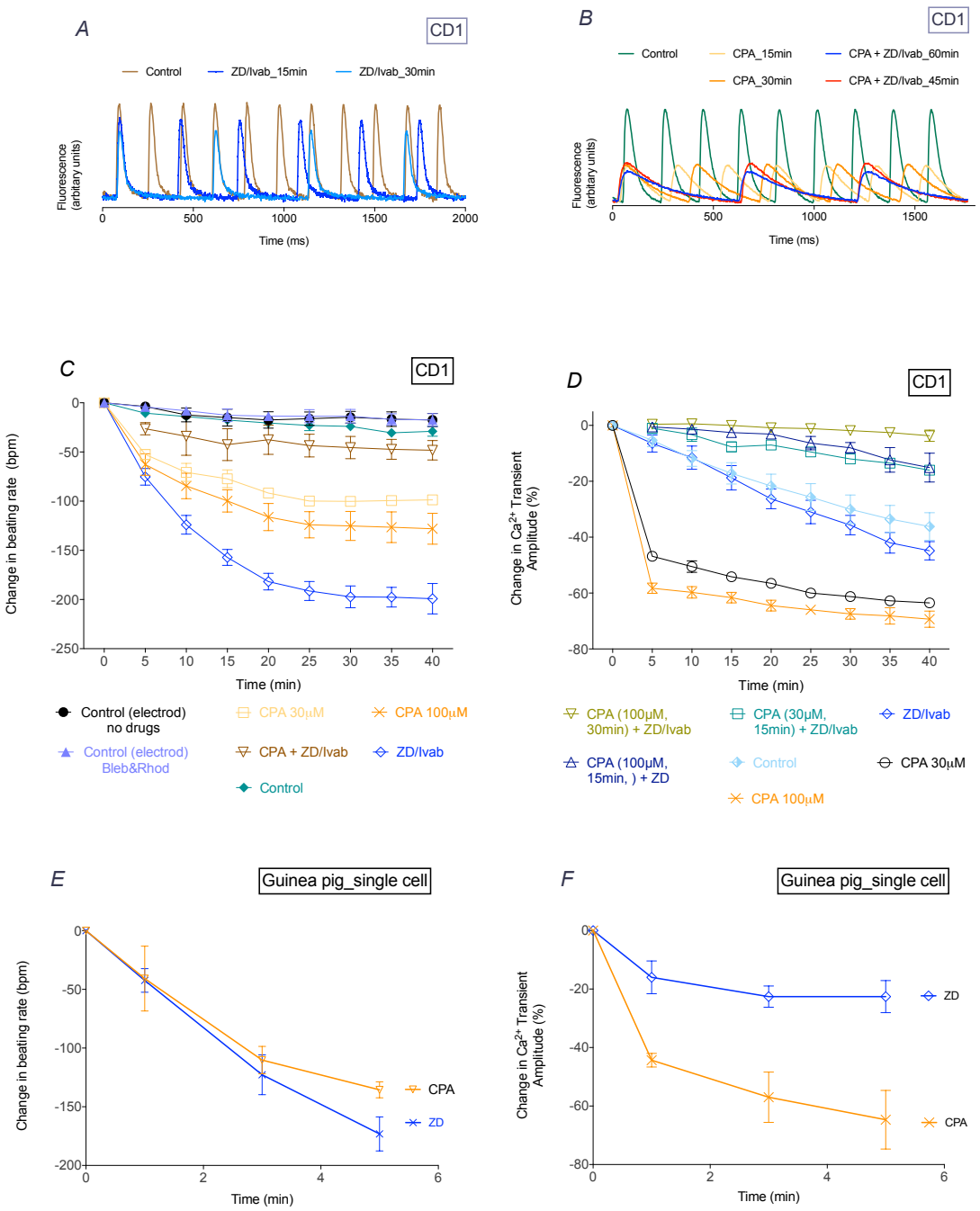


Figure 4.5 Representative traces of fluorescent Ca^{2+} transient measurements from the SAN region. ***(A)*** Control and 1 µM ZD7288 in combination with 3 µM ivabradine. ***(B)*** Control, 100 µM CPA, and 100 µM CPA in the presence of 1 µM ZD7288 in combination with 3 µM ivabradine. Graphs showing ***(C)*** the mean changes in rate of beating over time and ***(D)*** mean changes in amplitude of Ca^{2+} transients over the same time period in the presence of no drugs**,** control, (n = 6), 1 µM ZD7288 in combination with 3 µM ivabradine (n = 7), 30 µM CPA (n = 4), 100 µM CPA (n = 6) and 100 µM CPA in presence of 1 µM ZD7288/3 µM ivabradine (n = 6), measured from

the fluorescent Ca^{2+} transients recorded from the SAN region. Graphs showing ***(E)*** the mean changes in rate of beating over time and ***(F)*** mean changes in amplitude of Ca^{2+} transients over the same time period in the presence of 1 μM ZD7288 (n = 4) and 30 μM CPA (n = 4), measured from the fluorescent Ca^{2+} transients recorded from single SAN cells isolated from guinea pig. Data are expressed as mean ± S.E.M., n = number of experiments. GraphPad Prism (version 5.0) software was used to perform statistical analysis, including Student's t-test, and two-way ANOVA with Bonferroni post-test (significance level $P < 0.05$).

4.4.5. Effective time course and concentration of I_f and SR inhibitors assessed via Ca^{2+} transient measurements

To assess the concentration and the time period required by CPA to attenuate the actions of the ZD7288/ivabradine combination on beating rate, the effects of the drugs were tested with different combinations of incubation time and CPA concentration. Initially, the spontaneously beating mouse atrial preparation was incubated with 30 μM CPA for 15 min. 1 μM ZD7288 together with 3 μM ivabradine subsequently added for a further 40 min reduced the beating rate by 143 ± 20 ($P < 0.05$, n = 6, **Figure 4.6*A*)**. However, this was not substantially different from the 199 ± 15 bpm reduction induced by ZD7288/ivabradine alone (**Figure 4.5*C***). Over the 40 min period, the transient amplitude of Ca^{2+} was reduced by 15 ± 5% (**Figure 4.6*B***). Next, the above procedure was repeated with 100 μM CPA. This time, the effect of ZD7288/ivabradine in reducing beating rate was further dampened (rate reduced by 109 ± 12, $P < 0.05$, n = 7, **Figure 4.6*A***). This reduction was significantly lower than the response of ZD7288/ivabradine in the absence of CPA. Again, over the 40 min period, the transient amplitude of Ca^{2+} was

reduced by 15 ± 5% (**Figure 4.6*B***). Finally, 100 µM CPA was again applied and the pre-incubation time period was extended to 30 min. Under these conditions, the ZD7288/ivabradine combination in the presence of CPA reduced the rate by 48 ± 10 bpm or 19 ± 3% (*P < 0.05*, n = 6) at 40 min post 30 min incubation period with CPA (**Figure 4.6*A***). This was significantly lower than the 199 ± 15 bpm reduction induced by ZD7288/ivabradine in the absence of CPA. Over the same period, the Ca^{2+} transient amplitude was only marginally reduced by 4 ± 2% (n = 6) following addition of ZD7288/ivabradine in the presence of CPA (**Figure 4.6*A***).

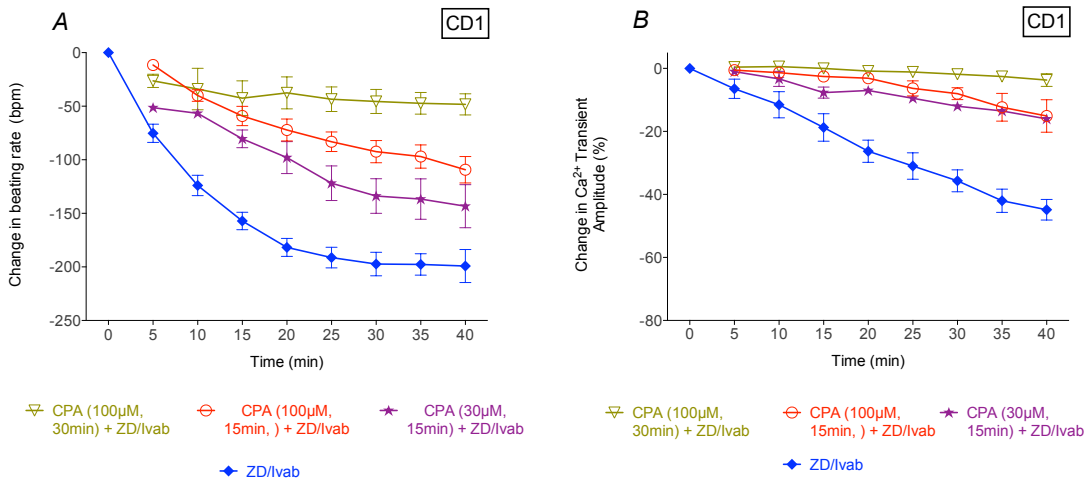


Figure 4.6 Graphs showing ***(A)*** the mean changes over time in rate of beating and ***(B)*** mean changes in amplitude of Ca^{2+} transients over the same time period in the presence of 1 µM ZD7288 in combination with 3 µM ivabradine in the presence of 30 µM CPA (15min pre-incubation, n = 6), 1 µM ZD7288 in combination with 3 µM ivabradine in the presence of 100 µM CPA (15 min pre-incubation, n = 7) and 1 µM ZD7288 in combination with 3 µM ivabradine in the presence of 100 µM CPA (30 min pre-incubation, n = 6), measured from the fluorescent Ca^{2+} transients recorded in the SAN region. Data are expressed as mean ± S.E.M., n = number of experiments. GraphPad Prism (version 5.0) software was used to perform statistical analysis, including Student's t-test and two-way ANOVA with Bonferroni post-test (significance level *P < 0.05*).

4.5. Modulation of β-adrenergic receptor-stimulated beating rate

4.5.1. The role of I_f in β-adrenergic pathway in mouse

A series of experiments were carried out with a range of blockers to investigate the contribution of I_f blockade and suppression of SR function on the spontaneous beating rate in the presence of β-adrenoceptor stimulation. 1-100 nM isoprenaline on its own caused a rapid increase in beating rate in mouse atrial preparation, and for each concentration, the effects reached a steady state within 2 min of exposure. At its maximum concentration of 100 nM, isoprenaline increased beating rate by 304 ± 41 bpm, from a basal rate of 380 ± 14 to 684 ± 22 bpm (an increase of 80 ± 3%, $P < 0.05$, n = 12; **Figure 4.7*A***).

When 1 - 100 nM isoprenaline was added to the spontaneously beating mouse atrial preparation in the presence of 1 μM ZD7288 (allowing 30 min pre-incubation for the preparations to reach a new reduced plateau steady state), the beating rate was reduced at each concentration and the reductions were all statistically significant compared to increase in the absence of 1 μM ZD7288 with the exception of the 1 nM concentration of isoprenaline (1 nM $P > 0.05$, 3 - 100 nM $P < 0.05$, two-way ANOVA with Bonferroni post-test, n = 6, **Figure 4.7*A***). When the log(concentration)-response curve was taken as a whole, there was also a statistically significant downward shift of the curve in the presence of 1 μM ZD7288 relative to control ($P < 0.05$, n = 6, **Figure 4.7*A***). At the highest concentration, 100 nM isoprenaline in the presence of 1 μM ZD7288, the beating rate was increased by 227 ± 21 bpm compared to a 303 ± 10 bmp

increase in the absence of 1 μM ZD7288. Pre-incubation with 1 μM ZD7288 together with 3 μM ivabradine (again, allowing 30 min pre-incubation time to reach new reduced plateau steady state) had a not significant effect that was very similar to that of 1 μM ZD7288 alone on the isoprenaline log(concentration)-response curve (**Figure 4.7*A***).

4.5.2. The role of Ca^{2+} release from SR in β-adrenergic pathway in mouse

Pretreatment with 30 or 100 μM CPA, followed by addition of 1 - 100 nM isoprenaline, reduced the increase in the mouse atrial beating rate at each concentration and the reductions were all statistically significant (1 - 100 nM, $P < 0.05$, two-way ANOVA with Bonferroni post-test, n = 13). Also when the isoprenaline log(concentration)-response curve was taken as a whole, there was a statistically significant downward shift of the curve in the presence of both 30 and 100 μM CPA relative to control ($P < 0.05$, n = 13). At its highest concentration of 100 nM, isoprenaline increased the beating rate by 193 ± 13 bpm (in presence of 100 μM CPA) and 173 ± 14 (in presence of 30 μM CPA) compared to a 303 ± 10 bmp increase in the absence of CPA. The difference between the curves produced in the presence of 100 μM CPA compared to 30 μM CPA was not statistically significant (**Figure 4.7*A***).

4.5.3. Contribution of Ca^{2+} release from SR and I_f combined on the β-adrenergic pathway in mouse

Incubation with 100 μM CPA followed by 1 μM ZD7288 reduced the isoprenaline-induced increase in the mouse atrial preparation spontaneous beating rate at each concentration of isoprenaline, and the reductions were all statistically significant (1 - 100 nM, $P < 0.05$, two-way ANOVA with Bonferroni post-test, n = 10). Also, when the isoprenaline log(concentration)-response curve was taken as a whole, there was a statistically significant downward shift of the curve in the presence of the 1 μM ZD7288 and 100 μM CPA combination relative to control ($P < 0.05$, n = 10). At its highest concentration of 100 nM, isoprenaline increased the beating rate by 51 ± 2 bpm compared to a 303 ± 10 bmp increase in the absence of 1 μM ZD7288 and 100 μM CPA (**Figure 4.7*A***).

4.5.4. The role of I_f in the β-adrenergic pathway in guinea pig

In line with the above described mouse experiments, similar observations were observed in guinea pig atrial preparations, even though the maximal bpm changes were generally smaller for the various drug combinations. 1 μM ZD7288 shifted the isoprenaline log(concentration)-response curve due to reductions in rate at all isoprenaline concentrations, and these rate reductions were all statistically significant, with the exception of the effect at 1 nM (1 nM $P > 0.05$, 3 - 100 nM $P < 0.05$,, two-way ANOVA with Bonferroni post-test, n = 6). Furthermore, combination of 1 μM ZD7288 and 3 μM ivabradine did not have any further substantial effects relative to the actions of 1 μM ZD7288 alone on

supressing the isoprenaline log(concentration)-response curve (1 - 100 nM, *P* > *0.05*, two-way ANOVA with Bonferroni post-test, n = 6). These observations indicate that 1 μM ZD7288 was sufficient to block the I_f channels. One thing to note is that substantial increases in spontaneous beating rate in response to isoprenaline were maintained in the presence of 1 μM ZD7288 alone or 1 μM ZD7288 combined with 3 μM ivabradine. At its highest concentration of 100 nM, isoprenaline increased the beating rate by 85 ± 16 bpm in the presence of 1 μM ZD7288 and by 88 ± 15 bpm in the presence of 1 μM ZD7288 & 3 μM ivabradine, compared to isoprenaline alone, which increased the rate by 132 ± 21 bpm (**Figure 4.7*B***).

4.5.5. Contribution of Ca^{2+} release from SR alone and in combination with I_f to β-adrenergic pathway in guinea pig

In the presence of 30 μM CPA, the isoprenaline log(concentration)-response curve from guinea pig atrial preparations was supressed at each concentration, with the exception of 1 nM (1 nM *P* > *0.05*, 3 – 100 nM, *P* < *0.05*, two-way ANOVA with Bonferroni post-test, n = 6). In presence of 30 μM CPA, the highest concentration of isoprenaline, 100 nM, increased the beating rate by only 57 ± 9 bpm. This was a significant reduction relative to the effect of isoprenaline alone, a 132 ± 21 bpm increase. Finally, in the presence of 30 μM CPA and 1 μM ZD7288, the isoprenaline log(concentration)-response curve was considerably supressed (1 - 100 nM, *P* < *0.05,* two-way ANOVA with Bonferroni post-test, n = 6), so that the response to the high concentration of

isoprenaline was reduced to an 8 ± 2 bpm increase compared to the control increase of 132 ± 21 bmp (**Figure 4.7*B***).

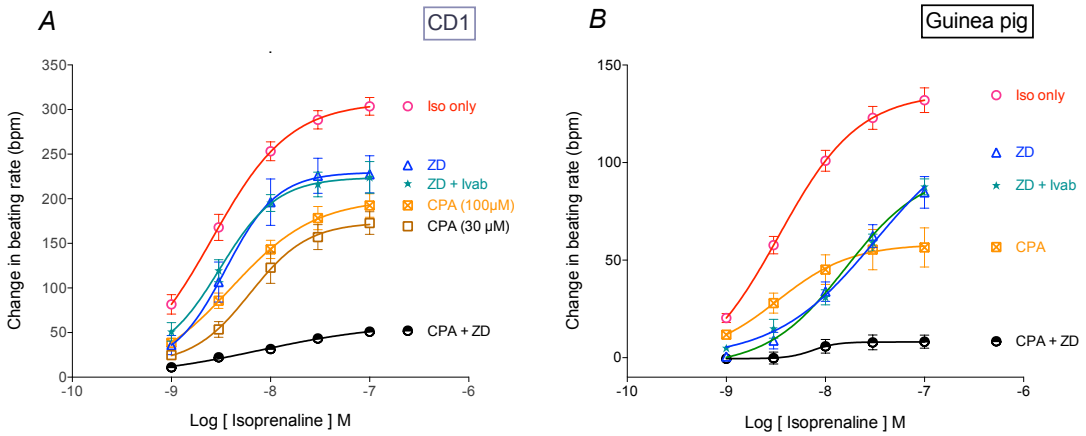


Figure 4.7 Graphs representing mean change in the positive chronotropic action of the β-adrenoceptor agonist isoprenaline by **(*A*)** 100 μM CPA (n = 13), 30 μM CPA (n = 13), 1 μM ZD7288 (n = 6), 1 μM ZD7288 in combination with 3 μM ivabradine (n = 6), and 1 μM ZD7288 in the presence of 100 μM CPA (n = 10) in the spontaneously beating mouse atrial preparation; **(*B*)** 30 μM CPA (n = 6), 1 μM ZD7288 (n = 6), 1 μM ZD7288 in combination with 3 μM ivabradine (n = 6) and 1 μM ZD7288 in the presence of 30 μM CPA (n = 6) in the spontaneously beating guinea pig atrial preparation. Data are expressed as mean ± S.E.M., n = number of experiments. GraphPad Prism (version 5.0) software was used to perform statistical analysis, including two-way ANOVA and Bonferroni post-test (significance level $P < 0.05$).

4.5.6. Contribution of PKA and I_f to pacemaking in the β-adrenergic pathway in mouse

In an attempt to dissect the different contributions of the PKA pathway and I_f to the chronotropic effects of β-adrenoceptor stimulation, H89 was used alone and in combination with ZD7288. Interestingly it was noted that inhibition of PKA together with 3 μM H89 had an asymmetrical effect, largely acting at the lower end of the isoprenaline log(concentration)-response curve. However, when H98 was combined with ZD7288, the isoprenaline log(concentration)-response curve was symmetrically supressed [with additional effects at the high concentration end of the log(concentration)-response curve].

Application of 1 - 100 nM isoprenaline increased the mouse basal spontaneous beating rate in a concentration dependent manner (reaching an increase of 261 ± 15 bpm at the highest concentration of 100 nM, n = 8). Pre-incubation with 3 μM H89 asymmetrically reduced the isoprenaline log(concentration)-response curve: statistically significant reductions were observed at the lower end of the curve (1 - 10 nM, $P < 0.05$; 30 nM & 100 nM, $P > 0.05$; two-way ANOVA with Bonferroni post-test, n = 8, **Figure 4.8*A***). In the presence of 3 μM H89, the highest concentration of isoprenaline (100 nM) increased the basal spontaneous beating rate by 258 ± 5 bpm, as compared to a 261 ± 15 bpm increase in the absence of 3 μM H89 (**Figure 4.8*A***). The largest attenuation in the isoprenaline log(concentration)-response curve was seen at the 3 nM concentration, where the rate only increased by 109 ± 8 bpm compared to 203 ± 13 bpm in absence of H89 (**Figure 4.8*A***).

Inhibiting both PKA together with I_f significantly reduced the isoprenaline log(concentration)-response curve at all the concentrations (1 - 100 nM, *P <0.001,* two-way ANOVA with Bonferroni post-test, n = 7). At the highest concentration of isoprenaline (100 nM) and in the presence of 3 μM H89 & 3 μM ivabradine, or 3 μM H89 together with 1 μM ZD7288 & 3 μM ivabradine, the rate only increased by 183 ± 14 bpm (n = 7) and 179 ± 10 bpm (n = 7), respectively. These effects were significantly lower than the response to isoprenaline alone (203 ± 13 bpm increase) (**Figure 4.8*A***). Also, as seen with previous experiments, inhibition of I_f with 1 μM ZD7288, either alone or in combination with 3 μM ivabradine, did not cause substantial changes in the isoprenaline log(concentration)-response curve in the presence of H89; no statistically significant difference was observed at any concentration of isoprenaline (*P >0.05*, two-way ANOVA with Bonferroni post-test, n = 7, **Figure 4.8*A***). These observations are also consistent with the suggestion that I_f channel inhibition in the presence of 1 μM ZD7288 was almost complete.

4.5.7. Contribution of PKA and I_f to pacemaking in mouse

The relative contributions of PKA and I_f to the control of spontaneous basal beating rate were also investigated in the absence of β_1-adrenoceptor stimulation. Initial pretreatment of mouse atrial preparations with 3 μM H89 caused a reduction of 116 ± 17 bpm, from 503 ± 15 bpm to 387 ± 17 bpm (a reduction of 31 ± 4 %, n = 6). Subsequent application of 1 μM ZD7288 & 3 μM ivabradine in combination further reduced the rate by 170 ± 10 bpm, from 387 ± 17 bpm to 215 ± 14 bpm (a reduction of 44 ± 3 %, *P < 0.05*, n = 6). This was

significantly smaller than the reduction of 284 ± 13 bpm by the ZD7288/ivabradine combination in the absence of H89 (n = 6, **Figure 4.8*B***).

Activation of β-adrenergic receptors with 30 nM isoprenaline increased the mouse spontaneous beating rate from 401 ± 19 to 638 ± 6 bpm (an increase of 37 ± 3%, expressed as % resting rate, $P < 0.05$, n = 13). Inhibition of PKA with 3 μM H89 reduced the mouse spontaneously beating rate from 439 ± 17 bpm to 327 ± 12 bpm (a reduction of 25 ± 2% expressed as % resting rate, $P < 0.05$, n = 13). Subsequent addition of 30 nM isoprenaline in the presence of 3 μM H89 increased the muse beating rate from 327 ± 12 bpm to 568 ± 9 bpm (an increase of 42 ± 2%, $P < 0.05$, n = 13). The inhibition of PKA did not significantly affect the chronotropic action of isoprenaline at 30 nM. Isoprenaline alone increased beating rate by 237 ± 18 bpm, and in the presence of H89, an increase of 241 ± 12 bpm was observed ($P > 0.05$, **Figure 4.8*D***). This is in line with the above dose response experiment observation that H89 asymmetrically attenuates the isoprenaline log(concentration)-response curve (**Figure 4.8*A***). 30 min was allowed for the full action of H89 to be reached.

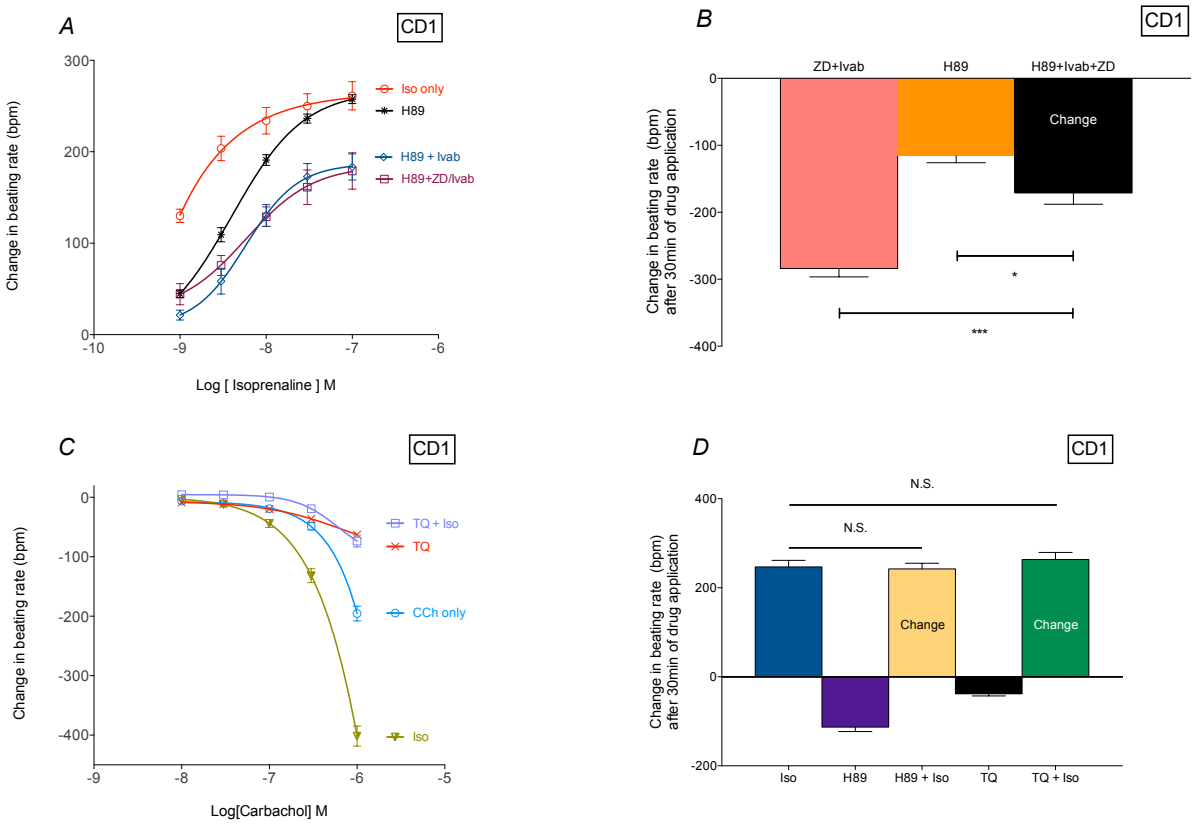


Figure 4.8. These data were collected in collaboration with Kamal Ibrahim (Terrar's group) (*A*) Graph representing mean change in the positive chronotropic action of the β-adrenoceptor agonist isoprenaline by 3 μM H89 (n = 8), 3 μM H89 in the presence of 3 μM ivabradine (n = 7) and 3 μM H89 in the presence of 1 μM ZD7288 + 3 μM ivabradine (n = 7) in the spontaneously beating rate mouse atrial preparation. ***(B)*** Bar chart representing the mean effect of 1 μM ZD7288 + 3 μM ivabradine (n = 6), 3 μM H89 (n = 6), and 1 μM ZD7288 + 3μM ivabradine in the presence of 3 μM H89 (n = 6) in the spontaneously beating mouse atrial preparation. ***(C)*** Graph representing mean change in the negative chronotropic action of the muscarinic receptor agonist CCh by 300 nM Tertiapin-Q (n = 7), 30 nM isoprenaline (n = 7) and 300 nM Tertiapin-Q in the presence of 30 nM isoprenaline (n = 7) on spontaneous beating rate in mouse atrial preparation. ***(D)*** Bar chart representing the mean effect of 30 nM isoprenaline (n = 13), 3 μM H89 (n = 13), 3 μM H89 in the presence of 30 nM isoprenaline (n = 13), 300 nM Tertiapin-Q (n = 20), and 300 nM Tertiapin-Q in the presence of 30 nM isoprenaline (n = 17) on the spontaneous beating rate in mouse atrial preparation. Data are expressed as mean ± S.E.M., n = number of experiments. GraphPad Prism (version 5.0) software was used to perform statistical analysis, including Student's t-test, one-way ANOVA with Dunnett post-test, two-way ANOVA with Bonferroni post-test (significance level $P < 0.05$).

4.6. Contribution of K_{ACh} to pacemaking

The components contributing to the negative chronotropic effects of stimulation of the muscarinic receptor signalling pathway by carbachol (CCh) were dissected using the pharmacological tools (Tertiapin-Q and isoprenaline). 10 - 1000 nM CCh on its own caused a decrease in spontaneous beating rate in mouse atrial preparation, with a new steady state for each concentration reached within 2 min of drug exposure. At its maximum concentration, 1000 nM, carbachol reduced beating rate by 195 ± 12 bpm from a basal rate of 411 ± 14 bpm (a decrease of 47 ± 3%, $P < 0.05$, n = 7, **Figure 4.8*C***). When the atrial preparations were pre-incubated with 30 nM isoprenaline to increase beating rate via activation of the β_1-adrenoceptor signalling pathway, the subsequent effects of CCh appeared to be larger than in the absence of isoprenaline, and the reductions were significantly larger at higher CCh concentrations in presence of isoprenaline compared to in the absence of isoprenaline (10 - 100 nM, $P > 0.05$; 300 - 1000 nM, $P < 0.001$; two-way ANOVA with Bonferroni post-test, n = 7). At its highest concentration, 1000 nM, CCh reduced the beating rate by 195 ± 12 bpm, compared to a 402 ± 17 bpm reduction in the presence of isoprenaline (**Figure 4.8*C***). Inhibition of K_{ACh} channels by 300 nM Tertiapin-Q attenuated the ability of CCh to reduce the beating rate. A statistically significant effect was only seen at the highest CCh concentration of 1000 nM. In the presence of Tertiapin-Q, 1000 nM CCh only reduced the beating rate by 63 ± 6 bpm relative to a 195 ± 12 bpm reduction on its own (10 - 300 nM, $P > 0.05$; 1000 nM, $P < 0.001$; two-way ANOVA with Bonferroni post-test, n = 7; **Figure 4.8*C***).

Next, in order to observe the contribution of the inhibition of K_{ACh} channels following β-adrenergic pathway stimulation on the CCh log(concentration)-response curve, the above experiments were repeated, but this time β-adrenergic receptors were stimulated with 30 nM isoprenaline following K_{ACh} channel inhibition. Under these conditions, the negative chronotropic effects of CCh were smaller at each concentration relative to when K_{ACh} channels were not inhibited by 300 nM Tertiapin-Q (**Figure 4.8*C***). However, the reductions were only statistically significant at the higher concentrations of CCh (10 & 30 nM, $P > 0.05$; 100 - 1000 nM, $P < 0.05$; two-way ANOVA with Bonferroni post-test, n = 7). In the presence of Tertiapin-Q and isoprenaline, 1000 nM, CCh reduced the beating rate by 73 ± 10 bpm. This was significantly lower than the 402 ± 17 bpm reduction when Tertiapin-Q was not present (**Figure 4.8*C***).

Activation of β-adrenergic receptors with 30 nM isoprenaline increased the spontaneous beating rate from 401 ± 19 to 638 ± 6 bpm (an increase of 37 ± 3%, expressed as % resting rate, $P < 0.05$, n = 13). Inhibition of K_{ACh} channels with 300 nM Tertiapin-Q reduced the spontaneously beating rate from 413 ± 13 bpm to 375 ± 10 bpm (a reduction of 9 ± 1% expressed as % resting rate, $P < 0.05$, n = 20). Subsequent addition of 30 nM isoprenaline in the presence of 300 nM Tertiapin-Q increased the beating rate from 375 ± 12 bpm to 638 ± 13 bpm (an increase of 41 ± 2%, $P < 0.05$, n = 17). However, Tertiapin-Q had no statistically significant effect on isoprenaline's positive chronotropic action. Isoprenaline alone increased beating rate by 237 ± 18 bpm, and in the presence of Tertiapin-Q, an increase of 264 ± 16 bpm was observed ($P > 0.05$,

Figure 4.8*D*). Approximately 30 min were allowed for the full action of Tertiapin-Q to be attained (Benavides-Haro *et al.,* 2003; Bolter and English, 2008).

4.7. Discussion

4.7.1. The role of I_f at rest

The results show that the basal spontaneous beating rate in both mouse and guinea pig atrial preparations is substantially reduced in the presence of I_f channel inhibition. 1 μM ZD7288 reduced the basal spontaneous beating rate by 222 ± 13 bpm (52 ± 5%) in mouse (**Figure 4.1*A***) and by 112 ± 12 (49 ± 4%) in guinea pig (**Figure 4.1*B***). In line with the organ bath atrial preparation results, the beating rate in intact mouse SAN preparations and isolated single SAN cells from guinea pig was reduced in the presence of 1 μM ZD7288 + 3 μM ivabradine, and 1 μM ZD7288B alone, by 199 ± 15 bpm (62 ± 3%, **Figure 4.5*C***) and 173 ± 15 bpm (78 ± 4%, **Figure 4.5*E***), respectively. The percentage change for the intact mouse SAN preparation was marginally larger compared to organ bath preparation; this is because the incubation temperature was kept at 34°C instead of 37°C, since even a small reduction in temperature is known to reduce extrusion of the Ca^{2+} probe. Thus, basal beating rates were slightly lower in mouse SAN preparations. Overall, the results from both species indicate that I_f channels make a substantial contribution to the basal spontaneous beating rate.

The above results support DiFrancesco's view on the importance of I_f channels in driving pacemaking and acting as a major contributor in determining the rate of diastolic depolarization in the SAN, even in the absence of β-adrenergic stimulation (DiFrancesco 2010). However, I do not support the view that the I_f channel is obligatory for pacemaking. This is because the inhibition of

I_f channels does not cause beating to cease, although it does substantially reduce the beating rate by 222 ± 13 bpm (52 ± 5%) in mouse (**Figure 4.1*A***) and by 112 ± 12 (49 ± 4%) in guinea pig (**Figure 4.1*B***). This finding supports previous experiments in mouse isolated SAN that showed a 50% increase in AP cycle length upon application of 3 μM ZD7288 (Liu *et al.,* 2008) and a 20% reduction in basal beating rate of the atrial preparation when exposed to 1 mM Cs^+ (Choate *et al.,* 2003). My results are also in line with BoSmith *et al.'s* (1993) observation in guinea pig SAN cells that 1 μM ZD7288 reduced the I_f current by 75% and did so without affecting voltage-gated Ca^{2+} or K^+ channels.

The effects of Cs^+ and ZD7288 in reducing the basal beating rate in other mammalian species support the above findings. However, the contribution of I_f at rest appears to be more significant in mice and guinea pig than in some other mammalian species. 2 mM Cs^+ reduced beating frequency by 21% in isolated working rabbit heart. 0.64 μM ZD7288 decreased beating rate by 38% in isolated working rabbit heart (Leitch *et al.,* 1995). Also, Gao *et al.,* (2011) showed that the 3 μM ZD77822 dramatically reduced I_f current in canine single SAN cells. The apparent difference in I_f contribution between species may be explained by differences in I_f channel density, as mouse SAN cells have a substantially higher I_f density relative to rabbit and canine SAN cells (Mangoni *et al.,* 2001; Gao *et al.,* 2011).

4.7.2. The role of Ca^{2+} release from SR at rest

The mouse atrial preparation's basal spontaneous beating rate was substantially reduced to similar extents by 30 μM ryanodine and 100 μM CPA, a sarcoendoplasmic reticulum Ca^{2+} ATPase (SERCA) blocker. 100 μM CPA reduced mouse basal beating rate by 148 ± 13 bpm (36 ± 4%), while in the case of 30 μM ryanodine, the mouse spontaneous beating rate was reduced by 105 ± 11 bpm (25 ± 6%) (**Figure 4.1*A***). In the guinea pig spontaneously beating atrial preparation, 30 μM CPA reduced the rate by 50 ± 14 bpm (23 ± 4%, **Figure 4.1*B***). Similar figures were deduced from Ca^{2+} transient measurements. 100 μM CPA reduced mouse beating rate by 129 ± 14 bpm (43 ± 5%), and 30 μM CPA reduced the rate by 99 ± 4 bpm (**Figure 4.5*C***). Also, in isolated single cell from guinea pig, 30 μM CPA reduced the rate by 134 ± 7 bpm (60 ± 4%, **Figure 4.5*E***). These results imply that Ca^{2+} from the SR store makes a substantial contribution to the basal spontaneous beating rate.

These observations support Rigg and Terrar's (1996) view on the importance of Ca^{2+} from SR in driving pacemaking and contributing to the determination of the diastolic depolarization rate in the SAN. When 2 μM ryanodine was added to spontaneously beating guinea pig SAN preparations, the rate of beating was reduced from 225 to 125 bpm, a reduction of 56%, while 30 μM CPA reduced the rate by 37% (Rigg and Terrar, 1996). I also support Lakatta's view on the importance of Ca^{2+} sparks in driving pacemaking. However, I do not support the view that Ca^{2+} sparks are the primary drivers of diastolic depolarization. This is because following the inhibition of Ca^{2+} sparks by 100 μM CPA, the frequency of beating was substantially reduced, but

beating did not cease. In support of this observation, Sanders *et al.* (2006) showed that in guinea pig SAN cells, 100 μM CPA suppresses Ca^{2+} sparks, resulting in a reduction in beating rate, but not cessation of beating.

My findings support previous experiments in mouse atrial and isolated SAN cells preparations, which showed a 64% and 55% decrease following the application of 2 μM ryanodine and 3 μM ryanodine on atrial preparations, respectively (Nikmaram *et al.,* 2008; Terrar group - unpublished data). Furthermore, treatment of mouse single SAN cells with 1 μM ryanodine reduced the basal rate by 60% (Wu *et al.,* 2009). Similar results were obtained in guinea pig single SAN cells, whereby application of 100 μM CPA reduced the basal beating rate by 45% (Rigg *et al.,* 2000). Also, 2 μM ryanodine marginally reduced basal SAN automaticity by 14% in isolated dog SAN cells (Gao *et al.,* 2010).

In contrast, in 2010, Noma's group challenged the importance of cytosolic Ca^{2+} transients (LCR) in pacemaker rhythm. Following rupture of the perforated patch membrane, where BAPTA was introduced into isolated guinea pig SAN cells (indicated by the arrow in **Figure 4.9**), generation of AP did not cease (Himeno *et al.,* 2011). However, Lakatta's group then challenged this result. Careful observation of the result in **Figure 4.9**, implies contraction following rupture of the membrane, where the length of the cells becomes transiently shorter before eventually reaching basal levels. This was proposal by Lakatta to be due to seal leakage, as extracellular Ca^{2+} would provide the background for APs to be generated. In my opinion, Lakatta's challenge is likely correct, as Sanders *et al.* (2006) and Vinogradova *et al.* (2000) observed that

generation of AP and spontaneous beating stopped following the application of BAPTA. Sanders also used the cell-permeable BAPTA (AM-BAPTA), which can be introduced into the intracellular environment without rupturing the membrane. Further convincing evidence has recently come from a study in which Himeno *et al.'s* (2011) experimental conditions were repeated by Capel *et al.* (2015). The addition of 10 mM BAPTA to the patch pipette led to prompt cessation of rhythmic generation of AP within 5.5 s following patch rupture. An additional experiment could also be carried out to see whether UV-induced activation of the Ca^{2+}-chelating agent Diazo-2 can be utilized to determine whether rapid buffering of cytosolic Ca^{2+} slows the pacemaker to below its baseline.

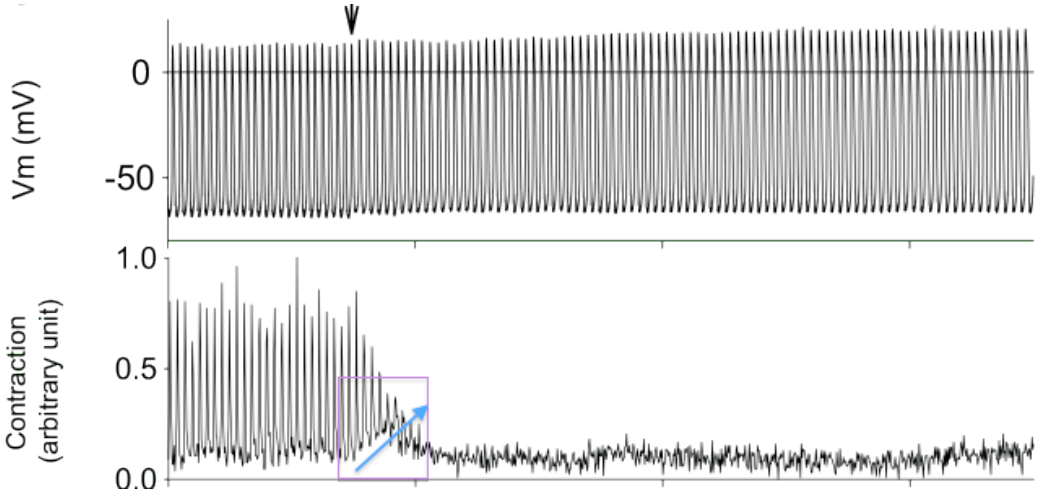


Figure 4.9 Effects of BAPTA on AP and contraction in SAN cells. One can see a contraction following rupture of the membrane, where the length of the cells becomes transiently shorter before eventually reaching basal level. This was said to be due to seal leakage, as extracellular Ca^{2+} would provide the background for APs to be generated and beating to occur [permission was granted by the American Physiological Society to reproduce **Figure 4.9**, Himeno *et al.,* (2011)].

4.7.3. Contribution of Ca^{2+} release from SR to I_f's modulation of basal beating rate

I tested the possibility that the influence of Ca^{2+} release from SR stores on SAN cell automaticity could partly be a result of modulation of I_f, through activation of Ca^{2+}-stimulated AC, leading to an increase in cytosolic cAMP.

The results suggest that both I_f channels and Ca^{2+} released from SR stores are important contributors to pacemaking in its basal state. However, in the presence of 100 μM CPA or 30 μM ryanodine, the effects of 1 μM ZD7288 on the mouse spontaneous beating rate were reduced: 1 μM ZD7288 in the presence of 100 μM CPA or 30 μM ryanodine (pre-incubation for 30 min) only reduced spontaneous beating rate by 79 ± 13 bpm and 57 ± 9 bpm, respectively. This is a significantly smaller reduction relative to the ability of 1 μM ZD7288 to reduce spontaneous beating rate on its own by 222 ± 13 bpm (**Figure 4.1*A***). In guinea pig spontaneous beating rate, the effect of 1 μM ZD7288 was also significantly attenuated in the presence of 30 μM CPA, with a reduction of 76 ± 15 bpm, which was again significantly lower than the 112 ± 12 bpm reduction in the absence of CPA (**Figure 4.1*B***). In line with the above observations, the results deduced from Ca^{2+} transient measurement experiments in mouse atrial SAN preparation showed a reduced effect of 1 μM ZD7288/ 3 μM ivabradine in the presence of CPA. Addition of ZD7288/ivabradine in the presence of CPA reduced the rate by 48 ± 10 bpm or 19 ± 3%, post CPA incubation. This is a significantly lower reduction than the 199 ± 15 bpm reduction induced by ZD7288/ivabradine in the absence of CPA (**Figure 4.5*C***). These findings suggest that calcium release from the SR Ca^{2+}

store is a major component contributing to the basal beating rate through modulation of I_f channels.

Results from the present experiments are in contrast to the observations of Gao *et al.,* (2011), who showed that 2 μM ryanodine did not significantly alter I_f current in dog SAN cells, using conventional patch clamp recording. Furthermore, past conventional voltage clamp experiments have shown that the I_f current is only fully active at -100mV (DiFrancesco *et al.,* 1986). As the SAN membrane potential only reaches approximately to -60 mV, this means that under basal conditions, the channels are not fully active. These observations have challenged the importance of I_f channels in the absence of β-adrenoceptor stimulation. However, as shown in the present study, the inhibition of I_f channels significantly reduced beating rate (60%) in the absence of β-adrenoceptor stimulation. Moreover, early experiments by Hagiwara *et al.* (1989) showed that for patch-clamp recordings of the I_f channel at intracellular Ca^{2+} concentrations as low as 0.1 to 100 nM (which was assumed to be the physiological range), an appreciable amount of I_f current was present (**Figure 4.10**). It was also shown that the threshold potential of I_f channel activation was dependent on the intracellular concentration of Ca^{2+}. At concentrations of 0.10 nM and 100 nM, the channel conductance was activated at -60 mV and -40 mV, respectively. The authors also ruled out the possibility of Ca^{2+} modulation of I_f channels via the calmodulin (CaM) pathway, since the addition of 1μM calmidazolium, a CaM inhibitor, did not affect the ability of Ca^{2+} to enhance the I_f current.

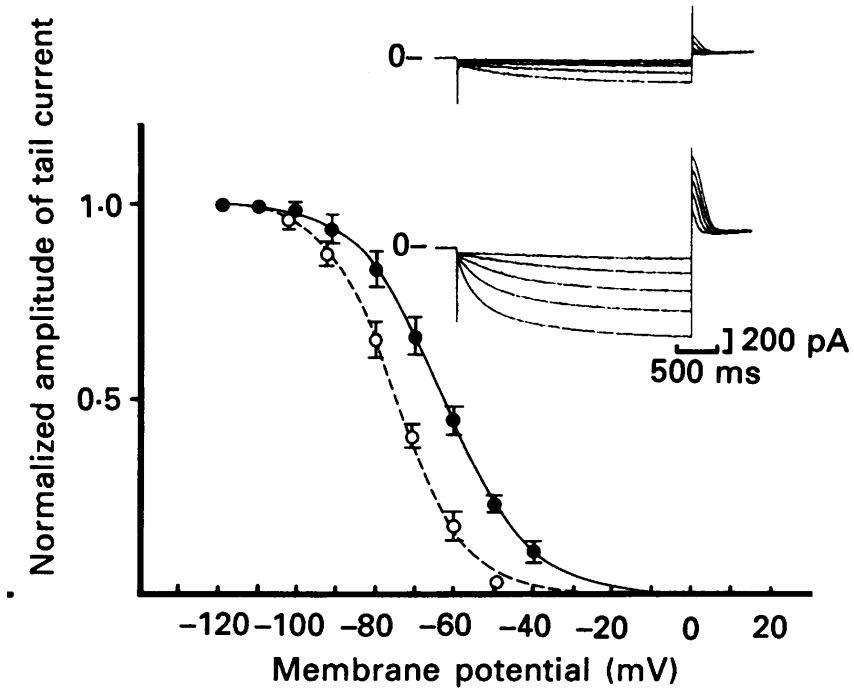


Figure 4.10. Effects of internal Ca^{2+} on the activation curve of I_f. The normalized amplitudes of the I_f tail current in twenty-one different cells are plotted against various membrane potentials. The activation curve shifted approximately 13 mV in a positive direction at pCa 7. The inset shows the I_f recorded with hyperpolarizing pulses between -40 and -80 mV at pCa 10 (above) and pCa 7 (below) in the pipette solution [permission was granted by Copyright Clearance Center to reproduce **Figure 4.10**, Hagiwara *et al.,* (1989), license number: 3830321299683]

Nevertheless, it is crucial to note that in those experiments, the I_f current was increased by approximately a factor of 2 when the intracellular Ca^{2+} concentration was increased from 10 nM to 100 nM (**Figure 4.11**). Thus, the activation of I_f current is very steep within the physiological Ca^{2+} concentration range.

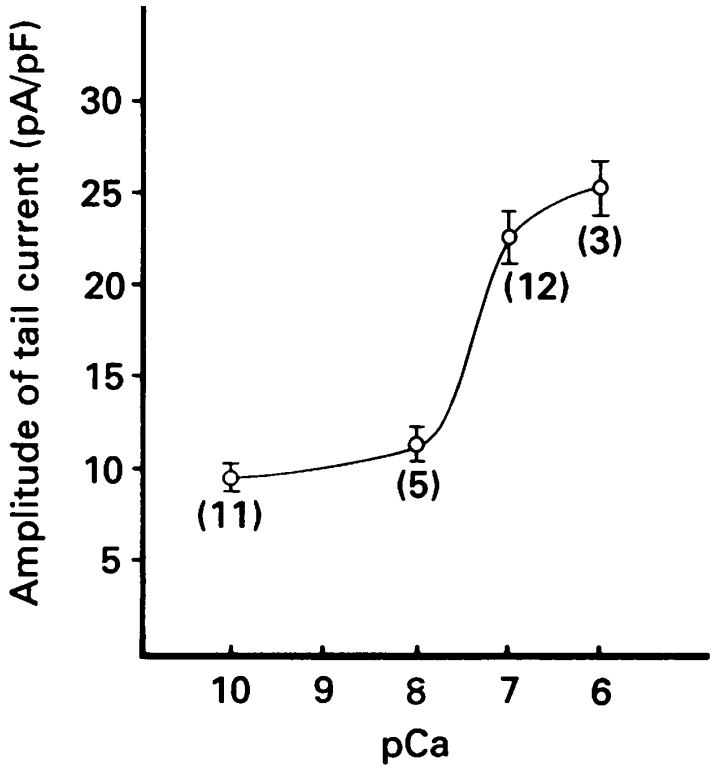


Figure 4.11 Dose-response relationship of I_f amplitude. The tail amplitudes of I_f are plotted against four different Ca^{2+} concentrations within the pipette in twenty-eight different cells. I_f was fully activated at -110 mV and the tail current was recorded at 20 mV. The numerals in parentheses below the curve indicate the number of experiments. I_f increased by 99 ± 7% between pCa 8 and 7, but increased only by 18 ± 5% between pCa 10 and 8. The curve was fitted by eye [permission was granted by Copyright Clearance Center to reproduce **Figure 4.11**, Hagiwara *et al.,* (1989), license number: 3830321299683]

However, as calmidazolium has been used at a range of concentrations up to 100 μM in subsequent experiments in cardiac myocytes (Colston J *et al.,* 1994; Nitta J *et al.,* 1994). Thus the 1 μM calmidazolium used by Hagiwara may not have been large enough to cause significant suppression of calmodulin-dependent pathways. In 2003, Rigg *et al.* showed that loading the guinea pig SAN cells with CaM antagonists (10 μM W-7; 25 μM calmidazolium)

caused a reduction in I_f amplitude by 69%, which was similar to when cells were loaded with BAPTA-AM. However, KN-93 (a CaMKII inhibitor) did not affect I_f, indicating that both Ca^{2+} and calmodulin are involved in I_f modulation via calmodulin (that is independent of CaMKII). Furthermore, when SAN cells were exposed to BAPTA in the presence of W-7, there was no significant change in I_f amplitude, indicating that the effects of Ca^{2+} act through calmodulin and not via direct activation of the I_f channel. Thus, it was speculated that a Ca^{2+}-sensitive AC might be involved in the underlying mechanism. In subsequent studies, it was shown that the Ca^{2+}-stimulated ACs (isoforms AC1 and AC8) in SAN cells are responsible for providing background production of cAMP (Mattick *et al.,* 2007).

It is important to note that the dependence of the I_f current on Ca^{2+} is at its steepest at concentrations of 10 to 100 nM cytosolic Ca^{2+}. Since Hagiwara *et al.* (1989) obtained this result through whole-cell patch recordings, and because Ca^{2+} stimulates AC8 and AC1 to produce cAMP, it might be questioned how much of the cAMP was being dialysed from the cytosol into the patch pipette during the experiment. Indeed, in rabbit SAN cells, Zaza *et al.* (1997) demonstrated that when using an action potential clamp, which maintains normal Ca^{2+} entry and extrusion, and a perforated patch technique, which would increase resistance to dialysis of cytosolic contents into the pipette, the amplitude of I_f was substantially larger than that observed by Hagiwara in standard whole-cell patch recordings. Thus, the I_f current may have even further underestimated the contribution of Ca^{2+} in modulating I_f current via stimulation of Ca^{2+}-stimulated ACs. Although it might be that Ca^{2+}-stimulated ACs are co-localised in the plasma membrane, as shown by Mattick *et al.* (2007), cAMP

could still dialyse from the cytosol into the pipette's solution. More importantly, experiments by Sanders *et al.* (2006) revealed that in spontaneously beating SAN cells, cytosolic Ca^{2+} concentration between beats is maintained at a higher level (225 nM) than in resting myocardial cells. Thus, even if cAMP is dialyzed, the fact that the physiological cytosolic Ca^{2+} concentration is much higher than previously thought (225 vs. 100 nM) implies that the I_f current would be higher than that suggested by Hagiwara.

It is also crucial to consider that under conventional step voltage clamping, where the membrane potential is held at -40 mV, the Ca^{2+} channels (L-type and T-type) are induced to be in their closed state, and this prevents the influx of Ca^{2+} into the cell that would normally occur during the action potentials occurring with spontaneous activity, thus reducing the cytosolic Ca^{2+} concentration directly and also indirectly via prevention of the CICR mechanism through ryanodine receptors. It is known that when the cell is kept in a quiescent state via conventional voltage clamp (at -40 mV), the cytosolic Ca^{2+} level decreases, and this most likely reduces the activity of Ca^{2+}-stimulated ACs, subsequently reducing cytosolic cAMP levels. Currently, Terrar's group is investigating this premise. If proven correct, it could explain Gao *et al.*'s (2011) contrasting observation, where inhibition of Ca^{2+} release from the SR by ryanodine did not affect the I_f current in single cell recordings. There would not be any spontaneous Ca^{2+} release because the CICR mechanism would be suppressed due to a drop in cytosolic Ca^{2+} level, and ryanodine would therefore not have any effect on Ca^{2+} release from SR stores.

4.7.4. The role of PKA at rest

So far, I have observed the modulation of I_f channels by Ca^{2+} release from SR stores, but it cannot be ruled out that elevated cAMP levels may upregulate PKA activity and increase PKA-dependent phosphorylation. Also, cAMP can directly modulate the I_f channels.

Inhibition of PKA through incubation of the atrial preparation with 3 μM H89 reduced the basal spontaneous beating rate by 113 ± 10 bpm **(Figure 4.8*B***). This observation is consistent with the suggestion that PKA plays a role in the generation of the basal beating rate. There are numbers of proteins known to be involved in pacemaking and which PKA phosphorylates in the basal state. These include voltage-gated L-type Ca^{2+} channels (De *et al.,* 1996; Sculptoreanu *et al.,* 1993), voltage-gated K^+ channels (K_s) (Lei *et al.,* 2002), and phospholamban (Li *et al.,* 1990; Mundina *et al.,* 1996). Phosphorylation of voltage-gated Ca^{2+} and K^+ channels results in increased Ca^{2+} influx and K^+ efflux, respectively, directly contributing to a positive chronotropic effect by shortening the duration of the AP. Phosphorylation of phospholamban increases the filling rate of the SR (due to disinhibition of the sarcoplasmic reticulum Ca^{2+}-ATPase), allowing the extra influxed Ca^{2+} to be pumped in. This would subsequently overload the SR stores with Ca^{2+} and increase the rhythmic releases of Ca^{2+} (Ca^{2+} sparks), which, through stimulation of sodium-calcium exchange (NCX), would also significantly contribute to membrane depolarization and pacemaking in SAN cells.

Vinogradova *et al.* (2006) revealed the presence of high cAMP levels in the SA node but not in rabbit ventricles or atria. However, this was first observed by Ohsumi's group in 1977, who reported that during tissue preparation, the concentration of cAMP was relatively higher in the rabbit SAN relative to atrial cells in the absence of β-adrenoceptor stimulation (Taniguchi *et al.,* 1977). Through experimental evidence, Vinogradova linked the generation of LCR to elevated cAMP concentrations in SAN cells by showing that inhibition of basal PKA activity (15 μM, PKI) abolishes LCR and spontaneous beating. It was suggested that this result may override the notion that cAMP imposes its effect via the I_f channel. The basal activity of PKA was driven by high basal activity of AC, as inhibition of AC by 400 μM MDL-12,330A had the same effect (Vinogradova *et al.,* 2006).

However, my results do not support those of Vinogradova *et al.,* (2006), as inhibition of PKA only reduced the beating rate by 113 ± 10 bpm (from 503 ± 15 bpm to 387 ± 17 bpm, or 31 ± 4%) and did not abolish the spontaneous beating (**Figure 4.8*B***). Furthermore, the subsequent addition of 1 μM ZD7288 in combination with 3 μM ivabradine in the presence of 3 μM H89 resulted in further reduction of the rate by 170 ± 10 bpm. This is significantly smaller than the reduction of 284 ± 13 bpm seen with the ZD7288/ivabradine combination in the absence of H89 (**Figure 4.8*B***). Firstly, this indicates that the basal PKA activity is not the only contributor driving the pacemaker, as inhibition of I_f further reduces the beating rate. My results suggest that PKA modulates the I_f channel. This is because effect of the ZD7288/ivabradine combination in reducing basal beating rate was attenuated in the presence of PKA inhibition by 170 ± 10 bpm. This is significantly smaller than the reduction of 284 ± 13 bpm

seen with the ZD7288/ivabradine combination in the absence of PKA inhibition (**Figure 4.8*B***). The observation that the effect of the ZD7288/ivabradine combination on basal beating rate is less in presence of PKA inhibition (170 ± 10 bpm reduction compared to the 284 ± 13 bpm reduction caused by ZD7288/ivabradine combination in the absence of PKA inhibition, **Figure 4.8*B***) is consistent with the suggestion that PKA modulates I_f. However, other interpretations are also possible. My findings support previous experiments by Liao *et al.* (2010) in isolated mouse SAN cells, which showed that PKA directly phosphorylates 13 sites on the N- and C-termini of HCN_4. The regulatory site resides at the distal C-terminus and, as is the case with cAMP, phosphorylation shifts the voltage dependence of I_f channel activation to more positive potentials. It has been confirmed that cAMP activates I_f channels independent of PKA (DiFrancesco and Tromba, 1988; Liao *et al.,* 2010). However, from Liao's (2010) observation, it was suggested that there may exists direct synergy between direct cAMP modulation of I_f channels and PKA phosphorylation of I_f channels. This is in line with the earlier observations of Accili *et al.* (1997).

4.7.5. Contribution of AC to modulation of basal beating rate by I_f

Previous experiments have shown that in addition to being activated by hyperpolarization, the I_f current can also be directly activated by cAMP (DiFrancesco and Tortora, 1991). Adenylyl cyclases (including those stimulated by cytosolic Ca^{2+}) are the enzymes responsible for generation of cAMP and these are inhibited by MDL-12,330A (Grupp *et al.,* 1980; Kanda *et al.,* 2001). I therefore wanted to assess the effect of AC inhibition prior to inhibition of I_f

channels. Application of 10 μM MDL-12,330A significantly reduced basal beating rate by 312 ± 21 bpm; however, in the presence of 10 μM MDL-12,330A, addition of 1 μM ZD7288 did not produce a statistically significant further reduction in the beating rate. The effect of ZD7288 in reducing spontaneous beating rate was abolished after MDL-12,330A (reduction of 7 ± 8 bpm, while ZD7288 alone reduced the rate by over 200 bpm, **Figure 4.2**). These observations suggest that the substantial contribution of I_f current to the basal spontaneous beating rate is maintained by constitutively active AC (which would include the Ca^{2+}-stimulated isoforms AC1 and AC8). Using the non-isoform-specific AC inhibitor MDL-12,330A would be expected to reduce cytosolic cAMP concentration. And since cAMP is an endogenous agonist of I_f channels, this reduces the open probability and shifts the activation potential of the I_f channel to a more negative potential.

4.8. Fluorescent Ca^{2+} transient measurements

4.8.1. The role of I_f in modulation of Ca^{2+} transient amplitude

The reduction of Ca^{2+} transient amplitude in the absence of any drugs (control) was comparable to the gradual reduction observed in the presence of 1 μM ZD7288 combined with 3 μM ivabradine. Over a period of 40 min, the Ca^{2+} transient amplitude was reduced by 45 ± 3%. The reduction was not significantly different from the 36 ± 5% reduction in Ca^{2+} transient amplitude in the absence of I_f blockers over the same time period (5 - 40 min, $P > 0.05$, **Figure 4.5*D***). Although my observations suggest that the 2ZD7288/ivabradine

combination does not impact Ca^{2+} handling of the SAN system, this is in contrast to the experimental observations of Yaniv *et al.* (2013) in rabbit-isolated SAN cells, where 3 μM ivabradine reduced the Ca^{2+} content of SR, as measured using the rapid caffeine "spritz" measurements. In these experiments, the caffeine-induced Ca^{2+} transient amplitude was lowered by 13% in the presence of 3 μM ivabradine. However, in subsequent studies, it was shown that the SR's Ca^{2+} content was significantly changed only when the concentration of ivabradine was increased to 10 μM and above (Yaniv *et al.,* 2014).

However, close inspection shows that a marginal increase in rate of reduction of the Ca^{2+} transient amplitude curve relative to control cannot be excluded, since all the points in the presence of the ZD7288/ivabradine combination appear to be lower than those in the absence of drugs (**Figure 4.5*D***). Even though there appeared to be no statistically significant difference using the applied methods, it seems prudent to keep an open mind about the possibility of a small change as a secondary consequence of the reduction in rate, possibly leading to changes in Ca^{2+} handling. Reducing the heart rate will reduce the number of action potentials per unit time and this will in turn reduce the amount of Ca^{2+} influx thorough voltage-gated Ca^{2+} channels, thus reducing the quantity of cytosolic Ca^{2+} available for uptake by SR. However, it is also important to note that in this context, the effect of inhibiting I_f channels on rate was substantial in the intact mouse SAN preparation (reduction of the rate by half), while a statistically significant impact on the amplitude of Ca^{2+} transients was not detected. Further experiments need to be carried out to see whether the difference between observations seen in Yaniv's experiments is due to a

species difference (difference in the density of ionic currents and/or basal heart rates).

4.8.2. The role of Ca^{2+} release from SR in modulation of Ca^{2+} transient amplitude

Unlike I_f inhibition (ZD7288/ivabradine), application of CPA induced a rapid reduction in the Ca^{2+} transient amplitude over the first 5 min (in the presence of 100 μM and 30 μM CPA, Ca^{2+} transient amplitude was reduced by 57 ± 2% and 48 ± 1%, respectively; **Figure 4.5*D***). Similarly, in an isolated single cell from guinea pig, an initial rapid reduction was seen within the first 1 min (reduction of 44 ± 2% over 1 min, **Figure 4.5*F***).

The observed rapid reduction is most likely due to suppression of SR function via inhibition of Ca^{2+} uptake by SERCA (Seidler *et al.,* 1989). This subsequently reduces the sodium-calcium exchange current associated with the reduced Ca^{2+} transient and suppression of local Ca^{2+} release events (Huser *et al.,* 2000; Bogdanov *et al.,* 2001). These effects are expected to develop in a short time frame. After the first 5 min in intact mouse SAN preparations, and after the first 1 min in SAN cells isolated from guinea pig, the Ca^{2+} transient amplitude was further reduced at a gradual rate, possibly due to dye extrusion and/or photobleaching (**Figure 4.5*D & F***).

However, looking at the rate of reduction, there was a significantly greater slowing in heart rate at 30 min than at 5 min ($P < 0.01$, paired t-test, **Figure 4.5*D***). Using first-order exponential decay, the fitted data showed a

gradual decline to a new steady rate of 129 ± 8 bpm, with a time constant of 9 ± 1.8 min (**Figure 4.12**). Therefore, I suggest that the slowing of beating rate in the presence of CPA could also in part reflect a reduction in the activity of Ca^{2+}-stimulated adenylyl cyclases and the subsequent reduction in the concentration of cytosolic cAMP, which regulates I_f channels. It is possible that the integration of changes in Ca^{2+} concentration in the cytosol by Ca^{2+}-stimulated adenylyl cyclases has slower kinetics.

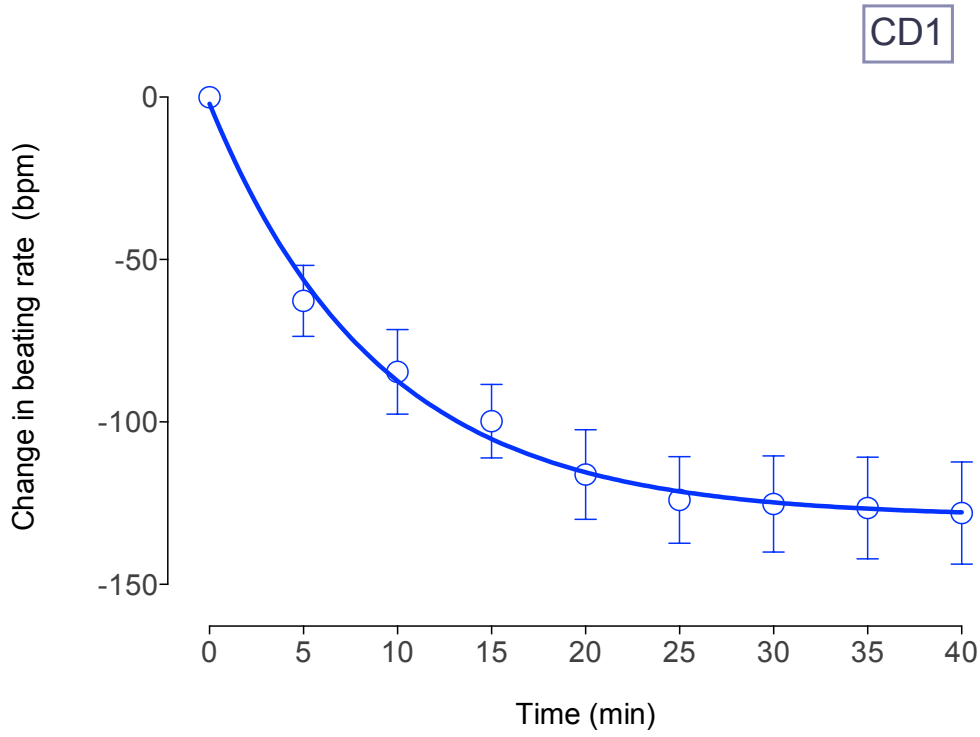


Figure 4.12 First-order exponential decay fitted using the mean changes over time in beating rate in the presence of 100 μM CPA (n = 6), as measured from the fluorescent Ca^{2+} transients recorded in the SAN region. Data are expressed as mean ± S.E.M. GraphPad Prism (version 5.0) software was used to perform statistical analysis, including paired Student's t-test (significance level $P < 0.05$).

4.9. Modulation of β-adrenergic receptor-stimulated beating rate

4.9.1. Role of I_f under β-adrenergic receptor stimulation

In the mouse and guinea pig SAN, the contribution of I_f to the positive chronotropic effect following β-adrenergic receptor stimulation was investigated. The isoprenaline log(concentration)-response curve was appreciably depressed following I_f inhibition. In mouse atrial preparations at the highest concentration of isoprenaline (100 nM), the maximum response was reduced by 76 ± 20 bpm in the presence of 1 μM ZD7288, either alone or in combination with 3 μM ivabradine (**Figure 4.7*A***). Similarly, in guinea pig atrial preparations at the highest concentration of isoprenaline (100 nM), the rate was reduced to 85 ± 16 bpm in the presence of 1 μM ZD7288, and to 88 ± 15 bpm in the presence of 1 μM ZD7288 + 3 μM ivabradine compared to 132 ± 21 bpm with isoprenaline alone (**Figure 4.7*B***). Thus, suppression of the isoprenaline response by I_f inhibitors indicates that the chronotropic effect of β-adrenergic receptor stimulation partly depends on the I_f signalling pathway.

The findings here are consistent with the results obtained by Choate *et al.* (2003), where intact mouse atrial sympathetic ganglia subjected to electrical stimulation in presence of 1 mM Cs^+ reduced the maximum response by 30%. This implies that noradrenaline is involved in I_f channel modulation. Also, a contribution of I_f to the positive chronotropic effect of β-adrenergic receptor stimulation has been seen in different mammalian species. Perfusion of dog isolated SAN cells with 1 μM isoprenaline after pretreatment with 1 μM ZD7288 reduced the chronotropic response of isoprenaline by 40% relative to 1 μM

isoprenaline alone (Joung *et al.,* 2009). In a separate experiment by Gao *et al.,* (2011) under the exact same conditions, there was a 35% reduction in the chronotropic effect of isoprenaline in the presence of 1 μM ZD7288, and a similar reduction in the presence of 3 mM Cs^+. Vinogradova *et al.* (2002) showed that in rabbit isolated SAN cells, in the presence of 1 mM Cs^+, 1 μM isoprenaline's chronotropic response was reduced by 11% relative to isoprenaline in the absence of Cs^+.

It is essential to note that inhibition of I_f only partially reduced the response to isoprenaline, and this is not attributed to incomplete inhibition of I_f channels. A precise way to assess the degree of ion channel blockade is through electrophysiological studies. However, with 'use-dependent' drugs such as ivabradine and ZD7288, this is difficult to assess, particularly since the drugs take over 30 min to reach their steady-state effect. Thus, the effect of I_f channel inhibition is most likely to be underestimated if the exposure time is too short. Also, recording over a long period of time may induce a current "rundown." Therefore, in the initial experiment carried out by BoSmith *et al.* (1993), the observed 74 ± 4% reduction in current by 1 μM ZD7288 might be an underestimate. In my experiment, 3 μM ivabradine caused a similar reduction in basal beating rate to 1 μM ZD7288, and the degree of blockade with this drug is expected to be at least as high as with ZD7288 (Bois *et al.,* 1996; Bucchi *et al.,* 2002).

Given that ZD7288 and ivabradine have the same magnitude of inhibition, it can be proposed that ivabradine also occupies a similar fraction of sites/channels at 3 μM. For the purpose of the following discussion it is

assumed that each drug separately occupies 75% of the channel sites (consistent with the 74 ± 4% blockade reported by BoSmith *et al.,* 1993). The fraction of sites blocked is = [D]/([D] + K_D), where K_D is the dissociation equilibrium constant and [D] is the drug concentration. And despite the fact that the magnitude of I_f inhibition might be underestimated, as alluded to above, a 75% blockade is expected to occur when the concentration of each drug is 3 times greater than the K_D. Thus, employing Jarvis and Thompson's (2013) models, the magnitude of total blockade can be assessed in a model whereby two different ion channel inhibitors either occupy the same or different sites on the channel protein. When both drugs occupy the same sites, and assuming that they show mutually exclusive binding to I_f channels, the total combined occupancy would be 86%, or (3 + 3)/(3 + 3 + 1). In a second model, in which the blockers occupy two different sites, the combined occupancy in this case would be 94%. This is because the first 75% is occupied by 1 μM ZD7288, while 3 μM ivabradine inhibits another 19% [since 75% of the remaining 25% (0.75*0.25 = 19%) is occupied by 3 μM ivabradine]. Thus, the combination of 1 μM ZD7288 and 3 μM ivabradine is most likely to result in a near complete blockade of I_f, especially since the magnitude of inhibition of each drug may be underestimated. This is also in line with the observations seen in the atrial preparation, where the concentration of ZD7288 was increased from 1 to 3 and then to 10 μM, with only marginal changes in beating rates (**Figure 4.3*A***). Furthermore, addition of 3 μM ivabradine in the presence of 1μM ZD7288 did not cause a statistically significant further change in the rate of spontaneous beating in mouse and guinea pig atrial preparations (**Figure 4.4*A* & *B***). The rate changes seen in mouse, a situation in which I believe little or no I_f remained

unblocked, were remarkably similar to those observed by Mesirca *et al.* (2014) using genetic techniques to silence I_f channels.

4.9.2. Role of Ca^{2+} release from the SR under β-adrenergic receptor stimulation

In mouse and guinea pig SAN cells, the contribution of Ca^{2+} from the SR store to the positive chronotropic effect of β-adrenergic receptor stimulation was revealed by the significant depression of the maximum of the isoprenaline-induced log(concentration)-response curve in the presence of CPA. In mouse at the highest isoprenaline concentration (100 nM), the beating rate was increased by 193 ± 13 bpm (in the presence of 100 μM CPA) and 173 ± 14 (in the presence of 30 μM CPA) compared to a 303 ± 10 bmp increase in the absence of CPA (**Figure 4.7*A***). Thus, 30 and 100 μM CPA suppressed the max isoprenaline response by 40% and 36%, respectively. In guinea pig at the highest concentration of isoprenaline (100 nM), the beating rate was increased by only 57 ± 9 bpm (in the presence of 30 μM CPA). This was a significant reduction from the change caused by isoprenaline alone, 132 ± 21 bpm (**Figure 4.7*B***). These results indicate that the chronotropic effect of β-adrenergic receptor stimulation partly depends on Ca^{2+} release from SR stores.

The contribution of Ca^{2+} release from SR stores has also been observed by different groups, in support of the above results. In rabbit SAN cells, Vinogradova *et al.* (2002) found that 3 μM ryanodine significantly reduced the positive chronotropic effect of isoprenaline. In guinea pig atria, Rigg *et al.* (2000)

showed that 2 μM ryanodine reduced the positive chronotropic effect of 100 nM isoprenaline by 30%. A significant part of the ryanodine suppression is most likely due to reduced activity of Ca^{2+}-stimulated ACs, leading to diminished cAMP-mediated upregulation of I_f.

In contrast, Goa *et al.'s* (2011) experiment on a dog isolated SAN cell using conventional voltage clamp recordings showed that 2 μM ryanodine had no significant effect on the chronotropic effect evoked by isoprenaline. However, as explained in detail above, there may be inherent flaws with conventional voltage clamp recording.

4.9.3. Contribution of I_f and the SR Ca^{2+} store to the chronotropic effect of isoprenaline

In the mouse and guinea pig preparations in the presence of both 1 μM ZD7288 and 100 μM CPA, the isoprenaline log(concentration)-response curve was substantially depressed. In mouse, 100 nM isoprenaline increased the beating rate by 51 ± 2 bpm in the presence of 1 μM ZD7288 + 100 μM CPA, compared to a 303 ± 10 bpm increase with isoprenaline alone. This represents a reduction of 83 ± 2% (**Figure 4.7*A***). In guinea pig, in the presence of 30 μM CPA + 1 μM ZD7288, the isoprenaline log(concentration)-response curve was considerably suppressed, with the response to the high concentration of isoprenaline reduced to 8 ± 2 bpm compared to a 132 ± 21 bmp increase with isoprenaline alone (**Figure 4.7*B***). These results are in line with recent experiments indicating that both Ca^{2+} release from SR and I_f current contribute

to pacemaker activity (Joung *et al.,* 2009; Gao *et al.,* 2010), although catecholamine effects were not assessed over a broad concentration range.

It is tempting to attempt to begin to dissect the individual effects of ZD7288 and CPA on the chronotropic effect of isoprenaline. In referring to **Figure 4.7*A***, one might conclude that the initial drop of 25 ± 3% seen in the presence of 1 μM ZD7288 is due to I_f current blockade and that the remaining 58% reduction is due to the inhibition of Ca^{2+} release from SR stores. At face value, this is a convincing proposition, as Ca^{2+} release from SR has control over I_f through up-regulation of PKA activity and increased PKA-dependent phosphorylation. However, this assumption does not hold if we look at the results from inhibition of Ca^{2+} release from SR stores. In other words, the initial drop of 36 ± 4% in the presence of 100μM CPA is due to inhibition of Ca^{2+} release from SR stores and the remaining 47% reduction is due to inhibition of the I_f current. Thus, this approach to the process of disentangling I_f current and Ca^{2+} release from SR seems too simplistic and it is not justified to assume that there is a linear relationship between these factors in the modulation of pacemaking. In evolutionary terms, it would make sense that there is more than one mechanism of pacemaking; indeed, it seems that the pacemaker is imbued with multiple defensive mechanisms to prevent the failure of a single layer, which would bring the heart to a standstill. Thus, under different circumstances, an alternate mechanism will take over to sustain the heart's beating. I propose that when Ca^{2+} release from SR stores is blocked by CPA, the residual I_f current becomes substantially more important for maintaining the basal beating rate and the chronotropic effect of isoprenaline, and vice versa. That is, when I_f currents are blocked by ZD7288, Ca^{2+} release from SR stores becomes crucial

for maintaining the basal beating rate and the chronotropic effect of isoprenaline.

4.9.4. Role of K_{ACh} at rest and under β-adrenergic and muscarinic receptor pre-stimulation

Under the initial experimental conditions prior to application of CCh, K_{ACh} only marginally contributes to modulation of pacemaking, both in the absence and presence of β-adrenergic stimulation. 300 nM Tertiapin-Q reduced the rate of spontaneous beating in the atrial preparation by 9 ± 1%. Also, in the presence of Tertiapin-Q, 30 nM isoprenaline increased beating rate by 41 ± 2% and this was not significantly different from the 37 ± 3% increase seen with 30 nM isoprenaline alone (**Figure 4.8*D***). These results are consistent with van Borren *et al.'s* (2010) observations, where K_{ACh} inhibition did not alter the pacemaker rate in the presence or absence of pre-stimulation of the β-adrenergic receptor with noradrenaline.

However, inhibition of K_{ACh} substantially reduced the negative chronotropic action of CCh. These reductions were apparent at higher concentrations of CCh, indicating that M_2 activation influences pacemaking through activation of K_{ACh} channels. Furthermore, the reduction was much more apparent subsequent to pre-stimulation of β-adrenergic receptors with 30 nM isoprenaline (**Figure 4.8*C***). These results support Yamada *et al.'s* (2002) experimental observations, where inhibition of K_{ACh} affected CCh's negative chronotropic effect at concentrations ≥ 300 nM but not ≤ 100 nM. Furthermore,

through patch-clamp experiments, the authors were able to deduce that there were two components of the post activation of M_2 receptors – the tertiapin-sensitive component and the tertiapin-insensitive component. The tertiapin-sensitive pathway through K_{ACh} activation contributed to approximately 75% of negative chronotropic action of CCh. This effect was observed in a concentration dependent manner with CCh concentrations > 100 nM. The remaining 25% of the maximum effect of CCh was driven through the tertiapin-insensitive pathway, via inhibition of AC by the G_i-protein α_i subunit. This effect was also concentration dependent, induced by 1 - 300 nM CCh.

The tertiapin-insensitive pathway's downstream target is the inhibition of I_f channels via reduced cytosolic cAMP concentration (DiFrancesco and Tromba, 1988; DiFrancesco *et al.,* 1989; DiFrancesco, 1994). Using rabbit isolated SAN cells, it was demonstrated that lower concentrations of ACh reduce I_f current without affecting K_{ACh} channels. More convincing experiments showed that when I_f and K_{ACh} channels were blocked with 2 mM Cs^+ and Tertiapin-Q, respectively, the tertiapin-insensitive component at 1 μM CCh was no longer present (Yamada *et al.,* 2002, van Borren *et al.,* 2010). These results suggest that K_{ACh} plays a significant role in the negative chronotropic effect of CCh at higher concentrations, with a minor contribution via inhibition of I_f at lower concentrations. However, the tertiapin-insensitive component cannot be fully attributed to the I_f-dependent pathway, as reduced AC activity will also reduce the PKA-phosphorylation pathway too. At IC_{50}, carbachol reduces cAMP and PKA-dependent phospholamban (PLB) phosphorylation by ~50%. The log(concentration)-response curve of carbachol in the presence of Tertiapin-Q resembles the carbachol-induced reduction of PLB phosphorylation (Lyashkov

et al., 2009). Thus, activation of the muscarinic receptor causes a negative chronotropic action via interplay between suppression of PKA-dependent Ca^{2+} signalling, I_f inhibition and $I_{K,ACh}$ activation.

4.9.5. Role of PKA under β-adrenergic receptor stimulation

Pre-incubation of the atrial preparation with 3 μM H89 asymmetrically reduced the isoprenaline log(concentration)-response curve; the statistically significant reductions were at the lower end of the isoprenaline concentration curve (**Figure 4.8*A***). However, addition of 1 μM ZD7288 subsequent to 3 μM H89 further reduced the isoprenaline log(concentration)-response curve, and the reduction was symmetrical relative to control curve. At the highest isoprenaline concentration of 100 nM, in the presence of H89 and 1 μM ZD7288 + 3 μM ivabradine, beating rate was increased by 184 ± 14 bpm compared to 261 ± 15 in the absence of any inhibitors (**Figure 4.8*A***). These results suggest that PKA-dependent mechanisms contribute mostly at low isoprenaline concentrations, while I_f contributes more at high isoprenaline concentrations. This implies that there are other mechanisms independent of cAMP/PKA are substantial.

4.10. Limitations

In this project, one main limitation was choosing the optimal concentrations of inhibitors to selectively block target proteins without having non-specific actions.

For example, ZD7288 is a selective I_f channel inhibitor (BoSmith *et al.,* 1993), but like any other drug, its specificity is reduced as its concentration increases. At higher concentrations, ZD7288 has been shown to modulate Ca^{2+} and K^+ channels. In this study, a 1 μM concentration was chosen, as experiments in guinea pig SAN cells by BoSmith *et al.* (1993) revealed that within a concentration range of 0.1 to 1 μM, ZD7288 was very effective at blocking I_f current, as ZD7288 concentrations of 0.1, 0.3 and 1 μM inhibited the I_f current by 44, 65 and 75%, respectively, without affecting voltage-gated Ca^{2+} or K^+ channels. In our experiments, 1 μM ZD7288 caused a 60 ± 4% reduction in basal beating rate, and a 25 ± 3% reduction in the chronotropic effect caused by 100 nM isoprenaline. It is possible that the effects of ZD7288 on I_f might have been underestimated in the electrophysiological experiments since the time course of action of ZD7288 is slow and patch-clamp electrophysiological experiments are limited in duration. As a 1 μM concentration of ZD7288 was effective, I was reluctant to increase its concentration above 1 μM. However, I still wanted to examine whether ZD7288 was effectively blocking I_f channels. Therefore, I initially looked for changes in beating rate when the concentration was increased from 1 to 3 to 10 μM in an incremental manner. The initial 253 ± 23 bpm reduction in mouse spontaneous beating rate in the presence of 1 μM ZD7288 was further reduced by 46 ± 9 bpm following the increase of

concentration to 3 μM (*P* > *0.05*, one-way ANOVA, Dunnett post-test, for comparison effect of increasing the concentration of ZD7288 from 1 to 3 μM). Subsequently increasing the concentration to 10 μM only marginally reduced the rate, by 2 ± 6 bpm (*P* > *0.05*, one-way ANOVA, Dunnett post-test, for comparison effect of increasing the concentration of ZD7288 from 3 to 10 μM **Figure 4.3*A***).

As I was reluctant to increase the concentration of ZD7288 above 1 μM due to its off-target effects (BoSmith *et al.,* 1993), I wanted to see whether 3 μM ivabradine (another I_f channel blocker) could further suppress I_f current in the presence of ZD7288. 3 μM ivabradine and 1 μM ZD7288 both had similar magnitudes of reduction of the mouse basal beating rate (reduction of 219 ± 20 bpm with ivabradine). Ivabradine has recently been reported to block hERG channels with a similar IC_{50} to I_f channels (Melgari *et al.,* 2015). It is emphasized above that in the original BoSmith *et al.* 1993 paper on ZD7288 the 1 μM concentrations used for the major part of our work were observed not to block voltage-gated Ca^{2+} or K^+ channels. Ivabradine is used mainly to ensure even greater fractional block of I_f while minimizing effects on other channels. In our experiments we have not recorded hERG current, but it is clear that addition of ivabradine in presence of ZD7288, did not induce further substantial reduction to rate of spontaneous basal beating of atrial preparations. If ivabradine were to substantially inhibit hERG channels as per Melgari *et al.* (2015) suggestion, considerable further reduction in basal beating rate would have been expected when ivabradine was subsequently added following ZD7288. However, this was not observed under our experimental conditions and it therefore appears that under our experimental conditions any blockade of

hERG channels by ivabradine made only a very minor contribution. In the presence of 1 μM ZD7288, 3 μM ivabradine caused little or no further change in mouse beating rate (reduction of 21 ± 5 bpm, **Figure 4.4*A***). Similarly, in guinea pig atrial preparation, any effects of 3 μM ivabradine in reducing the rate in presence of 1 μM ZD7288 were small and not statistically significant (only reducing the rate by 5 ± 30 bpm, **Figure 4.4*B***).

Instead of ivabradine, I initially used Cs^+ as an alternative I_f inhibitor, as it is widely used as a selective inhibitor of the I_f channel (DiFrancesco, 1981; Denyer and Brown, 1990; Bucchi *et al.,* 2002). Cs^+ was used at a 2 mM concentration, as it was proposed that its action in blocking I_f current is selective within a ≤ 2 mM range (Irisawa H. *et al.,* 1993). The purpose of using Cs^+ was to see whether it could further suppress the inhibitory action of 1 μM ZD7288 on basal beating rate. Applying 2 mM to block I_f caused a reduction of mouse spontaneous beating rate by 38 ± 3% but in the presence of 1 μM ZD7288, subsequent exposure to 2 mM Cs^+ surprisingly *increased* the spontaneous beating rate from 154 ± 16 bpm (ZD7288 alone) to 262 ± 9 bpm, an increase of 108 ± 17 bpm (70 ± 3%, **Figure 4.3*C***). This unexpected observation is discussed in detail in Section 4.11 below, titled “Underlying mechanism of Cs^+ action”.

Compared to a 30 μM concentration of CPA, a 100 μM concentration had a larger effect on reducing basal beating rate (30 μM, 23 ± 4%; 100 μM, 47 ± 4%). It was reassuring that the larger reduction appeared not to be due to toxic effects, as the subsequent wash-out of the drug caused the beating rate to return approximately to its original baseline. However, we could not rule out that

part of the further reduction in basal rate may have been due to inhibition of some voltage-gated Ca^{2+} channels. In a similar manner, increasing ryanodine from 3 to 30 μM caused a statistically further reduction in beating rate: at 3 μM, ryanodine reduced spontaneous beating rate by 9 ± 3%, and at 30 μM, spontaneous beating rate was reduced by 25 ± 4% (**Figure 4.3*B***). Although we observed a large decrease in basal rate in terms of suppressing the chronotropic effect of isoprenaline, 30 and 100 μM CPA had a similar effect to one another in mouse atrial preparation, with the difference between the curves being statistically not significant (**Figure 4.7*A***).

In addition to choosing the optimal concentrations of the abovementioned drugs, it was also crucial to choose the optimal incubation time, as governed by their target kinetics. The drugs used above, with the exception of isoprenaline and Cs^+ (2 min and 5 min, respectively), 30 min was optimal to reach the steady-state effect (**Figure 2.3*C* - *F***). For example, referring to the experiments in **Figure 4.6*A* & *B***, it was discovered that not only did the concentration of CPA need to be increased to 100 μM, but the pre-incubation time also had to be extended to 30 min in order to attenuate the effect of 1 μM ZD7288. This resulted in a significant change in Ca^{2+} transients modulated by I_f in the presence of CPA.

4.11. Underlying mechanism of Cs^+ action

It has been well documented that Cs^+ has a relatively smaller effect in reducing heart rate relative to ZD7288 (Denyer *et al.,* 1990; DiFrancesco *et al.,* 1982; lei). However, this apparent difference has not been previously addressed. Previous study by Rosenthal *et al.* (1998) suggested that Cs^+ directly activates AC. Therefore Cs^+ is indirectly stimulating I_f channels via the activation of adenylyl cyclase (AC). Consistent with this hypothesis, the addition of 2 mM Cs^+ did not increase beating rate in the presence of MDL-12,330A and ZD7288 (**Figure 4.3*C***). Cs^+ may directly/indirectly modulate ACs, which would lead to elevated cAMP levels, upregulated PKA activity, and increased PKA-dependent phosphorylation, contributing to the positive chronotropic effect.

Hence, the lower ability of Cs^+ to reduce the basal heart rate than ZD7288 may be due to a positive feedback loop on basal spontaneous beating rate through upregulation of PKA-dependent phosphorylation or membrane channels. Further experiments need to be carried out in order to reveal the exact underlying mechanism of Cs^+. Studies by Rosenthal *et al.* (1998) support this hypothesis, as they have shown that Cs^+ increases the rate of cAMP synthesis in a rat brain cortex membrane assay. The authors suggested that Cs^+ directly activates AC, as the blockade of muscarinic receptors with 1 mM atropine had no effect, and the omission of GTP in the reaction mixture did not affect the ability of Cs^+ to increase cAMP production. Further binding studies with [^{125}I]forskolin suggested that AC isoforms 1, 5 and 8 are stimulated by Cs^+ to produce cAMP. Cs^+ modulates Ca^{2+}-stimulated ACs, and it is now clear that Ca^{2+}-stimulated ACs are present in the SA node (Mattick *et al.,* 2007), further

supporting the above hypothesis. My observation has unmasked the potential ability of Cs^+ to upregulate the activity of AC and increase cytosolic cAMP levels, activating PKA. Targets of PKA include L-type Ca^{2+} channels, K_v channels, ryanodine receptors, phospholamban, and perhaps NCX (De *et al.,* 1996; Sculptoreanu *et al.,* 1993; Li *et al.,* 1990; Mundina *et al.,* 1996; Lei *et al.,* 2002), all of which can influence diastolic depolarization, therefore leading us to underestimate the ability of Cs^+ to act as an I_f channel blocker. I suggest that Cs^+ accesses the cytosolic environment by passing though nonselective cationic channels; Na^+ background channels could be one possible candidate (Hagiwara *et al.,* 1992; Cheng *et al.,* 2016). This discovery was coincidental, and for precisely this reason, one should be cautious when using the concentrations of drugs recommended in the literature.

This hypothesis fits well with the isoprenaline log(concentration)-response curve in the presence of 2 mM Cs^+, where isoprenaline's ability to increase the beating rate was only statistically significant above 30 nM (1 - 10 nM, $P > 0.05$, 30 - 100 nM, $P < 0.05$, two-way ANOVA with Bonferroni post-test, n = 6, **Figure 4.13**). This implies that at lower concentrations, isoprenaline has not saturated AC activity, and the contribution of Cs^+ to increasing cytosolic cAMP levels is substantial. It is also possible that isoprenaline concentrations ≥ 30 nM may saturate the activity of AC, and that the extra cAMP production by Cs^+ is not significant.

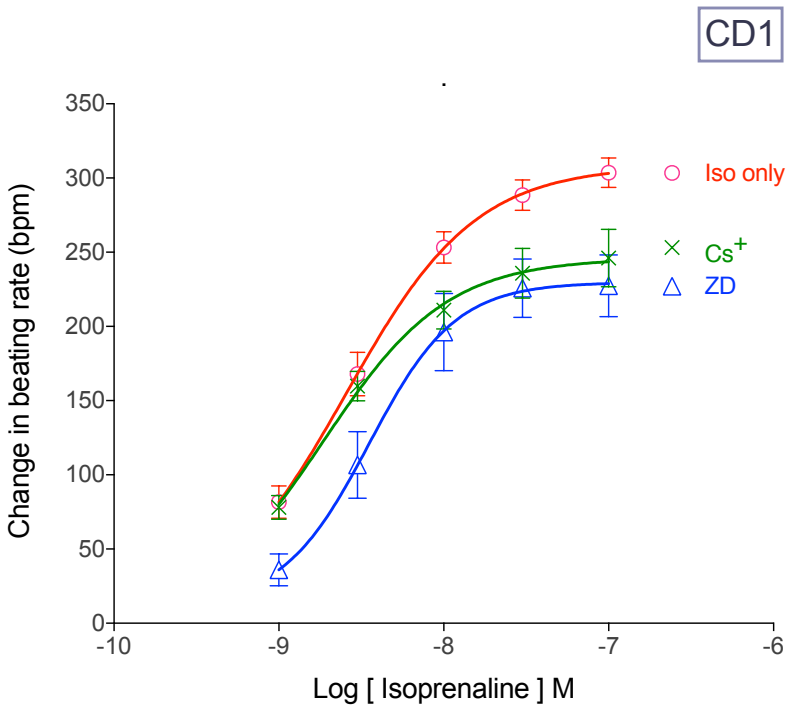


Figure 4.13. Graph representing mean change of the positive chronotropic action of the β-adrenoceptor agonist isoprenaline by **(*A*)** 2 mM Cs^+ (n = 6) and 1 μM ZD7288 (n = 6) in the spontaneously beating mouse atrial preparation. Data are expressed as mean ± S.E.M., n = number of experiments. GraphPad Prism (version 5.0) software was used to perform statistical analysis, including two-way ANOVA with Bonferroni post-test (significance level $P < 0.05$).

CHAPTER 5: EFFECTS OF I_F AND SR Ca^{2+} RELEASE INHIBITORS ON BASAL SPONTANEOUS BEATING RATE IN MICE WITH DIFFERENT EXPRESSION OF Ca^{2+}-STIMULATED ACS IN THE ABSENCE AND PRESENCE OF β_1 -ADRENOCEPTOR STIMULATION WITH ISOPRENALINE.

5.1. Introduction

Adenylyl cyclase (AC) is an enzyme responsible for catalysing cAMP synthesis from ATP. Nine AC isoforms have been identified, with some showing tissue-specific distribution (Deffer *et al.,* 2000). For example, while AC5 and AC6 are ubiquitously distributed throughout the body, AC1 is specifically expressed in neurons and AC3 in olfactory epithelial cells (Deffer *et al.,* 2000). In homogenised whole heart, the most abundant identified ACs are the AC5 and AC6 isoforms (Cooper *et al.,* 1995; *Defer et al.,* 2000). AC5 and AC6 are the most dominant isoforms present in ventricular cells (Katsushika *et al.,* 1992; Premont *et al.,* 1992; Yoshimura and Cooper, 1993). It was also revealed that some AC4 isoforms are present in ventricular cells (Belevych *et al.,* 2001). Work from Mattick *et al.* (2007) using RT-PCR and immunoblotting with a specific antibody showed that both Ca^{2+}-stimulated AC isoforms (AC1 and AC8) are present in the SAN, but not in the ventricular muscle of guinea pig. Also using quantitative RT-PCR, it was confirmed that in addition to the Ca^{2+}-stimulated AC isoforms (AC1 and AC8), the AC2, AC5 and AC6 isoforms are also present within rabbit SAN cells (Younes *et al.,* 2008).

In general, there are three AC isoforms (AC1, AC3 and AC8) that are activated by Ca^{2+}. Of these, AC1 and AC8 are activated at submicromolar cytosolic concentrations of Ca^{2+} through the calmodulin-dependent pathway and not through CaMKII (Deffer *et al.,* 2000). AC1 and AC8 have different Ca^{2+} sensitivity via CaM, with AC1 possessing a 5-fold lower EC_{50} for Ca^{2+} (150 nM) compared to AC8 (800 nM) (Diel *et al.,* 2006). It was suggested that the AC3 isoform is directly activated at relatively high concentrations, above the

micromolar range (Fagan *et al.,* 1996). In contrast, AC5 and AC6 are two isoforms that are directly inhibited by submicromolar concentrations of the cytosolic Ca^{2+} cation (Yoshimura and Cooper, 1993).

It is now known that the heart doesn't require any neurotransmitter or systemically circulating hormones to induce beating. In the 2nd century, Galen showed that a heart removed from body would continue to beat and it was suggested that there was no requirement for systemic circulating hormones or nerve innervation (autonomic) to maintain the beating of the heart (Silverman *et al.,* 2006). Therefore, the spontaneous depolarization of SAN cells, which drives pacemaking, does not depend on extrinsic nerves. However, the frequency of the pacemaker potential is modulated by the autonomic nervous system, predominantly through alteration of the AC system.

Sympathetic innervation increases heart rate predominantly by activating the β_1-adrenoceptors present on SAN cells (Piercy, 1988; Takei *et al.,* 1992). Sympathetic innervation releases noradrenaline, an adrenoceptor agonist, or systemically circulating adrenaline. Activation of the β_1-adrenoceptor (G_s-protein coupled) occurs following the binding of adrenaline/noradrenaline to β_1-adrenoceptors. Activated β_1-adrenoceptors via their α_s subunit activates the ACs (the detail mechanism is covered in chapter 1; 1.5.1. Sympathetic modulation of the pacemaker). However, the activation of AC does not account for all of the actions of sympathetic nerve stimulation. This is because activation of AC via neuronal sympathetic stimulation differs from direct activation of AC. It has been suggested that the non-AC effect of AC activation is due to ATP co-transmission (Bramich *et al.,* 1990; Choate *et al.,* 1993).

Parasympathetic nerve terminals release acetylcholine (ACh), a muscarinic agonist that reduces heart rate through activation of the M_2 muscarinic receptors present on SAN cells. Activated M_2 muscarinic receptor via its $\alpha_{i/o}$ subunit inhibits the ACs (the detail mechanism is covered in chapter 1; 1.5.2. Parasympathetic modulation of the pacemaker). Thus, AC modulation is the unifying point of interaction, where the sympathetic and parasympathetic signalling pathways directly antagonise one another (**Figure 1.3**). The autonomic modulation controls the cytosolic concentration of cAMP production and consequently the modulation of ion channels and the frequency of pacemaking. However, independent of AC, M_2 activation further reduces the rate of beating via the $\beta\gamma$ subunit through activation of the K_{ACh} channels (Breitwieser *et al.,* 1988) (**Figure 1.3**). The underlying mechanism of K_{ACh} channel activation via the $\beta\gamma$ subunit is through stabilisation of the PIP2-K_{ACh} complex, as explained in the chapter 1 [section 1.2.1.3. ACh activated K^+ channels (K_{Ach})]. Thus, activation of the muscarinic receptor causes a negative chronotropic action via the interplay between suppression of PKA-dependent Ca^{2+}-signalling, inhibition of I_f, and activation of $I_{K,Ach}$ (Giles *et al.*, 1989; DiFrancesco and Tromba, 1987; Trautwein *et al.,* 1986;).

Convincing evidence shows that unlike other cardiomyocytes, SAN cells have a constitutively active AC. Ohsumi's group in 1977 was the first to report that during tissue preparation, the concentration of cAMP was higher in the rabbit SAN relative to atrial cells in the absence of β-adrenoceptor stimulation (Taniguchi *et al.,* 1977).

The L-type Ca^{2+} channels in the SAN and ventricular cardiomyocytes are inhibited via inhibition of PKA activity. Such inhibition is induced by activation of M_2 receptors by ACh, as explained above (Trautwein *et al.,* 1986; Giles *et al.*, 1989; Tanaka *et al.,* 1996). At a basal state, the application of ACh to ventricular cells does not affect the L-type Ca^{2+} current, but in these cells pre-stimulation of β-adrenoceptors allows the subsequent application of ACh to reduce the L-type Ca^{2+} current through inhibition of AC activity, ultimately reducing PKA activity (detailed mechanism explained above). These observations suggest that there is no basal AC activity in ventricular cells (Fischmeister *et al.,* 1986). However, in SAN cells, application of ACh reduces the L-type Ca^{2+} channels in the absence of β-adrenoceptor stimulation. It has been suggested that cAMP is being produced, possibly through constitutively active ACs (Petit-Jacques *et al.,* 1993; Zaza *et al.,* 1996). Vinogradova *et al.,* (2006) showed that in rabbit SAN cells, the up-regulated activity of PKA is due to elevated cytosolic cAMP.

Moreover, Sanders *et al.*'s (2006) experiments reveal that in SAN cells' the cytosolic Ca^{2+} concentration between beats is maintained at a higher level (225 nM) than in resting cardiomyocytes. It was shown that this elevated level of Ca^{2+} drives NCX current throughout the pacemaker potential, which is critical for spontaneous beating in these cells. In a test of this suggestion, application of BAPTA-AM abolished spontaneous action potentials (Sanders *et al.,* 2006). Moreover, the elevated basal cytosolic Ca^{2+} levels found specifically in pacemaker cells help to explain the cause of increased cytosolic cAMP concentration and the upregulation of PKA (Vinogradova *et al.,* 2006), as elevated Ca^{2+} levels most likely keep the Ca^{2+}-stimulated AC1 and AC8 active

(Mattick et al., 2007; Younes *et al.,* 2008). This also provides a mechanism by which I_f might be physiologically relevant in contributing to SAN pacemaking. However, the mechanism underlying the increased cytosolic Ca^{2+} within SAN cells remains unknown.

The cytosolic concentration of cyclic nucleotides, including cAMP, is regulated by a family of enzymes known as phosphodiesterases (PDE), which are responsible for the breakdown of the cyclic nucleotides. Four isoforms of PDE have been identified, and of these, two specifically break down cAMP. PDE are modulated by cGMP, which in the SAN, is produced when nNOS activates guanylate cyclase (GC) (Komas *et al.,* 1991; Herring *et al.,* 2001). Activated GC converts GTP to cGMP. Cardiomyocytes are known to have high activity of AC and PDE, indicating that this system is highly active, with any alteration modifying cytosolic cAMP levels (Arch and Newsholme, 1976).

No isoform-specific inhibitors of AC enzymes have been found to date. In order to investigate the physiological contribution of AC enzymes, studies have used homozygous knockouts or overexpression of ACs (Wu *et al.,* 1995; Abdel-Majid *et al.,* 1998; Storm *et al.,* 1998; Wang *et al.,* 2003; Lipskaia *et al.,* 2000; Georget *et al.,* 2002). The contribution of the Ca^{2+}-stimulated AC enzymes has predominantly been studied in the context of the CNS. For example, despite their observed normal phenotypic features (in brain), AC1 knockout mice ($AC1^{(-/-)}$) showed a distinctive lack of barrel patterning in the sensory motor cortex (Abdel-Majid *et al.,* 1998). There was also reduction in CA1/CA3 hippocampal and cerebellar LTP, and a deficiency in spatial memory (Wu *et al.,* 1995; Storm *et al.,* 1998). With AC8 knockout mice ($AC8^{(-/-)}$), in addition to seeing reduced

Ca^{2+}-stimulated AC activity in various CNS locations (hypothalamus, brainstem, hippocampus and thalamus), short-term plasticity was also impaired (Wang *et al.,* 2003). With double knockouts, where both the AC1 and AC8 isoforms were lacking (AC1&8$^{(-/-)}$), there was an almost complete loss of mossy fiber LTP (Wang *et al.,* 2003). Overall, although the Ca^{2+}-stimulated AC system does not seem to play a crucial role in survival, it plays a major role in learning and memory.

Taking into account the above literature review and the observations presented in the previous chapter, the work presented in this chapter investigated the influence of Ca^{2+}-stimulated AC isoforms on pacemaking. The experimental approach was to use knockout mice models, AC1$^{(-/-)}$, AC8$^{(-/-)}$ and AC1&8$^{(-/-)}$, in conjunction with pharmacological intervention. The mice models [AC1$^{(-/-)}$, AC8$^{(-/-)}$ and AC1&8$^{(-/-)}$] were all homozygous mutants in which expression of the enzymes of interest is expected to be completely suppressed (Susik *et al.,* 2014). The knockouts were kindly provided by Dr. Alana Conti's Lab (Wayne State University, School of Medicine, Department of Neurosurgery). To date, very few studies have directly investigated influence of Ca^{2+}-stimulated AC on pacemaking. The only two studies that have indirectly looked at this issue were investigating the influence of AC8 overexpression on heart (Lipskaia *et al.,* 2000; Georget *et al.,* 2002). Interestingly, those studies showed that although the downstream signalling network was altered, no change in basal spontaneous heart rate was observed.

On the basis of the hypotheses that were developed in previous chapter (Chapter 4) using CD1 mouse atrial preparations, it was suggested that I_f was substantially supported by Ca^{2+}-stimulated AC (AC8 and AC1) enzymes. Then the following predictions and expectations might be made for the knockout models [$AC1^{(-/-)}$, $AC8^{(-/-)}$ and $AC1\&8^{(-/-)}$]:

- A lack of the AC1 and AC8 enzymes should reduce reduced atrial spontaneous basal beating rate relative to wiled type basal beating rate.

- A reduction in I_f blockers' ability to induce a decrease in basal beating rate would be expected.

- In the double knockout models ($AC1\&8^{(-/-)}$), the isoprenaline log(concentration)-response curve should not be greatly influenced by I_f inhibitors.

- If the AC1 and AC8 enzymes play a key role in downstream signalling pathway of the β-adrenoceptor stimulation, some depression of the isoprenaline log(concentration)-response curve in knockout animals would be expected.

However, most of these predictions were interestingly not supported by the observations described in this chapter. Thus, I will highlight any effects seen in the knockouts. In many instances, however, the responses to different drug combinations were very similar between the atrial preparations of knockout models and control (C57BL/6J strain mice). More specifically, most of the

observations in the absence of catecholamine (isoprenaline) seemed to show little or no difference between the control and knockout models.

The clear differences observed between knockout and control atrial preparations were:

- For control C57BL/6J, AC1$^{(-/-)}$ and AC8$^{(-/-)}$ atrial preparations, incremental increases of extracellular Ca^{2+}concentration increased the basal beating rate. In contrast, for AC1&8$^{(-/-)}$ an increased extracellular Ca^{2+} concentration reduced the spontaneous basal beating rate (**Figure 5.2**).

- In the presence of ZD7288/ivabradine, no isoprenaline log(concentration)-response curve could be constructed beyond 10 nM isoprenaline for the AC1&8$^{(-/-)}$ atrial preparation relative to control, AC1$^{(-/-)}$ and AC8$^{(-/-)}$. This is because isoprenaline above 10 nM in presence of ZD7288/ivabradine induced cyclical instability in beating rate in AC1&8$^{(-/-)}$ (**Figure 5.7*C***).

- In the presence of 100 μM CPA and the 1 μM ZD7288 & 3 μM ivabradine combination, the isoprenaline log(concentration)-response curve could not be constructed for the AC1&8$^{(-/-)}$ atrial preparation relative to the control, AC1$^{(-/-)}$ and AC8$^{(-/-)}$ atrial preparations. This is because as little as 1 nM isoprenaline induced cyclical instability in beating rate in AC1&8$^{(-/-)}$ (**Figure 5.7*D***).

- No isoprenaline log(concentration)-response curve could be constructed beyond 10 nM isoprenaline for the $AC1^{(-/-)}$ and $AC8^{(-/-)}$ atrial preparations in presence of 100 μM CPA and the 1 μM ZD7288 & 3 μM ivabradine combination. This is because isoprenaline above 10 nM in presence of 100 μM CPA and 1 μM ZD7288 + 3 μM ivabradine induced cyclical instability in beating rate in the $AC1^{(-/-)}$ and $AC8^{(-/-)}$ atrial preparations (**Figure 5.7*A* & *B***).

- Following inhibition of I_f channels with the ZD7288/ivabradine combination, there was a lower increase in the rate with isoprenaline for $AC8^{(-/-)}$ (small depression), and $AC1\&8^{(-/-)}$ (larger depression). This may suggest that I_f plays a larger role in the isoprenaline rate increase, which is not what would be expected unless there is a greater depression of PKA-dependent pathways (**Figure 5.8 *C&D***).

5.2. Results

5.3. The role of Ca^{2+}-stimulated ACs at rest

Knockout mice models $AC1^{(-/-)}$, $AC8^{(-/-)}$ and $AC1\&8^{(-/-)}$ [generated and kindly were provided by Dr Conti's laboratory (Conti *et al.,* 2009), refer to section 2.7. in chapter 2] were used to initially evaluate the influence of Ca^{2+}-stimulated AC isoforms on the spontaneously beating atrial preparation. C57BL/6J mice were used as a control. The basal spontaneous beating in the atrial preparations was recorded for 40 min to reach a stable steady state. The C57BL/6J, $AC1^{(-/-)}$, $AC8^{(-/-)}$ and $AC1\&8^{(-/-)}$ mouse preparations reached resting beating rates of 433 ± 11 bpm (n = 24), 414 ± 10 bpm (n = 25), 405 ± 11 bpm (n = 24) and 436 ± 7 bpm (n = 24), respectively. The rates in the knockout models were not different from the control (*P > 0.05*, one-way ANOVA, Dunnett post-test, **Figure 5.1**).

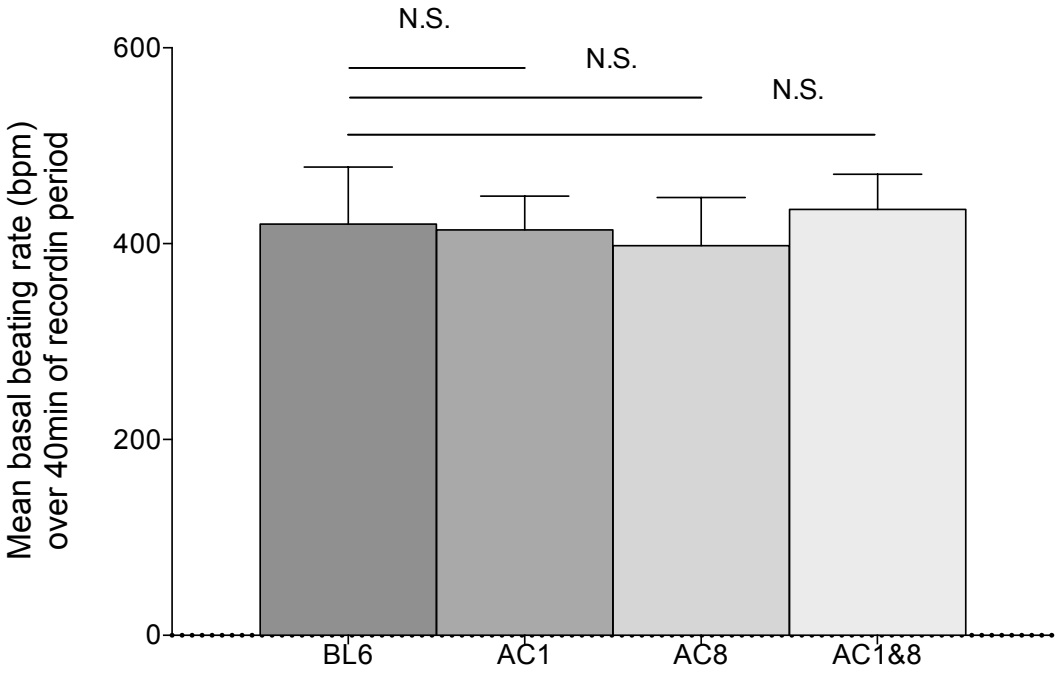


Figure 5.1 Bar chart representing the mean spontaneous beating rate in atrial preparations for wild type C57BL/6J (BL6, n = 24), AC1$^{(-/-)}$ (n = 25), AC8$^{(-/-)}$ (n = 24) and AC1&8$^{(-/-)}$ (n = 24) mice. Data are expressed as mean ± S.E.M., n = number of experiments. GraphPad Prism (version 5.0) software was used to perform statistical analysis, including one-way ANOVA with Dunnett post-test (significance level $P < 0.05$).

5.4. Effects of changes in extracellular Ca^{2+} concentration in modulating basal beating rate in mice with differential expression of Ca^{2+}-stimulated ACs.

The following experiments were done to assess the changes in extracellular Ca^{2+} concentration influence pacemaking in context of Ca^{2+}-stimulated ACs. Initially, atrial dissection was performed and the preparation was maintained in an organ bath at a base concentration of 1 mM Ca^{2+}. Next, the concentration was incrementally increased to 1.8 mM, then to 2.5 mM, and finally to 3.5 mM. For each incremental increase, a 20 min incubation period was allowed in order for the beating rate to reach a new steady state. Overall, with the exception of the AC1&8$^{(-/-)}$ atrial preparation, increasing the concentration of extracellular Ca^{2+} increased the basal beating rate. Increasing the extracellular Ca^{2+} concentration from 1 mM to 1.8 mM to 2.5 mM to 3.5 mM increased the beating rate by 9 ± 8 bpm, 35 ± 10 bpm and 53 ± 10 bpm, respectively, for the C57BL/6J strain (n = 8); 16 ± 3 bpm, 40 ± 6 bpm and 56 ± 16 bpm, respectively, for AC1$^{(-/-)}$ (n = 10); and 1 ± 6 bpm, 29 ± 8 bpm and 63 ± 7 bpm, respectively, for AC8$^{(-/-)}$ (n = 10). In contrast, for AC1&8$^{(-/-)}$, the beating rate *decreased* when extracellular Ca^{2+} concentration was increased. When the

concentration was increased from 1 mM to 1.8 mM, 2.5 mM and 3.5 mM, decreases of 32 ± 7 bpm, 55 ± 8 bpm and 68 ± 9 bpm, respectively, were seen (n = 8, **Figure 5.2**). Although it appears that knocking out both the AC1 and AC8 enzymes caused changes consistent with the physiological importance of these enzymes at rest (in the absence of autonomic influences), the observations with the knockouts of AC1 and AC8 alone can either indicate that these enzymes are unimportant, or that 'compensation' mechanisms came into play under the experimental conditions. Another possible explanation could be that either AC1 or AC8 activity alone is sufficient to maintain Ca^{2+} dependence.

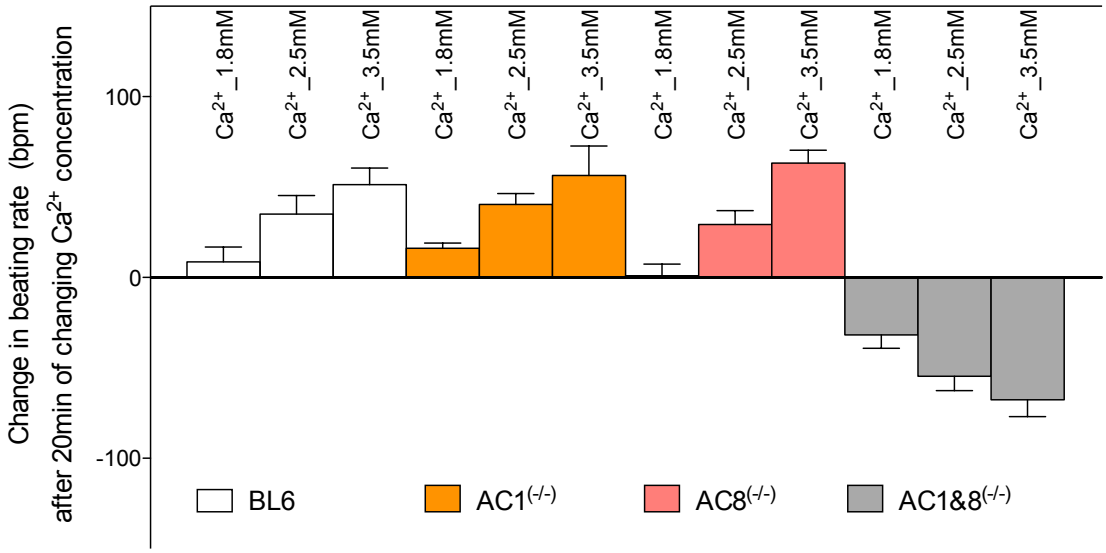


Figure 5.2 Bar chart representing the mean effect of incremental changes in $CaCl_2$ concentration, from 1 mM to 1.8 mM, 2.5 mM and 3.5 mM, on wild type C57BL/6J (BL6, n = 8), $AC1^{(-/-)}$ (n = 10), $AC8^{(-/-)}$ (n = 10) and $AC1\&8^{(-/-)}$ (n = 8) mice basal spontaneous beating rate in atrial preparations. Data are expressed as mean ± S.E.M., n = number of experiments. GraphPad Prism (version 5.0) software was used to perform statistical analysis, including Student's *t*-test, one-way ANOVA with Dunnett post-test (significance level $P < 0.05$).

5.5. Influence of ZD7288/ivabradine on basal beating rate at different extracellular Ca^{2+} concentrations in double knockout mouse model lacking both AC1&8 isoforms.

To assess how I_f inhibition influences the reduction in basal beating rate induced by increased extracellular Ca^{2+}, the above experiment (section 5.4.) was repeated for AC1&8$^{(-/-)}$, but this time in the presence of the 1 μM ZD7288 & 3 μM ivabradine combination. After a 30 min pre-incubation period to allow the preparation to reach new a reduced plateau steady state, the ability of increasing Ca^{2+} concentrations to reduce basal beating rate in AC1&8$^{(-/-)}$ was still apparent. Although the reductions were smaller than when no drug was present, the differences were not statistically significant. In the presence of the 1 μM ZD7288 & 3 μM ivabradine combination, increasing the extracellular Ca^{2+} concentration from 1 mM to 1.8 mM, 2.5 mM and 3.5 mM decreased the beating rate by 22 ± 3 bpm, 36 ± 3 bpm and 49 ± 5 bpm, respectively (n = 8, **Figure 5.3**).

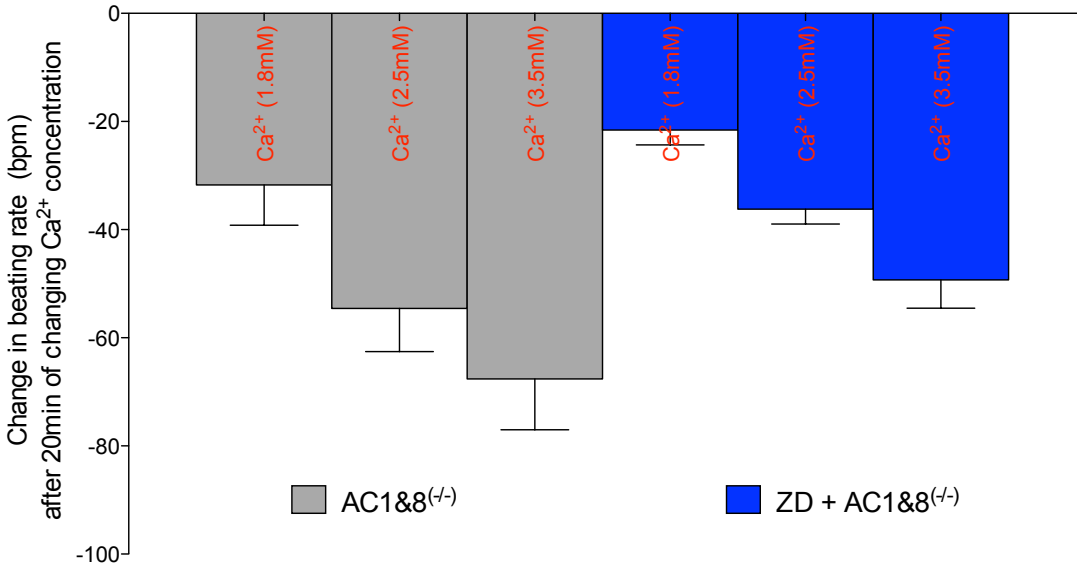


Figure 5.3. Bar chart representing the mean effect of incremental changes in $CaCl_2$ concentration, from 1 mM to 1.8 mM, 2.5 mM and 3.5 mM, in AC1&8$^{(-/-)}$ mice in the presence (n = 8) and absence of 1 μM ZD7288 + 3 μM Ivabradine (n = 8) on basal spontaneous beating rate of atrial preparations. Data are expressed as mean ± S.E.M., n = number of experiments. GraphPad Prism (version 5.0) software was used to perform statistical analysis, including Student's *t*-test (significance level $P < 0.05$).

5.6. Modulation of spontaneous beating rate at rest in mice with differential expression of Ca^{2+}-stimulated ACs

5.6.1. Influence of ZD7288/ivabradine (I_f inhibition) at rest in mice with differential expression of Ca^{2+} stimulated ACs

Possible changes in the influence of I_f channels on the spontaneous beating of atrial preparations due to lack of Ca^{2+}-stimulated AC was

investigated in the different knockout animals at an extracellular Ca^{2+} concentration of 1.8 mM. The atrial preparations from $AC1^{(-/-)}$, $AC8^{(-/-)}$ and $AC1\&8^{(-/-)}$ mice were incubated for 30 min with 1 μM ZD7288 + 3 μM ivabradine. The atrial preparations from the C57BL/6J mice were used as a control. The changes in beating rate observed were as follows: for the control (C57BL/6J) preparations, the rate was reduced by 55 ± 5%, a reduction of 233 ± 20 bpm from a resting beating rate of 420 ± 22 bpm ($P < 0.05$, n = 10, **Figure 5.4*A***); for $AC1^{(-/-)}$, beating rate was reduced by 56 ± 4%, a reduction of 232 ± 19 bpm from a resting rate of 414 ± 10 bpm ($P < 0.05$, n=12, **Figure 5.4*B***); for $AC8^{(-/-)}$, beating rate was reduced by 57 ± 4%, a reduction of 228 ± 13 bpm from a resting rate of 398 ± 11 bpm ($P < 0.05$, n = 12, **Figure 5.4*C***); and for $AC1\&8^{(-/-)}$, the rate was reduced by 48 ± 3%, a reduction of 210 ± 13 bpm from a resting beating rate of 435 ± 10 bpm ($P < 0.05$, n = 13, **Figure 5.4*D***).

The absolute reduction of basal spontaneous beating rates above are summarised in **Figure 5.4*E.*** The changes in basal beating rate induced by I_f inhibition in different knockout models relative to control were not significantly different ($P > 0.05$, one-way ANOVA with Dunnett post-test). Based on these observations, there appears to be no major contribution of AC1 and AC8 dependent pathways to the control of I_f at rest.

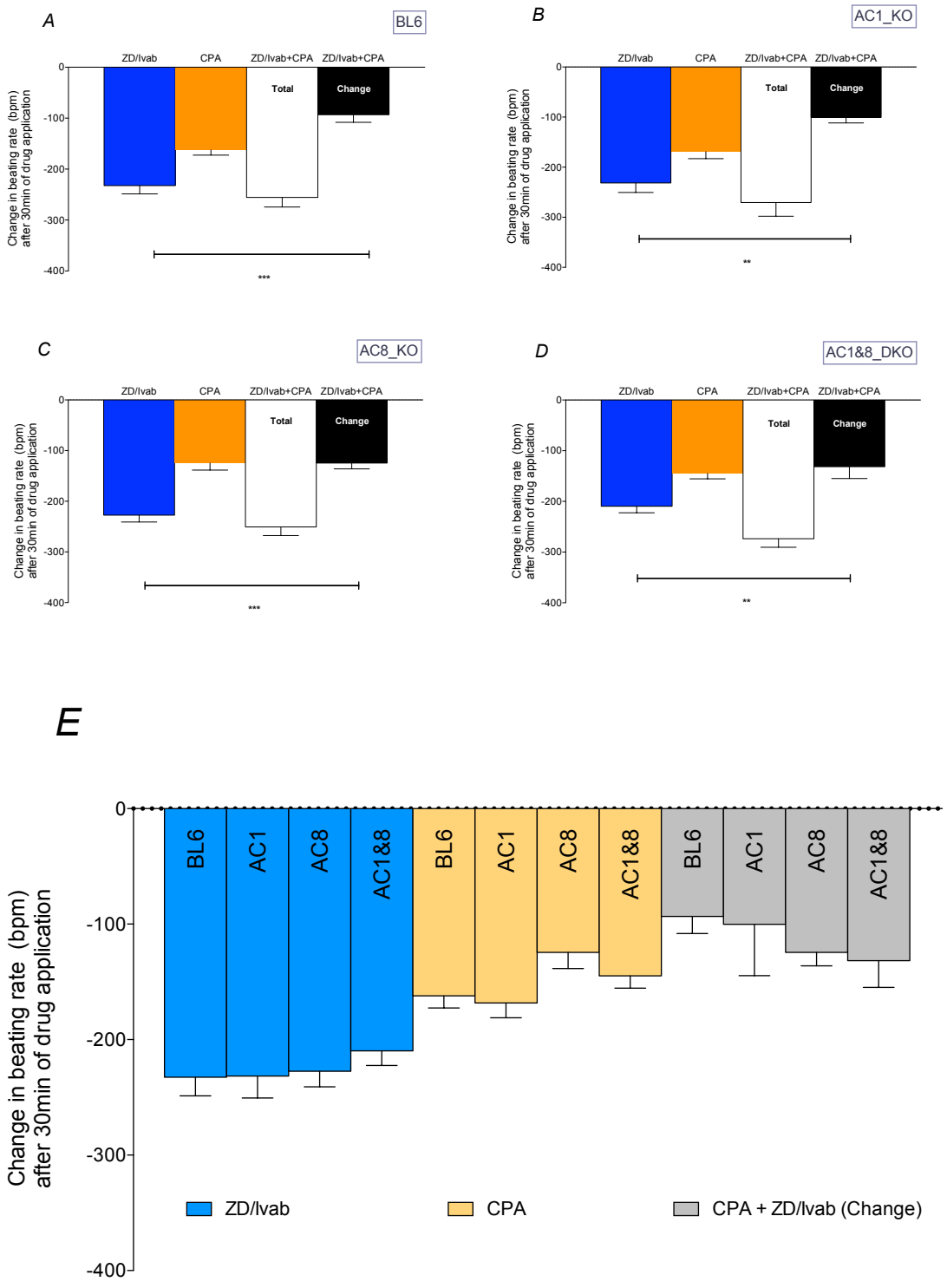


Figure 5.4 Bar chart representing the mean effect of 1 μM ZD7288 + 3 μM ivabradine, 100 μM CPA, and 1 μM ZD7288 + 3 μM ivabradine in the presence of 100 μM CPA on ***(A)*** wild type C57BL/6J (BL6, n = 10, n = 6 and n = 6 respectively), ***(B)*** $AC1^{(-/-)}$ (n = 12, n = 12 and n = 6 respectively), ***(C)*** $AC8^{(-/-)}$ (n = 12, n = 11 and n = 9 respectively) and ***(D)*** $AC1\&8^{(-/-)}$ (n = 13, n = 9 and n = 7 respectively) mice basal spontaneous beating rate in atrial preparations. 'Total'

represents cumulative change from baseline, while 'Change' represents the relative changes after CPA. ***(E)*** Regeneration of the summarized absolute reduction of basal spontaneous beating rate from ***(A) - (D)*** over the 40 min time period. Data are expressed as mean ± S.E.M., n = number of experiments. GraphPad Prism (version 5.0) software was used to perform statistical analysis, including Student's *t*-test, one-way ANOVA with Dunnett post-test, (significance level $P < 0.05$).

5.6.2. Influence of CPA (inhibition of Ca^{2+} release from SR) at rest in mice with differential expression of Ca^{2+}-stimulated ACs

The following experiments were done to assess the effect of a lack of Ca^{2+}-stimulated AC on the ability of Ca^{2+} release from SR to modulate basal beating rate. The atrial preparations from $AC1^{(-/-)}$, $AC8^{(-/-)}$ and $AC1\&8^{(-/-)}$ mice were incubated for 30 min with 100 µM CPA. The atrial preparation from the C57BL/6J mouse was used as a control, which was also incubated with 100 µM CPA for 30 min. The basal spontaneous beating for control (C57BL/6J) was reduced by 39 ± 4%, a reduction of 162 ± 11 bpm from a resting beating rate of 413 ± 13 bpm ($P < 0.05$, n = 6, **Figure 5.4*A***); for $AC1^{(-/-)}$, it was reduced by 39 ± 4%, a reduction of 160 ± 14 bpm from a resting beating rate of 408 ± 15 bpm ($P < 0.05$, n = 12, **Figure 5.4*B***); for $AC8^{(-/-)}$, beating rate was reduced by 29 ± 4%, a reduction of 125 ± 14 bpm from a resting beating rate of 426 ± 10 bpm ($P < 0.05$, n = 11, **Figure 5.4*C***); and for $AC1\&8^{(-/-)}$, the rate was reduced by 30 ± 4%, a reduction of 145 ± 11 bpm from a resting beating rate of 427 ± 14 bpm ($P < 0.05$, n = 9, **Figure 5.4*D***).

The absolute reductions of basal spontaneous beating rate are summarised in **Figure 5.4*E.*** The changes in basal beating rate induced by suppression of Ca^{2+} release from SR in the different knockout models relative to the control were not significantly different ($P > 0.05$, one-way ANOVA with Dunnett post-test). Therefore, there appears to be no major contribution of AC1 and AC8 dependent pathways in the ability of Ca^{2+} release from SR to modulate pacemaking at rest.

5.6.3. The influence of CPA (inhibition of Ca^{2+} release from SR) on I_f's modulation of basal beating rate in mice with differential expression of Ca^{2+} stimulated ACs

I next investigated how the lack of Ca^{2+}-stimulated AC influences ZD7288's ability to reduce the spontaneous beating rate of atrial preparations following inhibition of Ca^{2+} release with CPA. The atrial preparations from $AC1^{(-/-)}$, $AC8^{(-/-)}$ and $AC1\&8^{(-/-)}$ mice were pre-incubated for 30 min with 100 μM CPA, followed by a 30 min incubation with 1 μM ZD7288 + 3 μM ivabradine. The atrial preparation from the C57BL/6J mouse was used as a control, which was also pre-incubated with 100 μM CPA and 1 μM ZD7288 + 3 μM ivabradine, with each drug incubated for 30 min. In the presence of 100 μM CPA (pre-incubated for 30 min), 30 min incubation of 1 μM ZD7288 + 3 μM ivabradine reduced the basal spontaneous beating rate of atrial preparation for control (C57BL/6J) by 93 ± 15 ($P < 0.05$, n = 6, **Figure 5.4*A***); for $AC1^{(-/-)}$ by 101 ± 11 ($P < 0.05$, n = 6, **Figure 5.4*B***); for $AC8^{(-/-)}$ by 125 ± 12 ($P < 0.05$, n = 9, **Figure 5.4*C***); and for $AC1\&8^{(-/-)}$ by 131 ± 23 ($P < 0.05$, n = 7, **Figure 5.4*D***). These were significantly

smaller reductions compared 1 μM ZD7288 + 3 μM ivabradine on its own, which caused reductions of 218 ± 20 bpm (C57BL/6J), 232 ± 19 bpm ($AC1^{(-/-)}$), 228 ± 13 bpm ($AC8^{(-/-)}$), and 216 ± 13 bpm ($AC1\&8^{(-/-)}$) (**Figure 5.4*A-D***). The absolute reductions in basal spontaneous beating rate induced by ZD7288/ivabradine subsequent to suppression of Ca^{2+} release from SR by CPA are summarised in **Figure 5.4*E.*** The changes in basal beating rate in the different knockout models were not significantly different from control ($P > 0.05$, one-way ANOVA with Dunnett post-test). These observations suggest that there appears to be no major contribution of AC1 and AC8 dependent pathways to the cross-talk between I_f and Ca^{2+} release from SR.

5.7. Assessing effective I_f blockade

In order to assess the selectivity of ZD7288 and determine how completely the I_f channels were blocked, the ability of ivabradine [another selective I_f blocker with little or no effect on other currents at 3 μM (Bois *et al.,* 1996; Bucchi et al. 2002)] to further reduce the beating rate in the presence of 1 μM ZD7288 was assessed. To determine whether ZD7288 induces near complete inhibition, I applied 3 μM ivabradine subsequent to pretreatment with 1 μM ZD7288. Pre-treating the atrial preparation with 1 μM ZD7288 (over a 30 min time period) reduced the initial basal beating rate for C57BL/6J by 215 ± 18 bpm ($P < 0.05$, n = 6); for $AC1^{(-/-)}$ by 211 ± 11 bpm ($P < 0.05$, n = 6); for $AC8^{(-/-)}$ by 195 ± 18 bpm ($P < 0.05$, n = 6); and for $AC1\&8^{(-/-)}$ by 217 ± 15 bpm ($P < 0.05$, n = 6). Subsequent addition of 3 μM ivabradine (over another 30 min time period) in the presence of 1 μM ZD7288 further reduced the basal spontaneous

beating rate for control (C57BL/6J) by 19 ± 5 bpm (n = 6); for AC1$^{(-/-)}$ by 16 ± 6 bpm (n = 6); for AC8$^{(-/-)}$ by 27 ± 6 bpm (n = 6); and for AC1&8$^{(-/-)}$ by 16 ± 6 bpm (n = 6). However, none of the further reductions induced by ivabradine were statistically significant (**Figure 5.5**). This suggests that with 1 μM ZD7288, the I_f channels were almost fully blocked.

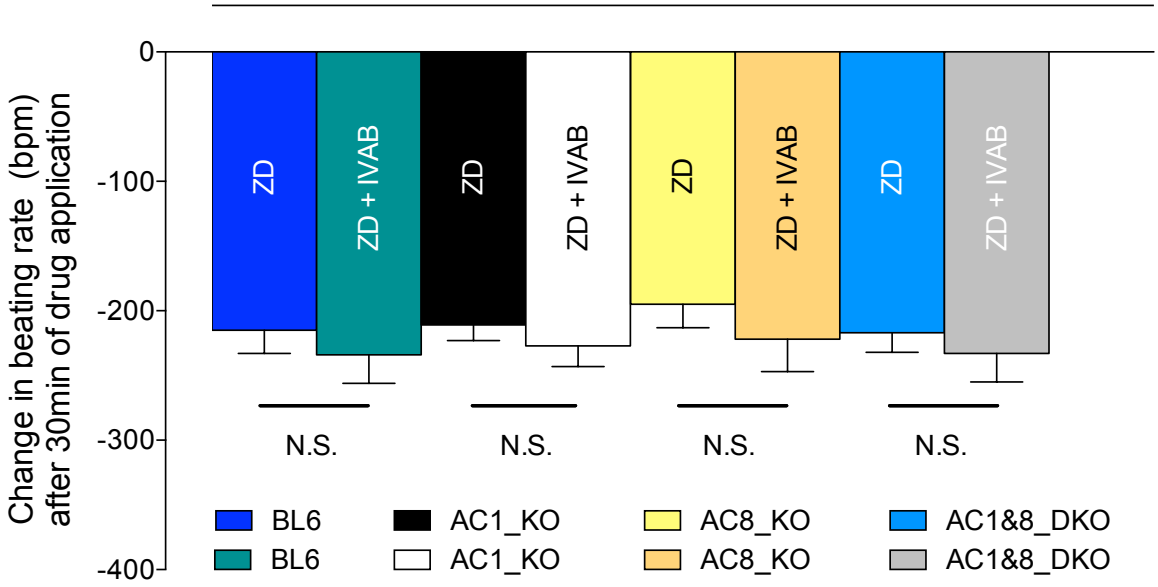


Figure 5.5. Bar chart representing the mean effect of 1 μM ZD7288 and 3 μM ivabradine in the presence of 1 μM ZD7288 on wild type C57BL/6J (BL6, n= 6), AC1$^{(-/-)}$ (n = 6), AC8$^{(-/-)}$ (n = 6) and AC1&8$^{(-/-)}$ (n = 6) mice basal spontaneous beating rate of atrial preparations, represented by respective colours. Data are expressed as mean ± S.E.M., n = number of experiments. GraphPad Prism (version 5.0) software was used to perform statistical analysis, including Student's *t*-test (significance level $P < 0.05$).

5.8. Fluorescent Ca^{2+} transient measurements

5.8.1. Influence of ZD7288/ivabradine (I_f inhibition) at rest in mice with differential expression of Ca^{2+}-stimulated ACs, assessed via Ca^{2+} transient measurements.

With the aim of assessing how the lack of Ca^{2+}-stimulated ACs influences I_f channels at a Ca^{2+} transient level, atrial preparations from $AC1^{(-/-)}$, $AC8^{(-/-)}$ and $AC1\&8^{(-/-)}$ mice were incubated for 40 min with 1 µM ZD7288 + 3 µM ivabradine. An atrial preparation from a C57BL/6J mouse was used as the control, which was also incubated with 1 µM ZD7288 + 3 µM ivabradine. The basal spontaneous beating rate of the atrial preparation was reduced for the control (C57BL/6J) by 169 ± 13 bpm or 54 ± 3% ($P < 0.05$, n = 6, after 40 min time period, **Figure 5.6*A***); for $AC1^{(-/-)}$ by 160 ± 12 bpm or 52 ± 3% ($P < 0.05$, n = 10, after 40 min time period, **Figure 5.6*C***); for $AC8^{(-/-)}$ by 154 ± 11 bpm or 47 ± 3% ($P < 0.05$, n = 6, after 40 min time period, **Figure 5.6*E***); and $AC1\&8^{(-/-)}$ by 147 ± 11 bpm or 49 ± 3% ($P < 0.05$, n = 6, after 40 min time period, **Figure 5.6*G***). Over the same 40 min period, the Ca^{2+} transient amplitude for the C57BL/6J was reduced by 42 ± 2% (**Figure 5.6*B***); for $AC1^{(-/-)}$ it was reduced by 38 ± 3% (**Figure 5.6*D***); for $AC8^{(-/-)}$ it was reduced by 34 ± 5% (**Figure 5.6*F***); and for $AC1\&8^{(-/-)}$ it was reduced by 37 ± 4% (**Figure 5.6*H***). These reductions in Ca^{2+} transient amplitude were not significantly different than in the absence of I_f inhibition (**Figure 5.6*B***). The absolute reductions in basal spontaneous beating rate over the 40 min time period are summarised in **Figure 5.6*I.*** The changes in basal beating rate induced by I_f inhibition in different knockout models were not significantly different from control. Therefore, there appears to be no major contribution of AC1 and AC8 dependent pathways to the effect of I_f at rest.

5.8.2. Influence of CPA (inhibition of Ca^{2+} release from SR) at rest in mice with differential expression of Ca^{2+}-stimulated ACs, assessed via Ca^{2+} transient measurements.

The following experiments were done in order to assess how the lack of Ca^{2+}-stimulated ACs affect the ability of Ca^{2+} release from SR to modulate basal beating rate in the SAN at a Ca^{2+} transient level. Atrial preparations from $AC1^{(-/-)}$, $AC8^{(-/-)}$ and $AC1\&8^{(-/-)}$ mice were incubated for 30 min with 100 μM CPA. The atrial preparation from a C57BL/6J mouse was used as a control, which was also incubated with 100 μM CPA for 30 min. The basal spontaneous beating rate for atrial preparations was reduced for C57BL/6J by 138 ± 6 bpm or 44 ± 3% ($P < 0.05$, n = 7, after 40 min, **Figure 5.6*A***); for $AC1^{(-/-)}$ by 128 ± 15 bpm or 40 ± 3% ($P < 0.05$, n = 10, after 40 min, **Figure 5.6*C***); for $AC8^{(-/-)}$ by 117 ± 13 bpm or 38 ± 3% ($P < 0.05$, n = 6, after 40 min, **Figure 5.6*E***); and for $AC1\&8^{(-/-)}$ by 117 ± 12 bpm or 37 ± 3% ($P < 0.05$, n = 6, after 40 min, **Figure 5.6*G***). Over the same 40 min period, the Ca^{2+} transient amplitude for C57BL/6J was reduced by 68 ± 1% (**Figure 5.6*B***); for $AC1^{(-/-)}$ it was reduced by 72 ± 3% (**Figure 5.6*D***); for $AC8^{(-/-)}$ it was reduced by 71 ± 1% (**Figure 5.6*F***); and for $AC1\&8^{(-/-)}$ it was reduced by 70 ± 3% (**Figure 5.6*H***). These reductions in Ca^{2+} transient amplitude were significantly different from amplitudes in the absence of CPA (**Figure 5.6*B***). The absolute reduction in basal spontaneous beating rate over the 40 min time period are summarised in **Figure 5.6*I.*** The changes in basal beating rate induced by suppression of Ca^{2+} release from SR in the different knockout models were not significantly different from control. Therefore, there appears to be no major contribution of the AC1 and AC8 dependent pathways to the effect of Ca^{2+} release from SR at rest.

5.8.3. The influence of CPA (inhibition of Ca^{2+} release from SR) on I_f's modulation of basal beating rate in mice with differential expression of Ca^{2+}-stimulated ACs, assessed via Ca^{2+} transient measurements

Subsequently, I investigated how the lack of Ca^{2+}-stimulated AC influences the ability of ZD7288/ivabradine to reduce spontaneous beating in atrial preparations following inhibition of Ca^{2+} release from SR with CPA at the Ca^{2+} transient level. The atrial preparations from $AC1^{(-/-)}$, $AC8^{(-/-)}$ and $AC1\&8^{(-/-)}$ mice were first pre-incubated for 30 min with 100 μM CPA, followed by 30 min incubation with 1 μM ZD7288 + 3 μM ivabradine. The C57BL/6J atrial preparation was used as a control and was pre-incubated with 100 μM CPA and 1 μM ZD7288 + 3 μM ivabradine, with each drug incubated for 30 min. In the presence of 100 μM CPA (pre-incubated for 30 min), 1 μM ZD7288 caused the basal spontaneous beating in atrial preparations to be reduced by 60 ± 8 bpm for C57BL/6J ($P < 0.05$, n = 6, **Figure 5.6*A***); 65 ± 7 bpm for $AC1^{(-/-)}$ ($P < 0.05$, n = 6, **Figure 5.6*B***); 65 ± 9 bpm for $AC8^{(-/-)}$ ($P < 0.05$, n = 6, **Figure 5.6*C***); and 95 ± 6 bpm for $AC1\&8^{(-/-)}$ ($P < 0.05$, n = 6, **Figure 5.6*D***). These were significantly smaller reductions than seen with 1 μM ZD7288 + 3 μM ivabradine alone, which caused reductions of 169 ± 13 bpm (C57BL/6J), 160 ± 12 bpm ($AC1^{(-/-)}$), 154 ± 11 bpm ($AC8^{(-/-)}$), and 147 ± 11 bpm ($AC1\&8^{(-/-)}$) (**Figure 5.6*A-D***). The absolute reductions in basal spontaneous beating rate over the 40 min period are summarised in **Figure 5.6*I*.** The changes in basal beating rate induced by ZD7288 + ivabradine subsequent to suppression of Ca^{2+} release from SR by CPA in the different knockout models were not significantly different from control. Therefore, there appears to be no major contribution of AC1 and AC8 dependent pathways in the crosstalk between I_f and Ca^{2+} release from SR.

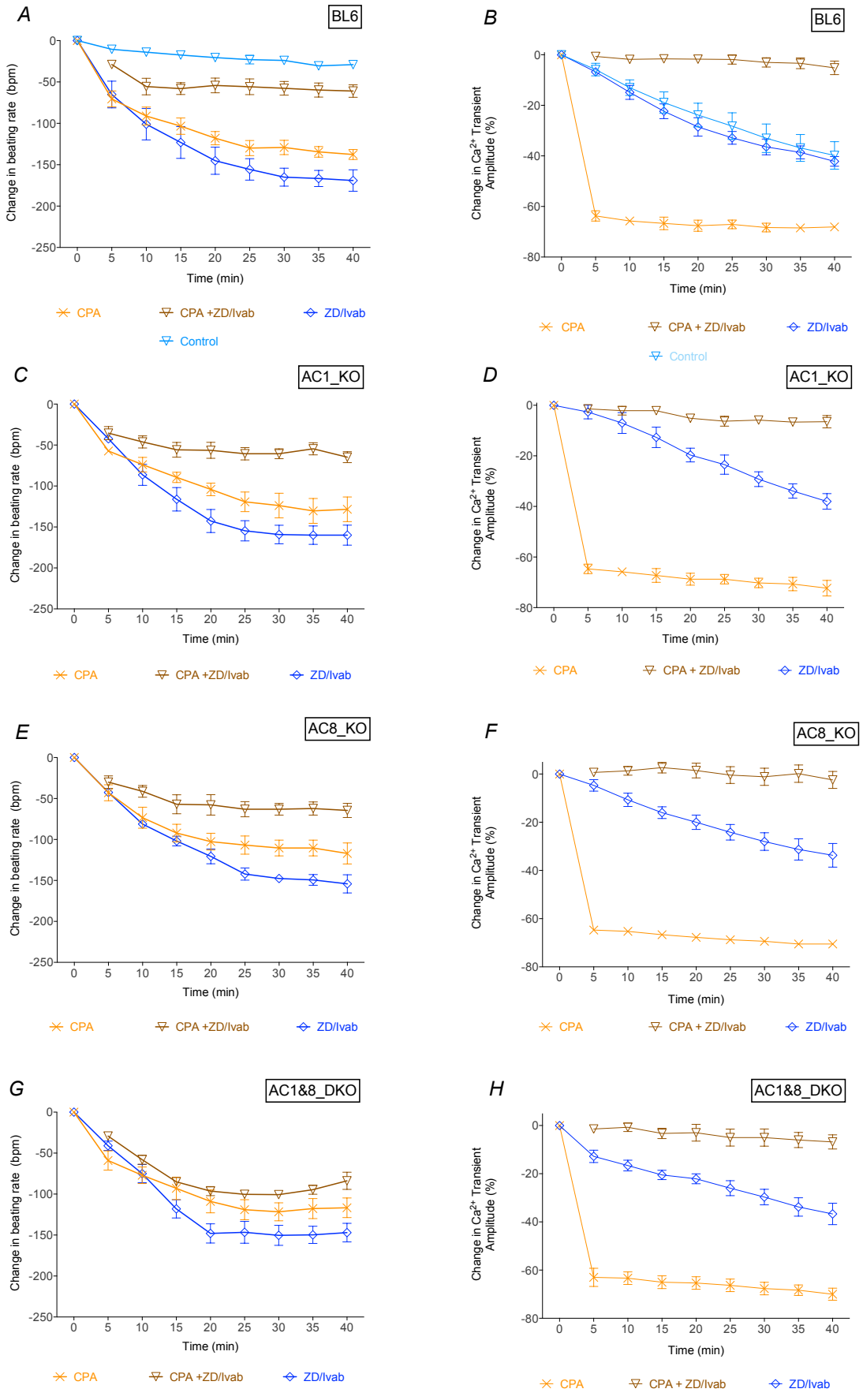

A
BL6
Change in beating rate (bpm)
Time (min)
CPA
CPA +ZD/Ivab
ZD/Ivab
Control
B
BL6
Change in Ca2+ Transient Amplitude (%)
Time (min)
CPA
CPA + ZD/Ivab
ZD/Ivab
Control
C
AC1_KO
Change in beating rate (bpm)
Time (min)
CPA
CPA +ZD/Ivab
ZD/Ivab
D
AC1_KO
Change in Ca2+ Transient Amplitude (%)
Time (min)
CPA
CPA + ZD/Ivab
ZD/Ivab
E
AC8_KO
Change in beating rate (bpm)
Time (min)
CPA
CPA +ZD/Ivab
ZD/Ivab
F
AC8_KO
Change in Ca2+ Transient Amplitude (%)
Time (min)
CPA
CPA + ZD/Ivab
ZD/Ivab
G
AC1&8_DKO
Change in beating rate (bpm)
Time (min)
CPA
CPA +ZD/Ivab
ZD/Ivab
H
AC1&8_DKO
Change in Ca2+ Transient Amplitude (%)
Time (min)
CPA
CPA + ZD/Ivab
ZD/Ivab

Figure 5.6

I

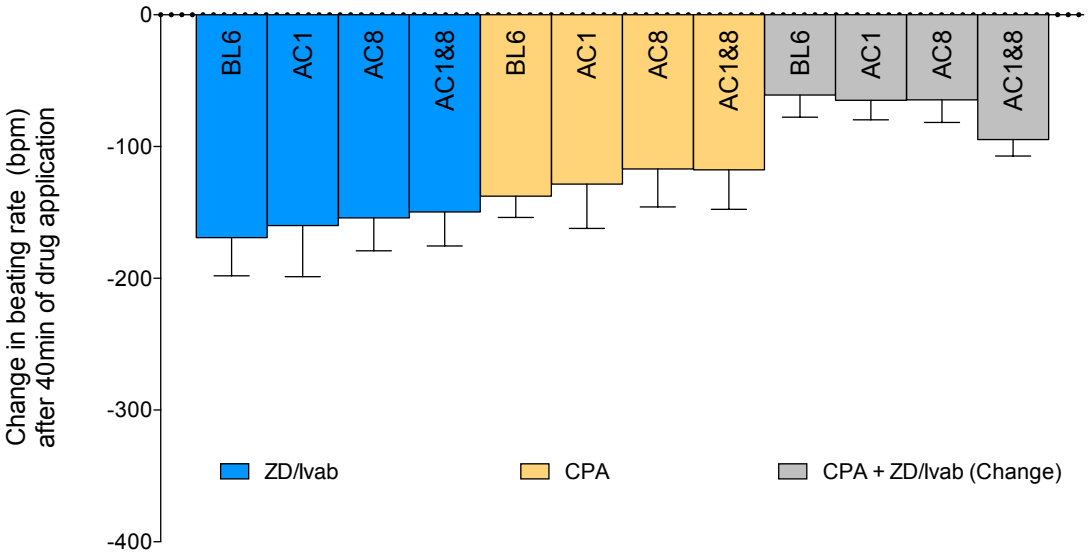


Figure 5.6 Graphs in the left column ***[(A)*** C57BL/6J, ***(C)*** *AC1*$^{(-/-)}$, ***(E)*** *AC8*$^{(-/-)}$ *and* ***(G)*** *AC1&8*$^{(-/-)}$***]*** show the mean changes in rate of beating over time, while graphs in the right column [***(B)*** C57BL/6J, ***(D)*** *AC1*$^{(-/-)}$, ***(F)*** *AC8*$^{(-/-)}$, ***(H)*** *AC1&8*$^{(-/-)}$] are the mean changes in amplitude of the Ca^{2+} transients over the same time in the presence of 1 μM ZD7288 + 3 μM ivabradine, 100 μM CPA, and 1 μM ZD7288 + 3 μM ivabradine in the presence of 100 μM CPA on ***(A & B)*** wild type C57BL/6J (BL6, n = 6, n = 7 and n = 6 respectively), ***(C & D)*** AC1$^{(-/-)}$ (n = 10, n = 10 and n = 6 respectively), ***(E & F)*** AC8$^{(-/-)}$ (n = 6, n = 6 and n = 6 respectively) and ***(G & H)*** AC1&8$^{(-/-)}$ (n = 6, n = 6 and n = 6 respectively) mice, measured from the fluorescent Ca^{2+} transients recorded from the SAN region. ***(I)*** Summary of absolute reductions in basal spontaneous beating rate from ***(A), (C), (E)*** *and* ***(G),*** for the 40 min time period. Data are expressed as mean ± S.E.M., n = number of experiments. GraphPad Prism (version 5.0) software was used to perform statistical analysis, including Student's *t*-test, one-way ANOVA with Dunnett post-test and two-way ANOVA with Bonferroni post-test (significance level $P < 0.05$).

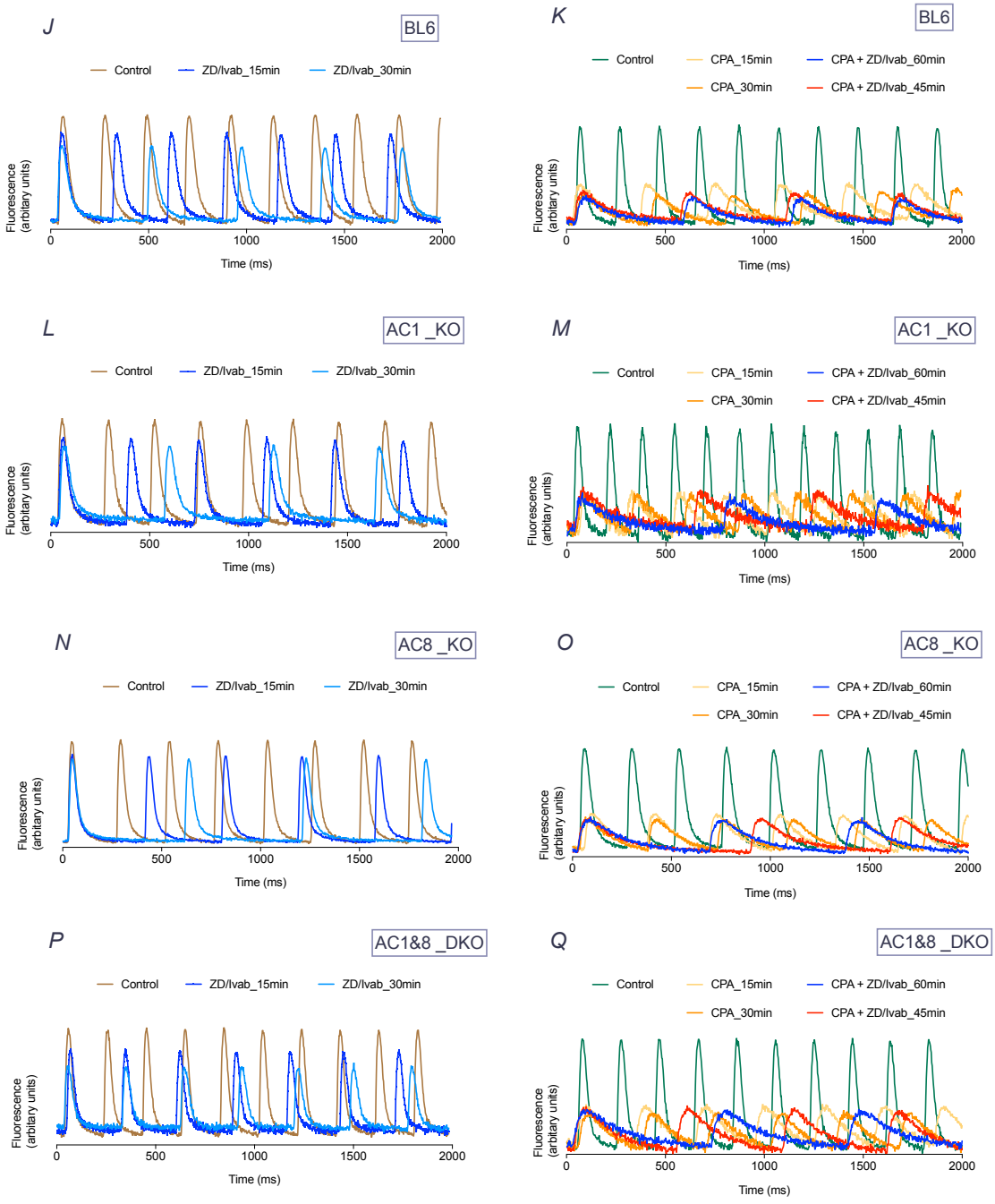


Figure 5.6 Representative traces of fluorescent Ca^{2+} transient measurements from the SAN region of ***(J & K)*** C57BL/6J, ***(L & M)*** *AC1*$^{(-/-)}$, ***(N & O)*** *AC8*$^{(-/-)}$ *and* ***(P & Q)*** *AC1&8*$^{(-/-)}$. ***(J, L, N & P)*** Control and 1 μM ZD7288 in combination with 3 μM ivabradine. ***(K, M, O & Q)*** Control, 100 μM CPA, and 100 μM CPA in the presence of 1 μM ZD7288 in combination with 3 μM ivabradine.

5.9. The effect of differential expression of Ca^{2+}-stimulated ACs on β-adrenergic receptor-stimulated beating rate

5.9.1. The contribution of Ca^{2+}-stimulated AC to I_f's influence on mouse beating rate in the presence of β-adrenergic pathway stimulation, assessed using I_f blockers.

Experiments were carried out to investigate the contribution of Ca^{2+}-stimulated ACs on influence of I_f blockade and suppression of SR function on spontaneous beating rate in the presence of β-adrenoceptor stimulation. 1-100 nM isoprenaline on its own caused a rapid increase in beating rate in mouse atrial preparation, reaching a steady state within 2 min of exposure at each concentration. At its maximum concentration of 100 nM, isoprenaline increased the beating rate by 217 ± 2 bpm for C57BL/6J (*P* < *0.05*, n = 12, **Figure 5.8*A***); by 219 ± 4 bpm for $AC1^{(-/-)}$ (*P* < *0.05*, n = 6, **Figure 5.8*B***); by 211 ± 3 bpm for $AC8^{(-/-)}$ (*P* < *0.05*, n = 7, **Figure 5.8*C***); and by 198 ± 3 bpm for $AC1\&8^{(-/-)}$ (*P* < *0.05*, n = 9, **Figure 5.8*D***).

When 1 - 100 nM isoprenaline was added to the spontaneously beating mouse atrial preparation in the presence of 1 μM ZD7288 + 3 μM ivabradine (30 min pre-incubation was required to reach new reduced plateau steady state), its effects were reduced at each concentration. The reductions were statistically significant for control (n = 9, **Figure 5.8*A***), $AC1^{(-/-)}$ (n = 6, **Figure 5.8*B***) and $AC8^{(-/-)}$ (n = 6, **Figure 5.8*C***) (1 - 100 nM, *P* < *0.05,* two-way ANOVA with Bonferroni post-test). For $AC1\&8^{(-/-)}$ (n = 6), the reduction in isoprenaline effect was significant at the lower end of the concentration spectrum (1 - 10 nM, *P* <

0.05, two-way ANOVA with Bonferroni post-test). Concentrations of isoprenaline above 10 nM in the presence of 1 μM ZD7288 induced cyclical instability in beating rate in AC1&8$^{(-/-)}$ (**Figure 5.7*C***). Also, when the dose response curve was taken as a whole, there was a statistically significant downward shift of the curves in the presence of 1 μM ZD7288 + 3 μM ivabradine relative to controls. At the highest concentration of 100 nM, isoprenaline in the presence of 1 μM ZD7288 + 3 μM ivabradine increased the beating rate by 168 ± 2 bpm, compared to a 217 ± 2 bpm increase in the absence of 1 μM ZD7288 + 3 μM ivabradine for C57BL/6J control (**Figure 5.8*A***); by 148 ± 3 bpm relative to a 219 ± 4 bpm increase in the absence of 1 μM ZD7288 + 3 μM ivabradine for AC1$^{(-/-)}$ (**Figure 5.8*B***); and by 143 ± 3 bpm relative to a 211 ± 3 bpm increase in the absence of 1 μM ZD7288 + 3 μM ivabradine for AC8$^{(-/-)}$ (**Figure 5.8*C***). In the case of AC1&8$^{(-/-)}$, I took 10 nM as the highest concentration. At 10 nM isoprenaline in presence of 1 μM ZD7288 + 3 μM ivabradine, the rate was increased by 71 ± 2 bpm compared to a 181 ± 3 bpm increase in the absence of 1 μM ZD7288 + 3 μM ivabradine for AC1&8$^{(-/-)}$ (**Figure 5.8*D***).

Unlike C57BL/6J, AC1$^{(-/-)}$ and AC8$^{(-/-)}$ atrial preparations no isoprenaline log(concentration)-response curve was possible to constructed in the presence of 1 μM ZD7288, beyond 10 nM isoprenaline for the AC1&8$^{(-/-)}$ atrial preparation. This is because isoprenaline above 10 nM in presence of 1 μM ZD7288 induces cyclical (very slow oscillation) instability in the beating rate in AC1&8$^{(-/-)}$ (**Figure 5.7*C***). Moreover, for the construction of the isoprenaline log(concentration)-response curve from 1 to 10 nM isoprenaline for AC1&8$^{(-/-)}$, only 3 out of 10 atrial preparations were viable to use. The remaining 7 displayed cyclical instability in beating rate at 1 nM isoprenaline. Cyclical

instability was also present in C57BL/6J, AC1$^{(-/-)}$ and AC8$^{(-/-)}$ atrial preparations for construction of the isoprenaline log(concentration)-response curve, occurring in 4 out of 10, 5 out of 10 and 7 out of 10 atrial preparations respectively.

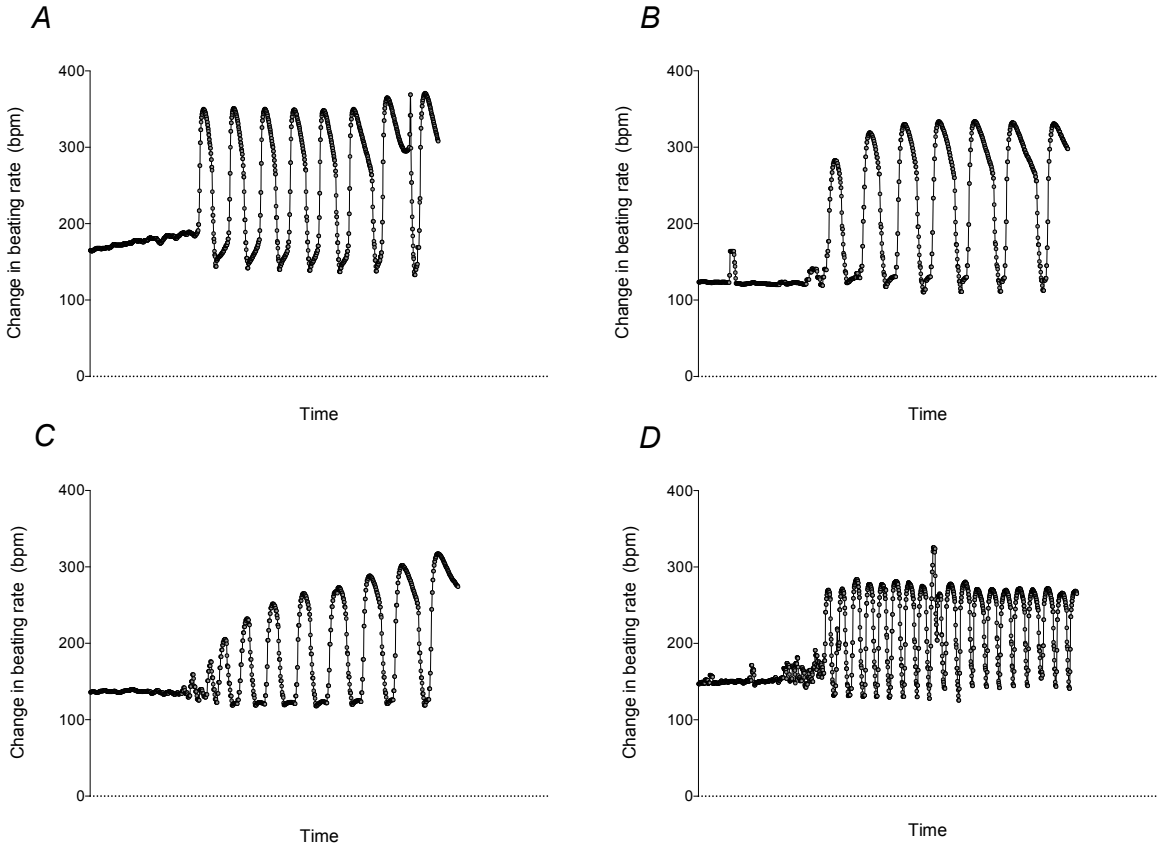


Figure 5.7 Representative traces of cyclical instability in beating rate induced by > 10nM isoprenaline in the presence of 100 μM CPA and 1 μM ZD7288 + 3 μM ivabradine pretreatment for ***(A)*** AC1$^{(-/-)}$, ***(B)*** AC8$^{(-/-)}$, and ***(C)*** AC1&8$^{(-/-)}$ in the presence of 1 μM ZD7288. **(*D*)** For AC1&8$^{(-/-)}$, as little as 1 nM isoprenaline induced arrhythmia in presence of 1 μM ZD7288 + 3 μM ivabradine and 100 μM CPA.

5.9.2. The contribution of Ca^{2+}-stimulated AC to Ca^{2+} release from SR's influence on mouse beating rate in the presence of β-adrenergic pathway stimulation, assessed using SR blocker.

Pre-treatment of C57BL/6J, $AC1^{(-/-)}$, $AC8^{(-/-)}$ and $AC1\&8^{(-/-)}$ atrial preparations with 100 μM CPA (30 min pre-incubation in order to reach a new reduced plateau steady state) followed by the addition of 1 - 100 nM isoprenaline reduced the increase in spontaneous beating rate of mouse atrial preparation at each concentration. The reductions were all statistically significant, with the only exception being 1 nM isoprenaline for $AC1\&8^{(-/-)}$. For control C57BL/6J (n = 8, **Figure 5.8*A***), $AC1^{(-/-)}$ (n = 7, **Figure 5.8*B***) and $AC8^{(-/-)}$ (n = 6**, Figure 5.8*C***), the statistical results were $P < 0.05$ for 1 - 100 nM (two-way ANOVA with Bonferroni post-test). For $AC1\&8^{(-/-)}$ (n = 10, **Figure 5.8*C***), the statistical result was $P < 0.05$ for 3 - 100 nM (two-way ANOVA with Bonferroni post-test). Also, when the dose response curve was taken as a whole, a statistically significant downward shift was observed in the presence of 100 μM CPA relative to respective controls. At the highest concentration of 100 nM, isoprenaline in the presence of 100 μM CPA increased the beating rate by 131 ± 11 bpm compared to a 217 ± 2 bpm increase in the absence of 100 μM CPA for C57BL/6J (**Figure 5.8*A***); by 84 ± 14 bpm relative to a 219 ± 4 bpm increase in the absence of 100 μM CPA for $AC1^{(-/-)}$ (**Figure 5.8*B***); by 71 ± 14 bpm relative to a 211 ± 3 bpm increase in the absence of 100 μM CPA for $AC8^{(-/-)}$ (**Figure 5.8*C***); and by 90 ± 11 bpm relative to a 198 ± 3 bpm increase in the absence of 100 μM CPA for $AC8\&1^{(-/-)}$ (**Figure 5.8*D***). Note that compared with C57BL/6J, the log(concentration)-response curve for isoprenaline was

depressed to a greater extent in AC8$^{(-/-)}$ after SR Ca^{2+} was depleted using CPA. However, this did not seem to be the case in AC8&1$^{(-/-)}$.

5.9.3. The influence of Ca^{2+}-stimulated AC on the contribution of Ca^{2+} release from SR and I_f combined on beating rate via the β-adrenergic pathway, assessed from the effects of combined application of CPA and I_f blockers

Incubating the preparation with 100 μM CPA followed by 1 μM ZD7288 + 3 μM ivabradine reduced the isoprenaline-induced increase in spontaneous beating rate at each concentration of isoprenaline, and the reductions were all statistically significant (1 - 100 nM, $P < 0.05$, two-way ANOVA with Bonferroni post-test). For AC1&8$^{(-/-)}$, the isoprenaline log(concentration)-response curve could not be built because as little as 1 nM isoprenaline induced cyclical instability in beating rate when the preparation was pre-incubated with 1 μM ZD7288 + 3 μM ivabradine and 100 μM CPA (**Figure 5.7*D***). For AC1$^{(-/-)}$ (n = 6) and AC8$^{(-/-)}$ (n = 4), however, the cyclical instability was only observed at isoprenaline concentrations above 10 nM (**Figure 5.7*A* & *B***). For C57BL/6J (n = 6) at the highest isoprenaline concentration (100 nM), beating rate was increased by 52 ± 2 bpm compared to a 217 ± 2 bpm increase in the absence of 100 μM CPA and 1 μM ZD7288 + 3 μM ivabradine (**Figure 5.8*A***). In the case of AC1$^{(-/-)}$ and AC8$^{(-/-)}$, I took 10 nM as the highest concentration. At 10 nM isoprenaline in the presence of 100 μM CPA and 1 μM ZD7288 + 3 μM ivabradine the rate was increased by 37 ± 2 bpm compared to a 186 ± 3 bpm increase in the absence of any drugs for AC1$^{(-/-)}$ (**Figure 5.8*B***), and it was

increased by 22 ± 2 bpm compared to a 205 ± 3 bpm increase observed in the absence of pretreatment for AC8$^{(-/-)}$ (**Figure 5.8*C***).

The above described observations provide further evidence for differences between the knockout models compared to control atrial preparations. In the presence of 100 μM CPA and 1 μM ZD7288 + 3 μM ivabradine, no isoprenaline log(concentration)-response curve could be constructed for AC1&8$^{(-/-)}$. This is because as little as 1 nM isoprenaline induced cyclical instability in beating rate in AC1&8$^{(-/-)}$ (**Figure 5.7*D***). Furthermore, no isoprenaline log(concentration)-response curve could be constructed beyond 10 nM isoprenaline for AC1$^{(-/-)}$ and AC8$^{(-/-)}$ in the presence of 100 μM CPA and 1 μM ZD7288 + 3 μM ivabradine combination (**Figure 5.7*A* & *B***). This was due to presence of cyclical instability in beating beyond 10 nM isoprenaline. Moreover, for the construction of the isoprenaline log(concentration)-response curve from 1 - 10 nM isoprenaline for AC1$^{(-/-)}$ and AC8$^{(-/-)}$ in the presence of 100 μM CPA and 1 μM ZD7288 + 3 μM ivabradine, only 3 out of 10 and 2 out of 10 atrial preparations, respectively, were viable to use. The remaining 7 and 6 respective preparations showed cyclical instability in beating rate at 1 nM isoprenaline. The cyclical instability was also present in C57BL/6J atrial preparations for the isoprenaline log(concentration)-response curve construction, occurring in 4 out of 10 atrial preparations under these conditions.

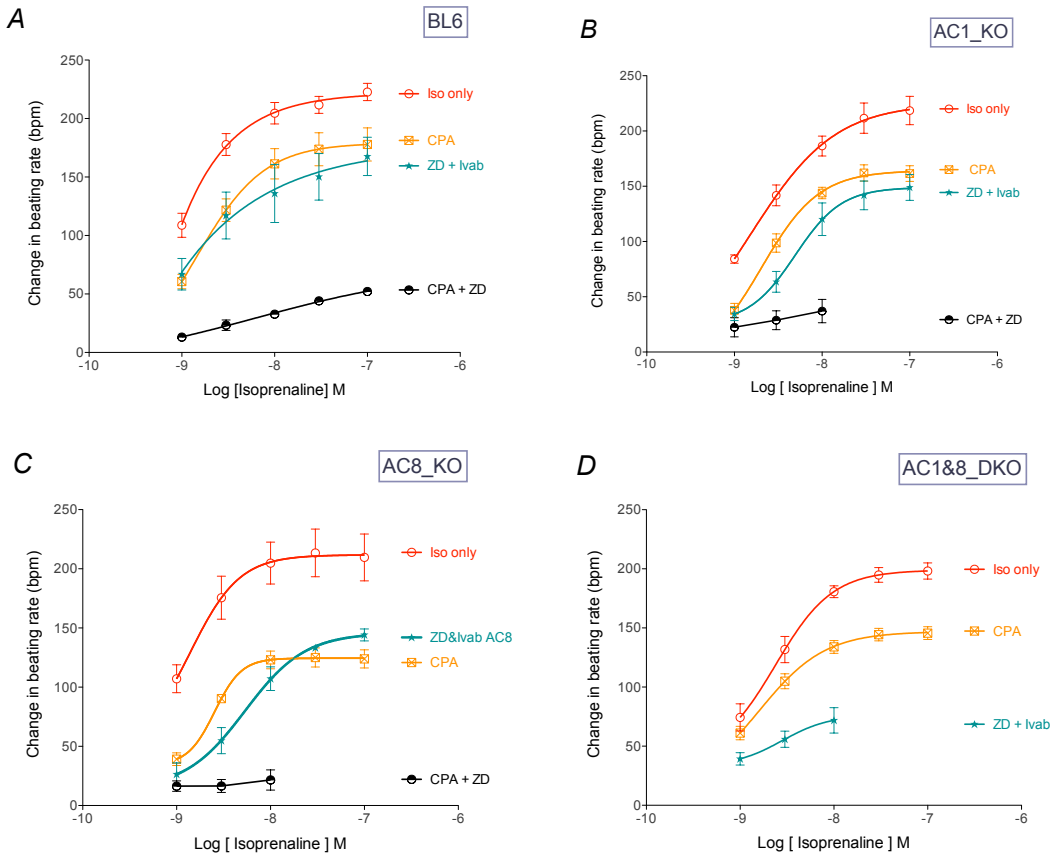


Figure 5.8. Graph representing mean change in the positive chronotropic action of the β-adrenoceptor agonist isoprenaline alone and in the presence of 1 μM ZD7288 + 3 μM ivabradine, 100 μM CPA, 1 μM ZD7288 + 3 μM ivabradine in the presence of 100 μM CPA on ***(A)*** wild type C57BL/6J (BL6, n = 12, n = 9, n = 8 and n = 6 respectively), ***(B)*** $AC1^{(-/-)}$ (n = 6, n = 6, n = 7 and n = 6 respectively), ***(C)*** $AC8^{(-/-)}$ (n = 7, n = 6, n = 6 and n = 4 respectively), and ***(D)*** $AC1\&8^{(-/-)}$ (n = 9, n = 6 and n = 10 respectively) mice basal spontaneous beating rate of atrial preparations. Data are expressed as mean ± S.E.M., n = number of experiments. GraphPad Prism (version 5.0) software was used to perform statistical analysis, including two-way ANOVA with Bonferroni post-test (significance level $P < 0.05$).

5.9.4. Contribution of Ca^{2+}-stimulated AC on the influence of L-type Ca^{2+} channels in the β-adrenergic pathway in mouse, assessed by partial blockade with nifedipine

Given that the change in extracellular Ca^{2+} concentration reduced the basal beating rate in AC1&8$^{(-/-)}$, the question arose of how the β-adrenergic pathway would be influenced when the Ca^{2+} influx through L-type Ca^{2+} channels was reduced. First, the beating rate changes induced by 1 - 100 nM isoprenaline alone were assessed. 1 - 100 nM isoprenaline caused a rapid increase in beating rate in mouse atrial preparation, reaching steady state within 2 min of exposure for each concentration. At its maximum concentration of 100 nM, isoprenaline increased beating rate by 219 ± 2 bpm for C57BL/6J ($P < 0.05$, n = 14, **Figure 5.9*A***) and by 195 ± 2 bpm for AC1&8$^{(-/-)}$ ($P < 0.05$, n = 22, **Figure 5.9*B***).

When 1 - 100 nM isoprenaline was added in the presence of 100 or 300 nM nifedipine (30 min pre-incubation was required to reach new reduced plateau steady state), the effects of isoprenaline on the spontaneously beating mouse atrial preparation for both C57BL/6J and AC1&8$^{(-/-)}$ were reduced at isoprenaline concentrations below 10 nM and *increased* above 10 nM compared to when nifedipine was not present (**Figure 5.9*A***). For C57BL/6J, only 3 nM isoprenaline induced a reduction, while 30 nM together with 100 nM isoprenaline induced increase. These effects were in the presence of 100 nM nifedipine and were significant relative to control (n = 6). Also, in the presence of 300 nM nifedipine, only 10 nM isoprenaline caused no significant change (n = 6). For AC1&8$^{(-/-)}$ in the presence of 100 nM nifedipine, only 10 nM isoprenaline

caused no significant change (n = 6). In the presence of 300 nM nifedipine, the only significant change was seen at 1 nM of isoprenaline (n = 6). At the highest concentration of isoprenaline (100 nM) in the presence of 100 and 300 nM nifedipine, beating rate was increased in C57BL/6J by 368 ± 8 bpm and 290 ± 8 bpm, respectively, compared to a 219 ± 3 bpm increase in the absence of nifedipine (**Figure 5.9*A***); and in AC1&8$^{(-/-)}$, beating rate was increased by 327 ± 7 and 249 ± 5 bpm, respectively, relative to a 195 ± 2 bpm increase in the absence of nifedipine (**Figure 5.9*B***).

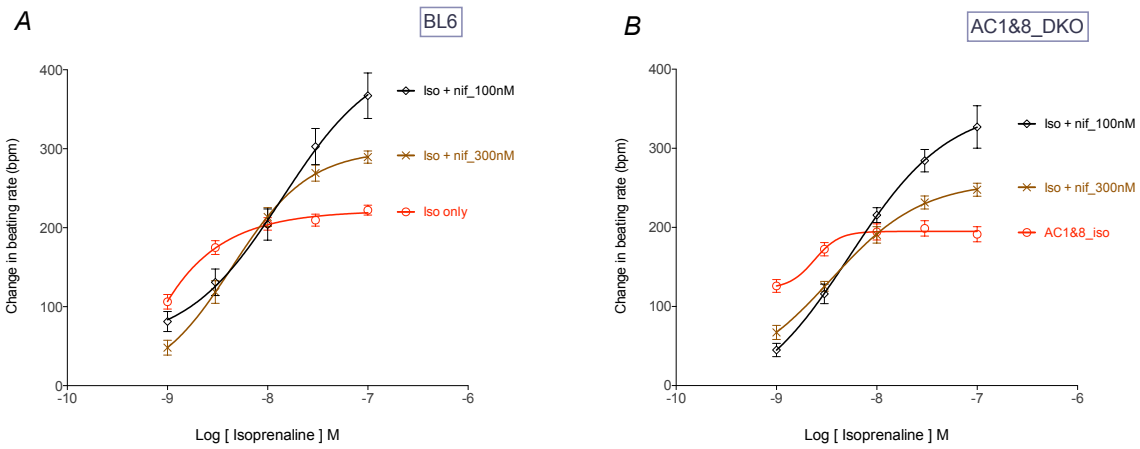


Figure 5.9. Graph representing mean change in the positive chronotropic action of the β-adrenoceptor agonist isoprenaline alone and in the presence of 100 nM and 300 nM nifedipine on ***(A)*** wild type C57BL/6J (BL6, n = 14, n = 6 and n = 6 respectively) and ***(B)*** AC1&8$^{(-/-)}$ (n = 22 n = 6 and n = 6 respectively) mice basal spontaneous beating rate of atrial preparations. Data are expressed as mean ± S.E.M., n = number of experiments. GraphPad Prism (version 5.0) software was used to perform statistical analysis, including two-way ANOVA with Bonferroni post-test (significance level $P < 0.05$).

5.10. Discussion

5.10.1. The role of Ca^{2+}-stimulated AC at rest in mice with differential expression of Ca^{2+}-stimulated ACs

Overall, the outcome of the above experiments was not clear-cut and the observations appeared not to allow a straightforward interpretation. It is possible that adaptation mechanisms are occurring. During development of the knockouts, it is possible that other AC isoforms might be overexpressed and/or other signalling pathways are upregulated to adapt to the loss of AC1 and/or AC8. Therefore, for future work it will be important to assess the expression and density of additional AC isoforms in the knockout models.

After recording for a 40 min period, the C57BL/6J, $AC1^{(-/-)}$, $AC8^{(-/-)}$ and $AC1\&8^{(-/-)}$ preparations reached resting beating rates of 433 ± 11 bpm, 414 ± 10 bpm, 405 ± 11 bpm and 436 ± 7 bpm, respectively. The hearts rates when AC1 and/or AC8 expression were suppressed were not significantly different from the heart rate in control C57BL/6J preparations (**Figure 5.1**). This finding indirectly supports the studies of Lipskaia *et al.* (2000) and Georget *et al.* (2002), in which overexpression of AC8 in the heart did not change the basal spontaneous heart rate, despite the fact that cytosolic cAMP concentration was elevated. Also, these studies observed no changes in global cardiac function.

Genetic studies on ubiquitously expressed AC5/6 isoforms, although they are not Ca^{2+}-stimulated isoforms, have revealed the following observations. Overexpression of the AC5 isoform induced upregulation of PKA and elevated

phospholamban phosphorylation as consequence of elevated cAMP levels. Consequently, the basal spontaneous beating rate was also elevated. However, there was no change in the β-adrenoceptor pathway (Tepe *et al.,* 1999; Esposito *et al.,* 2008). In the $AC5^{(-/-)}$ mouse model, there was a significant reduction in Ca^{2+}-mediated inhibition of cAMP production, and as a consequence, there was also a complete loss of acetylcholine-mediated, G_i inhibition. The basal spontaneous beating rate was also elevated, and this was partially explained by the loss of baroreflex function (Okumura *et al.,* 2003; Tang *et al.,* 2006). Deletion of the AC6 enzyme resulted in no change in cAMP levels under basal conditions and also no change in basal spontaneous beating rate. However, under β-adrenoceptor stimulation, the cAMP level was reduced by 70%, PKA activity was reduced by 40% and phospholamban phosphorylation was reduced by 45% (Tang *et al.,* 2008). In mice overexpressing the AC6 isoform, basal spontaneous rate was not affected and contractile function was unchanged. However, the cardiac responsiveness to β_2-adrenoceptor stimulation was upregulated (Gao *et al.,* 1999).

5.10.2. Influence of ZD7288/ivabradine (I_f inhibition) and CPA (inhibition of Ca^{2+} release from SR) at rest in mice with differential expression of Ca^{2+}-stimulated ACs

The studies from both organ bath and fluorescent Ca^{2+} transient measurements suggested that suppressed expression of Ca^{2+}-stimulated AC does not directly influence the effects of either Ca^{2+} release from SR or I_f channel activity on spontaneous beating rate. I would have expected the basal I_f

activity to be reduced for the AC1&8$^{(-/-)}$ preparation at least. This is because the lack of Ca^{2+}-stimulated ACs should have reduced the cytosolic concentration of cAMP, thus reducing basal I_f activity. This was expected to result in less channels available for inhibition by 1 μM ZD7288 + 3 μM ivabradine at basal spontaneous beating rate.

Even though the results were not statistically significant, a close inspection of marginal changes in the rate of reduction observed in **Figures 5.4*E*** and **5.6*I*** for AC1&8$^{(-/-)}$ relative to C57BL/6J may provide some clues. There was a slight tendency for the 1 μM ZD7288 + 3 μM ivabradine combination to reduce the basal beating rate for AC1&8$^{(-/-)}$ to a lesser extent than control C57BL/6J. There was a 10% smaller reduction in AC1&8$^{(-/-)}$ relative to C57BL/6J (= 210/233, **Figure 5.4*E***). Also, the same pattern was found in Ca^{2+} fluorescent measurements, where 1 μM ZD7288 + 3 μM ivabradine reduced the basal beating rate for AC1&8$^{(-/-)}$ to a lesser extent than control C57BL/6J. For AC1&8$^{(-/-)}$, there was 13% less reduction relative to C57BL/6J (= 147/169, **Figure 5.6*I***). These differences were small and not statistically significant but there appears to be a pattern indicating some influence of Ca^{2+}-stimulated AC on modulation of pacemaking by I_f channels. However, overcompensation may be occurring, in which other AC isoforms could be being up-regulated and thus masking the observation.

5.10.3. The influence of the CPA (inhibition of Ca^{2+} release from SR) on I_f's modulation of basal beating rate in mice with differential expression of Ca^{2+}-stimulated ACs

The experiments from the previous chapter (section 4.3.3. and 4.3.4.) on CD1 mice suggested that the Ca^{2+} release from SR activates Ca^{2+}-stimulated AC, subsequently increasing production of the endogenous I_f channel's agonist, cAMP. cAMP, in turn, keeps the basal I_f activity elevated. This suggestion is consistent with the observation that in the presence of CPA (pre-incubation), the effect of 1 μM ZD7288 + 3 μM ivabradine in wild type mouse spontaneous beating was reduced, as compared to the ability of 1 μM ZD7288 + 3 μM ivabradine to reduce spontaneous beating rate on its own. This is potentially due to reduced activity of Ca^{2+}-stimulated ACs as a consequence of supressing Ca^{2+} release from SR.

Therefore, I would have expected the 1 μM ZD7288 + 3 μM ivabradine combination to be able to reduce the basal beating rate to the same extent in presence and absence of SR disruption by 100 μM CPA in AC1&8$^{(-/-)}$. This is because crosstalk between Ca^{2+} release from SR and I_f channel modulation through Ca^{2+}-stimulated AC is disrupted; due to the lack of the Ca^{2+}-stimulated ACs in AC1&8$^{(-/-)}$ atrial preparation. The observations did not show statistically significant differences to support these suggestions, but perhaps these possibilities should not be entirely ruled out, since close inspection of **Figures 5.4*E*** and **5.6*I*** reveals marginal changes in the rate of reduction, possibly indicating a pattern. In the AC1&8$^{(-/-)}$ atrial preparation in the presence of 100 μM CPA pretreatment and 1 μM ZD7288 + 3 μM ivabradine basal beating rate

was reduced to larger extent than in C57BL/6J. In AC1&8$^{(-/-)}$ there was a further 40% reduction in basal beating rate relative to C57BL/6J (= 131/93 bpm; **Figure 5.4*E***). The same pattern was also found for Ca^{2+} fluorescent measurements, which showed a further 58% reduction in basal beating rate in AC1&8$^{(-/-)}$ relative to control (= 95/60 bpm; **Figure 5.6*I***). Despite the fact that the differences are not statistically significant, there appears to be a clear pattern indicating that in AC1&8$^{(-/-)}$, 1 μM ZD7288 + 3 μM ivabradine in the presence of CPA can further reduce basal beating rate relative to C57BL/6J.

5.10.4. The influence of ZD7288/ivabradine (I_f inhibition) and CPA (inhibition of Ca^{2+} release from SR) on β-adrenergic pathway activation in mice with differential expression of Ca^{2+}-stimulated ACs

In the presence of 1 μM ZD7288, the isoprenaline log(concentration)-response curve could not be extended to concentrations greater than 10 nM for AC1&8$^{(-/-)}$ atrial preparations (which would have allowed comparisons with the curves for control, AC1$^{(-/-)}$ and AC8$^{(-/-)}$). This is because isoprenaline above 10 nM in the presence of 1 μM ZD7288 induced cyclical instability in beating rate in AC1&8$^{(-/-)}$ (**Figure 5.7*C***). In the presence of 100 μM CPA and 1 μM ZD7288 + 3 μM ivabradine, it was not possible to construct a log(concentration)-response curve for isoprenaline even over a limited range of concentrations for AC1&8$^{(-/-)}$ (unlike AC1$^{(-/-)}$ and AC8$^{(-/-)}$) because as little as 1 nM isoprenaline induced cyclical instability in beating rate in AC1&8$^{(-/-)}$ (**Figure 5.7*D***). At the same time, no isoprenaline log(concentration)-response curve could be constructed for AC1$^{(-/-)}$ and AC8$^{(-/-)}$ at isoprenaline concentrations greater than 10 nM in the

presence of 100 μM CPA and 1 μM ZD7288 + 3 μM ivabradine (**Figure 5.7*A* & *B***). This suggests that AC1 and AC8 act as stabilising enzymes in preventing irregularity in heart rate. This stabilizing nature was more apparent when the 1 μM ZD7288 + 3 μM ivabradine combination was added in the presence of 100 μM CPA.

Following inhibition of I_f channels with the ZD7288/ivabradine combination, there was less increase in rate with isoprenaline for $AC8^{(-/-)}$ (small depression of isoprenaline log(concentration)-response curve), and $AC1\&8^{(-/-)}$ (larger depression of isoprenaline log(concentration)-response curve). This may suggest that I_f plays a larger role in the isoprenaline-induced rate increase for $AC8^{(-/-)}$ and $AC1\&8^{(-/-)}$, which is not what would be expected (less contribution from I_f would be expected if it was substantially activated by Ca^{2+}-stimulated ACs) unless there was a greater depression of PKA-dependent pathways (**Figure 5.8**).

5.10.5. Cyclical instability of knockout mice atrial preparations

The underlying mechanism of cyclical instability of beating rate in knockout mouse ($AC1^{(-/-)}$, $AC8^{(-/-)}$ and $AC1\&8^{(-/-)}$) atrial preparations observed above were not investigated. However, these cyclical events may be driven by a gradual change of Ca^{2+} in cytosol either thorough Ca^{2+} channels from extracellular domain and/or efflux of Ca^{2+} from Ca^{2+} stores, which then being counterbalanced by an uptake mechanism either through SERCA, membrane ATPase, and/or taken up by acidic organelles.

Previous studies shown that there are several oscillatory biochemical mechanisms present, where by single rate controlling enzyme can sustain stable non-equilibrium oscillatory states under distinct conditions. A work by Andres *et al.* (1990) on oscillatory synthesis of glucose 1,6-bisphosphate and frequency modulation of glycolytic oscillations in skeletal muscle extracts is a good example. Also slow waves of contraction in smooth muscle driven by the ubiquitous distribution of glycolytic enzymes another good example (Hess *et al.,* 1979). Moreover, an interesting study by O'Rourke et al. (1994) revealed that guinea pig ventricle cells can undergo oscillatory rhythm. This was due to cyclical activation of ATP-sensitive K^+ channels via oscillatory metabolic stress, together with simultaneous suppression of depolarization-evoked intracellular Ca^{2+} transients. Although these authors observed oscillatory alterations in the concentration of cytosolic Ca^{2+} it was shown that not this alteration but oscillatory metabolic stress drove the oscillatory rhythm. Perhaps in our knockout mouse models there is similar oscillatory metabolic stress present that may be driving the cyclical events observed during β-adrenoceptor stimulation.

5.10.6. Assessing effective I_f channel blockade in the modulation of beating rate.

In order to assess whether I_f channels are near full inhibition in the presence of 1 μM ZD7288, a different I_f channel blocker (3 μM ivabradine) was used to see whether additional blocking could further suppress I_f current in the presence of 1 μM ZD7288 (following an approach similar to that used in the previous chapter). In the presence of 1 μM ZD7288, addition of 3 μM ivabradine

caused little or no further change in mouse beating rate for the knockout models (**Figure 5.5**). The further not significant reductions caused by ivabradine were 19 bpm for C57BL/6J, 16 bpm for $AC1^{(-/-)}$, 27 bpm for $AC8^{(-/-)}$, and 16 bpm for $AC1\&8^{(-/-)}$. Despite these not significant effects of ivabradine, it was decided that 1 μM ZD7288 together with 3 μM ivabradine would be used to increase the confidence that blockade of I_f was near completion.

5.10.7. Effects of changes in extracellular Ca^{2+} concentration on its ability to modulate basal beating rate in mice with differential expression of Ca^{2+} stimulated ACs.

To assess the impact of changes in extracellular Ca^{2+} concentration on pacemaking in relation to Ca^{2+}-stimulated ACs, the concentration of Ca^{2+} was incrementally increased from 1 mM to 1.8 mM to 2.5 mM and finally to 3.5 mM. In $AC1^{(-/-)}$, $AC8^{(-/-)}$ and C57BL/6J (BL6) atrial preparations, increasing the cytosolic concentration of Ca^{2+} increased the basal beating rate. Raising extracellular Ca^{2+} would be expected to drive Ca^{2+} entry and increase the Ca^{2+} loading of the SR (Trafford *et al.,* 2001, observed in rat and ferret ventricular myocytes). These factors alone might lead to an increase in beating rate, however, the secondary effects of these changes on Ca^{2+}-stimulated ACs could also contribute to the observed increases in rate when at least one Ca^{2+}-stimulated AC remained functional. In contrast, increasing the cytosolic concentration of Ca^{2+} in the $AC1\&8^{(-/-)}$ atrial preparation reduced the basal beating rate (**Figure 5.2**). This might be due to an opposing influence from Ca^{2+} ACs that are inhibited by Ca^{2+}, namely the AC5 and AC6 isoforms, which could

lead to reduction of the cytosolic concentration of cAMP as extracellular concentration of Ca^{2+} is increased. This reduction in cAMP is does not appear to occur through reduction of I_f channel activity. This is because when AC1&8$^{(-/-)}$ atrial preparations were pre-incubated with the 1 μM ZD7288 + 3 μM ivabradine for 30 min prior to increasing the extracellular Ca^{2+}concentration, the reduction in basal beating rate was still present. I_f inhibition did not significantly alter the reduced basal beating rate induced by elevating extracellular Ca^{2+} concentration (**Figure 5.3**). It is possible that a reduction in PKA-phosphorylation activity due to reduced cytosolic cAMP concentration induces the reduction in rate.

5.10.8. The influence of nifedipine (L-type Ca^{2+} channel inhibition) on β-adrenergic pathway activation in mice with differential expression of Ca^{2+}-stimulated ACs

Given that the change in extracellular Ca^{2+} concentration reduced the basal beating rate for AC1&8$^{(-/-)}$ (**Figure 5.2**), I wanted to assess how the β-adrenergic pathway would be influenced when Ca^{2+} influx through L-type Ca^{2+} was reduced. Thus, 100 or 300 nM nifedipine was used to pre-incubate the atrial preparation over 30 min prior to constructing the isoprenaline log(concentration)-response curve. However, there was no difference between AC1&8$^{(-/-)}$ and control C57BL/6J in the isoprenaline log(concentration)-response curves observed in the presence of either 100 or 300 nM nifedipine (**Figure 5.9**). It should be noted that addition of nifedipine caused a substantial decrease in the resting beating rate, as expected. One point that arises from

this condition (inhibition of L-type Ca^{2+} channel) is that the low heart rate allows for a much greater increase in heart rate in terms of bpm before reaching a 'maximum' that is presumably determined by the inherent limits of the preparation, including those imposed by metabolic demands. This might account for the observation of larger bpm changes caused by isoprenaline in the presence of nifedipine (**Figure 5.9**).

5.11. Future experiments:

The following experiments would be informative in future work:

1) Electrophysiology experiments to study the I_f current density in the knockout models relative to control. In doing so, one would be able to assess the modulation of I_f currents by Ca^{2+} stimulated ACs.

2) Immunohistochemistry and Western blot analysis to assess the density of the AC isoforms in isolated SAN cells of control and knockout models.

3) It would also be important to measure AP profile from both wiled type and knockout mice ($AC1^{(-/-)}$, $AC8^{(-/-)}$ and $AC1\&8^{(-/-)}$) using perforated patch clamp technique. Unlike atrial preparation this will enable to assess the maximum diastolic potential and rate of diastolic depolarization. Perhaps some of the remodelling of knockout mice may be exposed.

CHAPTER 6: PHOTO-CROSSLINKING

6.1. Introduction

In the mid-90s, a novel inward current, I_{st}, was identified in spontaneously active SA node cells of rabbits, guinea pigs, and rats (Guo *et al.,* 1995; Guo *et al.,* 1997; Mitsuiye *et al.,* 2000). This channel has been implicated as playing an important role in pacemaking, and could be a unique potential target for angina and hypertension treatments. Inhibitors of the channel may provide a promising alternative to drugs that treat heart disease. However, unlike other ion channels that are believed to play an important role in driving the pacemaker potential, the I_{st} channel's biochemical characteristics remain unknown, and even its very existence has been somewhat controversial (comprehensive overview of the I_{st} channel provided above in the section 1.2.4. in Chapter 1). In this chapter photo-crosslinking method was chosen to design a photo-affinity probe to capture the I_{st} channel.

6.1.2. Ligand-protein interaction methods

Yeast two hybrid and protein enrichment using small molecules (probes) are some of the methods that have been used to study ligand-target interactions (Hamdi *et al.,* 2012; Sun *et al.,* 2013). In doing so, some of the signalling pathways and physiological functions of target proteins have been unravelled (Rix *et al.,* 2009). Probe compounds have been sophisticatedly designed to capture their targets. Typically, the simplest probes will consist of a selectivity function, which enables the probe to bind to its target, through either reversible or non-reversible binding. Second, the probe is designed to have a

reporter/handle group. The handle enables the probe-target complex to be visualised / captured / purified from highly complex protein samples (Vodovozova *et al.,* 2007; Heal *et al.,* 2011; Evans *et al.,* 2006). The simplest method is possibly the affinity enrichment method, in which the probe is immobilized on a solid support then exposed to a biological sample to capture the target protein.

The affinity enrichment method is one of the most common approaches to studying ligand-target interactions and has been successfully used (Ding *et al.,* 2003). However, it has number of shortfalls. It relies on a strong ligand-protein interaction but interactions are often weak and the proteins are easily washed away. Also, the immobilization of probe can disrupt the ligand-protein interaction. Therefore, affinity enrichment methods employing probes that covalently bind to their target protein have been developed. These covalently binding inhibitors encompass 'mechanism-based' probes (suicide inhibitors) and 'trap' probes (photo-affinity probes) (Cravatt *et al.,* 2008; Robinette *et al.,* 2006).

6.1.3. Photo-affinity probes

The photo-crosslinking method was chosen to design a photo-affinity probe to capture the I_{st} channel. The aim of this work was to synthesise photo-affinity probes to enable covalent photocapture of the I_{st} channel so that the channel could be defined. In doing so, I hoped to identify the biochemical identity of the channel. Photo-affinity probes are generally made up of three building blocks: a known inhibitor used as a scaffold (in this case, nicardipine), a photo-reactive group (in this case, an azide group), and a reporter (in this case,

an alkyne group) (Dubinsky *et al.,* 2012). The probes are then incubated with their target (in this case, the I_{st} channel) and allowed to reach dynamic equilibrium. Following irradiation with UV light, the azide group is activated to form a covalent bond with its target. An azide-biotin tag conjugate can then be used to react with the probe's alkyne group ('click reaction'). Following this, the target of interest can be isolated by affinity purification using the biotin group attached to the probe. The target protein may be analysed by gel electrophoresis, western blotting and/or mass spectrometry. A summary workflow is presented in **Figure 6.1.**

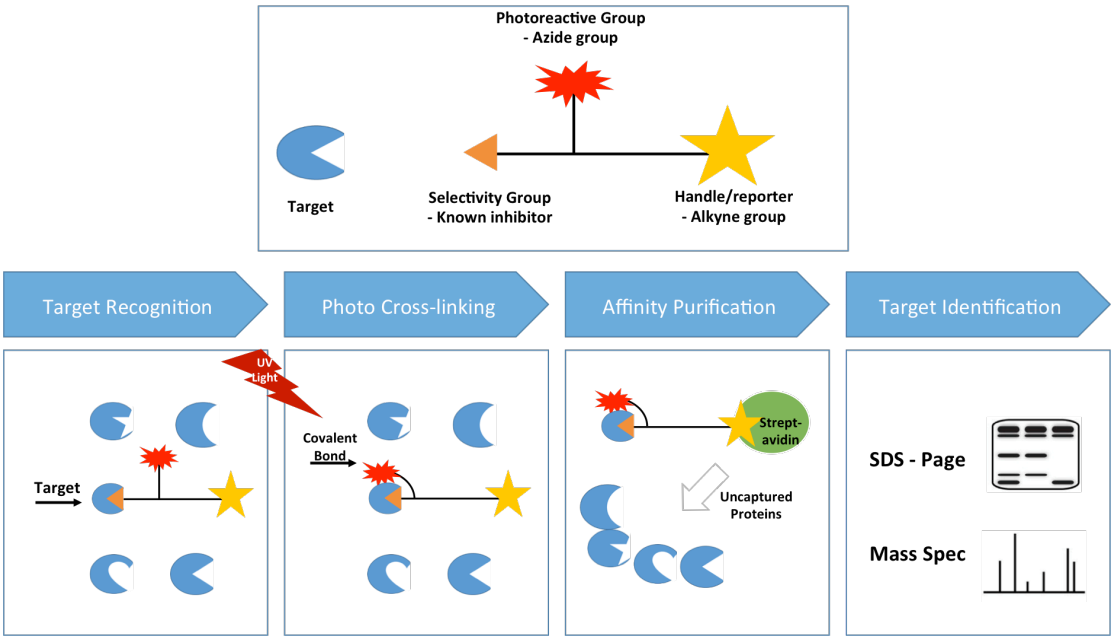
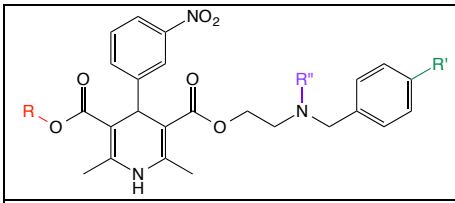
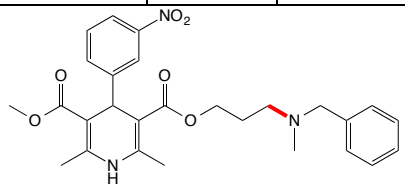


Figure 6.1 Photo-affinity probe pull-down workflow. The top panel represents photo-affinity probe made up of reactivity, selectivity and reporter groups. The bottom panel represents a typical experiment for performing pull-down: **Target recognition** is the process in which the probe is incubated with the cell lysate to allow the selectivity group to bind to its target. **Photo-crosslinking** is the process in which the photo-reactive group is activated following irradiation with UV light and the azide group is activated to produce a nitrene, which forms a covalent bond with the target. **Affinity purification** is the process by which probe's (biotin) handle is used to capture the protein-probe complex using streptavidin magnetic beads. **Target identification** is the process of analysing the captured protein by immunoblotting or mass spectrometry.

6.1.4. Development of Photo-affinity Probes

The L-type Ca^{2+} channel antagonist nicardipine, has been shown to fully inhibit the I_{st} current at a 0.5 μM concentration (Guo *et al.,* 1995). Thus, nicardipine was used as a selectivity function for the development of photo-affinity probes for the I_{st} channel. Structure-activity relationship (SAR) experiments on the interaction between nicardipine and L-type Ca^{2+} conducted by Iwanami *et al.* (1979) were key in designing the probes. Iwanami's experiments (see **Table 6.1**) showed that some manipulations of nicardipine (e.g. **36**, **42**, **44**-**46**) did not alter the ability of the molecules to inhibit L-type Ca^{2+} channels; i.e. they had the same potencies as nicardipine. These results indicated that there are possible additional pockets available in L-type Ca^{2+} channels for extending the size of nicardipine at **R**, **R'**, and **R"**, or that these regions are solvent exposed (**Table 6.1**). It was assumed that the nicardipine binding pocket in L-type Ca^{2+} channels would likely be similar to the binding pocket in the I_{st} channel, and therefore that modification of nicardipine in these regions may be tolerated by the I_{st} channel binding pocket.

Table 6.1 Probes that have the same potency as nicardipine in their ability to inhibit L-type Ca^{2+} channels (*adapted from Iwanami et al., 1979*).

	**R**	**R”**	**R’**
Nicardipine	Me	Me	H
Compound 42	Et	Me	H
Compound 46	Et	Et	Cl
Compound 45	Et	Et	OMe
Compound 44		Me	Me
Compound 36			

It was anticipated that photo-affinity probes could be accessed by installation of an azide group at **R’**, to afford a photo-reactive aryl azide. Alternatively, replacement of the NO_2 with an azide group would also give an aryl azide. Since it was unknown which of these would give best crosslinking to the protein, it was decided that both options should be synthesised. An alkyne group would be installed at **R** to enable click conjugation with a suitable handle.

6.2. Photo-affinity probes synthesis' results and discussion

Six photo-affinity probes were designed for the capture and subsequent identification of the I_{st} channel (**Table 6.2**, photo-affinity probe 1, 2, 3a, 3b, 4 and 5). The synthesis of the probes was based on a modification of the Hantzsch synthesis of pyridines, in which an aldehyde, an enamine and a 1,3-dicarbonyl are combined in one pot to afford the pyridine (a general reaction shown in **Figure 6.2**).

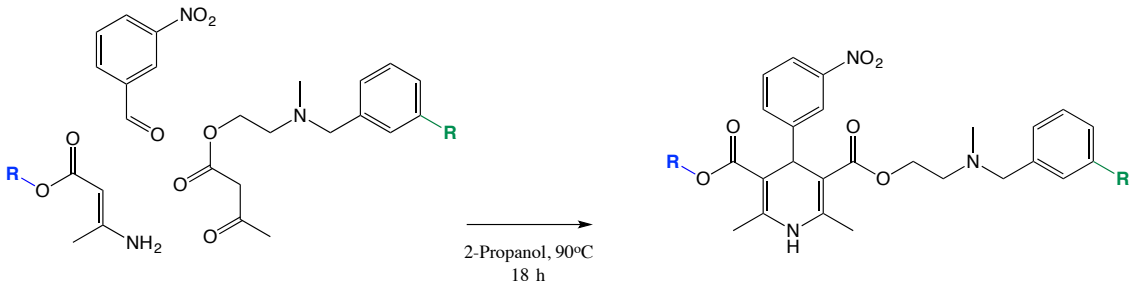


Figure 6.2 A general synthesis of probes using modified Hantzsch synthesis

6.2.1 Probe Synthesis

6.2.1.1 Probes 1 & 2

The insertion of the handles in the probes was achieved using alkyne containing enamine fragments **1.5** and **2.2**. For the synthesis of **1.5**, but-3-yn-1-ol was first reacted with methyl 3-oxobutanoate to afford the ester **1.4** in 47% yield. This was subsequently converted to the desired enamine by reaction with ammonium acetate to afford **1.5** in 85% yield. For the synthesis of **2.2**, an analogous procedure was attempted, however the reaction of propagyl alcohol with methyl 3-oxobutanoate was unsuccessful. Therefore, an alternative

strategy was employed in which the propargyl alcohol was reacted with 2,2,6-trimethyl-4*H*-1,3-dioxin-4-one. This provided the desired compound **2.1** in 65% yield. This ester was reacted with ammonium acetate to afford the fragment **2.2** in 75% yield (**Figure 6.3**).

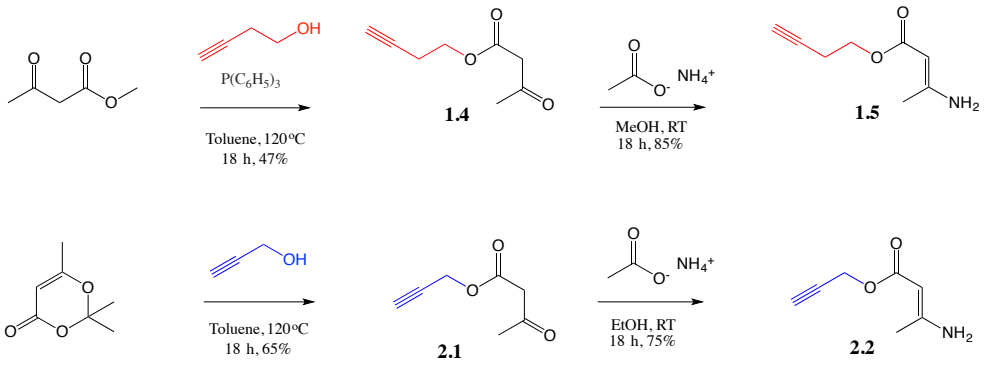


Figure 6.3. Representing synthesis of fragments **1.4, 1.5, 2.1** and **2.2.** For detailed explanations of the reactions, please refer to the experimental section 6.5**.**

The initial challenge I was faced with in synthesizing prop-2-yn-1-yl 3-oxobutanoate, (fragment **2.1**) and but-3-yn-1-yl 3-oxobutanoate (fragment **1.4**). I was unable to achieve a high enough yield when using 2,5-dioxocyclopentyl 3-oxobutanoate due to the predominant formation of 2-acetylcyclohexane-1,3,5-trione (**Figure 6.4**).

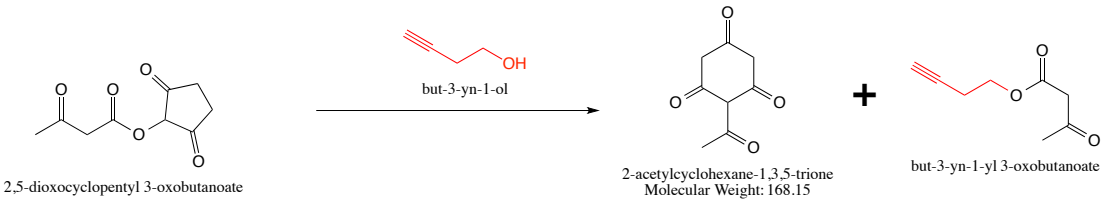


Figure 6.4 Reaction scheme for the production of 2-acetylcyclohexane-1,3,5-trione, an unwanted side product.

Next it was decided that 3-oxobutanoic acid would be formed from methyl 3-oxobutanoate in the presence of NaOH and H_2O over 18h. Following this it was envisaged that, 3-oxobutanoic acid would be added to form but-3-yn-1-yl 3-oxobutanoate (fragment **1.4**, **Figure 6.5**). However, the formed 3-oxobutanoic acid was trapped in the aqueous layer and I was therefore unable to extract it, despite using a range of organic solvents.

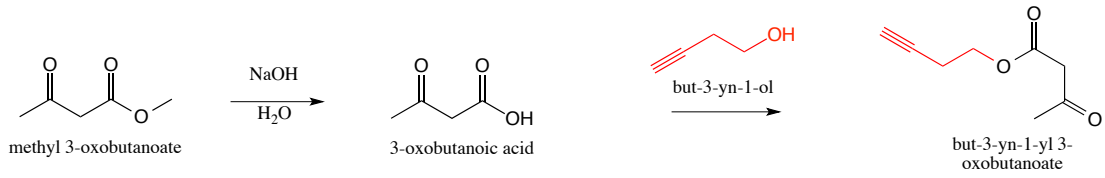


Figure 6.5 Reaction scheme illustrating the production of but-3-yn-1-yl 3-oxobutanoate using methyl 3-oxobutanoate as a starting material.

The above challenge for the synthesis of fragments **1.5** and **2.2** was overcome by following procedures outlined in **Figure 6.3**.

The photoreaction aryl azide was installed in probes 1 and 2 using the fragment **1.3**. This was synthesized by reaction of (3-formylphenyl)boronic acid with $TMSN_3$, to afford aryl azide intermediate **1.1** in 62 % yield. Reductive amination of methyl ethanolamine afforded **1.2** in 74% yield, and subsequent reaction with 2,2,6-trimethyl-4H-1,3-dioxine-4-one afforded the desired 1,3 dicarbonyl fragment **1.3** in 47% yield (**Figure 6.6**).

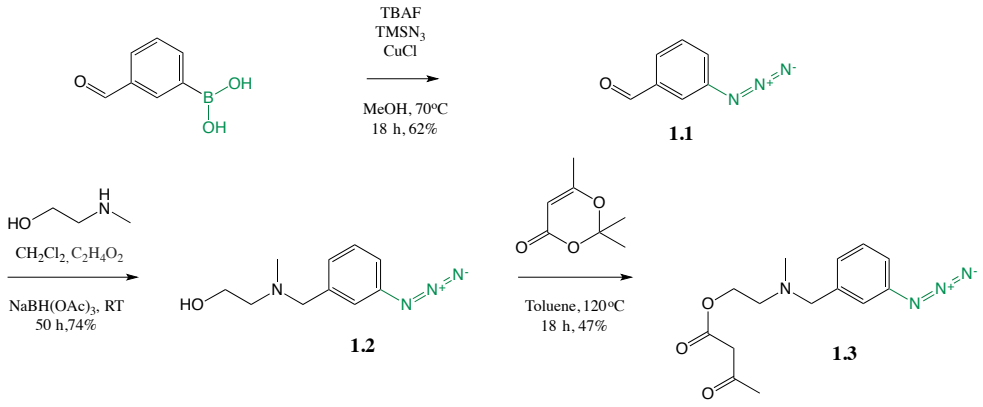


Figure 6.6 Representing synthesis of fragments **1.1, 1.2** and **1.3.** For detailed explanations of the reactions, please refer to the experimental section 6.5**.**

One challenge was faced during the synthesis of azidobenzaldehyde, (fragment **1.1**). I initially approached this using the reaction scheme shown in **Figure 6.7**, where iodobenzaldehyde was used as a starting material.

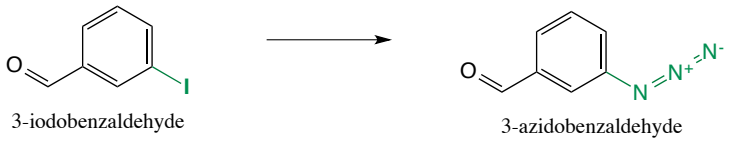
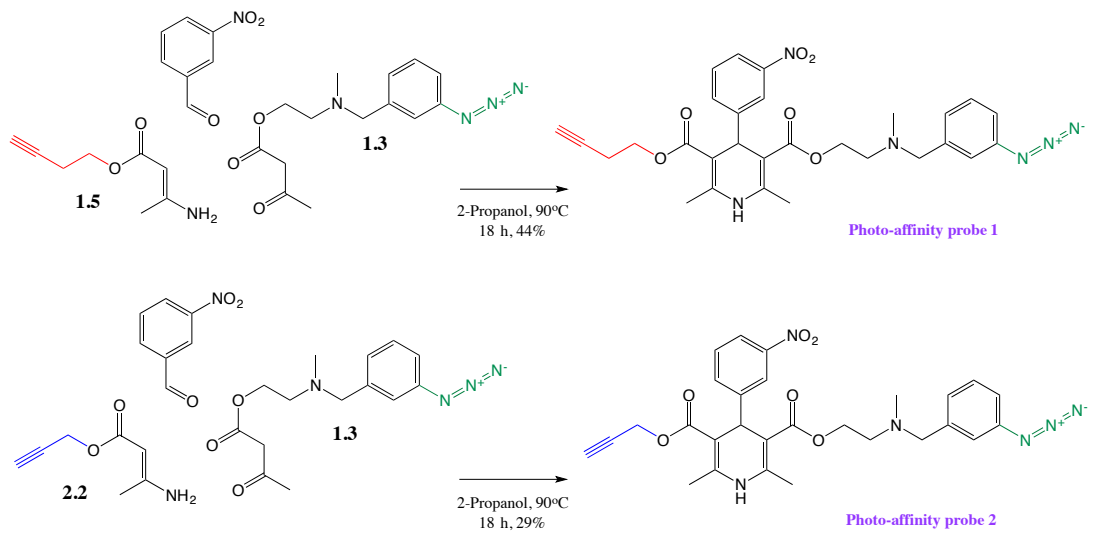


Figure 6.7 Reaction scheme for synthesis of azidobenzaldehyde using iodobenzaldehyde.

Iodobenzaldehyde, sodium azide, L-proline, NaOH and CuCl were added in succession to DMSO in a 50 ml round-bottomed flask. The mixture was heated to reflux (60°C) for 18 hours. However, azidobenzaldehyde was not formed. I therefore decided to try alternative methods of synthesising azidobenzaldehyde. Li *et al.* (2010) developed the optimal conditions for the synthesis of 3-azidobenzaldehyde.

Furthermore, It was challenging to successfully react the secondary amine with the aldehyde group to afford fragment **1.2**. Initially, $NaBH(OAc)_3$ was used as a reducing agent over 18h; however, a low product yield was obtained. The reducing agent was therefore changed to $NaCNBH_3$, but this produced an even lower yield. However when the original conditions with $NaBH(OAc)_3$ as a reducing agent was repeated and left over 50h instead of 18h a good yield (>70%) was obtained.

With the necessary fragments in hand, probes 1 and 2 were then synthesized using the Hantzsch reaction. Thus 3-nitrobenzaldehyde, fragment **1.3** and the required enamine (**1.5** and **2.2** respectively) were heated to 90 degrees overnight in propan-2-ol to afford the desired compounds probe 1 (44% yield) and probe 2 (29% yield) [**Figure 6.8**]



Scheme 6.8 Synthesis of **Photo-affinity Probes 1 and 2** using nicardipine as the scaffold; in **green** is the photo-reactive azide group, in **red** and **blue** are the reporter alkyne groups, in **black** is the nicardipine selectivity scaffold that when incubated binds to its target proteins (in this case, the $Ca_v1.2$, $Ca_v1.3$ and I_{st} channels). For detailed explanations of the reactions, please refer to the experimental section 6.5**.**

6.2.1.2 Probes 4 & 5

The photoreaction aryl azide was installed in probes 4 and 5 using the fragment **3.6**. First the reductive amination of methyl ethanolamine with (4-formylphenyl)boronic acid afforded **3.4** in 74% yield, this subsequently was reacted with $TMSN_3$, to afford 2-((4-azidobenzyl)(methyl)amino)ethan-1-ol intermediate **3.5** in 51% yield. Subsequent reaction with 2,2,6-trimethyl-4H-1,3-dioxine-4-one afforded the desired 2-((4-azidobenzyl)(methyl)amino)ethyl 3-oxobutanoate fragment **3.6** in 57% yield (**Figure 6.9**).

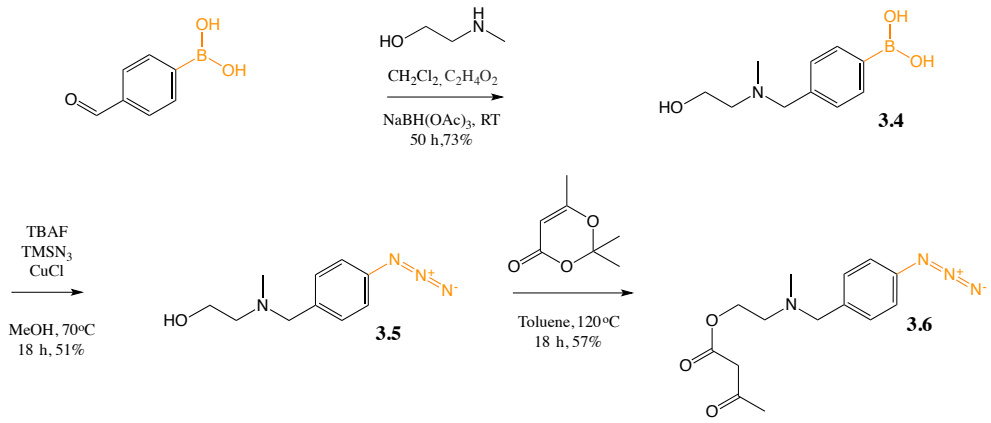


Figure 6.9 Representing synthesis of fragments **3.4, 3.5** and **3.6**. For detailed explanations of the reactions, please refer to the experimental section 6.5.

Initially, synthesis of 4-azidobenzaldehyde from (4-formlyphenyl)boronic acid using experimental conditions described by Li *et al.*'s (2010) was attempted. However, Li *et al.*'s (2010) experimental conditions were not optimal for the synthesis of 4-azidobenzaldehyde, as they produced a 5% yield. Therefore, the order of the steps was switched. The use of Li *et al.*'s (2010) experimental conditions after addition of 2-(methylamino)ethan-1-ol to (4-formlyphenyl)boronic acid resulted in a significantly improved yield of 73% for

the conversion of the boronic acid to the azide (**Figure 6.9)**. Note, however, that this reaction scheme cannot be carried out if an alkyne is present at the R" position (**Table 6.1**), because the alkyne would react with the newly formed azide bonds in the presence of Cu ('click reaction').

With the necessary fragments in hand, probes 4 and 5 were then synthesized using the Hantzsch reaction. Thus 4-nitrobenzaldehyde, fragment **3.6** and the required enamine (**1.5** and **2.2** respectively) were heated to 90 degrees overnight in propan-2-ol to afford the desired compounds probe 4 (74% yield) and probe 5 (54% yield) [**Figure 6.10**].

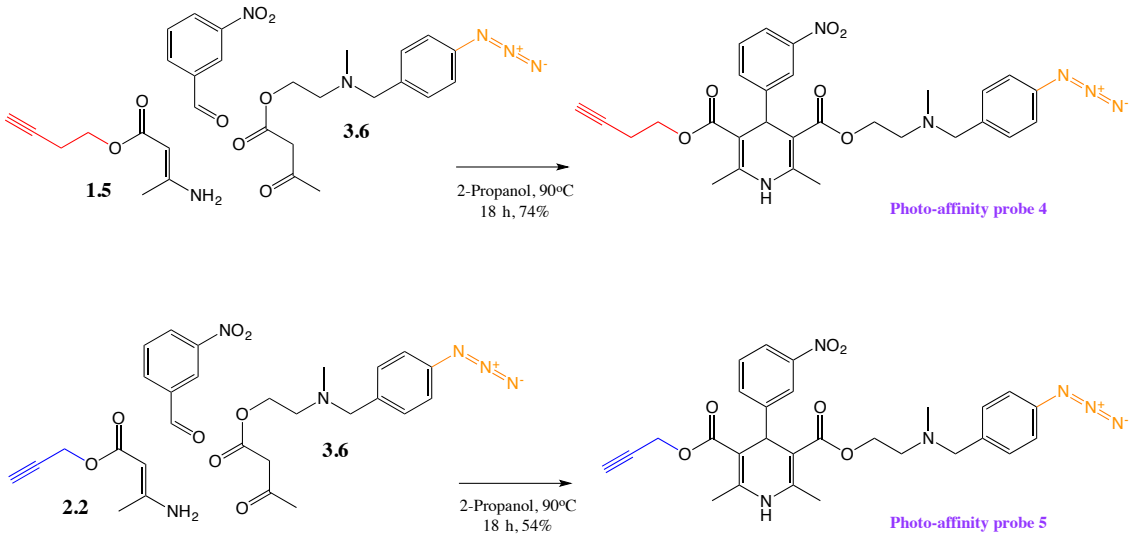


Figure 6.10 Synthesis of Photo-affinity Probes 4 and 5. In orange is the photo-reactive azide group, in **red** and **blue** are the reporter alkyne groups, and in **black** is the nicardipine selectivity scaffold that when incubated binds to its target proteins (in this case, the $Ca_v1.2$, $Ca_v1.3$ and I_{st} channels). For detailed explanations of the reactions, please refer to the experimental section 6.5.

6.2.1.3 Probes 3a & 3b

First 2-(benzyl(methyl)amino)ethan-1-ol was reacted with 2,2,6-trimethyl-4H-1,3-dioxine-4-one to afford the desired 2-(benzyl(methyl)amino)ethyl3-oxobutanoate fragment **3.1** in 51% yield (**Figure 6.11**).

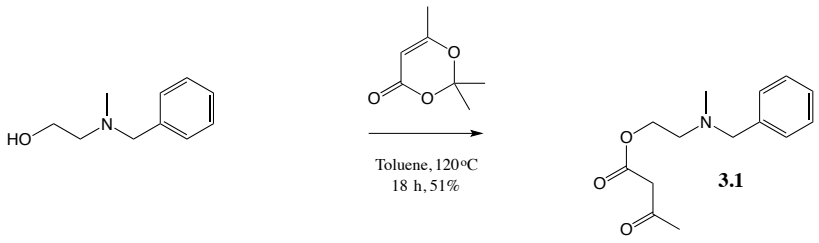


Figure 6.11 Representing synthesis of fragment **3.1.** For detailed explanations of the reaction, please refer to the experimental section 6.5**.**

Subsequently with the necessary fragments in hand, probes 3a and 3b were then synthesized using the Hantzsch reaction. Using fragment **3.1, 1.1 (**to add photoreaction aryl azide) and the required enamine (methyl aminocrotonate and **1.5** respectively) were heated to 90 degrees overnight in propan-2-ol to afford the desired compounds probe 3a (40% yield) and probe 3b (43% yield) [**Figure 6.12**]

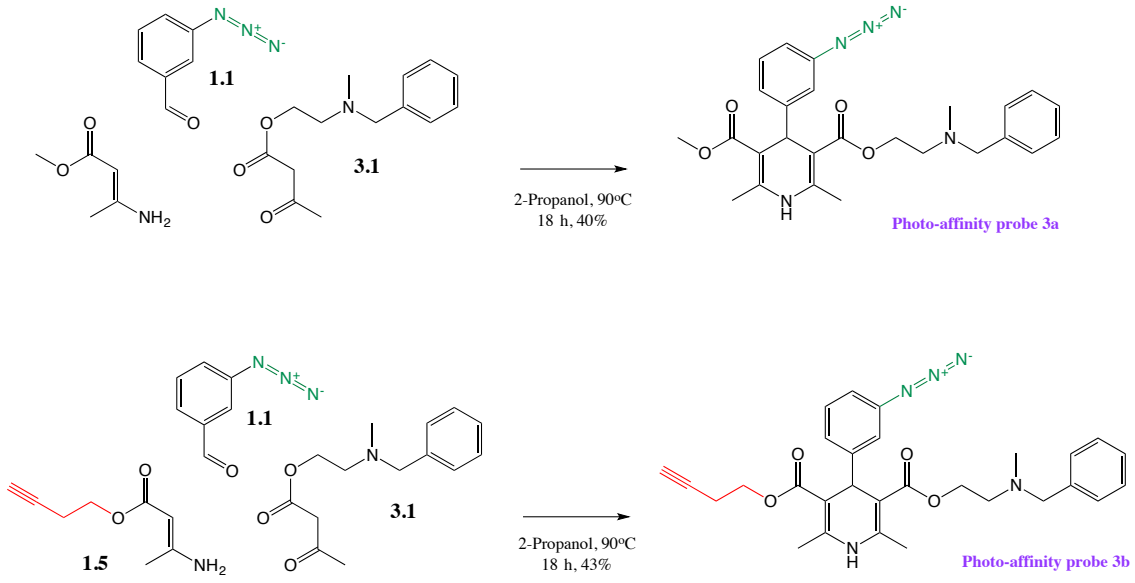


Figure 6.12. Synthesis of **Photo-affinity Probes 3a and 3b** using nicardipine as the scaffold; in **green** is the photo-reactive azide group, in **red** is the reporter alkyne group, and in **black** is the nicardipine selectivity scaffold that when incubated binds to its target proteins (in this case, the $Ca_v1.2$, $Ca_v1.3$ and I_{st} channels). For detailed explanations of the reactions, please refer to the experimental section 6.5**.**

In the synthesis of **1.3, 1.4, 2.1, 3.1** and **3.6** fragments, it was necessary to use a 3-oxobutanoate group at several stages in order to construct nicardapine's chemical scaffold. To achieve this, 2,5-dioxopyrrolidin-1-yl 3-oxobutanoate was used. A general reaction scheme illustrating this is shown in **Figure 6.13**. However, using these conditions a very low yield of the desired product was obtained. The major product had a molecular mass of 168, which was identified by NMR and mass spectroscopy analysis to be 2-acetylcyclohexane-1,3,5-trione. It was noted that the high temperatures (90 to 120°C) required for probe synthesis were causing 2,5-dioxocyclopentyl 3-oxobutanoate to react with itself, producing 2-acetylcyclohexane-1,3,5-trione (**Figure 6.14**).

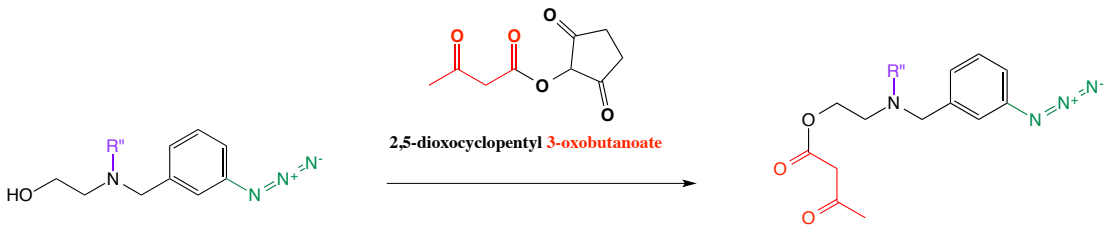


Figure 6.13 Reaction scheme for addition of the 3-oxobutanoate group.

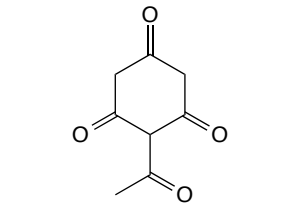


Figure 6.14. Unwanted side product, 2-acetylcyclohexane-1,3,5-trione, produced in the synthesis of **1.3, 1.4, 2.1, 3.1** and **3.6** fragments.

A literature search revealed an alternative way to add a 3-oxobutanoate group to the probe's chemical scaffold was to use 2,2,6-trimethyl-4H-1,3-dioxine-4-one instead of 2,5-dioxocyclopentyl 3-oxobutanoate (Miri *et al.,* 2006; **Figure 6.15**).

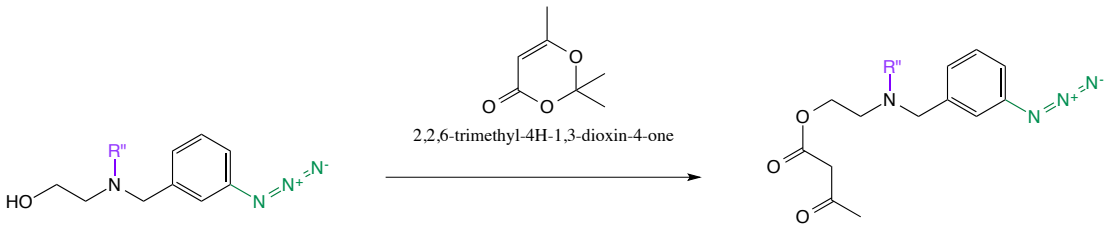
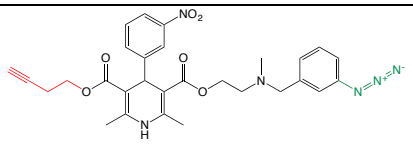
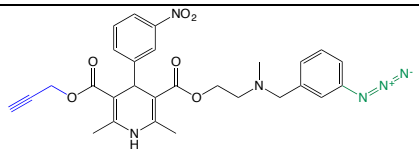
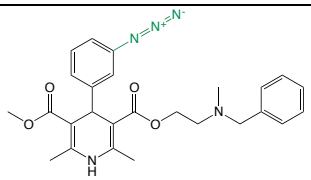
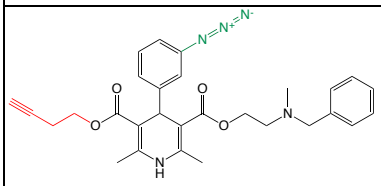
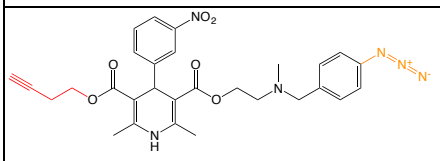
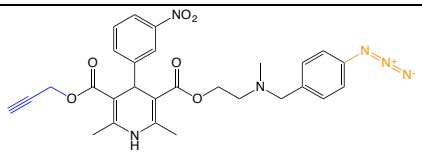


Figure 6.15 Reaction scheme showing an alternative way to add a 3-oxobutanoate group to the probe scaffold.

In total, six individual probes were successfully synthesised, characterised, and tested for biological function using a mouse atrial preparation. The synthesised probes, as well as the results from the biological assay, are summarised in **Table 6.2** below.

Table 6.2 Yield of successfully synthesised probes and their effects on a mouse atrial preparation.

Probe structure	Name assigned	Weight in mg	Results from mouse atrial preparation
	Photo-affinity probe 1	71	Comparable to nicardipine in reducing spontaneous beating rate
	Photo-affinity probe 2	46	Comparable to nicardipine in reducing spontaneous beating rate
	Photo-affinity probe 3a	90	No significant reduction in spontaneous beating rate
	Photo-affinity probe 3b	151	No significant reduction in spontaneous beating rate
	Photo-affinity probe 4	157	Comparable to nicardipine in reducing spontaneous beating rate
	Photo-affinity probe 5	111	Comparable to nicardipine in reducing spontaneous beating rate

6.3. Biological assay's results and discussion

The CD1 mouse atrial preparation was the chosen model to represent SAN function. The functional readout of the assay was observed changes in the basal beating rate of the atrial preparation (which is directly driven and controlled by SAN cells). Please refer to chapter 2 (method, section 2.2. organ bath sinoatrial node preparations) for the detailed description of setup and information captured by the assay. Thus inhibition of both L-type Ca^{2+} and I_{st} channel would expect to reduce the basal beating rate due to reduction of slope of diastolic depolarisation.

The reduction of basal beating rate induced by nicardipine and the probes are irreversible, thus different mouse atrial preparations were used in assessing their effects. First, the response to nicardipine was measured, and then to each individual photo-affinity probe was recorded. The atrial preparations were incubated for 30 min with either nicardipine, probe 1, probe 2, probe 3a, probe 3b, probe 4 or probe 5, all at 1 μM (30 min incubation period required a reduced plateau steady beating rate to be reached). In the mouse atrial preparations, basal spontaneous beating rate reduced by 306 ± 17 (n = 8), 270 ± 14 bpm (n = 7), 312 ± 15 bpm (n = 6), 289 ± 10 bpm (n = 5), 302 ± 19 bpm (n = 5), 26 ± 4 bpm (n = 6) and 27 ± 6 bpm (n = 6), respectively (**Figure 6.16**). To show the effectiveness of all the individual compounds I was testing the statistical difference in beating rate in presence and absence of of each compound (including nicardipine). Thus all of the reductions, with the exception of probes 3a & b, were statistically significant relative to baseline. Also, the reductions in basal beating rate induced by probes 1, 2, 4 and 5 were not

significantly different from that of nicardipine (*P > 0.05,* one-way ANOVA with Dunnett post-test).

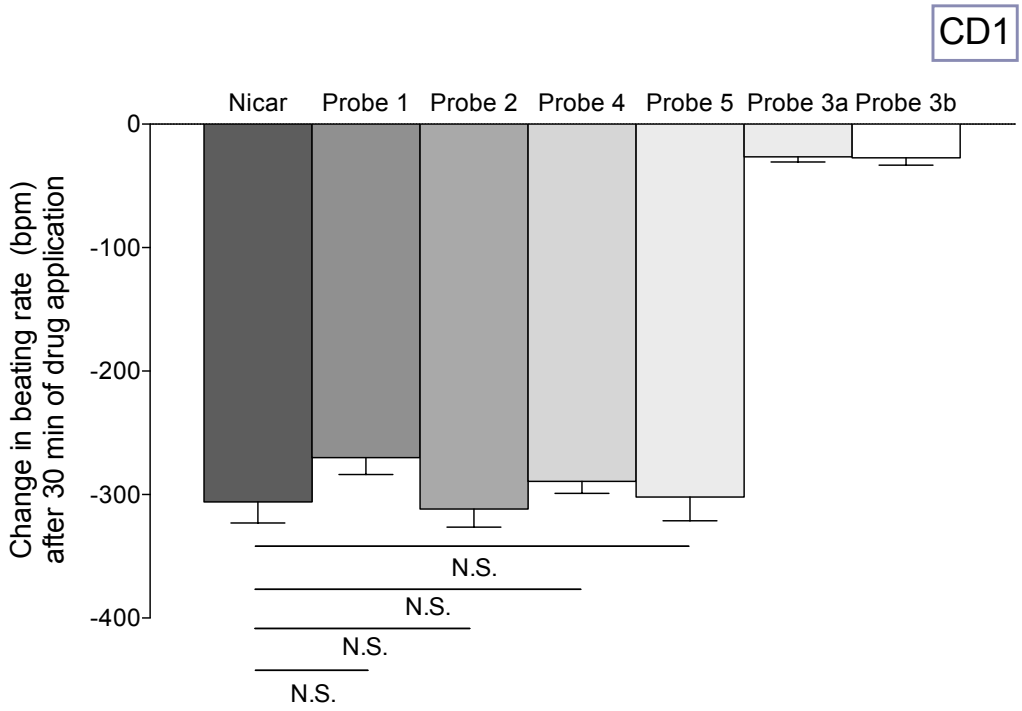


Figure 6.16 Bar chart representing the mean effect of 1 μM nicardipine (n = 8), 1 μM photo-affinity probe 1 (n = 7), 1 μM photo-affinity probe 2 (n = 6), 1 μM photo-affinity probe 3a (n = 5), 1 μM photo-affinity probe 3b (n = 5), 1 μM photo-affinity probe 4 (n = 6) and 1 μM photo-affinity probe 5 (n = 6) on mouse basal spontaneous beating rate of atrial preparations. Data are expressed as mean ± S.E.M., n = number of experiments. GraphPad Prism (version 5.0) software was used to perform statistical analysis, including one-way ANOVA with Dunnett post-test (significance level *P < 0.05*).

Inability of reducing the atrial basal beating rate by probes 3a & b may be due to exchange of NO_2 group with an azide group, and this indicates that the NO_2 group is crucial in the activity of nicardipine. Overall, the comparable potency of probes 1, 2, 4, 5 and nicardipine suggested that the chemical modification did not alter probes ability to reduce basal beating rate. Therefore probe 1, 2, 4 or 5 could be taken forward for photo-affinity enrichment of the I_{st} channels; probe 1 was selected to proceed with the enrichment experiments.

6.3.1. Photo-affinity enrichment of the I_{st} channel

In the previous section photo-affinity probes were synthesised, using nicardipine as the selectivity function. This section describes the application of these photo-affinity probes to attempt to capture, isolate and identify the as yet unidentified I_{st} channel.

Since Nicardipine is also known to bind to $Ca_v1.2$ and $Ca_v1.3$, it was anticipated that the probe might also capture these channels. Therefore, it was anticipated that a capture experiment might afford three bands in a resulting western blot, resulting from I_{st} channel $Ca_v1.2$ and $Ca_v1.3$. Experiments were performed using SAN cells, since these are known to express the I_{st} channel.

First, isolated SAN cells from guinea pig were incubated with 1 μM of a photo-affinity probe for 40 min at 4 °C in PSS solution (100 μL). The samples were then irradiated with UV light (CaproBox, 310 nm, 4 °) using 5 min pulses separated by 2 min intervals for a total of 9 pulses. In control experiments, the procedure was the same, with the exception being that either the photo-affinity

probe was not added or a competitive inhibitor was added (1 μM nicardipine). The cells were subsequently lysed [detail procedure outlined in chapter 2, 2.15. Cell lysis (guinea pig)]. Then the probe was conjugated with biotin [detail procedure outlined in chapter 2, 2.17. Click Chemistry reaction]. The probe and captured proteins were then isolated using streptavidin beads [detail procedure outlined in chapter 2, 2.18. Magnetic beads pull-down]. Captured proteins were eluted from the beads [detail procedure outlined in chapter 2, 2.18. Magnetic beads pull-down] and visualised by SDS-PAGE and western blotting using a streptvadin-HRP conjugate. Unfortunately, no signal was observed, which was believed to be because the number of SAN cells was too low.

It was then decided that as proof of principle, the ability of the probes to photo-crosslink to $Ca_v1.2$ and $Ca_v1.3$ ion channels would be examined. Since these proteins are known, and there are antibodies available for immuneblotting, their capture should be more easily studied than the for the I_{st} channel. Therefore, it was envisioned that the capture protocol could be optimised against these known channels and subsequently applied to the capture and identification of the I_{st} channel.

Thus, guinea pig isolated ventricular cells and homogenized fresh whole heart from C57BL/6 were chosen as samples from which to pull out the L-type Ca^{2+} channel ($Ca_v1.2$ isoform). For the isolation of ventricular cells, please refer to the methods section. The homogenized sample was prepared using the Dounce homogenizer; a fresh whole heart from a C57BL/6 mouse was mechanically homogenized in the presence of 100 μL lysis buffer A/B. Another 900 μL of lysis buffer A/B was added to the final homogenized preparation. The

preparation was then left for further digestion for 45 min at 4°C. The membrane proteins were recovered in supernatant after 15 min of centrifugation at 13,500 rpm at 4°C. The sample was then irradiated with 310 nm wavelength light it was identified that this would insure that the photo-affinity probe was irreversibly bound to its target protein (**Figure 6.1** *Photo Cross-linking*). Next, the biotin was attached to the alkene group (handle) through click chemistry (Dubinsky *et al.,* 2012), resulting in the formation of biotin-probe-target protein complex. Subsequently, the protein capture was loaded into the gel lane and analysed by gel electrophoresis (see method for further description, **Figure 6.1** *Target Identification*). This was followed by Western blotting, where the transferred protein bands were analysed.

Unlike the homogenized tissue preparation, the single cells were first irradiated with photo-affinity probe 1 in an open top PCR Eppendorf viol for 45 min. The cells were then manually spun down and re-suspended in lysis buffer A/B (100µl) replacing PSS. Subsequently, the sample was sonicated with 3 x 5 seconds pulses separated by 30-second intervals. Next, the membrane proteins were recovered in supernatant after 15 min of centrifugation at 13,500 rpm at 4°C. Then, in a similar manner to the homogenized tissue procedure, the samples were loaded into the gel lanes and analysed by gel electrophoresis (see method for further description), Western blot analysis was then carried out.

6.3.2. Immunoblotting for $Ca_v1.2$ using ACC-003

Initially, it was difficult to obtain the desired band with the primary antibody (ACC-003) for the $Ca_v1.2$ channel. As the bands were not clearly

defined, systematic adjustment of the parameters was required. It was then discovered that ACC-003 required further dilution to 1:1000, as the manufacturing guidance of 1:200 dilution was not optimal under the experimental conditions. The optimised antibody detection method is detailed below.

First, a range of homogenized whole heart concentrations (protein concentrations from 30 - 100 mg/mL) was loaded onto the gel. The samples were immunoblotted for $Ca_v1.2$ using ACC-003 as a primary antibody (polyclonal antibody raised in rabbit against $Ca_v1.2$, Alomone, Israel) diluted in T-BST buffer at a 1:1000 dilution. The secondary antibody was the goat anti-rabbit IgG HRP (Santa Cruz Biotech) diluted in T-BST buffer at 1:1000 dilution. 5% milk in T-BST buffer was used as a blocking buffer. A band consistent with $Ca_v1.2$ at ~190 kD was observed in agreement with Zhao *et al.'s* observations (2002). As a control, the first four lanes (L1-4) were incubated with the ACC-003 control peptide, an antigen blocking peptide ($Ca_v1.2_{848-865}$ peptide, Alomone, Israel), represented as "+ peptide". Following this treatment, the band corresponding to $Ca_v1.2$ was no longer observed (lanes 1-4) (**Figure 6.17**).

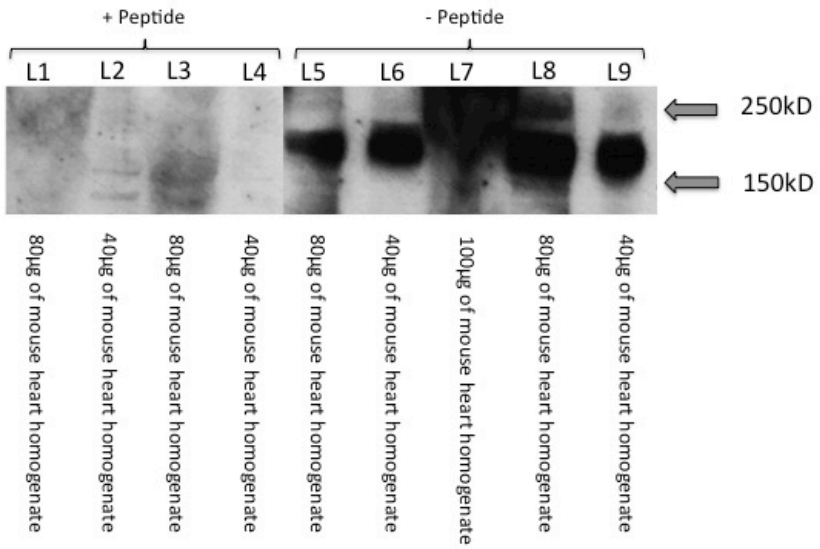


Figure 6.17 Detection of $Ca_v1.2$ channels by Western blot analysis. A range of sample concentrations (40 - 100 mg/mL) were loaded and immunoblotted. In 30 mg/mL homogenized mouse whole heart samples, $Ca_v1.2$ (~190 kDa) was successfully detected after blotting with primary and secondary antibodies (Lanes 5 - 9). No band was observed in the presence of $Ca_v1.2_{848-865}$ peptide (Lanes 1 - 4). The full Western blot gel (**Figure *A*6.17**) is available in the Appendix section**.**

6.3.3. Blotting for $Ca_v1.2$ using streptavidin-horseradish peroxidase conjugate

In attempts to blot for $Ca_v1.2$ using the streptavidin-horseradish peroxidase conjugate, the signal-to-noise ratio was too large to detect the desired band of ~190 kD. It was then realized that heart tissue would naturally have an endogenous biotinylated protein. Therefore, an initial step was included to remove the endogenous biotinylated proteins prior to the click reaction. A representative Western blot, in the presence of endogenous biotinylated

proteins, is shown in **Figure 6.18.**

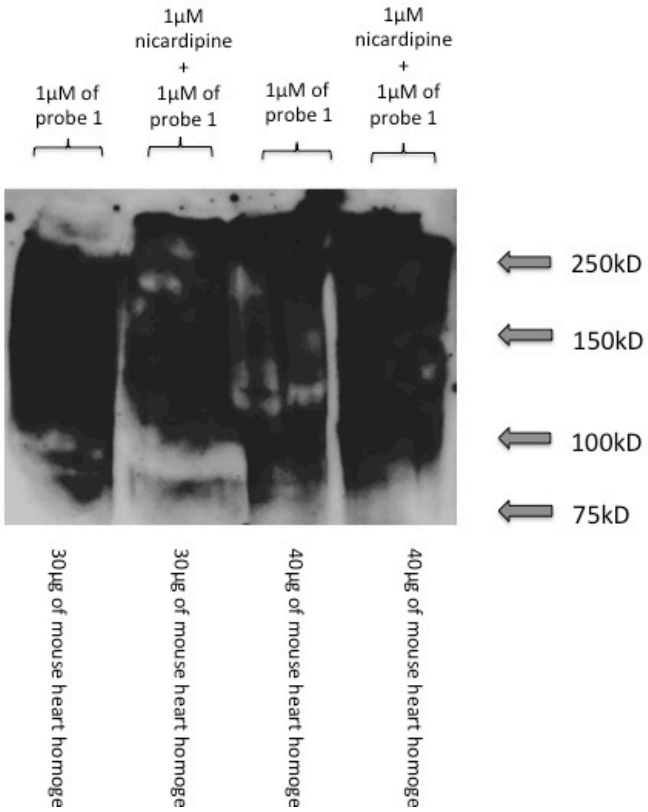


Figure 6.18 Photo-capture of $Ca_v1.2$ channel by Probe 1 in homogenized mouse whole heart samples. Due to high signal to noise ratio, no obvious band of ~190 kD, representing the $Ca_v1.2$ channel, was observed.

Following removal of the endogenous biotinylated proteins with an aid of streptavidin beads, streptavidin-horseradish peroxidase conjugate (1:15,000 dilution in T-TBS) was used to detect biotinylated $Ca_v1.2$ (biotin-probe-$Ca_v1.2$ complex) post click reaction derivatisation. Nicardipine was used as a competitive antagonist in order to prevent photo-affinity probe 1 from binding to its target protein, the $Ca_v1.2$ channel. It was observed that nicardipine successfully competed with probe 1 for binding to $Ca_v1.2$; i.e. in lanes 2 and 4

to 8, no band was found at ~190 kD corresponding to $Ca_v1.2$. However, in the absence of nicardipine, the ~190 kD band was present, although it was weak in the ventricular cell lysate sample (lane 3) (**Figure 6.19**).

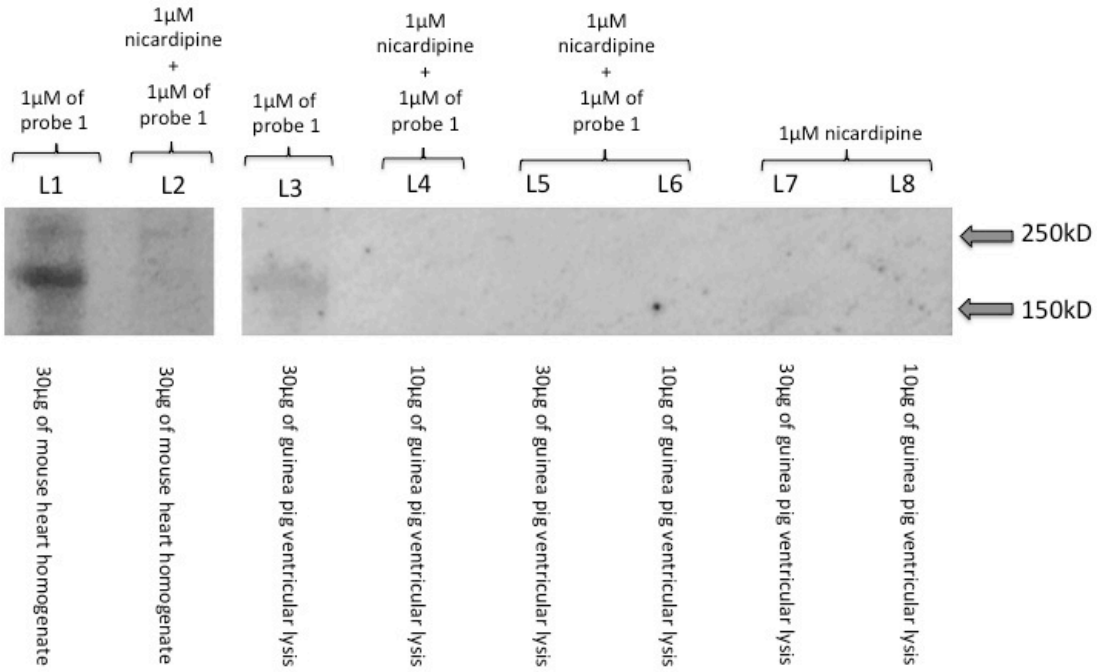


Figure 6.19 Photo-capture of $Ca_v1.2$ channel by photo-affinity probe 1 in (L3 - 8) ventricular guinea pigs cell lysate or (L1-2) homogenized mouse whole heart samples. In 30 mg/mL cell lysate and homogenized tissue, cross-linked $Ca_v1.2$ (~190 kDa) could be detected after irradiation with 1 μM photo-affinity probe 1 (Lanes 1 and 3). No crosslinking was observed in the presence of 1 μM nicardipine (Lanes 2, 4 to 8). The full Western blot gel (**Figure *A*6.19**) is available in the Appendix section**.**

Using homogenized sample from mouse the above experiment was repeated with the photo-affinity probe 1, except this time the concentration was increased from 1 μM to 3 μM. Again, the desired band of ~190 kDa corresponding to $Ca_v1.2$ was successfully detected in the absence of

nicardipine (**Figure 6.20**).

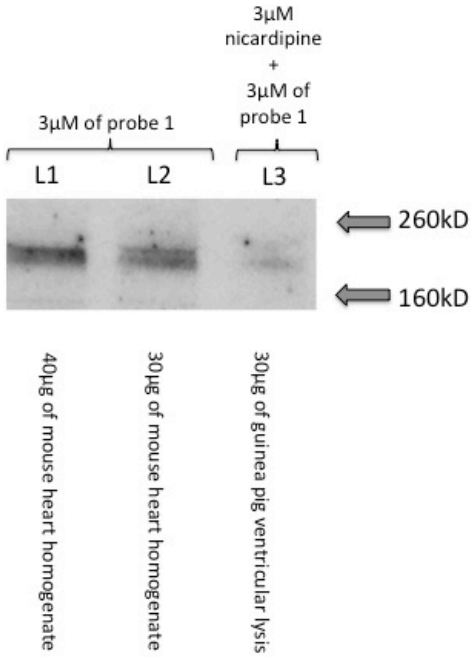


Figure 6.20 Evidence for photo-capture of $Ca_v1.2$ channel by photo-affinity probe 1 in homogenized mouse whole heart samples. Cross-linked $Ca_v1.2$ (~190 kDa) could be detected after irradiation with 3 μM photo-affinity Probe 1 (L1 - 2). No obvious crosslinking was observed in the presence of 3 μM nicardipine (L3). The full Western blot gel (**Figure *A*6.20**) is available in the Appendix section**.**

Overall a proof of concept was successfully established demonstrating that the L-type Ca^{2+} channel can be captured and enriched using photo-crosslinking probe. A natural extension of this work would involve use of the synthesised photo-affinity probes to identify the I_{st} channel in the SA node. However, in attempting to do so it seems likely that more than one guinea pig heart may need to be used to isolate sufficient SAN cells. Then the subsequent

pulled down protein needs to be analysed in mass spectrometry (LC-MS/MS) to reveal the amino acid sequence of the target protein.

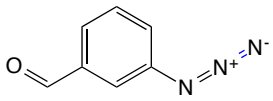
6.4. Experimental section

6.4.1 Chemical syntheses

Reagents and solvents were obtained, unless otherwise stated, from Sigma Aldrich UK. Solvents were removed under reduced pressure using a BuchiTM rotary evaporator. Analytical thin layer chromatography (TLC) was carried out on Merck silica gel 60 F254 aluminium supported thin layer chromatography sheets. Visualisation was by absorption of UV light (λ max 254 nm). Flash column chromatography was carried out using a Biotage SP1 automated flash column chromatography machine, eluting with solvents under a positive pressure of compressed air. Spectra were recorded using a Bruker Tensor 27 spectrometer and a representative number of absorption maxima are reported in wavenumbers (cm-1). ^{1}H NMR spectra and ^{13}C NMR were recorded on a Bruker Avance AV500 (125.8 MHz) spectrometer in CDCl3 or MeOD-d6. Chemical shift values are given as δH in units of parts per million (ppm) relative to tetramethylsilane (TMS) where δ(TMS) = 0.00 ppm. The multiplicity of each signal is indicated by: s (singlet); br s (broad singlet); d (doublet); t (triplet); q (quartet); dd (doublet of doublets) or m (multiplet). The number of protons (n) for a given resonance signal is indicated by nH. Coupling constants (J) are expressed in Hz and are recorded to the nearest 0.5 Hz. Identical proton coupling constants (J) are averaged in each spectrum and reported to the nearest 0.5 Hz. ^{1}H and ^{13}C spectra were assigned using 2D NMR experiments including COSY and HSQC, and by comparison with related compounds. Mass spectra (m/z) under the conditions of electrospray ionisation (ESI) were recorded on a Fisons Platform Accurate mass (HRMS) data were recorded under conditions of ESI on a Brucker Micro-CT of spectrometer (resolution 10000 FWHM)

using a lock spray source. Values are reported as ratio of mass to charge in Daltons and relative intensities of peaks observed are quoted as a percentage value.

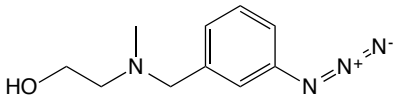
6.4.1.1 3-Azidobenzaldehyde (Li *et al.,* 2010) [1.1]



TBAF (4.18 g, 16 mmol), $TMSN_3$ (1.84 g, 16 mmol) and CuCl (204 mg, 1.3 mmol) were added in succession to (3-formylphenyl)boronic acid (2.0 g, 13.3 mmol) in 60 ml methanol in a 250 ml round-bottomed flask. The mixture was heated to reflux (70°C) for 18 hours, and reaction progress was monitored by TLC (product R_f 0.20, EtOAc:n-hexane, 10:90). The reaction mixture was cooled, and the methanol was removed using a rotary evaporator. The resultant residue, a dark orange liquid, was re-dissolved in the minimum volume of dichloromethane then purified by flash column chromatography on a silica column. The column was eluted with a gradient of EtOAc:c-hexane, which was increased linearly from 4:96 to 10:90 over 12 CVs. The desired fractions were combined and evaporated using a rotary evaporator to yield the product as a dark orange liquid (1.25 g, 62%).

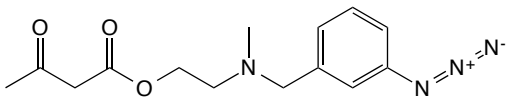
^{1}H NMR (500 MHz, chloroform-*d*) d ppm 7.28 (1 H, ddd, *J*=8.0, 2.5, 1.0 Hz, C(Ar)*H*)), 7.52 - 7.57 (2 H, m, C(Ar)*H*)), 7.66 (1 H, d, *J*=7.5 Hz, C(Ar)*H*)), 10.01 (1 H, s, C=O*H*Ph-N_3).^{13}C NMR (126 MHz, chloroform-*d*) d ppm 119.0, 124.9, 126.6, 130.5, 137.8, 141.4, 191.2.

6.4.1.2 2-((3-azidobenzyl)(methyl)amino)ethan-1-ol [1.2]



1.1 (250 mg, 1.7 mmol) was added to 2-(methylamino)ethan-1-ol (128 mg, 1.7 mmol) in 6 ml dichloromethane and placed in a 25 ml round-bottomed flask. Acetic acid (112 mg, 1.9 mmol) was added to the flask. The mixture was stirred at room temperature for 15 minutes before adding $NaBH(OAc)_3$ (376 mg, 1.79 mmol). The mixture was stirred at room temperature for 50 hours. Reaction progress was monitored by TLC (product R_f 0.20, EtOAc:n-hexane, 10:90). On completion of the reaction, dichloromethane was removed using a rotary evaporator. The resultant residue, a yellow liquid, was re-dissolved in the minimum volume of dichloromethane then purified by flash column chromatography on a silica column. The column was eluted with a gradient of EtOAc:c-hexane, which was increased linearly from 4:96 to 10:90 over 12 CVs. The desired fractions were combined and evaporated using a rotary evaporator to yield the product as a light brown liquid (260 mg, 74%), which was used directly in the next step (**6.4.1.3**; Compound **1.3**).

6.4.1.3 2-((3-azidobenzyl)(methyl)amino)ethyl 3-oxobutanoate [1.3]

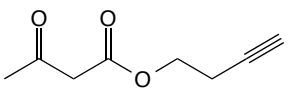


The methods used were adapted from Miri *et al.,* (2006). **1.2** (260 mg, 1.26 mmol) was added to 2,2,6-trimethyl-4H-1,3-dioxine-4-one (179 mg, 1.26 mmol) in 2 ml

toluene and placed in a 25 ml round-bottomed flask. The mixture was stirred and heated to reflux (120°C) for 18 hours, and reaction progress was monitored by TLC (product R_f 0.20, MeOH:DCM, 1:99). The reaction mixture was cooled, and the toluene was removed using a rotary evaporator. The resultant residue, a pale yellow liquid, was re-dissolved in the minimum volume of dichloromethane then purified by flash column chromatography on a silica column. The column was eluted with a gradient of MeOH:DCM, which was increased linearly from 0:100 to 1:99 over 12 CVs. The desired fractions were combined and evaporated using a rotary evaporator to yield the product as a pale yellow liquid (171 mg, 47%).

v_{max} (thin film) 2792 (C-H), 2361, 2326, 2163 (C≡C), 2113 (N_3), 1717 (C=O, ester). ^{1}H NMR (500 MHz, chloroform-*d*) d ppm 2.28 (3 H, s, NC*H*$_3$), 2.28 (3 H, s, C*H*$_3$C=O), 2.68 (2 H, t, *J*=6.0 Hz, OCH$_2$C*H*$_2$N), 3.49 (2 H, s, CH$_3$C=OC*H*$_2$), 3.54 (2 H, s, NC*H*$_2$Ph-N$_3$), 4.28 (2 H, t, *J*=6.0 Hz, OC*H*$_2$CH$_2$N), 6.93 (1 H, dd, *J*=8.0, 1.3 Hz, C(Ar)*H*), 7.01 - 7.05 (1 H, m, C(Ar)*H*), 7.06 - 7.10 (1 H, m, C(Ar)*H*), 7.28 - 7.32 (1 H, m, C(Ar)*H*). ^{13}C NMR (126 MHz, chloroform-*d*) d ppm 30.2, 42.5, 50.0, 55.3, 62.0, 62.9, 117.8, 119.3, 125.4, 129.6, 140.0, 141.0, 167.1, 200.5. *m/z* HRMS (ESI$^+$) $C_{14}H_{18}N_4NaO_3^+$ ([M+Na]$^+$) requires 313.1271; found 313.1271.

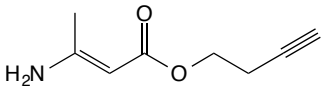
6.4.1.4 But-3-yn-1-yl 3-oxobutanoate (Yadav *et al.,* 2007) [1.4]



The methods used were adapted from Yadav *et al.,* (2007). Triphenylphosphine (452 mg, 1.73 mmol) was added to a stirred mixture of methyl-3-oxobutanoate (2 g, 17.2 mmol) and but-3-yn-1-ol (966 mg, 17.2 mmol) in 87 ml toluene in a 250 ml round-bottomed flask. The mixture was heated to reflux (120°C) for 18 hours, and reaction

progress was monitored by TLC (product R_f 0.20, EtOAc:n-hexane, 15:85). The reaction mixture was cooled, and the toluene was removed using a rotary evaporator. The resultant residue, a yellow liquid, was re-dissolved in the minimum volume of dichloromethane then purified by flash column chromatography on a silica column. The column was eluted with a gradient of EtOAc:c-hexane, which was increased linearly from 5:95 to 15:85 over 12 CVs. The desired fractions were combined and evaporated using a rotary evaporator to yield the product as a yellow liquid (1.25 g, 47%), which was used directly in the next step (6.**5.1.5**; Compound **1.5**).

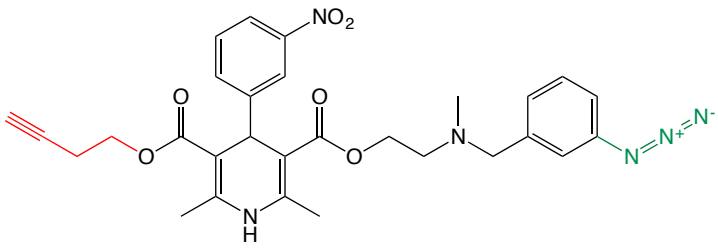
6.4.1.5 But-3-yn-1-yl-(E)-3-aminobut-2-enoate[1.5]



The methods used were adapted from Filipan-Litvić *et al.,* (2007). **1.4** (500 mg, 3.25 mmol) was added to ammonium carbamate (NH_4OOCNH_2, 192 mg, 3.25 mmol) in 5 ml methanol in a 50 ml round-bottomed flask. The mixture was stirred overnight (18 hours) at room temperature until all solid material in the suspension was dissolved. The solvent was then evaporated off to yield crude white colorless liquid of 1.5 (422 mg, 85%).

v_{max} (thin film) 3463 (N-H), 3338 (C-H, alkyne), 3292, 3004, 2970 (C-H), 1739 (C=O, ester), 1664, 1620, 1562. ^{1}H NMR (500 MHz, chloroform-*d*) d ppm 1.92 (3 H, s, CCH_3), 2.00 (1 H, t, *J*=2.5 Hz, C*H*CCH_2), 2.54 (2 H, td, *J*=7.0, 2.5 Hz, CHCCH_2), 4.18 (2 H, t, *J*=7.0 Hz, CHCCH_2CH_2O), 4.52 - 4.58 (1 H, m, OC=OC*H*), 7.88 (2 H, s, NH_2). ^{13}C NMR (126 MHz, chloroform-*d*) d ppm 19.3, 22.4, 60.5, 69.5, 80.7, 83.7, 160.1, 169.7. *m/z* HRMS (ESI$^+$) $C_8H_{11}NNaO_2^+$ ([M+Na]$^+$) requires 176.0682; found 176.0677.

6.4.1.6 3-(2-((3-azidobenzyl)(methyl)amino)ethyl) 5-(but-3-yn-1-yl) 2,6-dimethyl-4-(3-nitrophenyl)pyridine-3,5-dicarboxylate [*Probe 1*]

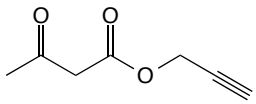


The methods used were adapted from Iwanami *et al.,* (1979). **1.3** (85.5 mg, 0.29 mmol) was added to **1.5** (45 mg, 0.29 mmol) and 3-nitrobenzaldehyde (45 mg, 0.29 mmol) in 3 ml 2-propanol and placed in a 25 ml round-bottomed flask. The mixture was heated to reflux (90°C) for 18 hours, and reaction progress was monitored by TLC (product R_f 0.20, EtOAc:n-hexane, 45:55). The reaction mixture was cooled, and the 2-propanol was removed using a rotary evaporator. The resultant residue, a yellow liquid, was re-dissolved in the minimum volume of dichloromethane then purified by flash column chromatography on a silica column. The column was eluted with a gradient of EtOAc:c-hexane, which was increased linearly from 15:85 to 50:50 over 12 CVs. The desired fractions were combined and evaporated using a rotary evaporator to yield the product as a yellow liquid (71 mg, 44%).

ν_{max} (thin film) 3459.86 (N-H), 3304 (C-H, alkyne), 3016 (C-H), 2970 (C-H), 2113 (N_3, C≡C), 1739 (C=O, ester), 1527 & 1366 (-NO_2). ^{1}H NMR (500 MHz, METHANOL-d_4) d ppm 2.21 (3 H, s, NCH_3), 2.26 (1 H, t, *J*=2.5 Hz, CHCCH_2), 2.36 (3 H, s, NCCH_3), 2.37 (3 H, s, NCCH_3), 2.47 (2 H, td, *J*=6.5, 2.7 Hz, CHCCH_2), 2.59 - 2.72 (2 H, m, OCH_2CH_2N), 3.49 (2 H, q, *J*=11.0 Hz, NCH_2Ph-N_3), 4.05 - 4.16 (2 H, m, CHCCH_2CH_2), 4.20 (2 H, t, *J*=5.5 Hz, OCH_2CH_2N), 5.13 (1 H, s, NO_2-PhCH), 5.51 (1 H, s, NH), 6.93 - 6.99 (2 H, m, C(Ar)H), 7.06 (1 H, d, *J*=7.0 Hz, C(Ar)H), 7.30 (1 H, t, *J*=8.0 Hz, C(Ar)H),

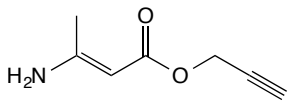
7.42 (1 H, t, *J*=8.0 Hz, C(Ar)*H*), 7.71 (1 H, d, *J*=8.0 Hz, C(Ar)*H*), 7.93 - 7.99 (1 H, m, C(Ar)*H*), 8.13 (1 H, t, *J*=2.0 Hz, C(Ar)*H*). ^{13}C NMR (126 MHz, METHANOL-d_4) d ppm 18.86, 18.96, 19.81, 40.99, 42.88, 56.95, 62.61, 62.96, 63.34, 71.09, 81.58, 103.14, 103.35, 118.95, 120.62, 122.24, 123.88, 126.94, 130.30, 130.90, 135.62, 141.59, 142.38, 148.51, 148.69, 149.54, 151.83, 168.83, 168.96. *m/z* HRMS (ESI$^+$) $C_{29}H_{31}N_6O_6^+$ ([M+H]$^+$) requires 559.2300; found 559.2275.

6.4.1.7 Prop-2-yn-1-yl 3-oxobutanoate [2.1]



The methods used were adapted from Miri et al. (2006). 2,2,6-trimethyl-4H-1,3-dioxine-4-one (1.0 g, 7.04 mmol) was added to a solution of prop-2-yn-1-ol (395 mg, 7.04 mmol) in 4 ml toluene and placed in a 25 ml round-bottomed flask. The mixture was stirred and heated to reflux (120°C) for 18 hours, for the reaction to be complete. The reaction mixture was cooled, and the toluene was removed using a rotary evaporator. The resultant crude product, a dark brown viscous liquid, was carried forward to the next step (640 mg, ~ 65%), which was used directly in the next step (6.**5.1.8**; Compound **2.2**).

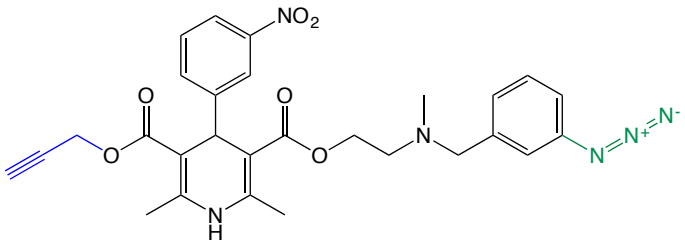
6.4.1.8 Prop-2-yn-1-yl-(E)-3-aminobut-2-enoate [2.2]



The methods used were adapted from Miri *et al.,* (2006). **2.1** (640 mg, ~ 4.6 mmol) and ammonium acetate (408 mg, 6.9 mmol) in 8 ml ethanol was placed in a 50 ml round-bottomed flask. The mixture was stirred and heated to reflux (90°C) for 18 hours, for the reaction to be complete (monitored by TLC, product R_f 0.20, EtOAc:n-hexane, 15:85). The reaction mixture was cooled, and the ethanol was removed using a rotary evaporator. The resultant residue, a burgundy viscous liquid, was re-dissolved in the minimum volume of dichloromethane then purified by flash column chromatography on a silica column. The column was eluted with a gradient of EtOAc:c-hexane, which was increased linearly from 5:95 to 15:85 over 12 CVs. The desired fractions were combined and evaporated using a rotary evaporator to yield the product as an orange viscous liquid (480 mg, 75%).

v_{max} (thin film) 3470 (N-H), 3341 (C-H, alkyne), 3291, 2921 (C-H), 1666 (C=O, ester), 1624, 1561. ^{1}H NMR (500 MHz, chloroform-*d*) d ppm 1.93 (3 H, s, CCH_3), 2.43 (1 H, t, *J*=2.5 Hz, CHCCH_2), 4.58 (1 H, s, OC=OCH), 4.67 (2 H, s, CHCCH_2), 7.93 (2 H, br. s, NH_2). ^{13}C NMR (126 MHz, chloroform-*d*) d ppm 22.4, 50.2, 73.8, 79.0, 83.1, 160.8, 169.0. *m/z* HRMS (ESI$^+$) $C_7H_9NNaO_2^+$ ([M+Na]$^+$) requires 162.0525; found 162.0520.

6.4.1.9 3-(2-((3-azidobenzyl)(methyl)amino)ethyl) 5-(prop-2-yn-1-yl) 2,6-dimethyl-4-(3-nitrophenyl)pyridine-3,5-dicarboxylate [*Probe 2*]

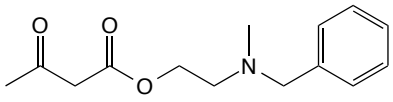


The methods used were adapted from Iwanami *et al.,* (1979). **1.3** (85.5 mg, 0.29 mmol) was added to **2.2** (41 mg, 0.29 mmol) and 3-nitrobenzaldehyde (45 mg, 0.29 mmol) in 3 ml 2-propanol and placed in a 25 ml round-bottomed flask. The mixture was heated to reflux (90°C) for 18 hours, and reaction progress was monitored by TLC (product R_f 0.20, EtOAc:n-hexane, 45:55. The reaction mixture was cooled, and the 2-propanol was removed using a rotary evaporator. The resultant residue, a yellow liquid, was re-dissolved in the minimum volume of dichloromethane then purified by flash column chromatography on a silica column. The column was eluted with a gradient of EtOAc:c-hexane, which was increased linearly from 15:85 to 50:50 over 12 CVs. The desired fractions were combined and evaporated using a rotary evaporator to yield the product as a yellow liquid (46 mg, 29%).

ν_{max} (thin film) 3344 (C-H, alkyne, N-H), 2934 (C-H), 2788 (C-H), 2593, 2484, 2366, 2113 (N_3, C≡C), 1692 (C=O, ester) 1587, 1527 & 1348 (-NO_2). ^{1}H NMR (500 MHz, METHANOL-d_4) d ppm 2.21 (3 H, s, NCH_3), 2.36 (3 H, s, NCCH_3), 2.37 (3 H, s, NCCH_3), 2.65 (2 H, m, OCH$_2$CH_2N), 2.83 (1 H, t, *J*=2.5 Hz, CHCCH$_2$), 3.49 (2 H, q, *J*=13.0 Hz, NCH_2Ph-N_3), 4.12 - 4.25 (2 H, m, OCH_2CH$_2$N), 4.59 - 4.72 (2 H, m, CHCCH_2), 5.12 (1 H, s, NO_2-PhCH), 5.51 (1 H, s, NH), 6.92 - 6.99 (2 H, m, C(Ar)H), 7.06 (1 H, d, *J*=7.5 Hz, C(Ar)H), 7.30 (1 H, t, *J*=8.0 Hz, C(Ar)H), 7.42 (1 H, t, *J*=8.0 Hz,

C(Ar)*H*), 7.69 (1 H, d, *J*=8.0 Hz, C(Ar)*H*), 7.97 (1 H, m, *J*=7.0, 1.5, 1.5 Hz, C(Ar)*H*), 8.13 (1 H, t, *J*=2.0 Hz, C(Ar)*H*). ^{13}C NMR (126 MHz, METHANOL-d_4) d ppm 18.7, 18.7, 40.9, 42.8, 52.1, 56.8, 62.5, 62.9, 75.9, 79.1, 102.6, 103.3, 118.8, 120.5, 122.1, 123.8, 126.8, 130.2, 130.8, 135.4, 141.4, 142.2, 148.3, 149.0, 149.4, 151.6, 167.9, 168.8. *m/z* HRMS (ESI$^+$) $C_{28}H_{29}N_6O_6^+$ ([M+H]$^+$) requires 545.2143; found 545.2117.

6.4.1.10. 2-(benzyl(methyl)amino)ethyl3-oxobutanoate (Noyola *et al.,* 2003) [3.1]

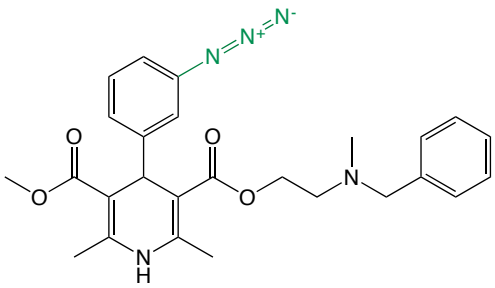


The methods used were adapted from Noyola *et al.,* (2003). 2-(benzyl(methyl)amino)ethan-1-ol (500 mg, 3.5 mmol) was added to 2,2,6-trimethyl-4H-1,3-dioxine-4-one (581 mg, 3.5 mmol) in 2 ml toluene and placed in a 25 ml round-bottomed flask. The mixture was stirred and heated to reflux (120°C) for 18 hours, and reaction progress was monitored by TLC (product R_f 0.20, MeOH:DCM, 10:90). The reaction mixture was cooled, and the toluene was removed using a rotary evaporator. The resultant residue, a light yellow liquid, was re-dissolved in the minimum volume of dichloromethane then purified by flash column chromatography on a silica column. The column was eluted with a gradient of MeOH:DCM, which was increased linearly from 0:100 to 10:90 over 12 CVs. The desired fractions were combined and evaporated using a rotary evaporator to yield the product as light yellow liquid (447 mg, 51%).

^{1}H NMR (500 MHz, chloroform-*d*) d ppm 2.27 (3 H, s, NCH_3), 2.28 (3 H, s, CH_3C=O), 2.68 (2 H, t, *J*=6.0 Hz, OCH$_2$CH_2N), 3.46 (2 H, s, CH$_3$C=OCH_2), 3.55 (2 H, s, NCH_2Ph), 4.27 (2 H, t, *J*=6.0 Hz, OCH_2CH$_2$N), 7.24 - 7.34 (5 H, m, C(Ar)*H*). ^{13}C NMR

(126 MHz, chloroform-*d*) d ppm 30.1, 42.5, 50.0, 55.2, 62.4, 63.0, 127.1, 128.2, 128.9, 138.6, 167.1, 200.5.

6.4.1.11 3-(2-(benzyl(methyl)amino)ethyl) 5-methyl 4-(3-azidophenyl)-2,6 dimethylpyridine-3,5-dicarboxylate [*Probe 3a*]

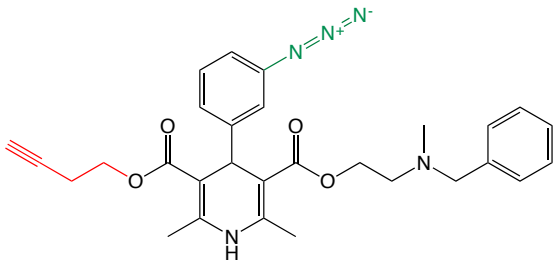


The methods used were adapted from Iwanami *et al.,* (1979). **3.1** (116 mg, 0.48 mmol) was added to **1.1** (70 mg, 0.48 mmol) and methyl aminocrotonate (54 mg, 0.48 mmol) in 3 ml 2-propanol and placed in a 25 ml round-bottomed flask. The mixture was heated to reflux (90°C) for 18 hours, and reaction progress was monitored by TLC (product R_f 0.20, MeOH:DCM, 10:90). The reaction mixture was cooled, and the 2-propanol was removed using a rotary evaporator. The resultant residue, a yellow liquid, was re-dissolved in the minimum volume of dichloromethane then purified by flash column chromatography on a silica column. The column was eluted with a gradient of MeOH:DCM, which was increased linearly from 0:100 to 10:90 over 12 CVs. The desired fractions were combined and evaporated using a rotary evaporator to yield the product as a yellow liquid (90 mg, 40%).

ν_{max} (thin film) 3332 (N-H), 3088 (C-H), 2952 (C-H), 2844 (C-H), 2791 (C-H), 2115 (N_3), 1682 (C=O, ester). ^{1}H NMR (500 MHz, chloroform-*d*) d ppm 2.22 (3 H, s, NCH_3), 2.34 (3 H, s, NCCH_3), 2.35 (3 H, s, NCCH_3), 2.63 - 2.71 (2 H, m, OCH$_2$CH_2N), 3.52 (2 H, d, *J*=2.0 Hz, NCH_2Ph), 3.65 (3 H, s, OCH_3), 4.20 (2 H, t, *J*=6.0 Hz, OCH_2CH$_2$N),

5.03 (1 H, s, N_3-PhC*H*), 5.67 (1 H, s, N*H*), 6.77 - 6.83 (1 H, m, C(Ar)*H*), 6.93 (1 H, t, *J*=2.0 Hz, C(Ar)*H*), 7.07 (1 H, d, *J*=8.0 Hz, C(Ar)*H*), 7.14 - 7.20 (1 H, m, C(Ar)*H*), 7.23 - 7.27 (1 H, m, C(Ar)*H*), 7.28 - 7.33 (4 H, m, C(Ar)*H*). ^{13}C NMR (126 MHz, chloroform-*d*) d ppm 19.60, 19.67, 39.32, 42.27, 51.02, 55.57, 61.73, 62.47, 103.53, 103.56, 116.82, 118.41, 124.56, 126.98, 128.20, 128.91, 129.28, 138.86, 139.47, 144.33, 144.48, 149.42, 167.23, 167.75. *m/z* HRMS (ESI^+) $C_{26}H_{30}N_5O_4^+$ ([M+H^+) requires 476.2292; found 476.2276.

6.4.1.12 3-(2-(benzyl(methyl)amino)ethyl) 5-(but-3-yn-1-yl) 4-(3-azidophenyl)-2,6-dimethylpyridine-3,5-dicarboxylate [*Probe 3b*]

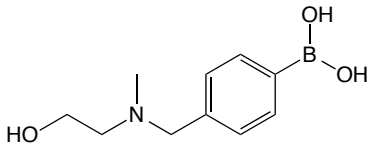


The methods used were adapted from Iwanami *et al.,* (1979). **3.1** (171 mg, 0.68 mmol) was added to **1.1** (100 mg, 0.68 mmol) and **1.5** (105 mg, 0.68 mmol) in 5 ml 2-propanol and placed in a 25 ml round-bottomed flask. The mixture was heated to reflux (90°C) for 18 hours, and reaction progress was monitored by TLC (product R_f 0.20, EtOAc:n-hexane, 45:55). The reaction mixture was cooled, and the 2-propanol was removed using a rotary evaporator. The resultant residue, a yellow liquid, was re-dissolved in the minimum volume of dichloromethane then purified by flash column chromatography on a silica column. The column was eluted with a gradient of EtOAc:n-hexane, which was increased linearly from 15:85 to 55:45 over 12 CVs. The desired

fractions were combined and evaporated using a rotary evaporator to yield the product as a yellow liquid (151 mg, 43%).

v_{max} (thin film) 3307 (C-H, alkyne, N-H), 3088 (C-H), 3030 (C-H), 2960 (C-H), 2844 (C-H), 2790 (C-H), 2116 (N_3, C≡C), 1696 (C=O, ester). ^{1}H NMR (500 MHz, chloroform-*d*) d ppm 2.20 - 2.24 (3 H, m, NCH_3), 2.28 (1 H, d, *J*=1.5 Hz, CHCCH_2), 2.34 (3 H, s, NCCH_3), 2.36 (3 H, s, NCCH_3), 2.46 (2 H, td, *J*=6.5, 3.0 Hz, CHCCH_2), 2.63 - 2.70 (2 H, m, OCH_2CH_2N), 3.45 - 3.57 (2 H, m, NCH_2Ph), 4.11 - 4.21 (4 H, m, CHCCH_2CH_2, OCH_2CH_2N), 5.01 - 5.04 (1 H, m, N_3-PhCH), 5.69 (1 H, s, NH), 6.80 (1 H, ddd, *J*=8.0, 2.5, 1.0 Hz, C(Ar)H), 6.94 (1 H, t, *J*=2.0 Hz, C(Ar)H), 7.08 - 7.12 (1 H, m, C(Ar)H), 7.14 - 7.19 (1 H, m, C(Ar)H), 7.23 - 7.33 (5 H, m, C(Ar)H). ^{13}C NMR (126 MHz, chloroform-*d*) d ppm 19.0, 19.6, 19.8, 39.4, 42.4, 55.5, 61.7, 61.8, 62.5, 69.8, 80.4, 103.3, 103.8, 116.8, 118.6, 124.8, 127.0, 128.2, 128.9, 129.2, 138.9, 139.4, 144.3, 144.8, 149.5, 166.9, 167.2. *m/z* HRMS (ESI$^+$) $C_{29}H_{32}N_5O_4^+$ ([M+H$^+$) requires 514.2449; found 514.2430.

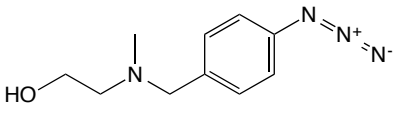
6.4.1.13 (4-((methyl(2-((3-oxobutanoyl)oxy)ethyl)amino)methyl)phenyl)boronic acid [3.4]



(4-formylphenyl)boronic acid (550 mg, 3.7 mmol) was added to 2-(methylamino)ethan-1-ol (255 mg, 3.7 mmol) in 12 ml dichloromethane and placed in a 50 ml round-bottomed flask. 4 ml ethanol was added. Acetic acid (244 mg, 4.1 mmol) was then added to the flask, and the mixture was stirred at room temperature for 15 minutes before adding $NaBH(OAc)_3$ (823 mg, 3.9 mmol). The mixture was stirred at

room temperature for 50 hours. The reaction progress was monitored by TLC. On completion of the reaction, the solvents were removed using a rotary evaporator. The resultant residue, a yellow/green viscous liquid, was re-dissolved in methanol and then purified by running the product through an SCX column. The eluted solution of NH_4:MeOH 5:95 containing the product was evaporated using a rotary evaporator to yield the product as a very viscous pale green liquid (561 mg, 73%), which was used directly in the next step (6.**5.1.14**; Compound **3.5**).

6.4.1.14 2-((4-azidobenzyl)(methyl)amino)ethan-1-ol [3.5]

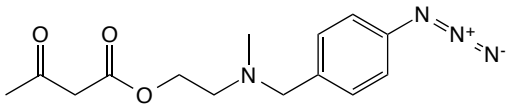


The methods used were adapted from Li *et al.,* (2010). TBAF (835 mg, 3.2 mmol), $TMSN_3$ (368 mg, 3.2 mmol) and CuCl (49 mg, 0.32 mmol) were added in succession to 3.4 (561 mg, 2.68 mmol) in 11 ml methanol in a 50 ml round-bottomed flask. The mixture was heated to reflux (70°C) for 18 hours, and reaction progress was monitored by TLC (product R_f 0.20, MeOH:DCM, 5:95). The reaction mixture was cooled, and the methanol was removed using a rotary evaporator. The resultant residue, a yellow liquid, was re-dissolved in the minimum volume of dichloromethane then purified by flash column chromatography on a silica column. The column was eluted with a gradient of MeOH:DCM, which was increased linearly from 0:100 to 5:95 over 12 CVs. The desired fractions were combined and evaporated using a rotary evaporator to yield the product as a yellow liquid (282 mg, 51%).

ν_{max} (thin film) 3457 (O-H), 3016 (C-H), 2970 (C-H), 2947 (C-H), 2361, 2115 (N_3), 1739. ^{1}H NMR (500 MHz, chloroform-*d*) d ppm 2.22 (3 H, s, NC*H*$_3$), 2.59 (2 H, t, *J*=5.5 Hz, OHCH$_2$C*H*$_2$N), 2.73 (1 H, s, O*H*), 3.54 (2 H, s, NC*H*$_2$Ph-N$_3$), 3.63 (2 H, q, *J*=5.0 Hz,

OHCH_2CH_2N), 7.00 (2 H, d, *J*=8.5 Hz, C(Ar)*H*), 7.29 (2 H, d, *J*=8.5 Hz, C(Ar)*H*). ^{13}C NMR (126 MHz, chloroform-*d*) d ppm 41.4, 58.2, 58.3, 61.6, 118.9, 130.3, 135.4, 138.9. *m/z* HRMS (ESI$^+$) $C_{10}H_{15}N_4O^+$ ([M+H]$^+$) requires 207.1240; found 207.1237.

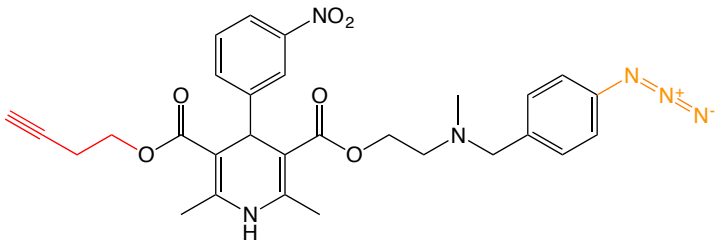
6.4.1.15 2-((4-azidobenzyl)(methyl)amino)ethyl 3-oxobutanoate [3.6]



The methods used were adapted from Miri *et al.,* (2006). **3.5** (282 mg, 1.35 mmol) was added to 2,2,6-trimethyl-4H-1,3-dioxine-4-one (192 mg, 1.35 mmol) in 2 ml toluene and placed in a 25 ml round-bottomed flask. The mixture was stirred and heated to reflux (120°C) for 18 hours, and reaction progress was monitored by TLC (product R_f 0.20, EtOAc:n-hexane, 40:60). The reaction mixture was cooled, and the toluene was removed using a rotary evaporator. The resultant residue, a pale yellow liquid, was re-dissolved in the minimum volume of dichloromethane then purified by flash column chromatography on a silica column. The column was eluted with a gradient of EtOAc:n-hexane, which was increased linearly from 15:85 to 45:55 over 12 CVs. The desired fractions were combined and evaporated using a rotary evaporator to yield the product as a pale yellow liquid (225 mg, 57%).

v_{max} (thin film) 2980 (C-H), 2958 (C-H), 2791 (C-H), 2114 (N_3, C≡C), 2035, 1650 (C=O, ketone), 1506. ^{1}H NMR (500 MHz, chloroform-*d*) d ppm 2.26 (3 H, s, NCH_3), 2.28 (3 H, s, CH_3C=O), 2.67 (2 H, t, *J*=6.0 Hz, OCH_2CH_2N), 3.47 (2 H, s, CH_3C=OCH_2), 3.52 (2 H, s, NCH_2Ph-N_3), 4.27 (2 H, t, *J*=6.0 Hz, OCH_2CH_2N), 6.99 (2 H, d, *J*=8.0 Hz, C(Ar)*H*), 7.27 - 7.32 (2 H, m, C(Ar)*H*). ^{13}C NMR (126 MHz, chloroform-*d*) d ppm 30.2, 42.4, 50.0, 55.1, 61.7, 62.9, 118.9, 130.3, 135.5, 138.8, 167.0, 200.4 (s). *m/z* HRMS (ESI$^+$) $C_{14}H_{18}N_4NaO_3^+$ ([M+Na]$^+$) requires 313.1271; found 313.1271.

6.4.1.16 3-(2-(4-azido-N-methylbenzamido)ethyl) 5-(but-3-yn-1-yl) 2,6-dimethyl-4-(3-nitrophenyl)pyridine-3,5-dicarboxylate [*Probe 4*]

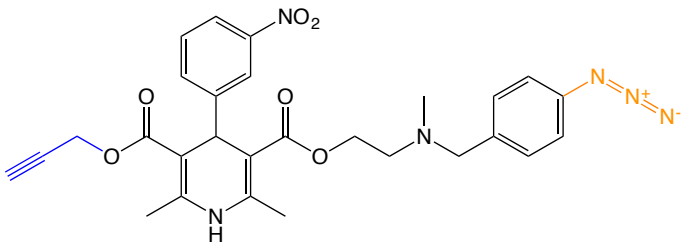


The methods used were adapted from Iwanami *et al.,* (1979). **3.6** (112 mg, 0.38 mmol) was added to **1.5** (59 mg, 0.38 mmol) and 3-nitrobenzaldehyde (59 mg, 0.38 mmol) in 4 ml 2-propanol and placed in a 25 ml round-bottomed flask. The mixture was heated to reflux (90°C) for 18 hours, and reaction progress was monitored by TLC (product R_f 0.20, EtOAc:n-hexane, 45:55). The reaction mixture was cooled, and the 2-propanol was removed using a rotary evaporator. The resultant residue, a yellow liquid, was re-dissolved in the minimum volume of dichloromethane then purified by flash column chromatography on a silica column. The column was eluted with a gradient of EtOAc:c-hexane, which was increased linearly from 15:85 to 50:50 over 12 CVs. The desired fractions were combined and evaporated using a rotary evaporator to yield the product as a yellow liquid (157 mg, 74%).

ν_{max} (thin film) 3301 (C-H, alkyne, N-H), 2955 (C-H), 2793 (C-H), 2485, 2114 (N3, C≡C), 1739 (C=O, ester), 1682, 1583, 1527 & 1349 (-NO_2), 1505. ^{1}H NMR (500 MHz, METHANOL-d_4) d ppm 2.21 (3 H, s, NCH_3), 2.26 (1 H, t, *J*=2.5 Hz, CHCCH_2), 2.35 (3 H, s, NCCH_3), 2.38 (3 H, s, NCCH_3), 2.45 - 2.50 (2 H, m, CHCCH_2), 2.56 - 2.70 (2 H, m, OCH_2CH_2N), 3.48 (2 H, d, *J*=5.0 Hz, NCH_2Ph-N_3), 4.07 - 4.15 (2 H, m, CHCCH_2CH_2), 4.15 - 4.22 (2 H, m, OCH_2CH_2N), 5.11 - 5.14 (1 H, m, NO_2-PhCH), 5.51 (1 H, s, NH), 6.96 - 7.00 (2 H, m, C(Ar)H), 7.28 (2 H, d, *J*=8.0 Hz, C(Ar)H), 7.41 - 7.46

(1 H, m, C(Ar)*H*), 7.71 (1 H, d, *J*=7.5 Hz, C(Ar)*H*), 7.95 - 8.00 (1 H, m, C(Ar)*H*), 8.13 (1 H, t, *J*=2.0 Hz, C(Ar)*H*). ^{13}C NMR (126 MHz, METHANOL-d_4) d ppm 18.7, 18.9, 19.7, 40.8, 42.7, 54.8, 56.5, 62.5, 63.2, 71.0, 81.5, 103.0, 103.2, 119.9, 122.1, 123.7, 130.2, 131.8, 135.5, 136.7, 140.3, 148.4, 148.5, 149.4, 151.7, 168.7, 168.8. *m/z* HRMS (ESI$^+$) $C_{29}H_{31}N_6O_6^+$ ([M+H]$^+$) requires 559.2300; found 559.2283.

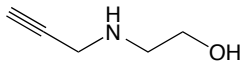
6.4.1.17 3-(2-((4-azidobenzyl)(methyl)amino)ethyl) 5-(prop-2-yn-1-yl) 2,6-dimethyl-4-(3-nitrophenyl)pyridine-3,5-dicarboxylate [*Probe 5*]



The methods used were adapted from Iwanami *et al.,* (1979). **3.6** (112 mg, 0.38 mmol) was added to **2.2** (54 mg, 0.38 mmol) and 3-nitrobenzaldehyde (59 mg, 0.38 mmol) in 4 ml 2-propanol and placed in a 25 ml round-bottomed flask. The mixture was heated to reflux (90°C) for 18 hours, and reaction progress was monitored by TLC (product R_f 0.20, EtOAc:n-hexane, 45:55). The reaction mixture was cooled, and the 2-propanol was removed using a rotary evaporator. The resultant residue, a yellow liquid, was re-dissolved in the minimum volume of dichloromethane then purified by flash column chromatography on a silica column. The column was eluted with a gradient of EtOAc:c-hexane, which was increased linearly from 15:85 to 50:50 over 12 CVs. The desired fractions were combined and evaporated using a rotary evaporator to yield the product as a yellow liquid (111 mg, 54%).

v_{max} (thin film) 3343 (C-H, alkyne, N-H), 2978 (C-H), 2949 (C-H), 2794 (C-H), 2591, 2114 (N_3, C≡C), 1693 (C=O, ester), 1527 & 1348 (-NO_2), 1505. ^{1}H NMR (500 MHz, METHANOL-d_4) d ppm 2.22 (3 H, s, NCH_3), 2.35 (3 H, s, NCCH_3), 2.36 (3 H, s, NCCH_3), 2.54 - 2.72 (2 H, m, OCH$_2$CH_2N), 2.84 (1 H, t, CHCCH$_2$), 3.45 - 3.53 (2 H, m, NCH_2Ph-N_3), 4.15 - 4.22 (2 H, m, OCH_2CH$_2$N), 4.59 - 4.73 (2 H, m, CHCCH_2), 5.10 - 5.14 (1 H, m, NO_2-PhCH), 5.51 (1 H, s, NH), 6.96 - 7.01 (2 H, m, C(Ar)H), 7.26 - 7.30 (2 H, m, C(Ar)H), 7.41 - 7.46 (1 H, m, C(Ar)H), 7.69 (1 H, d, J=8.0 Hz, C(Ar)H), 7.96 - 8.00 (1 H, m, C(Ar)H), 8.11 - 8.13 (1 H, m, C(Ar)H). ^{13}C NMR (126 MHz, METHANOL-d_4) d ppm 18.7, 18.8, 40.8, 42.7, 52.1, 54.8, 56.5, 62.6, 75.9, 78.5 - 79.2, 102.6, 103.3, 119.9, 122.2, 123.7, 130.2, 131.8, 135.4, 136.7, 140.3, 148.3, 148.9 , 149.4, 151.5, 167.9, 168.7. *m/z* HRMS (ESI$^+$) $C_{28}H_{29}N_6O_6^+$ ([M+H$^+$) requires 545.2143; found 545.2130.

6.4.1.18 2-(prop-2-yn-1-ylamino)ethan-1-ol (Vergnaud *et al.,* 2011) [4.1]

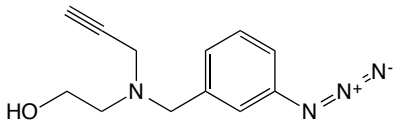


The methods used were adapted from Vergnaud *et al.,* (2011). 2-aminoethanol (27 g, 0.449 mol) was added to 100 ml dichloromethane in a 250 ml round-bottomed flask. Propargyl bromide (10.6 g, 89.8 mmol, 80% in toluene) was added dropwise to the mixture while stirring vigorously. The reaction was kept at room temperature for 18 hours, with use of an ice bath when necessary and reaction progress was monitored by TLC (product R_f 0.20, MeOH:DCM 10:90). Using a separating funnel, the bottom layer, containing dichloromethane (DCM), was removed, and the top layer, containing mainly 2-aminoethanol, was extracted three times with DCM. The DCM layers were combined in a conical flask, and dried over $MgSO_4$. The solvent was then removed using a rotatory evaporator. The resultant residue, a dark yellow viscous liquid, was re-

dissolved in the minimum volume of dichloromethane then purified by flash column chromatography on a silica column. The column was eluted with a gradient of MeOH:DCM, which was increased linearly from 0:100 to 10:90 over 12 CVs. The desired fractions were combined and evaporated using a rotary evaporator to yield the product as a dark yellow viscous liquid (2.95 g, 33%).

v_{max} (thin film) 3292 (C-H, alkyne, N-H), 3016 (C-H), 2970 (C-H), 2946 (C-H), 1739. ^{1}H NMR (500 MHz, chloroform-*d*) d ppm 2.24 (1 H, t, *J*=2.5 Hz, C*H*CCH_2), 2.38 (2 H, s, O*H* & N*H*), 2.84 - 2.88 (2 H, m, NC$H_2$$CH_2$OH), 3.46 (2 H, d, *J*=2.5 Hz, CHCCH_2), 3.67 - 3.70 (2 H, m, NC$H_2$$CH_2$OH). ^{13}C NMR (126 MHz, chloroform-*d*) d ppm 37.7, 49.9, 60.7, 71.7, 81.7.

6.4.1.19 2-((3-azidobenzyl)(prop-2-yn-1-yl)amino)ethan-1-ol [4.2]

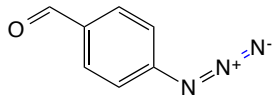


1.1 (250 mg, 1.7 mmol) was added to **4.1** (170 mg, 1.7 mmol) in 6 ml dichloromethane and placed in a 25 ml round-bottomed flask. Acetic acid (112 mg, 1.9 mmol) was added to the flask, and the mixture was stirred at room temperature for 15 minutes before adding $NaBH(OAc)_3$ (376 mg, 1.79 mmol). The mixture was stirred at room temperature for 48 hours. The reaction progress was monitored by TLC (product R_f 0.20, EtOAc:n-hexane, 30:70). On completion of the reaction, dichloromethane was removed using a rotary evaporator. The resultant residue, a yellow liquid, was re-dissolved in the minimum volume of dichloromethane then purified by flash column chromatography on a silica column. The column was eluted with a gradient of EtOAc:c-hexane, which was increased linearly from 10:90 to 35:65 over 12 CVs. The desired

fractions were combined and evaporated using a rotary evaporator to yield the product as a yellow liquid (262 mg, 67%).

v_{max} (thin film) 3295 (O-H), 2836 (C-H), 2113 (N3, C≡C), 1606, 1588. ^{1}H NMR (500 MHz, chloroform-*d*) d ppm 2.28 (1 H, t, *J*=2.5 Hz, C*H*CCH$_2$N), 2.33 - 2.51 (1 H, m, O*H*), 2.80 (2 H, t, *J*=5.5 Hz, OHC*H*$_2$CH$_2$N), 3.35 (2 H, d, *J*=2.5 Hz, NC*H*$_2$Ph-N$_3$), 3.66 (2 H, t, *J*=5.5 Hz, OHCH$_2$C*H*$_2$N), 3.69 (2 H, s, CHCC*H*$_2$N), 6.96 (1 H, dd, *J*=8.0, 1.5 Hz, C(Ar)*H*), 7.01 (1 H, s, C(Ar)*H*), 7.13 (1 H, d, *J*=7.5 Hz, C(Ar)*H*), 7.32 (1 H, t, *J*=8.0 Hz, C(Ar)*H*).^{13}C NMR (126 MHz, chloroform-*d*) d ppm 41.3, 54.8, 57.2, 58.5, 73.7, 77.8, 118.1, 119.6, 125.6, 129.8, 140.2. *m/z* HRMS (ESI$^+$) $C_{12}H_{14}N_4NaO^+$ ([M+Na]$^+$) requires 253.1060; found 253.1058

6.4.1.20 4-azidobenzaldehyde (Grimes *et al.,* 2010) [5.1]



The methods used were adapted from Grimes *et al.,* (2010). TBAF (4.18 g, 16 mmol), TMSN$_3$ (1.84 g, 16 mmol) and CuCl (204 g, 1.3 mmol) were added in succession to (4-formylphenyl)boronic acid (2.0 g, 13.3 mmol) in 60 ml methanol in a 250 ml round-bottomed flask. The mixture was heated to reflux (70°C) for 18 hours, and reaction progress was monitored by TLC (product R_f 0.20, EtOAc:n-hexane, 10:90). The reaction mixture was cooled, and the methanol was removed using a rotary evaporator. The resultant residue, a dark orange liquid, was re-dissolved in the minimum volume of dichloromethane then purified by flash column chromatography on a silica column. The column was eluted with a gradient of EtOAc:c-hexane, which was increased linearly from 4:96 to 10:90 over 12 CVs. The desired fractions were

combined and evaporated using a rotary evaporator to yield the product as a dark orange liquid (90 mg, 5%).

^{1}H NMR (500 MHz, chloroform-*d*) d ppm 7.17 (2 H, d, *J*=8.5 Hz, C(Ar)*H*), 7.89 (2 H, d, C(Ar)*H*), 9.96 (1 H, s, C=O*H*Ph-N_3). ^{13}C NMR (126 MHz, chloroform-*d*) d ppm 119.5, 131.5, 133.2, 146.3, 190.6.

CHAPTER 7: GENERAL DISCUSSION

7.1. General Dissuasion

The observations made during the course of the work described in this thesis have revealed that the contribution of I_f to pacemaker activity, as assessed from the action of ZD7288, is substantial in the mouse heart in the absence of adrenoceptor stimulation (Chapter 4). A CPA-sensitive contribution of SR appears to be a major influence in setting the resting level of I_f in wild type mice atrial preparations. The observations support the proposal that Ca^{2+} release from SR Ca^{2+} stores activates Ca^{2+}-stimulated ACs (via activation of calmodulin), which in turn activates I_f channels, as schematic diagram showed in **Figure 7.1**. In support of the proposal, the inhibition of AC enzymes (using 10 μM MDL-12,330A) attenuated the ability of I_f inhibitors to reduce the basal beating rate (Chapter 4).

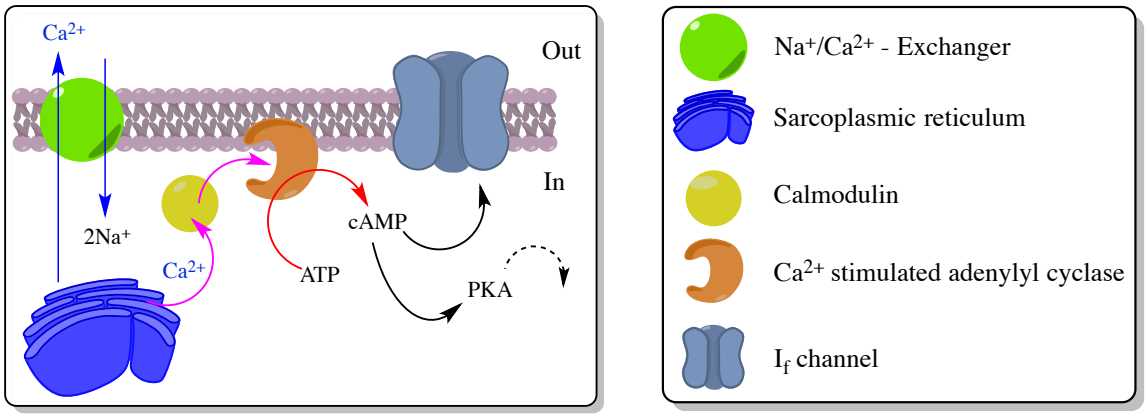


Figure 7.1. Simplified proposed mechanism of constitutive activation of the I_f channels via Ca^{2+} release from the sarcoplasmic reticulum.

Further tests of the hypothesis developed in Chapter 4 were subsequently carried out using genetically modified mice (Chapter 5). Specific knockout models [$AC1^{(-/-)}$, $AC8^{(-/-)}$ and $AC1\&8^{(-/-)}$] were used to study how the lack of the Ca^{2+}-stimulated ACs affects I_f channels (Chapter 5). Although there were clear differences between these models and control C57BL/6J mice, interestingly the results of the knockout models did not support the aforementioned proposal (Figure 7.1). In the knockout mice this may possibly be due to compensation of the loss of the AC enzymes by other pathways during development. During development of the knockouts, it is possible that other AC isoforms might be overexpressed to adapt to the loss of AC1 and/or AC8. In this regard the work of Lipskaia *et al.* (2000) and Georget *et al.* (2002) is notable; these results in mice showed that overexpression of AC8 in the heart did not change the basal spontaneous heart rate, despite the fact that the cytosolic cAMP concentration was elevated (Lipskaia *et al.,* 2000; Georget *et al.,* 2002). In addition no change in global cardiac function was observed. Knockout model mice lacking the AC6 enzyme resulted in no change in cAMP levels under basal conditions and no change in basal spontaneous beating rate (Tang *et al.,* 2008). However, under β-adrenoceptor stimulation, the cAMP level was reduced by 70%, PKA activity was reduced by 40%, and phospholamban phosphorylation was reduced by 45% (Tang *et al.,* 2008). In mice overexpressing the AC6 isoform, the basal spontaneous rate was not affected and contractile function was unchanged. However, the cardiac responsiveness to β_2-adrenoceptor stimulation was upregulated (Gao *et al.,* 1999). Thus it is possible that compensatory mechanisms may exist in the knockout models, which prevents changes to the basal spontaneous rate.

The limitations for drugs used in this thesis (Chapter 4 & 5) concerned selectivity, and whether the concentration and time course of incubation of particular drugs were appropriate (for example for drugs inhibiting I_f and Ca^{2+} release from SR). These limitations are discussed below.

To assess whether 1 μM ZD7288 induces near complete inhibition of I_f channels, I applied 3 μM ivabradine (another I_f inhibitor) subsequent to pretreatment of the tissue with 1 μM ZD7288. In the presence of ZD7288, ivabradine caused marginal change in beating rate, which was statistically not significant. This provided reassurance that 1 μM ZD7288 induced near complete inhibition both in mouse and in guinea pig atrial preparations (**Figure 4.4*A & B,* Figure 5.5**). Also, inhibition of I_f with 1 μM ZD7288, either alone or in combination with 3 μM ivabradine, did not cause substantial changes in the isoprenaline log(concentration)-response curve; no statistically significant difference was observed at any concentration of isoprenaline both in mouse and in guinea pig atrial preparation (**Figure 4.7*A & B***). These observations are also consistent with the suggestion that I_f channel inhibition in the presence of 1 μM ZD7288 was almost complete.

Compared to a 30 μM concentration of CPA, a 100 μM concentration had a larger effect on reducing basal beating rate (30 μM, 23 ± 4%; 100 μM, 47 ± 4%). It was reassuring that the larger reduction appeared not to be due to toxic effects, as the subsequent wash-out of the drug caused the beating rate to return approximately to its original baseline. However, we could not rule out that part of the further reduction in basal rate may have been due to inhibition of some voltage-gated Ca^{2+} channels. Although we observed a large decrease in

basal rate in terms of suppressing the chronotropic effect of isoprenaline, 30 and 100 μM CPA had a similar effect to one another in mouse atrial preparation, with the difference between the curves being statistically not significant (**Figure 4.7*A***). Reassuring that there are no toxic effects.

In addition to choosing the optimal concentrations of the abovementioned drugs, it was also crucial to choose the optimal incubation time, as governed by their target kinetics. The drugs used above, with the exception of isoprenaline and Cs^+ (2 min and 5 min, respectively), 30 min was optimal to reach the steady-state effect (**Figure 2.3*C* - *F***). For example, referring to the experiments in **Figure 4.6*A* & *B***, it was discovered that not only did the concentration of CPA need to be increased to 100 μM, but the pre-incubation time also had to be extended to 30 min in order to attenuate the effect of 1 μM ZD7288. This resulted in a significant change in Ca^{2+} transients modulated by I_f in the presence of CPA.

Given that we don't have a specific Ca^{2+}-stimulated AC inhibitor I used non-isoform-specific AC inhibitor MDL-12,330A to assess the contribution of Ca^{2+}-stimulated AC action on I_f channels. However, we could not rule out that part of the further inhibition is as a result of inhibition of non Ca^{2+}-stimulated AC. To overcome this issue specifically knockout mice models ($AC1^{(-/-)}$, $AC8^{(-/-)}$ and $AC1\&8^{(-/-)}$) were used to assess the lack of Ca^{2+}-stimulated AC's effect on I_f channel in Chapter 5. Overall, the outcome of the experiments in Chapter 5 were not clear-cut and the observations appeared not to allow a straightforward interpretation. It is possible that adaptation mechanisms are occurring. During development of the knockouts, it is possible that other AC isoforms might be

overexpressed and/or other signalling pathways are upregulated to adapt to the loss of AC1 and/or AC8. Therefore, for future work immunohistochemistry and RT-PCR techniques should be used to assess the spatiotemporal expressions and density of AC isoforms in the wild type and knockout models. Furthermore, the source of cAMP in terms of spatiotemporal production should be assessed using FRET techniques, this can reveal if there are difference in local production of cAMP in specific micro domains of wild type relative to knockout mice (Koschinski *et al.,* 2015).

It would also be important to measure AP profile from both wild type and knockout mice ($AC1^{(-/-)}$, $AC8^{(-/-)}$ and $AC1\&8^{(-/-)}$) on single cells using perforated patch-clamp technique. Unlike atrial preparation this will enable to assess the maximum diastolic potential and rate of diastolic depolarization. Perhaps some of the remodelling of knockout mice may be exposed.

Six photo-affinity probes were successfully synthesised and characterised (Chapter 6). When these were assessed in mouse spontaneously beating atrial preparations, it was revealed that 4 of the photo-affinity probes had the desired pharmacological action. One of the probes was selected and preliminary evidence was accrued that an ion channel, $Ca_v1.2$, could be successfully 'fished out' using the photo-crosslinking method. This shows that identification of a target molecule such as an ion channel, which is not only a macrostructure (~ 190 kD) but also a trans-membrane target, can also be achieved.

Although probe 1,2,4 and 5 all had a similar potency to nicardipine in reducing the mouse atrial preparations' spontaneously beating rate, the preparations are limited only to beating rate readouts. For future experiments it would be more informative to assess the effect of synthesised photo-affinity probes in reducing I_{st} current using single cell patch-clap protocols proposed by Noma's group (Guo *et al.,* 1995; Guo *et al.,* 1997; Mitsuiye *et al.,* 2000). A natural extension of this work would then involve use of the synthesised photo-affinity probes to identify the I_{st} channel in the SA node. However, in attempting to do so it may be necessary to use more than one guinea pig heart to isolate sufficient SAN cells for protein identification. Then the subsequent pulled down protein needs to be analysed in mass spectrometry (LC-MS/MS) to reveal the amino acid sequence of the target protein.

Over all in this thesis most of the drugs required over 30 min incubation time period to have a full desired action (**Figure 2.3*C* - *F***). In some instances, over 60 and 70 min incubation period were required, addition of If inhibitor in presence of CPA in organ bath and optical mapping experiments respectively. Thus it would be very difficult to perform these protocols under electrophysiological experiments. Thus using electrophysiological technique to test for the effectiveness of blockade is technically difficult particularly with If inhibitors. This is because ivabradine and ZD7288 are thought to be "use dependent" and which take a long time (30 min) to reach a steady-state effect and therefore blockade may be underestimated if the exposure time is too short. Therefore, under electrophysiological protocols current "rundown" and dialysis can also be a problem over long time periods. Even more importantly, the conditions used by most experimenters to measure I_f would not give 'normal' or

physiological levels of Ca^{2+} load into the SR (since conventional patch-clamp protocols do not allow the $Ca2^{+}$ loading of the SR that accompanies normal action potentials), and would therefore not be helpful. To overcome this limitation, experiments to measure I_f might be done for example using 'action potential clamp' to maintain SR Ca^{2+} load, and our lab planning these for the future work. Thus the spontaneously beating atrial preparation was selected due to its robustness and resilience, enabling prolonged measurements of drug incubations. However, despite number of advantages listed above it need to be pointed out that the disadvantage of using atrial preparation was that I was not able to observe the AP profile, specifically maximum diastolic potential and rate of diastolic depolarization of SAN cells.

REFERENCES

References

ABDEL-MAJID, R. M., LEONG, W. L., SCHALKWYK, L. C., SMALLMAN, D. S., WONG, S. T., STORM, D. R., FINE, A., DOBSON, M. J., GUERNSEY, D. L. & NEUMANN, P. E. (1998). Loss of adenylyl cyclase I activity disrupts patterning of mouse somatosensory cortex. *Nature genetics.* **19**, pp 289-291.

ACCILI, E., REDAELLI, G. & DIFRANCESCO, D. (1997). Differential control of the hyperpolarization-activated current I(f) by cAMP gating and phosphatase inhibition in rabbit sino-atrial node myocytes. *The Journal of physiology.* **500**, pp 643-651.

ALTOMARE, C., TERRAGNI, B., BRIOSCHI, C., MILANESI, R., PAGLIUCA, C., VISCOMI, C., MORONI, A., BARUSCOTTI, M. & DIFRANCESCO, D. (2003). Heteromeric HCN1–HCN4 channels: a comparison with native pacemaker channels from the rabbit sinoatrial node. *The Journal of physiology.* **549**, pp 347-359.

ANDRES, V., SCHULTZ, V. & TORNHEIM, K., (1990). Oscillatory synthesis of glucose 1,6-bisphosphate and frequency modulation of glycolytic oscillations in skeletal muscle extracts. *The Journal of biological chemistry,* **265**, pp 21441-21447.

ANUMONWO, J., FREEMAN, L., KWOK, W. & KASS, R. (1992). Delayed rectification in single cells isolated from guinea pig sinoatrial node. *American Journal of Physiology-Heart and Circulatory Physiology.* **262**, pp 921-925.

ARCH, J. R., NEWSHOLME, E. A. (1976). Activities and some properties of adenylate cyclase and phosphodiesterase in muscle, liver and nervous tissues from vertebrates and invertebrates in relation to the control of the concentration of adenosine 3':5'-cyclic monophosphate. *The Biochemical journal.* **158**, pp 603-622.

BAKER, J.G. (2005). The selectivity of β-adrenoceptor antagonists at the human β1, β2 and β3 adrenoceptors. *British journal of pharmacology,* **144**, pp 317-322.

BARBUTI, A., TERRAGNI, B., BRIOSCHI, C. & DIFRANCESCO, D. (2007). Localization of I_f-channels to caveolae mediates specific β_2-adrenergic receptor modulation of rate in sinoatrial myocytes. *Journal of Molecular and Cellular Cardiology.* **42**, pp 71-78.

BELEVYCH, A. E., SIMS, C. & HARVEY, R. D. (2001). ACh-induced rebound stimulation of L-type Ca^{2+} current in guinea-pig ventricular myocytes, mediated by $G_{\beta\gamma}$-dependent activation of adenylyl cyclase. *The Journal of physiology.* **536**, pp 677-692.

BENAVIDES-HARO, D. E., NAVARRO-POLANCO, R. A. & SÁNCHEZ-CHAPULA, J. A. (2003). The cholinomimetic agent bethanechol activates IK

(ACh) in feline atrial myocytes. *Naunyn-Schmiedeberg's archives of pharmacology.* **368**, pp 309-315.

BENNETT, H. J., DAVENPORT, J. B., COLLINS, R. F., TRAFFORD, A. W., PINALI, C. & KITMITTO, A. (2013). Human junctophilin-2 undergoes a structural rearrangement upon binding PtdIns(3,4,5)P_3 and the S101R mutation identified in hypertrophic cardiomyopathy obviates this response. *The Biochemical journal.* **456**, pp 205-217.

BENSON, D.W., WANG, D.W., DYMENT, M., KNILANS, T.K., FISH, F.A., STRIEPER, M.J., RHODES, T.H. & GEORGE, A.L.,JR, 2003. Congenital sick sinus syndrome caused by recessive mutations in the cardiac sodium channel gene (SCN5A). *The Journal of clinical investigation,* **112**, pp 1019-1028.

BOGDANOV, K. Y., VINOGRADOVA, T. M. & LAKATTA, E. G. (2001). Sinoatrial nodal cell ryanodine receptor and Na^+-Ca^{2+} exchanger: molecular partners in pacemaker regulation. *Circulation research.* **88**, pp 1254-1258.

BOIS, P., BESCOND, J., RENAUDON, B. & LENFANT, J. (1996). Mode of action of bradycardic agent, S 16257, on ionic currents of rabbit sinoatrial node cells. *British journal of pharmacology.* **118**, pp 1051-1057.

BORGDORFF, P., VERLATO, G. & CEVESE, A. (1987). Cardiac alpha-1 adrenoceptors are not involved in heart rate control of the anaesthetized dog. *Pflugers Archiv : European journal of physiology.* **410**, pp 495-500.

BOSMITH, R. E., BRIGGS, I. & STURGESS, N. C. (1993). Inhibitory actions of ZENECA ZD7288 on whole-cell hyperpolarization activated inward current I(f) in guinea-pig dissociated sinoatrial node cells. *British journal of pharmacology.* **110**, pp 343.

BOYETT, M.R., HONJO, H. and KODAMA, I., (2000). The sinoatrial node, a heterogeneous pacemaker structure. *Cardiovascular research,* **47**, pp. 658-687.

BRAMICH, N. J., EDWARDS, F. & HIRST, G. (1990). Sympathetic nerve stimulation and applied transmitters on the sinus venosus of the toad. *The Journal of physiology.* **429**, pp 349-375.

BRODDE, O., O'HARA, N., ZERKOWSKI, H. and ROHM, N., 1984. Human Cardiac [beta]-Adrenoceptors: Both β_1 and β_2 Adrenoceptors Are Functionally Coupled to the Adenylate Cyclase in Right Atrium. *Journal of cardiovascular pharmacology,* **6**, pp. 1184-1191.

BROWN, H., DIFRANCESCO, D. & NOBLE, S. (1979). How does adrenaline accelerate the heart? *Nature.* **120**, pp 235-236.

BUCCHI, A., BARUSCOTTI, M. & DIFRANCESCO, D. (2002). Current-dependent block of rabbit sino-atrial node I(f) channels by ivabradine. *The Journal of general physiology.* **120**, pp 1-13.

BURNSTOCK, G. (1969). Evolution of the autonomic innervation of visceral and cardiovascular systems in vertebrates. *Pharmacological reviews.* **21**, pp 247-324.

CAPEL, R. A., TERRAR, D. A. (2015). Cytosolic calcium ions exert a major influence on the firing rate and maintenance of pacemaker activity in guinea-pig sinus node. *Name: Frontiers in Physiology.* **6**, pp 1-8.

CHAMET, P., QUADID, H., RICHARD, S. & NARGET, J. (1987). Electrophysiological analysis of the action of nifedipine and nicardipine on myocardial fibres. *Fundam Clin Pharmacol,* **1**, pp 413-431.

CHENG, H., JAMES DPHIL, A.F., BOYETT, M.R. & HANCOX, J.C. (2016). Cardiac background sodium current: Elusive but important. *Channels,* **97**, pp 114-124.

CHIJIWA, T., MISHIMA, A., HAGIWARA, M., SANO, M., HAYASHI, K., INOUE, T., NAITO, K., TOSHIOKA, T. & HIDAKA, H. (1990). Inhibition of forskolin-induced neurite outgrowth and protein phosphorylation by a newly synthesized selective inhibitor of cyclic AMP-dependent protein kinase, N-[2-(p-bromocinnamylamino)ethyl]-5-isoquinolinesulfonamide (H-89), of PC12D pheochromocytoma cells. *The Journal of biological chemistry.* **265**, pp 5267-5272.

CHO, C., KIM, S. S., JEONG, M., LEE, C. O. & SHIN, H. (2000). The Na^{+}-Ca^{2+} exchanger is essential for embryonic heart development in mice. *Molecules and cells.* **10**, pp 712-722.

CHOATE, J. K., FELDMAN, R. (2003). Neuronal control of heart rate in isolated mouse atria. *American Journal of Physiology-Heart and Circulatory Physiology.* **285**, pp 1340-1346.

CHOATE, J. K., EDWARDS, F. R., HIRST, G. D. & O'SHEA, J. E. (1993). Effects of sympathetic nerve stimulation on the sino-atrial node of the guinea-pig. *The Journal of physiology.* **471**, pp 707-727.

COLSTON, J., KUMAR, P., CHAMBERS, J. & FREEMAN, G. (1994). Altered sarcolemmal calcium channel density and Ca^{2+}-pump ATPase activity in tachycardia heart failure. *Cell calcium.* **16**, pp 349-356.

COLLINS, T.P., BAYLISS, R., CHURCHILL, G.C., GALIONE, A. and TERRAR, D.A. (2011). NAADP influences excitation–contraction coupling by releasing calcium from lysosomes in atrial myocytes. *Cell calcium.* **50**, pp 449-458.

CONTI, A.C., YOUNG, C., OLNEY, J.W. and MUGLIA, L.J. (2009). Adenylyl cyclases types 1 and 8 promote pro-survival pathways after ethanol exposure in the neonatal brain. *Neurobiology of disease,* **33**, pp 111-118.

CONVERY, M.K. & HANCOX, J.C., (2000). Na^{+}-Ca^{2+} exchange current from rabbit isolated atrioventricular nodal and ventricular myocytes compared using action potential and ramp waveforms. *Acta Physiologica Scandinavica.* **168**, pp 393-401.

COOPER, D. M., MONS, N. & KARPEN, J. W. (1995). Adenylyl cyclases and the interaction between calcium and cAMP signalling. *Nature.* **374**, pp 421-424.

CORKEY, B.E., TORNHEIM, K., DEENEY, J.T., GLENNON, M.C., PARKER, J.C., MATSCHINSKY, F.M., RUDERMAN, N.B. & PRENTKI, M. (1989). Metabolic Regulation of Ca^{2+} Handling in Permeabilized Insulinoma Cells. *Cell Calcium Metabolism.* Springer. pp 369-377.

CRAVATT, B. F., WRIGHT, A. T. & KOZARICH, J. W. (2008). Activity-based protein profiling: from enzyme chemistry to proteomic chemistry. *Annu.Rev.Biochem.* **77**, pp 383-414.

DAVIES, F., FRANCIS, E. T. B. (1946). The conducting system of the vertebrate heart. *Biological Reviews.* **21**, pp 173-188.

DE JONGH, K.S., MURPHY, B.J., COLVIN, A.A., HELL, J.W., TAKAHASHI, M. & CATTERALL, W.A. (1996). Specific phosphorylation of a site in the full-length form of the α_1 subunit of the cardiac L-type calcium channel by adenosine 3', 5'-cyclic monophosphate-dependent protein kinase. *Biochemistry.* **35**, pp 10392-10402.

DEFER, N., BEST-BELPOMME, M. & HANOUNE, J. (2000). Tissue specificity and physiological relevance of various isoforms of adenylyl cyclase. *American journal of physiology.Renal physiology.* **279**, pp 400-416.

DENYER, J., BROWN, H. (1990). Pacemaking in rabbit isolated sino-atrial node cells during Cs block of the hyperpolarization-activated current if. *The Journal of physiology.* **429**, pp 401-409.

DIEL, S., KLASS, K., WITTIG, B. & KLEUSS, C. (2006). Gbetagamma activation site in adenylyl cyclase type II. Adenylyl cyclase type III is inhibited by Gbetagamma. *The Journal of biological chemistry.* **281**, pp 288-294.

DIFRANCESCO, D. (2010). The role of the funny current in pacemaker activity. *Circulation research.* **106**, pp 434-446.

DIFRANCESCO, D. (1986). Characterization of single pacemaker channels in cardiac sino-atrial node cells. *The Journal of physiology.* **429**, pp 385-407.

DIFRANCESCO, D. (1982). Block and activation of the pace-maker channel in calf Purkinje fibres: effects of potassium, cesium and rubidium. *The Journal of physiology.* **329**, pp 485-507.

DIFRANCESCO, D., CAMM, J. A. (2004). Heart rate lowering by specific and selective I_f current inhibition with ivabradine: a new therapeutic perspective in cardiovascular disease. *Drugs.* **64**, pp 1757-1765.

DIFRANCESCO, D., TORTORA, P. (1991). Direct activation of cardiac pacemaker channels by intracellular cyclic AMP. *Nature.* **351**, pp 145-147.

DIFRANCESCO, D., TROMBA, C. (1988). Muscarinic control of the hyperpolarization-activated current I_f in rabbit sino-atrial node myocytes. *The Journal of physiology.* **405**, pp 493-510.

DIFRANCESCO, D., MANGONI, M. (1994). Modulation of single hyperpolarization-activated channels I_f by cAMP in the rabbit sino-atrial node. *The Journal of physiology.* **474**, pp 473-482.

DIFRANCESCO, D., TROMBA, C. (1987). Acetylcholine inhibits activation of the cardiac hyperpolarizing-activated current, I_f. *Pflügers Archiv.* **410**, pp 139-142.

DIFRANCESCO, D. (1981). A new interpretation of the pace-maker current in calf Purkinje fibres. *The Journal of physiology.* **314**, pp 359-376.

DIFRANCESCO, D., DUCOURET, P. & ROBINSON, R. B. (1989). Muscarinic modulation of cardiac rate at low acetylcholine concentrations. *Science (New York, N.Y.).* **243**, pp 669-671.

DIXON, R. A., KOBILKA, B., STRADER, D., BENOVIC, J., DOHLMAN, H., FRIELLE, T., BOLANOWSKI, M., BENNETT, C. D., RANDS, E. & DIEHL, R. E. (1986). Cloning of the gene and cDNA for mammalian ß-adrenergic receptor and homology with rhodopsin. *Nature.* **321**, pp 75-79.

DOBRZYNSKI, H., BOYETT, M.R. and ANDERSON, R.H. (2007). New insights into pacemaker activity: promoting understanding of sick sinus syndrome. *Circulation.* **115**, pp 1921-1932.

DOOLEY, D.J., BITTIGER, H. & REYMANN, N.C. (1986). CGP 20712 A: a useful tool for quantitating β_1-and β_2-adrenoceptors. *European journal of pharmacology.* **130**, pp 137-139.

EMORINE, L. J., MARULLO, S., BRIEND-SUTREN, M. M., PATEY, G., TATE, K., DELAVIER-KLUTCHKO, C. & STROSBERG, A. D. (1989). Molecular characterization of the human beta 3-adrenergic receptor. *Science (New York, N.Y.).* **245**, pp 1118-1121.

ESPOSITO, G., PERRINO, C., OZAKI, T., TAKAOKA, H., DEFER, N., PETRETTA, M. P., DE ANGELIS, M. C., MAO, L., HANOUNE, J. & ROCKMAN, H. A. (2008). Increased myocardial contractility and enhanced exercise function in transgenic mice overexpressing either adenylyl cyclase 5 or 8. *Basic research in cardiology.* **103**, pp 22-30.

"European Medicine Agency, Procoralan Summary of Product Characteristics". Retrieved 2010-09-13.

EVANS, M. J., CRAVATT, B. F. (2006). Mechanism-based profiling of enzyme families. *Chemical reviews.* **106**, pp 3279-3301.

FAGAN, K. A., MAHEY, R. & COOPER, D. M. (1996). Functional co-localization of transfected Ca^{2+}-stimulable adenylyl cyclases with capacitative Ca^{2+} entry sites. *Journal of Biological Chemistry.* **271**, pp 12438-12444.

FILIPAN-LITVIĆ, M., LITVIĆ, M., CEPANEC, I. & VINKOVIĆ, V. (2007). Hantzsch Synthesis of 2, 6-Dimethyl-3, 5-dimethoxycarbonyl-4-(o-methoxyphenyl)-1, 4-dihydropyridine; a Novel Cyclisation Leading to an Unusual Formation of 1-Amino-2-methoxycarbonyl-3, 5-bis (o-methoxyphenyl)-4-oxa-cyclohexan-1-ene. *Molecules.* **12**, pp 2546-2558.

FLAVAHAN, N., MCGRATH, J. (1981). α-adrenoceptors can mediate chronotropic responses in the rat heart. *British journal of pharmacology.* **73**, pp 586-588.

FLEET, G., PORTER, R. and KNOWLES, J. (1969). Affinity labelling of antibodies with aryl nitrene as reactive group. *Nature.* **224.** pp. 511-512.

FRIELLE, T., COLLINS, S., DANIEL, K. W., CARON, M. G., LEFKOWITZ, R. J. & KOBILKA, B. K. (1987). Cloning of the cDNA for the human beta 1-adrenergic receptor. *Proceedings of the National Academy of Sciences of the United States of America.* **84**, pp 7920-7924.

GAO, Z., CHEN, B., MEI-LING, A. J., WU, Y., GUAN, X., KOVAL, O. M., CHAUDHARY, A. K., CUNHA, S. R., MOHLER, P. J. & MARTINS, J. B. (2010). I_f and SR Ca^{2+} release both contribute to pacemaker activity in canine sinoatrial node cells. *Journal of Molecular and Cellular Cardiology.* **49**, pp 33-40.

GAO, M. H., LAI, N. C., ROTH, D. M., ZHOU, J., ZHU, J., ANZAI, T., DALTON, N. & HAMMOND, H. K. (1999). Adenylylcyclase increases responsiveness to catecholamine stimulation in transgenic mice. *Circulation.* **99**, pp 1618-1622.

GAO, Z., SINGH, M. V., HALL, D. D., KOVAL, O. M., LUCZAK, E. D., JOINER, M. L., CHEN, B., WU, Y., CHAUDHARY, A. K., MARTINS, J. B., HUND, T. J., MOHLER, P. J., SONG, L. S. & ANDERSON, M. E. (2011). Catecholamine-independent heart rate increases require Ca^{2+}/calmodulin-dependent protein kinase II. *Circulation. Arrhythmia and electrophysiology.* **4**, pp 379-387.

GEORGET, M., MATEO, P., VANDECASTEELE, G., JUREVICIUS, J., LIPSKAIA, L., DEFER, N., HANOUNE, J., HOERTER, J. & FISCHMEISTER, R. (2002). Augmentation of cardiac contractility with no change in L-type Ca^{2+} current in transgenic mice with a cardiac-directed expression of the human adenylyl cyclase type 8 (AC8). *FASEB journal: official publication of the Federation of American Societies for Experimental Biology.* **16**, pp 1636-1638.

GILES, W., VAN GINNEKEN, A. & SHIBATA, E. (1986). Ionic currents underlying cardiac pacemaker activity: a summary of voltage-clamp data from single cells. *Cardiac Muscle: The Regulation of Excitation and Contraction.* pp 1-27.

GILES, W., NAKAJIMA, T., ONO, K. & SHIBATA, E. (1989). Modulation of the delayed rectifier K^+ current by isoprenaline in bull-frog atrial myocytes. *The Journal of physiology.* **415**, pp 233-249.

GRAND, T., DEMION, M., NOREZ, C., METTEY, Y., LAUNAY, P., BECQ, F., BOIS, P. & GUINAMARD, R. (2008). 9-Phenanthrol inhibits human TRPM4 but

not TRPM5 cationic channels. *British journal of pharmacology.* **153**, pp 1697-1705.

GREENE, D., KANG, S., KOSENKO, A. & HOSHI, N. (2012). Adrenergic regulation of HCN4 channel requires protein association with β_2-adrenergic receptor. *The Journal of biological chemistry.* **287**, pp 23690-23697.

GRIMES, K. D., GUPTE, A. & ALDRICH, C. C. (2010). Copper (II)-Catalyzed Conversion of Aryl/Heteroaryl Boronic Acids, Boronates, and Trifluoroborates into the Corresponding Azides: Substrate Scope and Limitations. *Synthesis.* **2010**, pp 1-23.

GROENKE, S., LARSON, E. D., ALBER, S., ZHANG, R., LAMP, S. T., REN, X., NAKANO, H., JORDAN, M. C., KARAGUEUZIAN, H. S., ROOS, K. P., NAKANO, A., PROENZA, C., PHILIPSON, K. D. & GOLDHABER, J. I. (2013). Complete atrial-specific knockout of sodium-calcium exchange eliminates sinoatrial node pacemaker activity. *PloS one.* **8**, pp 81633.

GRUPP, G., GRUPP, I., JOHNSON, C., MATLIB, M., ROUSLIN, W., SCHWARTZ, A., WALLICK, E., WANG, T. & WISLER, P. (1980). Effects of RMI 12330A, a new inhibitor of adenylate cyclase on myocardial function and subcellular activity. *British journal of pharmacology.* **70**, pp 429-442.

GUINAMARD, R., RAHMATI, M., LENFANT, J. & BOIS, P. (2002). Characterization of a Ca^{2+} -activated nonselective cation channel during dedifferentiation of cultured rat ventricular cardiomyocytes. *The Journal of membrane biology.* **188**, pp 127-135.

GUINAMARD, R., CHATELIER, A., DEMION, M., POTREAU, D., PATRI, S., RAHMATI, M. & BOIS, P., 2004. Functional characterization of a Ca^{2+} -activated non-selective cation channel in human atrial cardiomyocytes. *The Journal of physiology.* **558**, pp 75-83.

GUINAMARD, R., DEMION, M., CHATELIER, A. & BOIS, P. (2006). Calcium-activated nonselective cation channels in mammalian cardiomyocytes. *Trends in cardiovascular medicine.* **16**, pp 245-250.

GUINAMARD, R., DEMION, M., MAGAUD, C., POTREAU, D. & BOIS, P. (2006). Functional expression of the TRPM4 cationic current in ventricular cardiomyocytes from spontaneously hypertensive rats. *Hypertension.* **48**, pp 587-594.

GUO, J., MITSUIYE, T. & NOMA, A. (1997). The sustained inward current in sino-atrial node cells of guinea-pig heart. *Pflügers Archiv European Journal of Physiology.* **433**, pp 390-396.

GUO, J., ONO, K. & NOMA, A. (1995). A sustained inward current activated at the diastolic potential range in rabbit sino-atrial node cells. *The Journal of physiology.* **483**, pp 1-13.

HAGIWARA, N., IRISAWA, H. (1989). Modulation by intracellular Ca^{2+} of the hyperpolarization-activated inward current in rabbit single sino-atrial node cells. *The Journal of physiology.* **409**, pp 121-141.

HAGIWARA, N., IRISAWA, H. & KAMEYAMA, M. (1988). Contribution of two types of calcium currents to the pacemaker potentials of rabbit sino-atrial node cells. *The Journal of physiology.* **395**, pp 233-253.

HAGIWARA, N., IRISAWA, H., KASANUKI, H. & HOSODA, S. (1992). Background current in sino-atrial node cells of the rabbit heart. *The Journal of physiology.* **448**, pp 53-72.

HAMDI, A., COLAS, P. (2012). Yeast two-hybrid methods and their applications in drug discovery. *Trends in pharmacological sciences.* **33**, pp 109-118.

HASEGAWA, T., YASUDA, N. & YOSHIOKA, M. (1996). Photocyclization of 2-(dialkylamino) ethyl acetoacetates: Remote proton transfer and Stern-Volmer quenching kinetics in the system involving two reactive excited states. *Journal of physical organic chemistry.* **9**, pp 221-226.

HEAL, W. P., DANG, T. T. & TATE, E. W. (2011). Activity-based probes: discovering new biology and new drug targets. *Chemical Society Reviews.* **40**, pp 246-257.

HERRING, N., RIGG, L., TERRAR, D. A. & PATERSON, D. J. (2001). NO-cGMP pathway increases the hyperpolarisation-activated current, I(f), and heart rate during adrenergic stimulation. *Cardiovascular research.* **52**, pp 446-453.

HERRMANN, S., LIPP, P., WIESEN, K., STIEBER, J., NGUYEN, H., KAISER, E. & LUDWIG, A. (2013). The cardiac sodium-calcium exchanger NCX1 is a key player in the initiation and maintenance of a stable heart rhythm. *Cardiovascular research.* **99**, pp 780-788.

HESS, B. & PLESSER, T. (1979). Temporal and spatial order in biochemical systems. *Annals of the New York Academy of Sciences.* **316**, pp 203-213.

HEWINGS, D. S., WANG, M., PHILPOTT, M., FEDOROV, O., UTTARKAR, S., FILIPPAKOPOULOS, P., PICAUD, S., VUPPUSETTY, C., MARSDEN, B. & KNAPP, S. (2011). 3, 5-Dimethylisoxazoles act as acetyl-lysine-mimetic bromodomain ligands. *Journal of medicinal chemistry.* **54**, pp 6761-6770.

HIMENO, Y., TOYODA, F., SATOH, H., AMANO, A., CHA, C. Y., MATSUURA, H. & NOMA, A. (2011). Minor contribution of cytosolic Ca^{2+} transients to the pacemaker rhythm in guinea pig sinoatrial node cells. *American Journal of Physiology-Heart and Circulatory Physiology.* **300**, pp 251-261.

HIRANO, Y., HIRAOKA, M. (1988). Barium-induced automatic activity in isolated ventricular myocytes from guinea-pig hearts. *The Journal of physiology.* **395**, pp 455-472.

HONJO, H., BOYETT, M., KODAMA, I. & TOYAMA, J. (1996). Correlation between electrical activity and the size of rabbit sino-atrial node cells. *The Journal of physiology.* **496**, pp 795-808.

HUANG, C. L., FENG, S. & HILGEMANN, D. W. (1998). Direct activation of inward rectifier potassium channels by PIP_2 and its stabilization by $G_{\beta\gamma}$. *Nature.* **391**, pp 803-806.

HÜSER, J., BLATTER, L. A. & LIPSIUS, S. L. (2000). Intracellular Ca^{2+} release contributes to automaticity in cat atrial pacemaker cells. *The Journal of physiology.* **524**, pp 415-422.

HUTTER, O. F., TRAUTWEIN, W. (1956). Vagal and sympathetic effects on the pacemaker fibers in the sinus venosus of the heart. *The Journal of general physiology.* **39**, pp 715-733.

IRISAWA, H., BROWN, H. & GILES, W. (1993). Cardiac pacemaking in the sinoatrial node. *Physiological Reviews.* **73**, pp 197-227.

IWANAMI, M., SHIBANUMA, T., FUJIMOTO, M., KAWAI, R., TAMAZAWA, K., TAKENAKA, T., TAKAHASHI, K. & MURAKAMI, M. (1979). Synthesis of new water-soluble dihydropyridine vasodilators. *Chemical & pharmaceutical bulletin.* **27**, pp 1426-1440.

Jackson, V. Rakovic, S. & Terrar, D. (2002). Effects of isoproterenol on calcium transients and calcium sparks in guinea-pig sino-atrial node cells imaged by confocal microscopy. **82**, pp 648.

JARVIS, G. E., THOMPSON, A. J. (2013). A golden approach to ion channel inhibition. *Trends in pharmacological sciences.* **34**, pp 481-488.

JOUNG, B., TANG, L., MARUYAMA, M., HAN, S., CHEN, Z., STUCKY, M., JONES, L. R., FISHBEIN, M. C., WEISS, J. N., CHEN, P. S. & LIN, S. F. (2009). Intracellular calcium dynamics and acceleration of sinus rhythm by beta-adrenergic stimulation. *Circulation.* **119**, pp 788-796.

JU, Y., ALLEN, D. G. (1999). How does β-adrenergic stimulation increase the heart rate? The role of intracellular Ca^{2+} release in amphibian pacemaker cells. *The Journal of physiology.* **516**, pp 793-804.

KAMEYAMA, M., HOFMANN, F. & TRAUTWEIN, W. (1985). On the mechanism of β-adrenergic regulation of the Ca channel in the guinea-pig heart. *Pflügers Archiv.* **405**, pp 285-293.

KANDA, N., WATANABE, S. (2001). Regulatory roles of adenylate cyclase and cyclic nucleotide phosphodiesterases 1 and 4 in interleukin-13 production by activated human T cells. *Biochemical pharmacology.* **62**, pp 495-507.

KANG, T. M., HILGEMANN, D. W. (2004). Multiple transport modes of the cardiac Na+-Ca^{2+}; exchanger. *Nature.* **427**, pp 544-548.

KATSUSHIKA, S., CHEN, L., KAWABE, J., NILAKANTAN, R., HALNON, N. J., HOMCY, C. J. & ISHIKAWA, Y. (1992). Cloning and characterization of a sixth adenylyl cyclase isoform: types V and VI constitute a subgroup within the mammalian adenylyl cyclase family. *Proceedings of the National Academy of Sciences of the United States of America.* **89**, pp 8774-8778.

KEITH, A., FLACK, M. (1907). The form and nature of the muscular connections between the primary divisions of the vertebrate heart. *Journal of anatomy and physiology.* **41**, pp 172.

KO, E.A., WAN, J., YAMAMURA, A., ZIMNICKA, A.M., YAMAMURA, H., YOO, H.Y., TANG, H., SMITH, K.A., SUNDIVAKKAM, P.C., ZEIFMAN, A., AYON, R.J., MAKINO, A. and YUAN, J.X. (2013). Functional characterization of voltage-dependent Ca^{2+} channels in mouse pulmonary arterial smooth muscle cells: divergent effect of ROS. *American journal of physiology. Cell physiology.* **304**. pp 1042-1052.

KOMAS, N., LE BEC, A., STOCLET, J. C. & LUGNIER, C. (1991). Cardiac cGMP-stimulated cyclic nucleotide phosphodiesterases: effects of cGMP analogues and drugs. *European journal of pharmacology.* **206**, pp 5-13.

KOSCHINSKI, A. & ZACCOLO, M. (2015). A novel approach combining real-time imaging and the patch-clamp technique to calibrate FRET-based reporters for cAMP in their cellular microenvironment. *cAMP Signaling: Methods and Protocols.* pp 25-40.

KOUSHIK, S. V., WANG, J., ROGERS, R., MOSKOPHIDIS, D., LAMBERT, N. A., CREAZZO, T. L. & CONWAY, S. J. (2001). Targeted inactivation of the sodium-calcium exchanger (Ncx1) results in the lack of a heartbeat and abnormal myofibrillar organization. *FASEB journal: official publication of the Federation of American Societies for Experimental Biology.* **15**, pp 1209-1211.

KOVACS, M., TOTH, J., HETENYI, C., MALNASI-CSIZMADIA, A. & SELLERS, J.R. (2004). Mechanism of blebbistatin inhibition of myosin II. *The Journal of biological chemistry.* **279**, pp 35557-35563.

KRAPIVINSKY, G., GORDON, E., WICKMAN, K., VELIMIROVIC, B., KRAPIVINSKY, L. & CLAPHAM, D. (1995). The G-protein-gated atrial 1C channel Ikach is a heteromultimer of two inwardly rectifying 1C-channel proteins. *Nature.* **374**, pp 9.

KREITNER, D. (1985). Electrophysiological study of the two main pacemaker mechanisms in the rabbit sinus node. *Cardiovascular research.* **19**, pp 304-318.

KRYUKOVA, Y. N., PROTAS, L. & ROBINSON, R. B. (2012). Ca^{2+} -activated adenylyl cyclase 1 introduces Ca^{2+} -dependence to beta-adrenergic stimulation of HCN_2 current. *Journal of Molecular and Cellular Cardiology.* **52**, pp 1233-1239.

LAKATTA, E. G., DIFRANCESCO, D. (2009). What keeps us ticking: a funny current, a calcium clock, or both? *Journal of Molecular and Cellular Cardiology.* **47**, pp 157-170.

LAKATTA, E. G., MALTSEV, V. A. & VINOGRADOVA, T. M. (2010). A coupled SYSTEM of intracellular Ca^{2+} clocks and surface membrane voltage clocks controls the timekeeping mechanism of the heart's pacemaker. *Circulation research.* **106**, pp 659-673.

LATTANZIO, F. A.,JR, SCHLATTERER, R. G., NICAR, M., CAMPBELL, K. P. & SUTKO, J. L. (1987). The effects of ryanodine on passive calcium fluxes across sarcoplasmic reticulum membranes. *The Journal of biological chemistry.* **262**, pp 2711-2718.

LEE, P., BOLLENSDORFF, C., QUINN, T.A., WUSKELL, J.P., LOEW, L.M. and KOHL, P. (2011). Single-sensor system for spatially resolved, continuous, and multiparametric optical mapping of cardiac tissue. *Heart Rhythm,* **8**, pp 1482-1491.

LEI, M., BROWN, H. F. (1996). Two components of the delayed rectifier potassium current, I_K, in rabbit sino-atrial node cells. *Experimental physiology.* **81**, pp 725-741.

LEI, M., COOPER, P.J., CAMELLITI, P. & KOHL, P. (2002). Role of the 293b-sensitive, slowly activating delayed rectifier potassium current, $I(K_s)$, in pacemaker activity of rabbit isolated sino-atrial node cells. *Cardiovascular research.* **53**, pp 68-79.

LEI, M., JONES, S. A., LIU, J., LANCASTER, M. K., FUNG, S. S., DOBRZYNSKI, H., CAMELLITI, P., MAIER, S. K., NOBLE, D. & BOYETT, M. R. (2004). Requirement of neuronal-and cardiac-type sodium channels for murine sinoatrial node pacemaking. *The Journal of physiology.* **559**, pp 835-848.

LEITCH, S. P., SEARS, C. E., BROWN, H. F. & PATERSON, D. J. (1995). Effects of high potassium and the bradycardic agents ZD7288 and cesium on heart rate of rabbits and guinea pigs. *Journal of cardiovascular pharmacology.* **25**, pp 300.

LEVY, F. O., ZHU, X., KAUMANN, A. J. & BIRNBAUMER, L. (1993). Efficacy of beta 1-adrenergic receptors is lower than that of beta 2-adrenergic receptors. *Proceedings of the National Academy of Sciences of the United States of America.* **90**, pp 10798-10802.

LI, C., WANG, J. H. & COLYER, J. (1990). Immunological detection of phospholamban phosphorylation states facilitates the description of the mechanism of phosphorylation and dephosphorylation. *Biochemistry.* **29**, pp 4535-4540.

LI, Y., GAO, L. & HAN, F. (2010). Reliable and Diverse Synthesis of Aryl Azides through Copper-Catalyzed Coupling of Boronic Acids or Esters with $TMSN_3$. *Chemistry-A European Journal.* **16**, pp 7969-7972.

LIAO, Z., LOCKHEAD, D., LARSON, E. D. & PROENZA, C. (2010). Phosphorylation and modulation of hyperpolarization-activated HCN4 channels by protein kinase A in the mouse sinoatrial node. *The Journal of general physiology.* **136**, pp 247-258.

LIPSIUS, S.L. and VASSALLE, M. (1978). Dual excitatory channels in the sinus node. *Journal of Molecular and Cellular Cardiology.* **10**, pp. 753-767.

LIPSKAIA, L., DEFER, N., ESPOSITO, G., HAJAR, I., GAREL, M. C., ROCKMAN, H. A. & HANOUNE, J. (2000). Enhanced cardiac function in transgenic mice expressing a Ca^{2+}-stimulated adenylyl cyclase. *Circulation research.* **86**, pp 795-801.

LIU, J., NOBLE, P. J., XIAO, G., ABDELRAHMAN, M., DOBRZYNSKI, H., BOYETT, M. R., LEI, M. & NOBLE, D. (2008). Role of pacemaking current in cardiac nodes: insights from a comparative study of sinoatrial node and atrioventricular node. *Progress in biophysics and molecular biology.* **96**, pp 294-304.

LUO, W., GRUPP, I.L., HARRER, J., PONNIAH, S., GRUPP, G., DUFFY, J.J., DOETSCHMAN, T. and KRANIAS, E.G. (1994). Targeted ablation of the phospholamban gene is associated with markedly enhanced myocardial contractility and loss of beta-agonist stimulation. *Circulation research.* **75**, pp 401-409.

LUPU, V. D., KAZNACHEYEVA, E., KRISHNA, U. M., FALCK, J. R. & BEZPROZVANNY, I. (1998). Functional coupling of phosphatidylinositol 4, 5-bisphosphate to inositol 1, 4, 5-trisphosphate receptor. *Journal of Biological Chemistry.* **273**, pp 14067-14070.

LYASHKOV, A. E., VINOGRADOVA, T. M., ZAHANICH, I., LI, Y., YOUNES, A., NUSS, H. B., SPURGEON, H. A., MALTSEV, V. A. & LAKATTA, E. G. (2009). Cholinergic receptor signaling modulates spontaneous firing of sinoatrial nodal cells via integrated effects on PKA-dependent Ca^{2+} cycling and I(KACh). *American journal of physiology. Heart and circulatory physiology.* **297**, pp 949-59.

MALTSEV, V. A., LAKATTA, E. G. (2012). The funny current in the context of the coupled-clock pacemaker cell system. *Heart Rhythm.* **9**, pp 302-307.

MALTSEV, V. A., LAKATTA, E. G. (2007). Normal heart rhythm is initiated and regulated by an intracellular calcium clock within pacemaker cells. *Heart, Lung and Circulation.* **16**, pp 335-348.

MANGONI, M. E., COUETTE, B., BOURINET, E., PLATZER, J., REIMER, D., STRIESSNIG, J. & NARGEOT, J. (2003). Functional role of L-type $Ca_v1.3$ Ca^{2+} channels in cardiac pacemaker activity. *Proceedings of the National Academy of Sciences.* **100**, pp 5543.

MANGONI, M. E., NARGEOT, J. (2001). Properties of the hyperpolarization-activated current (I_f) in isolated mouse sino-atrial cells. *Cardiovascular research.* **52**, pp 51-64.

MANGONI, M. E., COUETTE, B., MARGER, L., BOURINET, E., STRIESSNIG, J. & NARGEOT, J. (2006). Voltage-dependent calcium channels and cardiac pacemaker activity: from ionic currents to genes. *Progress in biophysics and molecular biology.* **90**, pp 38-63.

MARX, S. O., REIKEN, S., HISAMATSU, Y., JAYARAMAN, T., BURKHOFF, D., ROSEMBLIT, N. & MARKS, A. R. (2000). PKA phosphorylation dissociates FKBP12.6 from the calcium release channel (ryanodine receptor): defective regulation in failing hearts. *Cell.* **101**, pp 365-376.

MARX, S.O., KUROKAWA, J., REIKEN, S., MOTOIKE, H., D'ARMIENTO, J., MARKS, A.R. and KASS, R.S. (2002). Requirement of a macromolecular signaling complex for beta adrenergic receptor modulation of the KCNQ1-KCNE1 potassium channel. *Science,* **295**, pp 496-499.

MATTICK, P., PARRINGTON, J., ODIA, E., SIMPSON, A., COLLINS, T. & TERRAR, D. (2007). Ca^{2+}-stimulated adenylyl cyclase isoform AC1 is preferentially expressed in guinea-pig sino-atrial node cells and modulates the I_f pacemaker current. *The Journal of physiology.* **582**, pp 1195-1203.

MEISSNER, G. (1994). Ryanodine receptor/Ca^{2+} release channels and their regulation by endogenous effectors. *Annual Review of Physiology.* **56**, pp 485-508.

MESIRCA, P., ALIG, J., TORRENTE, A. G., MÜLLER, J. C., MARGER, L., ROLLIN, A., MARQUILLY, C., VINCENT, A., DUBEL, S. & BIDAUD, I. (2014). Cardiac arrhythmia induced by genetic silencing of 'funny' (f) channels is rescued by GIRK4 inactivation. *Nature communications.* **5**, pp 1-15.

MIAKE, J., MARBÁN, E. & NUSS, H. B. (2002). Gene therapy: biological pacemaker created by gene transfer. *Nature.* **419**, pp 132-133.

DE MIGUEL, G., WIELOPOLSKI, M., SCHUSTER, D.I., FAZIO, M.A., LEE, O.P., HALEY, C.K., ORTIZ, A.L., ECHEGOYEN, L., CLARK, T. & GULDI, D.M. (2011). Triazole bridges as versatile linkers in electron donor–acceptor conjugates. *Journal of the American Chemical Society.* **133**, pp 13036-13054.

MILANESI, R., BARUSCOTTI, M., GNECCHI-RUSCONE, T. and DIFRANCESCO, D. (2006). Familial sinus bradycardia associated with a mutation in the cardiac pacemaker channel. *New England Journal of Medicine.* **354**, pp 151-157.

MIRI, R., JAVIDNIA, K., SARKARZADEH, H. & HEMMATEENEJAD, B. (2006). Synthesis, study of 3D structures, and pharmacological activities of lipophilic nitroimidazolyl-1, 4-dihydropyridines as calcium channel antagonist. *Bioorganic & medicinal chemistry.* **14**, pp 4842-4849.

MITSUIYE, T., SHINAGAWA, Y. & NOMA, A. (2000). Sustained inward current during pacemaker depolarization in mammalian sinoatrial node cells. *Circulation research.* **87**, pp 88-91.

MUNDIÑA-WEILENMANN, C., VITTONE, L., ORTALE, M., DE CINGOLANI, G. C. & MATTIAZZI, A. (1996). Immunodetection of phosphorylation sites gives new insights into the mechanisms underlying phospholamban phosphorylation in the intact heart. *Journal of Biological Chemistry.* **271**, pp 33561-33567.

NAKAYAMA, T., KURACHI, Y., NOMA, A. & IRISAWA, H. (1984). Action potential and membrane currents of single pacemaker cells of the rabbit heart. *Pflügers Archiv.* **402**, pp 248-257.

NATHAN, R. D. (1986). Two electrophysiologically distinct types of cultured pacemaker cells from rabbit sinoatrial node. *American Journal of Physiology-Heart and Circulatory Physiology.* **250**, pp 325-329.

NIKMARAM, M. R., LIU, J., ABDELRAHMAN, M., DOBRZYNSKI, H., BOYETT, M. R. & LEI, M. (2008). Characterization of the effects of ryanodine, TTX, E-4031 and 4-AP on the sinoatrial and atrioventricular nodes. *Progress in biophysics and molecular biology.* **96**, pp 452-464.

NILIUS, B., PRENEN, J., VOETS, T. & DROOGMANS, G. (2004). Intracellular nucleotides and polyamines inhibit the Ca^{2+} -activated cation channel TRPM4b. *Pflügers Archiv.* **448**, pp 70-75.

NILIUS, B., PRENEN, J., DROOGMANS, G., VOETS, T., VENNEKENS, R., FREICHEL, M., WISSENBACH, U. & FLOCKERZI, V. (2003). Voltage dependence of the Ca^{2+}-activated cation channel TRPM4. *The Journal of biological chemistry.* **278**, pp 30813-30820.

NITTA, J., FURUKAWA, T., MARUMO, F., SAWANOBORI, T. & HIRAOKA, M. (1994). Subcellular mechanism for Ca^{2+}-dependent enhancement of delayed rectifier K current in isolated membrane patches of guinea pig ventricular myocytes. *Circulation research.* **74**, pp 96-104.

NOBLE, D., TSIEN, R. (1969). Reconstruction of the repolarization process in cardiac Purkinje fibres based on voltage clamp measurements of membrane current. *The Journal of physiology.* **200**, pp 233-254.

NOYOLA, M., GALLEGOS, Z. H. (2003). Síntesis y actividad relajante en músculo liso vascular de una serie de 1, 4-dihidropiridinas análogas de nicardipina. *Journal of the Mexican Chemical Society.* **47**, pp 34-37.

O'ROURKE, B., RAMZA, B.M. & MARBAN, E. (1994). Excitability Driven by Metabolic Oscillations in Heart Cells. *Science.* **265**, pp 12.

OKUMURA, S., KAWABE, J., YATANI, A., TAKAGI, G., LEE, M. C., HONG, C., LIU, J., TAKAGI, I., SADOSHIMA, J., VATNER, D. E., VATNER, S. F. & ISHIKAWA, Y. (2003). Type 5 adenylyl cyclase disruption alters not only sympathetic but also parasympathetic and calcium-mediated cardiac regulation. *Circulation research.* **93**, pp 364-371.

ONO, K. & ITO, H. (1995). Role of rapidly activating delayed rectifier K^+ current in sinoatrial node pacemaker activity. *The American Journal of Physiology.* **269**, pp 453-462.

PETIT-JACQUES, J., BOIS, P., BESCOND, J. & LENFANT, J. (1993). Mechanism of muscarinic control of the high-threshold calcium current in rabbit sino-atrial node myocytes. *Pflügers Archiv.* **423**, pp 21-27.

PIERCY, V. (1988). Method for assessing the activity of drugs at β1-and β2-adrenoceptors in the same animal. *Journal of pharmacological methods.* **20**, pp 125-133.

POWELL, T., TERRAR, D. & TWIST, V. (1980). Electrical properties of individual cells isolated from adult rat ventricular myocardium. *The Journal of physiology.* **302**, pp 131-153.

PREMONT, R. T., CHEN, J., MA, H. W., PONNAPALLI, M. & IYENGAR, R. (1992). Two members of a widely expressed subfamily of hormone-stimulated adenylyl cyclases. *Proceedings of the National Academy of Sciences of the United States of America.* **89**, pp 9809-9813.

Rakovic, S. Rigg, L. & Terrar, D. (2000). Calcium transients in guinea-pig sino-atrial node cells imaged by confocal microscopy. **78**, pp 106.

REUTER, H., HENDERSON, S. A., HAN, T., MATSUDA, T., BABA, A., ROSS, R. S., GOLDHABER, J. I. & PHILIPSON, K. D. (2002). Knockout Mice for Pharmacological Screening Testing the Specificity of Na^+-Ca^{2+} Exchange Inhibitors. *Circulation research.* **91**, pp 90-92.

REUTER, H., HENDERSON, S. A., HAN, T., ROSS, R. S., GOLDHABER, J. I. & PHILIPSON, K. D. (2002). The Na^+-Ca^{2+} exchanger is essential for the action of cardiac glycosides. *Circulation research.* **90**, pp 305-308.

RIGG, L., HEATH, B. M., CUI, Y. & TERRAR, D. A. (2000). Localisation and functional significance of ryanodine receptors during β-adrenoceptor stimulation in the guinea-pig sino-atrial node. *Cardiovascular research.* **48**, pp 254-264.

RIGG, L., MATTICK, P. A. D., HEATH, B. M. & TERRAR, D. A. (2003). Modulation of the hyperpolarization-activated current (I_f) by calcium and calmodulin in the guinea-pig sino-atrial node. *Cardiovascular research.* **57**, pp 497-504.

RIGG, L., TERRAR, D. A. (1996). Possible role of calcium release from the sarcoplasmic reticulum in pacemaking in guinea-pig sino-atrial node. *Experimental physiology.* **81**, pp 877-880.

RIGG, L., TERRAR, D. (1998). Influence of ryanodine on the positive chronotropic response to β-adrenergic stimulation with isoprenaline in guinea-pig sino-atrial node. *British Journal of Pharmacology-Proceedings Supplement.*, pp 254-264.

RIX, U., SUPERTI-FURGA, G. (2009). Target profiling of small molecules by chemical proteomics. *Nature chemical biology.* **5**, pp 616-624.

ROBINETTE, D., NEAMATI, N., TOMER, K. B. & BORCHERS, C. H. (2006). Photoaffinity labeling combined with mass spectrometric approaches as a tool for structural proteomics. *Expert review of proteomics.* **3**, pp 399-408.

ROHRER, D. K., DESAI, K. H., JASPER, J. R., STEVENS, M. E., REGULA, D. P.,JR, BARSH, G. S., BERNSTEIN, D. & KOBILKA, B. K. (1996). Targeted

disruption of the mouse beta$_1$-adrenergic receptor gene: developmental and cardiovascular effects. *Proceedings of the National Academy of Sciences of the United States of America.* **93**, pp 7375-7380.

ROSEN, M. R., BRINK, P. R., COHEN, I. S. & ROBINSON, R. B. (2004). Genes, stem cells and biological pacemakers. *Cardiovascular research.* **64**, pp 12-23.

ROSENTHAL, K., LEMBER, J., KARELSON, E. & JÄRV, J. (1998). Activation of cAMP synthesis in rat brain cortical membranes by rubidium and cesium ions. *IUBMB life.* **45**, pp 745-751.

ROSTOVTSEV, V.V., GREEN, L.G., FOKIN, V.V. and SHARPLESS, K.B. (2002). A stepwise huisgen cycloaddition process: copper (I)-catalyzed regioselective "ligation" of azides and terminal alkynes. *Angewandte Chemie.* **114**. pp 2708-2711.

ROUGIER, J.S., ALBESA, M., ABRIEL, H. and VIARD, P. (2011). Neuronal precursor cell-expressed developmentally down-regulated 4-1 (NEDD4-1) controls the sorting of newly synthesized $Ca_V1.2$ calcium channels. *The Journal of biological chemistry.* **286**, pp 8829-8838.

ROUSSEAU, E., SMITH, J. S. & MEISSNER, G. (1987). Ryanodine modifies conductance and gating behavior of single Ca^{2+} release channel. *The American Journal of Physiology.* **253**, pp 364-368.

SANDERS, L., RAKOVIC, S., LOWE, M., MATTICK, P. A. D. & TERRAR, D. A. (2006). Fundamental importance of Na^+-Ca^{2+} exchange for the pacemaking mechanism in guinea-pig sino-atrial node. *The Journal of physiology.* **571**, pp 639-649.

SATOH, H. (2003). Sino-atrial nodal cells of mammalian hearts: ionic currents and gene expression of pacemaker ionic channels. *Journal of Smooth Muscle Research.* **39**, pp 175-193.

SCHULZE-BAHR, E., NEU, A., FRIEDERICH, P., KAUPP, U.B., BREITHARDT, G., PONGS, O. and ISBRANDT, D. (2003). Pacemaker channel dysfunction in a patient with sinus node disease. *The Journal of clinical investigation.* **111**, pp 1537-1545.

SCULPTOREANU, A., ROTMAN, E., TAKAHASHI, M., SCHEUER, T. & CATTERALL, W.A. (1993). Voltage-dependent potentiation of the activity of cardiac L-type calcium channel alpha 1 subunits due to phosphorylation by cAMP-dependent protein kinase. *Proceedings of the National Academy of Sciences of the United States of America.* **90**, pp 10135-10139.

SEIDLER, N. W., JONA, I., VEGH, M. & MARTONOSI, A. (1989). Cyclopiazonic acid is a specific inhibitor of the Ca^{2+}-ATPase of sarcoplasmic reticulum. *The Journal of biological chemistry.* **264**, pp 17816-17823.

SEVERS, N. J., SLADE, A. M., POWELL, T., TWIST, V. W. & JONES, G. E. (1985). Morphometric analysis of the isolated calcium-tolerant cardiac myocyte.

Organelle volumes, sarcomere length, plasma membrane surface folds, and intramembrane particle density and distribution. *Cell and tissue research.* **240**, pp 159-168.

SHI, W., WYMORE, R., YU, H., WU, J., WYMORE, R. T., PAN, Z., ROBINSON, R. B., DIXON, J. E., MCKINNON, D. & COHEN, I. S. (1999). Distribution and prevalence of hyperpolarization-activated cation channel (HCN) mRNA expression in cardiac tissues. *Circulation research.* **85**, pp 1-6.

SILVERMAN, M. E., GROVE, D. & UPSHAW, C. B.,JR (2006). Why does the heart beat? The discovery of the electrical system of the heart. *Circulation.* **113**, pp 2775-2781.

STORM, D. R., HANSEL, C., HACKER, B., PARENT, A. & LINDEN, D. J. (1998). Impaired cerebellar long-term potentiation in type I adenylyl cyclase mutant mice. *Neuron.* **20**, pp 1199-1210.

STRADER, C. D., FONG, T. M., GRAZIANO, M. P. & TOTA, M. R. (1995). The family of G-protein-coupled receptors. *FASEB journal : official publication of the Federation of American Societies for Experimental Biology.* **9**, pp 745-754.

SUN, H., CHEN, G. Y. & YAO, S. Q. (2013). Recent advances in microarray technologies for proteomics. *Chemistry & biology.* **20**, pp 685-699.

SUSICK, L. L., LOWING, J. L., PROVENZANO, A. M., HILDEBRANDT, C. C. & CONTI, A. C. (2014). Postnatal ethanol exposure simplifies the dendritic morphology of medium spiny neurons independently of adenylyl cyclase 1 and 8 activity in mice. *Alcoholism: Clinical and Experimental Research.* **38**, pp 1339-1346.

TAKEI, M., FURUKAWA, Y., NARITA, M., MURAKAMI, M., REN, L., KARASAWA, Y. & CHIBA, S. (1992). Sympathetic Nerve Stimulation Activates Both. BETA. 1-and. BETA. 2-Adrenoceptors of SA and AV Nodes in Anesthetized Dog Hearts. *The Japanese Journal of Pharmacology.* **59**, pp 23-30.

TANAKA, H., CLARK, R. B. & GILES, W. R. (1996). Positive chronotropic responses of rabbit sino-atrial node cells to flash photolysis of caged isoproterenol and cyclic AMP. *Proceedings.Biological sciences / The Royal Society.* **263**, pp 241-248.

TANG, T., LAI, N., ROTH, D. M., DRUMM, J., GUO, T., LEE, K., HAN, P., DALTON, N. & GAO, M. H. (2006). Adenylyl cyclase type V deletion increases basal left ventricular function and reduces left ventricular contractile responsiveness to β–adrenergic stimulation. *Basic research in cardiology.* **101**, pp 117-126.

TANG, T., GAO, M. H., LAI, N. C., FIRTH, A. L., TAKAHASHI, T., GUO, T., YUAN, J. X., ROTH, D. M. & HAMMOND, H. K. (2008). Adenylyl cyclase type 6 deletion decreases left ventricular function via impaired calcium handling. *Circulation.* **117**, pp 61-69.

TANIGUCHI, T., FUJIWARA, M. & OHSUMI, K. (1977). Possible involvement of cyclic adenosine 3':5'-monophosphate in the genesis of catecholamine-induced tachycardia in isolated rabbit sinoatrial node. *The Journal of pharmacology and experimental therapeutics.* **201**, pp 678-688.

TEPE, N. M., LORENZ, J. N., YATANI, A., DASH, R., KRANIAS, E. G., DORN, G. W. & LIGGETT, S. B. (1999). Altering the receptor-effector ratio by transgenic overexpression of type V adenylyl cyclase: enhanced basal catalytic activity and function without increased cardiomyocyte β-adrenergic signalling. *Biochemistry.* **38**, pp 16706-16713.

THOLLON, C., BEDUT, S., VILLENEUVE, N., COGE, F., PIFFARD, L., GUILLAUMIN, J., BRUNEL-JACQUEMIN, C., CHOMARAT, P., BOUTIN, J. & PEGLION, J. (2007). Use-dependent inhibition of hHCN4 by ivabradine and relationship with reduction in pacemaker activity. *British journal of pharmacology.* **150**, pp 37-46.

TRAFFORD, A. W., DIAZ, M. E. & EISNER, D. A. (2001). Coordinated control of cell Ca^{2+} loading and triggered release from the sarcoplasmic reticulum underlies the rapid inotropic response to increased L-type Ca^{2+} current. *Circulation research.* **88**, pp 195-201.

TRAUTWEIN, W., KAMEYAMA, M. (1986). Intracellular control of calcium and potassium currents in cardiac cells. *Japanese heart journal.* **27 Suppl 1**, pp 31-50.

TU, J. C., XIAO, B., YUAN, J. P., LANAHAN, A. A., LEOFFERT, K., LI, M., LINDEN, D. J. & WORLEY, P. F. (1998). Homer binds a novel proline-rich motif and links group 1 metabotropic glutamate receptors with IP_3 receptors. *Neuron.* **21**, pp 717-726.

UEDA, K., NAKAMURA, K., HAYASHI, T., INAGAKI, N., TAKAHASHI, M., ARIMURA, T., MORITA, H., HIGASHIUESATO, Y., HIRANO, Y., YASUNAMI, M., TAKISHITA, S., YAMASHINA, A., OHE, T., SUNAMORI, M., HIRAOKA, M. and KIMURA, A. (2004). Functional characterization of a trafficking-defective HCN4 mutation, D553N, associated with cardiac arrhythmia. *The Journal of biological chemistry,* **279**, pp 27194-27198.

VAN BORREN, M. M., VERKERK, A. O., WILDERS, R., HAJJI, N., ZEGERS, J. G., BOURIER, J., TAN, H. L., VERHEIJCK, E. E., PETERS, S. L. & ALEWIJNSE, A. E. (2010). Effects of muscarinic receptor stimulation on Ca2 transient, cAMP production and pacemaker frequency of rabbit sinoatrial node cells. *Basic research in cardiology.* **105**, pp 73-87.

VAN GINNEKEN, A., GILES, W. (1991). Voltage clamp measurements of the hyperpolarization-activated inward current I(f) in single cells from rabbit sino-atrial node. *The Journal of physiology.* **434**, pp 57-83.

VERGNAUD, J., FAUGERAS, P., CHALEIX, V., CHAMPAVIER, Y. & ZERROUKI, R. (2011). Design of a new oligotriazole peptide nucleic acid analogue (oT-PNA). *Tetrahedron letters.* **52**, pp 6185-6189.

VINOGRADOVA, T. M., BOGDANOV, K. Y. & LAKATTA, E. G. (2002). β-Adrenergic stimulation modulates ryanodine receptor Ca^{2+} release during diastolic depolarization to accelerate pacemaker activity in rabbit sinoatrial nodal cells. *Circulation research.* **90**, pp 73-79.

VINOGRADOVA, T. M., LYASHKOV, A. E., ZHU, W., RUKNUDIN, A. M., SIRENKO, S., YANG, D., DEO, S., BARLOW, M., JOHNSON, S. & CAFFREY, J. L. (2006). High Basal Protein Kinase A–Dependent Phosphorylation Drives Rhythmic Internal Ca^{2+} Store Oscillations and Spontaneous Beating of Cardiac Pacemaker Cells. *Circulation research.* **98**, pp 505-514.

VINOGRADOVA, T. M., ZHOU, Y. Y., BOGDANOV, K. Y., YANG, D., KUSCHEL, M., CHENG, H. & XIAO, R. P. (2000). Sinoatrial node pacemaker activity requires Ca2 /calmodulin-dependent protein kinase II activation. *Circulation research.* **87**, pp 760-767.

VODOVOZOVA, E. (2007). Photoaffinity labeling and its application in structural biology. *Biochemistry (Moscow).* **72**, pp 1-20.

WANG, H., PINEDA, V. V., CHAN, G. C., WONG, S. T., MUGLIA, L. J. & STORM, D. R. (2003). Type 8 adenylyl cyclase is targeted to excitatory synapses and required for mossy fiber long-term potentiation. *The Journal of neuroscience: the official journal of the Society for Neuroscience.* **23**, pp 9710-9718.

WU, Y., GAO, Z., CHEN, B., KOVAL, O. M., SINGH, M. V., GUAN, X., HUND, T. J., KUTSCHKE, W., SARMA, S. & GRUMBACH, I. M. (2009). From the Cover: Calmodulin kinase II is required for fight or flight sinoatrial node physiology. *Science's STKE.* **106**, pp 5972.

WU, J., SCHUESSLER, R. B., RODEFELD, M. D., SAFFITZ, J. E. & BOINEAU, J. P. (2001). Morphological and membrane characteristics of spider and spindle cells isolated from rabbit sinus node. *American journal of physiology. Heart and circulatory physiology.* **280**, pp 1232-40.

WU, Z. L., THOMAS, S. A., VILLACRES, E. C., XIA, Z., SIMMONS, M. L., CHAVKIN, C., PALMITER, R. D. & STORM, D. R. (1995). Altered behavior and long-term potentiation in type I adenylyl cyclase mutant mice. *Proceedings of the National Academy of Sciences of the United States of America.* **92**, pp 220-224.

YADAV, J., REDDY, B., KRISHNA, A., REDDY, C. S. & NARSAIAH, A. V. (2007). Triphenylphosphine: An efficient catalyst for transesterification of β-ketoesters. *Journal of Molecular Catalysis A: Chemical.* **261**, pp 93-97.

YAMADA, M. (2002). The role of muscarinic K^+ channels in the negative chronotropic effect of a muscarinic agonist. *The Journal of pharmacology and experimental therapeutics.* **300**, pp 681-687.

YANAGIHARA, K., IRISAWA, H. (1980). Inward current activated during hyperpolarization in the rabbit sinoatrial node cell. *Pflugers Archiv: European journal of physiology.* **385**, pp 11-19.

YANIV, Y., LAKATTA, E. G. & MALTSEV, V. A. (2015). From two competing oscillators to one coupled-clock pacemaker cell system. *Frontiers in physiology.* **6**, pp 1-8.

YANIV, Y., SIRENKO, S., ZIMAN, B. D., SPURGEON, H. A., MALTSEV, V. A. & LAKATTA, E. G. (2013). New evidence for coupled clock regulation of the normal automaticity of sinoatrial nodal pacemaker cells: bradycardic effects of ivabradine are linked to suppression of intracellular Ca 2 cycling. *Journal of Molecular and Cellular Cardiology.* **62**, pp 80-89.

YARD, N. J., CHIESI, M. & BALL, H. A. (1994). Effect of cyclopiazonic acid, an inhibitor of sarcoplasmic reticulum Ca^{2+}-ATPase, on the frequency-dependence of the contraction-relaxation cycle of the guinea-pig isolated atrium. *British journal of pharmacology.* **113**, pp 1001-1007.

YOSHIMURA, M., COOPER, D. M. (1993). Type-specific stimulation of adenylyl cyclase by protein kinase C. *The Journal of biological chemistry.* **268**, pp 4604-4607.

YOUNES, A., LYASHKOV, A. E., GRAHAM, D., SHEYDINA, A., VOLKOVA, M. V., MITSAK, M., VINOGRADOVA, T. M., LUKYANENKO, Y. O., LI, Y., RUKNUDIN, A. M., BOHELER, K. R., VAN EYK, J. & LAKATTA, E. G. (2008). Ca^{2+}-stimulated basal adenylyl cyclase activity localization in membrane lipid microdomains of cardiac sinoatrial nodal pacemaker cells. *The Journal of biological chemistry.* **283**, pp 14461-14468.

ZAZA, A., MACCAFERRI, G., MANGONI, M. & DIFRANCESCO, D. (1991). Intracellular calcium does not directly modulate cardiac pacemaker I(f) channels. *Pflügers Archiv European Journal of Physiology.* **419**, pp 662-664.

ZAZA, A., MICHELETTI, M., BRIOSCHI, A. & ROCCHETTI, M. (1997). Ionic currents during sustained pacemaker activity in rabbit sino-atrial myocytes. *The Journal of physiology.* **505**, pp 677-688.

ZAZA, A., ROBINSON, R. & DIFRANCESCO, D. (1996). Basal responses of the L-type Ca^{2+} and hyperpolarization-activated currents to autonomic agonists in the rabbit sino-atrial node. *The Journal of physiology.* **491**, pp 347-355.

ZHAO, P., WANG, X., ZHANG, X., CEBOTARU, V., CEBOTARU, L., GUO, G., MORALES, M. & GUGGINO, S. E. (2002). Tubular and cellular localization of the cardiac L-type calcium channel in rat kidney. *Kidney international.* **61**, pp 1393-1406.

ZHOU, Z., LIPSIUS, S. (1993). Na^{+}- Ca^{2+} exchange current in latent pacemaker cells isolated from cat right atrium. *The Journal of physiology.* **466**, pp 263-285.

Appendix

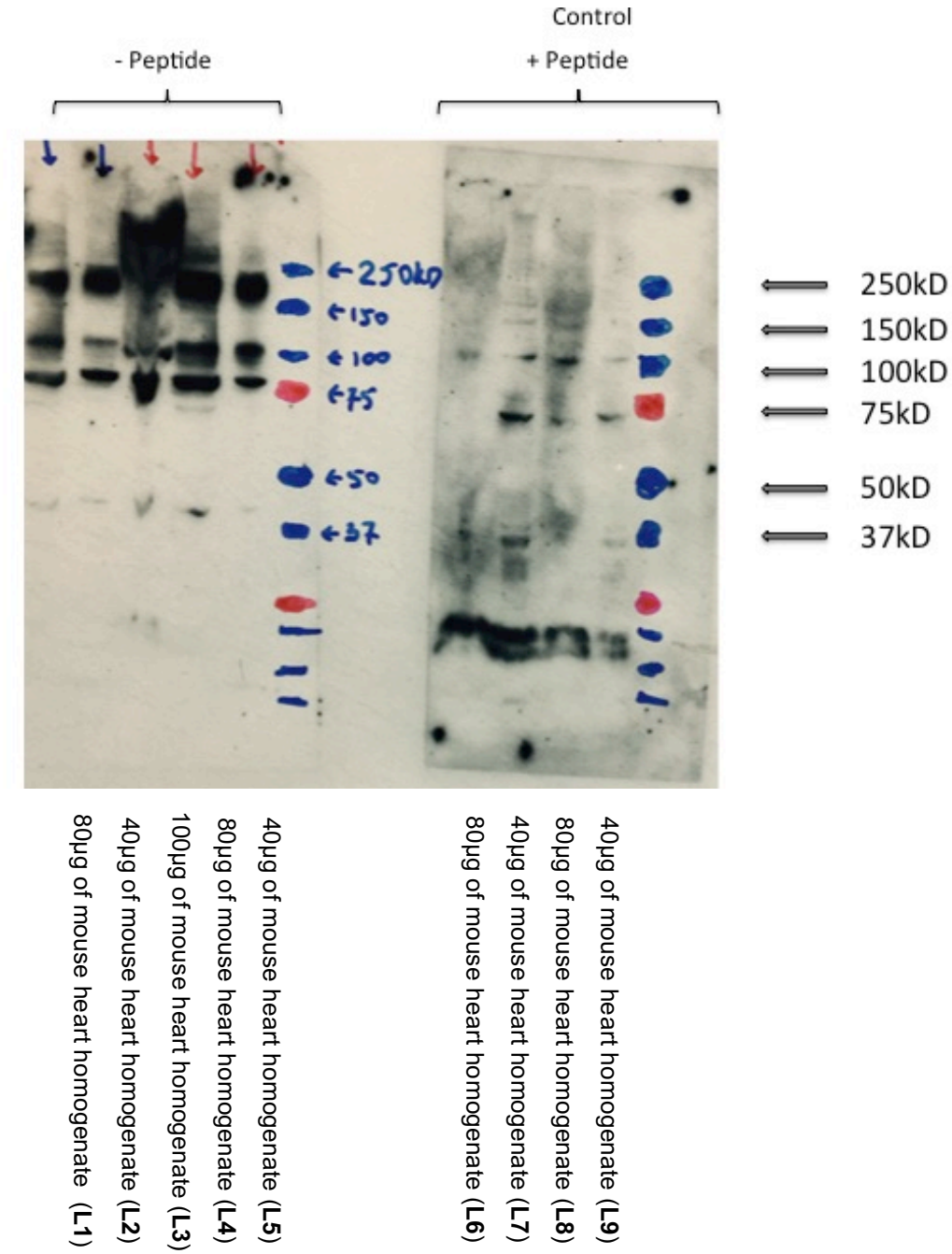


Figure *A*6.17 Detection of $Ca_v1.2$ channels by Western blot analysis. A range of sample concentrations (40 - 100 mg/mL) were loaded and immunoblotted. In 30 mg/mL homogenized mouse whole heart samples, $Ca_v1.2$ (~190 kDa) was successfully detected after blotting with primary and secondary antibodies (Lanes 5 - 9). No band was observed in the presence of $Ca_v1.2_{848\text{-}865}$ peptide (Lanes 1 - 4).

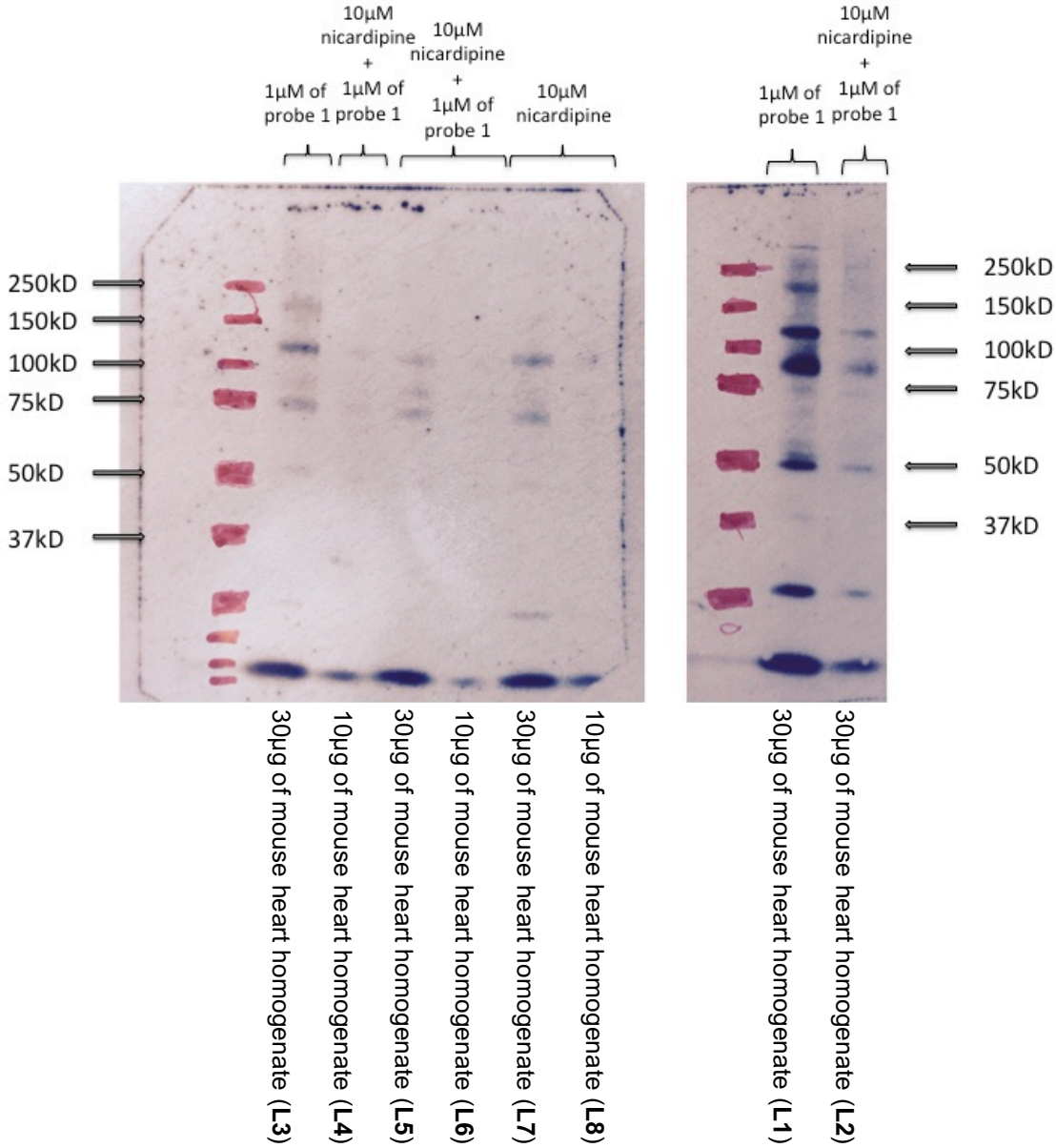


Figure *A*6.19 Photocapture of $Ca_v1.2$ channel by photo-affinity probe 1 in (L3 - 8) ventricular guinea pigs cell lysate or (L1-2) homogenized mouse whole heart samples. In 30 mg/mL cell lysate and homogenized tissue, cross-linked $Ca_v1.2$ (~190 kDa) could be detected after irradiation with 1 µM photo-affinity probe 1 (Lanes 1 and 3). No crosslinking was observed in the presence of 1 µM nicardipine (Lanes 2, 4 to 8).

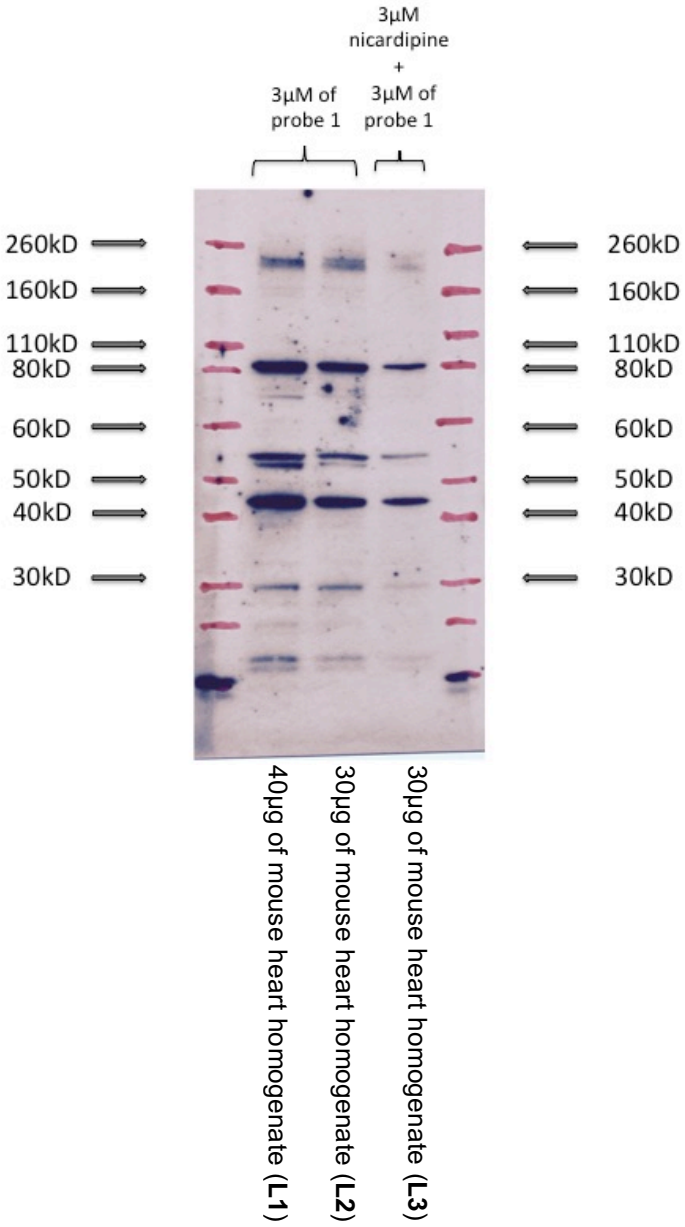


Figure *A*6.20 Evidence for photocapture of $Ca_v1.2$ channel by photo-affinity probe 1 in homogenized mouse whole heart samples. Cross-linked $Ca_v1.2$ (~190 kDa) could be detected after irradiation with 3 µM photo-affinity Probe 1 (L1 - 2). No obvious crosslinking was observed in the presence of 3 µM nicardipine (L3).